

Copyright is owned by the Author of the thesis. Permission is given for a copy to be downloaded by an individual for the purpose of research and private study only. The thesis may not be reproduced elsewhere without the permission of the Author.

**Synthetic targets as mechanistic probes for the key  
biosynthetic enzyme, dehydroquinate synthase**

A dissertation submitted to

Massey University

in partial fulfilment of the requirements for the degree of

Doctor of Philosophy

by

**Leonardo Negrón**

INSTITUTE OF FUNDAMENTAL SCIENCES

Palmerston North

April 2009

Para mis padres Ruth y Antonio

## **Acknowledgements**

I would like to thank my supervisor Dr. Emily J. Parker for all her help, enthusiasm and encouragement. I am particularly grateful to her for continuing to supervise me despite the distance.

I would also like to thank my co-supervisor Dr. Geoffrey B. Jameson for all his support and assistance. I wish to express a special thank you to Dr. Linley Schofield, Dr. Fiona Cochrane and all the members of Dr. Gill Norris' lab for the excellent biological support that helped me through many experiments.

Many thanks go to the members of the EJP group and the staff and students of the Institute of Fundamental Sciences.

I wish to express my appreciation to my parents and my siblings for being there for me always and encouraging me to succeed.

Finally, I wish to give my dearest thanks to my partner Dr. Mike Roguski for his unconditional love and support during these arduous few years.

## Abstract

Dehydroquinate synthase (DHQS) catalyses the five-step transformation of the seven carbon sugar 3-deoxy-D-*arabino*-heptulosonate 7-phosphate (DAH7P) to the carbacycle dehydroquinate (DHQ). Multiple studies have described in detail the mechanism of most of the steps carried out by DHQS with the exception of the final cyclisation step. In this study, (3*S*)-3-fluoro-DAH7P and (3*R*)-3-fluoro-DAH7P (fluorinated analogues of DAH7P) were produced and assayed across three phylogenetically distinct sources of DHQS in order to determine the role of the enzyme during the cyclisation step of the reaction.

Incubation of (3*S*)-3-fluoro-DAH7P with DHQS from *Escherichia coli*, *Pyrococcus furiosus*, and Kiwifruit resulted in the production of different ratios of (6*S*)-6-fluoro-DHQ and 1-*epi*-(6*S*)-6-fluoro-DHQ for each enzyme. In addition, enzyme catalysis showed a slowing of reaction rates when (3*S*)-3-fluoro-DAH7P was used, suggesting that the fluorine at C-3 is stabilising the enol pyranose. An increase in the stabilisation of the fluoro-enol pyranose would allow release of this substrate intermediate from the enzyme to compete with the on-going on-enzyme reaction.

The differences in the ratio of products formed suggest that the cyclisation occurs in part on the enzyme and that the epimeric product arises only by an abortive reaction pathway where the (3*S*)-3-fluoro-enol pyranose is prematurely released and allowed to cyclise free in solution. Once in solution, the (3*S*)-3-fluoro-enol pyranose could undergo a conformational change in the ring leading to the formation of the epimeric product. Furthermore, it is suspected that the position of fluorine influences the likely transition-state in carbacycle formation leading to the production of the epimeric product.

This research has illuminated the role of the enzyme in guiding the correct stereochemistry of the product and illustrates the important molecular interplay between the enzyme and substrate.

## Contents

1. Background.....	1
1.1 Shikimate pathway.....	1
1.2 Dehydroquinase synthase (DHQS).....	3
1.3 Structure and function of DHQS.....	4
1.4 Mechanism of DHQS.....	5
1.5 Structural involvement of DHQS in the catalysis of DHQ formation.....	7
1.6 DHQS from other sources.....	9
1.7 Studies investigating steps one, two, and three catalysed by DHQS.....	9
1.8 Studies investigating steps four and five of the DHQS reaction mechanism.....	13
1.9 Further studies involving the role of the enzyme during ring closure.....	15
1.10 Purpose of the study.....	20
1.11 Thesis objectives.....	22
2. Expression and purification of DHQS and DHQase from <i>Escherichia coli</i> and <i>Pyrococcus furiosus</i> . Characterisation of DHQS from <i>Escherichia coli</i> , <i>Pyrococcus furiosus</i> , and Kiwifruit.....	23
2.1 Introduction.....	23
2.2 Expression of <i>E. coli</i> DHQS.....	23
2.3 Purification of <i>E. coli</i> DHQS.....	26
2.4 Expression of <i>P. furiosus</i> DHQS.....	28
2.5 <i>P. furiosus</i> DHQS purification trials.....	29
2.6 Expression of <i>P. furiosus</i> DHQS using Rosetta-gami B™ cells.....	30
2.7 <i>P. furiosus</i> DHQS lysis trials.....	33
2.8 Final purification of <i>P. furiosus</i> DHQS.....	34
2.9 Expression and purification of <i>E. coli</i> DHQase.....	36
2.10 Expression and purification of <i>P. furiosus</i> DHQase.....	37
2.11 Characterisation of <i>E. coli</i> DHQS, <i>P. furiosus</i> DHQS, and Kiwifruit DHQS.....	38
2.12 Metal dependency of <i>P. furiosus</i> DHQS and Kiwifruit DHQS.....	45
2.13 Tagged versus untagged Kiwifruit DHQS experiment.....	50
2.14 Discussion.....	53
2.15 Summary.....	55
3. Chemo-enzymatic preparation of DAH7P, (3 <i>S</i> )-3-fluoro-DAH7P, and (3 <i>R</i> )-3-fluoro-DAH7P.....	56
3.1 Introduction.....	56
3.2 Preparation of E4P.....	56
3.3 Preparation of (Z)-3-fluoro-PEP and (E)-3-fluoro-PEP.....	57
3.4 Preparation and isolation of DAH7P.....	60
3.5 Preparation and isolation of (3 <i>S</i> )-3-fluoro-DAH7P and (3 <i>R</i> )-3-fluoro-DAH7P.....	62

3.6	Substrate concentration .....	68
3.7	Summary .....	69
4.	Interaction of (3 <i>S</i> )-3-fluoro-DAH7P and (3 <i>R</i> )-3-fluoro-DAH7P with DHQS enzymes .....	70
4.1	Introduction .....	70
4.2	Partitioning results from <sup>19</sup> F NMR spectroscopy .....	71
4.3	Kinetic experiments .....	81
4.4	Partitioning experiments using UV spectroscopy .....	90
4.5	Discussion .....	95
4.6	Summary .....	103
5.	Approaches to the synthesis of the modified DAH7P analogues.....	104
5.1	Methodology.....	104
5.2	Methodology and synthesis of 7-carbon phosphate sugars.....	106
5.3	Other syntheses .....	122
5.4	Summary .....	138
6.	Overall conclusions and future work .....	139
7.	Experimental .....	149
7.1	General methods.....	149
7.2	General biological methods.....	152
7.3	Experimental for chapter 2.....	156
7.4	Experimental for chapter 3.....	167
7.5	Experimental for chapter 4.....	174
7.6	Experimental for chapter 5.....	178
	Appendices .....	203
	References .....	209

## Abbreviations

Bn	Benzyl
BTP	1,3-bis(tris(hydroxymethyl)amino)propane
DAH7P	3-deoxy-D- <i>arabino</i> -heptulosonate-7-phosphate
DAST	diethylaminosulfur trifluoride
DCM	dichloromethane
DHQ	dehydroquinate
DHQase	dehydroquinase
DHQS	dehydroquinase synthase
DMAP	4-dimethylaminopyridine
DMSO	dimethyl sulfoxide
DNA	deoxyribonucleic acid
DTT	dithiothreitol
E4P	erythrose-4-phosphate
E	extinction coefficient
EDTA	ethylenediaminetetraacetic acid disodium salt
ESMS	electrospray mass spectrometry
ESPS	5-enolpyruvyl-shikimate-3-phosphate
Et	ethyl
G-6-P	glucose-6-phosphate
IPTG	isopropylthio- $\beta$ -D-galactoside
$K_M$	Michaelis constant
$k_{cat}$	catalytic constant
LB	Luria Bertani
Me	methyl
NAD <sup>+</sup>	nicotinamide adenine dinucleotide
NaHMDS	sodium hexamethyldisilazide
NBS	<i>N</i> -bromosuccinamide
NMR	nuclear magnetic resonance
NOE	nuclear Overhauser enhancement
OD <sub>600</sub>	optical density at 600nm
PAGE	polyacrylamide gel electrophoresis
PEP	phosphoenol pyruvate
Ph	phenyl
P <sub>i</sub>	inorganic phosphate
Ppm	parts per million
<i>p</i> Ts	<i>p</i> -toluenesulfonic acid
Rt	room temperature
SDS	sodium dodecyl sulfate
TBAF	tetra- <i>n</i> -butylammonium fluoride
<i>t</i> -Bu	potassium <i>tert</i> -butoxide
THF	tetrahydrofuran

TLC thin layer chromatography  
TMP Trimethyl phosphite  
UV ultra violet

## 1. Background

### 1.1 Shikimate pathway

Antibacterial agents are compounds that halt or completely inhibit the growth of bacteria. This alteration in bacterial growth can be accomplished by blocking the operation of biochemical pathways, which in turn result in a cascade of events leading to stasis or complete disruption of cell function and growth.<sup>1</sup> One such biochemical pathway that serves as an interesting area of research for potential antibacterial and antifungal agents is the shikimate pathway. The enzymes of the shikimate pathway are prime targets for drug design because they are not found in humans, thus, reducing the risk of potential adverse effects from drugs that inhibit this pathway.

The shikimate pathway is responsible for producing the precursors of aromatic amino acids (phenylalanine, tyrosine, and tryptophan).<sup>2</sup> The biosynthesis of these amino acids are vital for the homeostasis of various plants, fungi, and bacteria. In addition, this biochemical pathway generates aromatic precursors essential for folic acid and ubiquinone production.<sup>3</sup> A total of seven enzymes are responsible for the conversion of phosphoenol pyruvate (PEP) **1** and erythrose 4-phosphate (E4P) **2** to chorismate **9** (see figure 1.1). At chorismate the shikimate pathway branches into three; one pathway leading to phenylalanine and tyrosine, a second pathway leading to tryptophan, and a third pathway leading to folate and ubiquinone.<sup>4</sup>

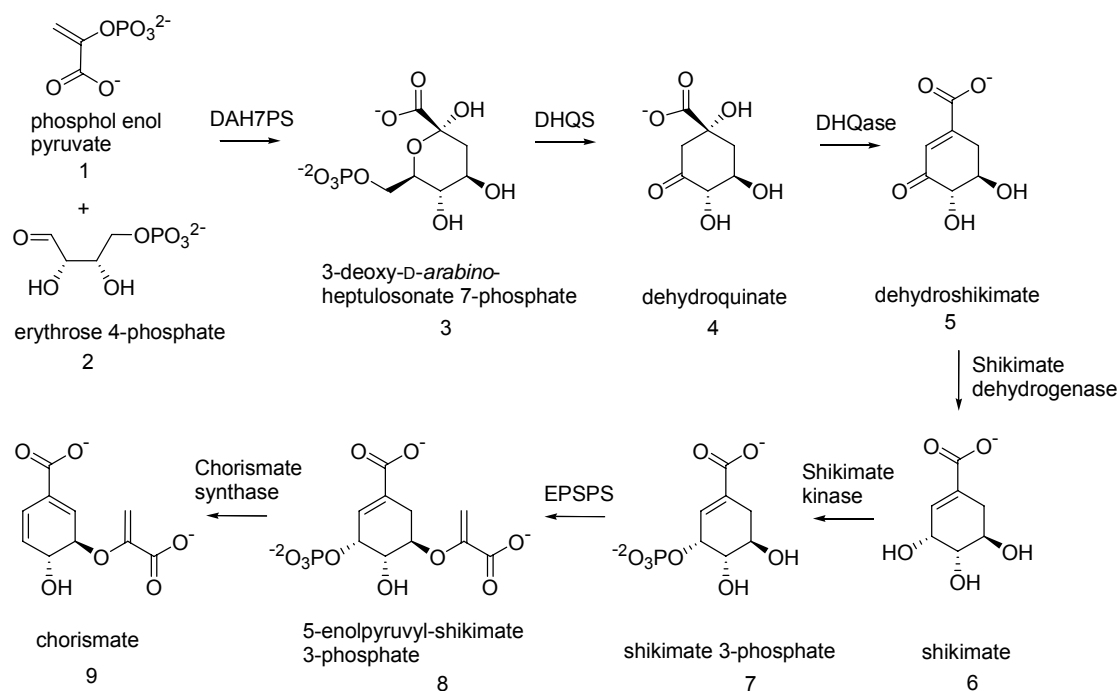


Figure 1.1. The shikimate pathway

The first enzyme in the shikimate pathway is 3-deoxy-D-*arabino*-heptulosonate 7-phosphate synthase (DAH7PS). DAH7PS is responsible for catalysing the condensation of PEP **1** and EAP **2** to form 3-deoxy-D-*arabino*-heptulosonate 7-phosphate (DAH7P). DAH7P is the substrate for the second enzyme dehydroquininate synthase (DHQS). DHQS converts DAH7P **3** to the carbocycle dehydroquininate (DHQ) **4**, which is then used by the third enzyme, dehydroquinase (DHQase). DHQase catalyses the dehydration of DHQ to make dehydroshikimate **5**. The fourth enzyme, shikimate dehydrogenase, is responsible for the formation of shikimate **6** through the reduction of the ketone functionality of dehydroshikimate. Shikimate kinase, the fifth enzyme, continues the pathway by catalysing the phosphorylation of shikimate thereby forming shikimate 3-phosphate **7**. The sixth enzyme, 5-enolpyruvyl-shikimate 3-phosphate synthase (EPSPS), catalyses the formation of 5-enolpyruvyl-shikimate 3-phosphate (EPSP) **8** by adding an enolpyruvate moiety to the

hydroxyl on the fifth carbon of shikimate 3-phosphate. Finally, the seventh enzyme of the pathway, chorismate synthase, catalyses the dephosphorylation of EPSP, forming chorismate **9**. To date, only one inhibitor of these enzymes has been developed for commercial use. Glyphosate [*N*-(phosphonomethyl)glycine], which specifically targets EPSPS, is the active ingredient found in Roundup<sup>®</sup>, a product developed as a herbicide by J.E. Franz from Monsanto Corporation in 1971.<sup>5</sup> Of these seven enzymes, DHQS will be the subject of study in this doctoral research.

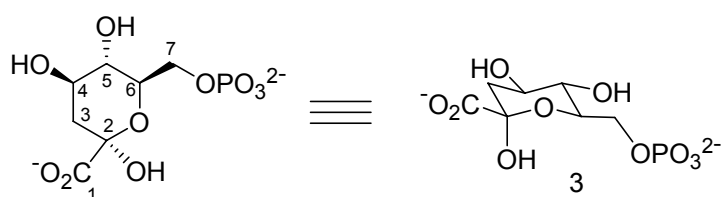
## 1.2 Dehydroquinase synthase (DHQS)

DHQS (EC 4.2.3.4) is monofunctional in most plants and bacteria.<sup>6</sup> However, in microbial eukaryotes DHQS forms the N-terminal domain of the AROM protein complex. The AROM protein complex is a multidomain pentafunctional polypeptide containing enzymes two, three, four, five, and six of the shikimate pathway.<sup>7</sup> DHQS has been an enzyme of much interest due to the complexity and variety of reactions that it catalyses despite its relatively small size.

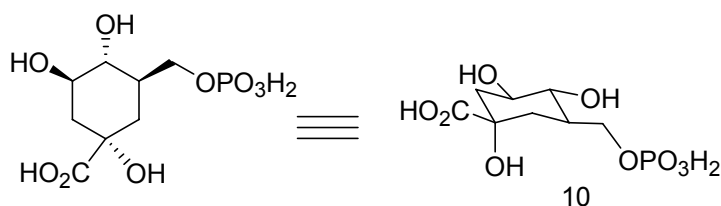
Currently, there are four DHQS crystal structures available in the RCSB protein data bank ([www.rcsb.org/pdb](http://www.rcsb.org/pdb)); these are from *Aspergillus nidulans* (code 1DQS), *Staphylococcus aureus* (code 1XAG), *Thermus thermophilus* (code 1UJN), and *Helicobacter pylori* (code 3CLH), which is pending release.<sup>8-11</sup> A fifth crystal structure of DHQS from *Xanthomonas oryzae pv. oryzae* has been published in Acta Crystallographica but the data are not available in the protein data bank.<sup>12</sup>

### 1.3 Structure and function of DHQS

Using x-ray crystallography, Carpenter and co-workers solved the structure of DHQS from *Aspergillus nidulans* (*An*DHQS); this was accomplished by crystallising the enzyme with nicotinamide adenine dinucleotide ( $\text{NAD}^+$ ), zinc and a high affinity inhibitor (a carbaphosphonate analogue of DAH7P) (see figure 1.2).



3-deoxy-D-*arabino*-heptulosonate 7-phosphate; DAH7P



(1S,3R,4R,5S)-1,3,4-trihydroxy-5-(phosphonomethyl)cyclohexane-1-carboxylic acid;  
Carbaphosphonate

Figure 1.2. Structures of DAH7P and a Carbaphosphonate

The data showed that *An*DHQS is a homodimer composed of two protein chains, each 362 amino acids long (see figure 1.3).<sup>8</sup> In addition to an independent active site for the substrate, each monomer contains one tightly bound divalent metal ion and one molecule of  $\text{NAD}^+$ . Zinc is the divalent metal thought to be present in *An*DHQS *in vivo*; however, cobalt functions better than zinc *in vitro*.<sup>13</sup> The N-terminal end of the amino acid chain forms an  $\alpha/\beta$  domain and the C-terminal end forms an  $\alpha$ -helical domain. The active site lies in a cleft between these two domains. The residues involved in catalysis, substrate binding, and coordination of the metal ion all mainly

reside in the C-terminal domain, whereas the residues that interact with  $\text{NAD}^+$  reside in the N-terminal domain.

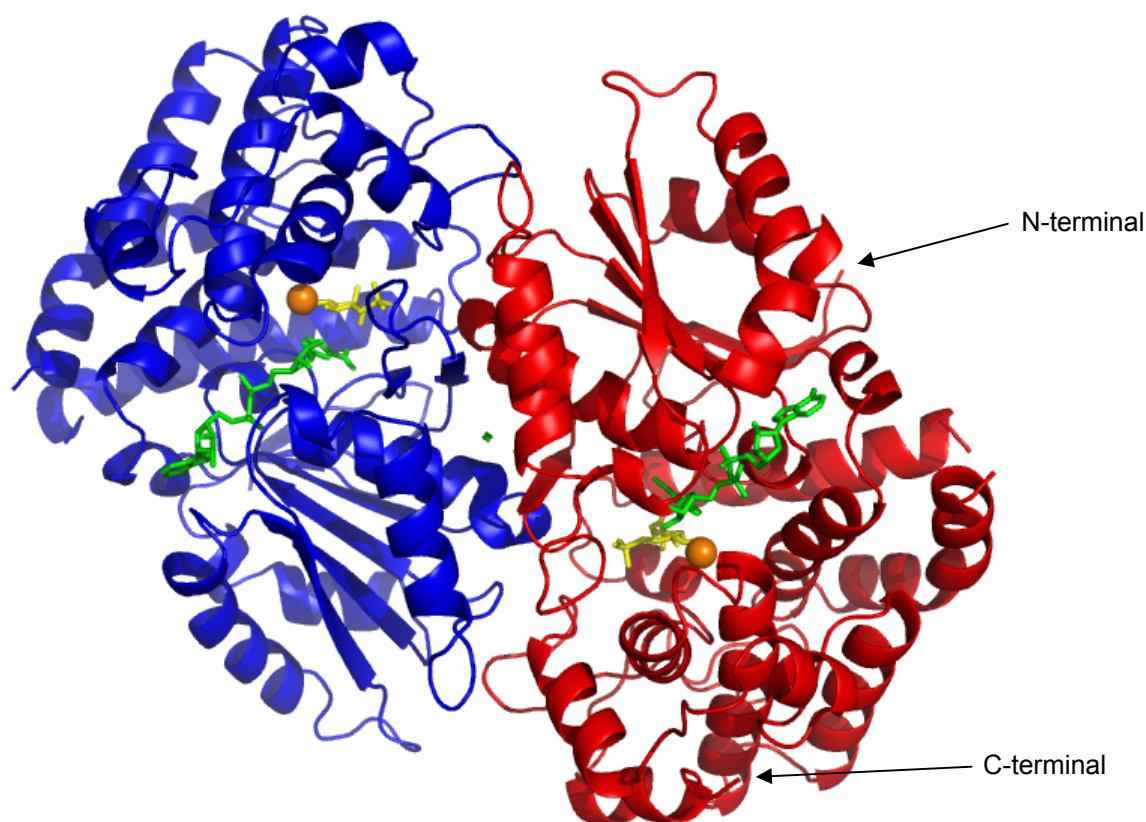


Figure 1.3. Ribbon diagram of the *An*DHQS dimer showing chain A (blue), chain B (red), the inhibitor carbaphosphonate (yellow),  $\text{NAD}^+$  (green), and  $\text{Zn}^{2+}$  (orange).<sup>8</sup>

#### 1.4 Mechanism of DHQS

There are five steps involved in the overall transformation of DAH7P **3** to DHQ **4** (see figure 1.4). The initial step uses  $\text{NAD}^+$  as a co-substrate and involves the oxidation of the hydroxyl on the fifth carbon (C-5) of DAH7P to form a ketone **11**. The second step involves  $\beta$ -elimination of phosphate across carbon six (C-6) and seven (C-7) to yield an enone **12**. The ketone functionality at C-5 from the first step makes the hydrogen on C-6 more acidic, thereby facilitating this E1cb elimination. The third step involves reduction of the ketone at C-5 via NADH (the reduced form of  $\text{NAD}^+$ ),

thereby regenerating the hydroxyl at C-5 and forming an enol pyranose **13**. The fourth step of the mechanism involves opening of the enol pyranose ring, which is initiated by the abstraction of the proton from the hydroxyl on the second carbon (C-2) forming an enolate **14**. This is followed by the fifth and final step involving an intramolecular aldol reaction resulting in ring closure and formation of a carbocycle **4**.

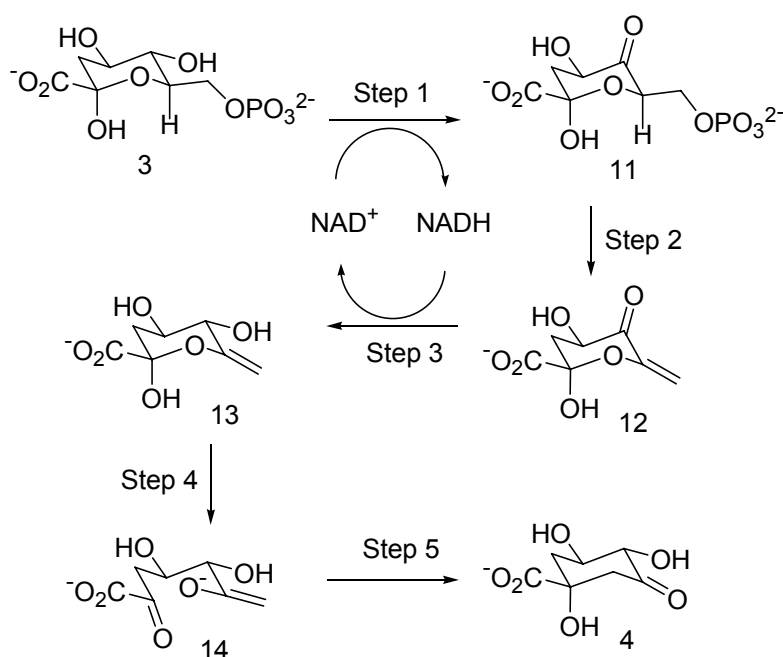


Figure 1.4. Mechanism of DHQS

It has been proposed that the cyclisation step occurs through a chair-like transition state that requires a 180° rotation of the sigma bond between C-5 and C-6 (see figure 1.5). The rotation would allow for the enolate carbon (C-7) to easily attack the electrophilic carbonyl group at C-2, thus forming the carbocycle dehydroquinate.<sup>14-16</sup> This was demonstrated by monitoring the conformation of the product formed from the incubation of a stereospecifically labelled DAH7P analogue with DHQS. Enzymatic catalysis of (7*R*)-[7-<sup>2</sup>H]-DAH7P with DHQS results in the formation of

DHQ exclusively by way of *syn* elimination of phosphate and inversion of configuration at C-7.<sup>17</sup>

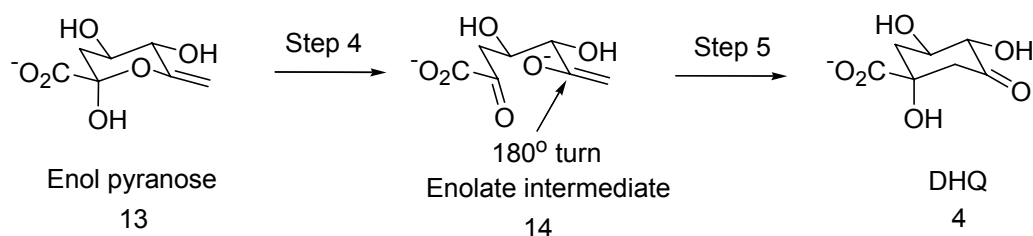


Figure 1.5. Cyclisation step of DHQS

### 1.5 Structural involvement of DHQS in the catalysis of DHQ formation

As noted above, Carpenter and co-workers determined the structure of DHQS and showed the interactions between the amino acids of DHQS and carbaphosphonate,  $\text{NAD}^+$ , and zinc (see figure 1.6).<sup>8</sup> In the first step of the mechanism, oxidation of the C-5 hydroxyl is accomplished by a hydride transfer from C-5 of DAH7P to the fourth carbon of  $\text{NAD}^+$ . This step is initiated by proton loss of the C-5 hydroxyl, which is relayed through a proton-shuffling system involving a water molecule and His275. It is proposed that the zinc ion facilitates the hydride transfer and proton loss by polarising the C-5 hydroxyl. In the second step,  $\beta$ -elimination of phosphate is mediated by the removal of the C-6 proton. It has been proposed that the enzyme could facilitate the loss of phosphate by providing a phosphate-binding pocket that could stabilise the elimination transition state as well as orientate the phosphate oxygens to a position favourable for the removal of the C-6 proton (see section 1.6). The phosphate-binding pocket is formed by Lys152, Asn162, Asn268, His275 and Lys356. The third step of the mechanism involves the reduction of the C-5 ketone back to a hydroxyl using NADH. Enzyme involvement proceeds through a reversal

of the proton-shuffling system shown in step one. The ring-opening or fourth step involves removal of the proton from the C-2 hydroxyl. It is likely that a water molecule removes the proton and the guanidino functionality of Arg260 acts as a base to accept the proton from the water molecule. The final step involves an attack on the C-2 carbonyl carbon by the C-7 enolate carbon. Interactions between the carboxylic acid at C-2 and the functional groups of Lys152, Lys250 and Arg264 restrict rotation of the bond between C-2 and C-3 thereby ensuring that the enolate attacks the *re* face of the ketone to generate the correct stereochemistry of DHQ.<sup>8</sup>

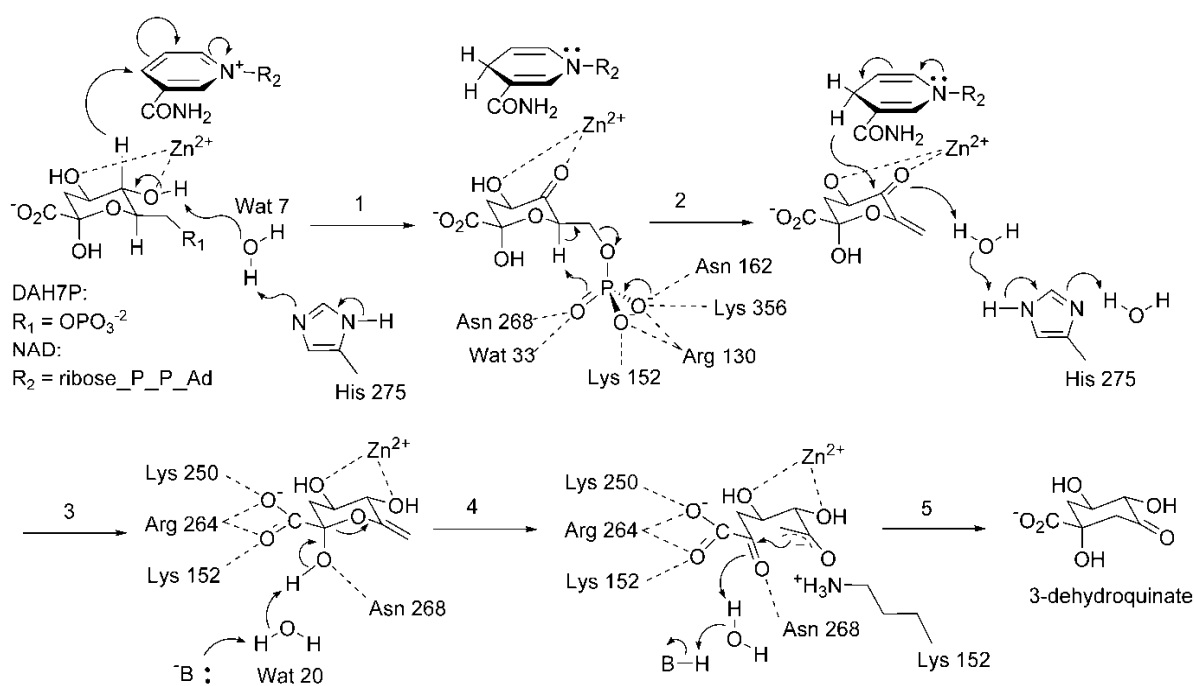


Figure 1.6. Interactions between DAH7P,  $\text{NAD}^+$ , zinc, and DHQS<sup>8</sup>

## 1.6 DHQS from other sources

In addition to *Aspergillus nidulans*, *Staphylococcus aureus*, *Thermus thermophilus*, and *Helicobacter pylori*, other sources of DHQS that have been studied include *Escherichia coli*, *Neurospora crassa*, *Bacillus subtilis*, *Phaseolus mungo*, and *Sorghum bicolor*.<sup>13,18-21</sup> Some of these studies discuss the isolation of DHQS from multifunctional protein complexes, whereas others attempt to explore biophysical and kinetic properties of the enzyme from bacterial, plant, and fungal sources. A comparison between these broader groups show structural similarities such as the N-terminal Rossmann-fold domain and the C-terminal  $\alpha$ -helical domain, and requirements of NAD<sup>+</sup> and a divalent metal for activity. In terms of size, fungal and plant sources of DHQS appear to be larger than bacterial sources.

## 1.7 Studies investigating steps one, two, and three catalysed by DHQS

DHQS has generated much interest primarily because it manages, despite its relatively small size, to catalyse a reaction sequence involving four different types of chemical transformations. Rotenberg and Sprinson postulated that DHQS performs the function of a dehydrogenase, a phospho-lyase, a pyranose ring-opening enzyme, and an aldolase.<sup>15</sup> However, it has been questioned whether DHQS actually carries out all five steps of the mechanism and that perhaps it is merely a dehydrogenase capable of controlling the stereospecificity of the final product.<sup>3</sup> For the purpose of studying the mechanism of DHQS, various research groups have made substrate analogues of DAH7P with structural alterations that would cause the substrate to halt at different

stages of the catalytic pathway. These analogues have allowed for a closer examination of each step in isolation.

To assess the first step in the enzymatic pathway Widlanski and co-workers designed an analogue that was not capable of eliminating phosphate.<sup>17,22</sup> Phosphonate **15** was made so that it contained a phosphonate instead of a phosphate substituent on C-7 thereby stopping catalysis after oxidation by  $\text{NAD}^+$  (see figure 1.7). A second alteration involved the replacement of the pyranose oxygen with carbon. This was done to push the redox equilibrium towards oxidation. DHQS was saturated with phosphonate **15**, and the reaction was assayed by monitoring the formation of enzyme-bound NADH at 340nm via UV spectroscopy. A rise in absorbance at 340nm is consistent with oxidation being the first step in the conversion of DAH7P to DHQ catalysed by DHQS.

To investigate steps two and three of the DHQS-catalyzed reaction, Widlanski and co-workers made a cyclic 2-deoxy substrate analogue **16** and a C-7 deuterium-labelled form of the cyclic 2-deoxy substrate analogue **17**; see figure 1.7.<sup>17,22</sup> The absence of a hydroxyl group at C-2 of the 2-deoxy substrate analogues **16** or **17** prevents the ring from opening, thereby preventing the fourth step from occurring. DHQS was saturated with cyclic 2-deoxy substrate analogue **16** and the product was analysed by NMR. Results confirmed a loss of inorganic phosphate ( $\text{P}_i$ ) and the reduction of the ketone at C-5.

Deuterated 2-deoxy substrate analogue **17** was then used to investigate the stereochemical course of the phosphate elimination by monitoring the position of the deuterium label at C-7 via nuclear Overhauser enhancement (NOE) experiments.

After deuterated 2-deoxy substrate analogue **17** was incubated with the enzyme, the extracted product was converted to the bicyclic lactone **18** in order to flip and lock its conformation. The NOE experiment allowed for the assignment of the deuterium label to the *E* position and confirmed elimination of phosphate with *syn* stereochemistry. Several studies have been done to assess the elimination of phosphate and the role of the enzyme in this step. As suggested by Widlanski and co-workers, the loss of P<sub>i</sub> begins with the initial abstraction of the acidic proton at C-6 followed by the elimination of phosphate via a E1cB process.<sup>17,22</sup>

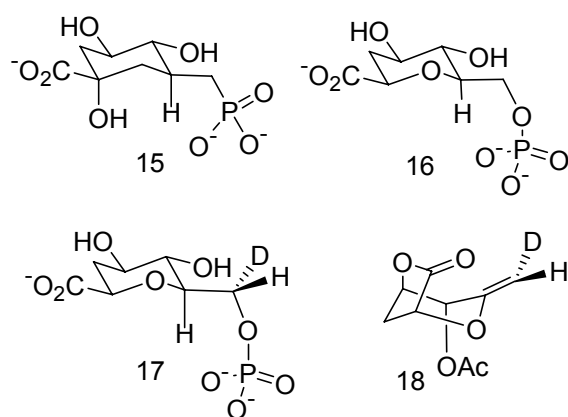


Figure 1.7. Modified substrate analogues of DAH7P

Widlanski and co-workers, demonstrated that one of the oxygens on the phosphate serves as the base responsible for removing the proton at C-6.<sup>23</sup> With the use of *E*-vinyl and *Z*-vinyl homophosphonates (**19** and **20** respectively) it was shown that removal of the C-6 proton could only occur when the phosphate group was closest to the proton, that being with *Z*-vinyl homophosphonate (see figure 1.8). This fits in well with the crystal-complex structure of DHQS, which shows that the phosphate is held via contact with the enzyme in such a conformation so that the phosphate oxygens are directed towards the C-6 proton thereby facilitating proton removal.

Results from the work by Montchamp and co-workers reinforce that DAH7P **3** mediates its own  $P_i$  loss with no apparent assistance from the enzyme.<sup>24</sup> An analogue of DAH7P containing inverse stereochemical configuration at C-6, carbacycle **21**, had no effect on the elimination of phosphate (see Figure 1.8). Had the enzyme favoured a specific configuration at C-6, inversion of configuration at this site would have affected the progress of the elimination. These studies suggest that the enzyme does not play a significant catalytic role in the formation of the enone during step two and that the phosphate-binding pocket could be a region of stereochemical tolerance. The results do not rule out the function of the enzyme in influencing the stereochemistry during the elimination of phosphate.

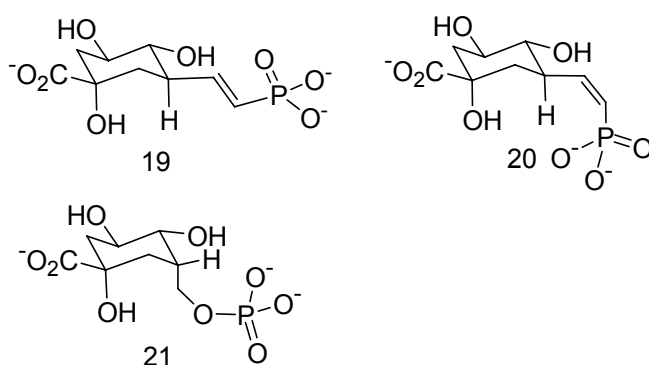


Figure 1.8. Carbacycle substrate analogues of DAH7P

## 1.8 Studies investigating steps four and five of the DHQS reaction mechanism

Although steps four and five have been well studied, there still remain questions regarding the mechanism and enzyme involvement with these last two steps. In this section studies that have investigated steps four and five of the DHQS reaction mechanism are discussed.

Based on the overall stereochemical course of the on-enzyme reaction, the formation of DHQ **4** involves cyclisation of an enolate intermediate with inversion of configuration at C-7 of DAH7P. This was confirmed using  $^3\text{H}$  labelled DAH7P at C-7. Incubation of this substrate with DHQS showed retention of the  $^3\text{H}$  label through to DHQ. Rotenberg and Sprinson showed that the *pro-R* hydrogen at C-7 of DAH7P becomes the *pro-R* hydrogen at C-6 of DHQ.<sup>14,15</sup> Widlanski and co-workers suggested that, given the *syn* elimination of the phosphate, the only possible transition state that satisfies the stereochemical requirement for the subsequent aldol reaction is that of a chairlike geometry. This is based on the least reorganisation required of the molecular geometry of the enol pyranose whereby the aldol reaction can be achieved by a simple  $180^\circ$  rotation about C-5 and C-6, hence, allowing the C-7 enolate to attack the C-2 carbonyl to form DHQ **4**.<sup>22</sup>

Bartlett and Satake, by non-enzymatic generation of an enolate intermediate, have shown that the enol pyranose ring opening and intramolecular aldol reaction steps can occur spontaneously to form DHQ **4** without the assistance of the enzyme.<sup>25</sup> The non-

enzymatic generation of DHQ **4** brings into question the extent to which DHQS plays a role in the last two steps of the mechanism.

In order to study steps 4 and 5, a modified version of the enol pyranose was made containing a photo-labile *o*-nitrobenzyl protecting group at C-2 and a deuterium label at C-7 (see nitrobenzyl enol pyranose analogue **22**, figure 1.9). Nitrobenzyl enol pyranose analogue **22** was placed in a neutral buffered aqueous solution and exposed to light, thus resulting in the removal of the *o*-nitrobenzyl protecting group. NMR analysis demonstrated a rapid rearrangement of nitrobenzyl enol pyranose analogue **22** to give DHQ **4**. Although the enol pyranose and open-ring intermediate were observed at  $-78^{\circ}\text{C}$ , their presence was short-lived, emphasising the rapid conversion of the enol pyranose to DHQ **4**. Monitoring of the deuterium label at C-7 of nitrobenzyl enol pyranose analogue **22** showed that only the (2*R*)-[2- $^2\text{H}$ ]-DHQ isomer **23** was formed (see figure 1.9). These data are consistent with the ring closure step occurring through a chair-like configuration, with the same overall stereochemistry outcome as is seen with the enzyme-catalysed formation of DHQ **4**.<sup>16</sup> As a result, Bartlett and Satake suggested that perhaps the enzyme only performs the first three steps of the mechanism, followed by the release of the enol pyranose with no further involvement in the catalysis of DHQ **4** after the third step, thereby making DHQS simply a dehydrogenase.

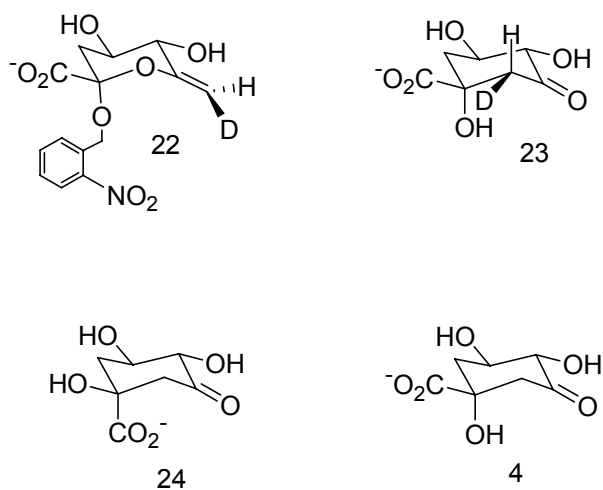


Figure 1.9. Modified substrate analogue of DAH7P, (2R)-[2-<sup>2</sup>H]-DHQ, 1-*epi*-DHQ, and DHQ

It was later found by Bartlett and co-workers that when nitrobenzyl enol pyranose analogue **22** was allowed to cyclise off the enzyme 2.5-4% of 1-*epi*-DHQ **24** was formed in addition to DHQ **4** (see figure 1.9).<sup>26</sup> 1-*epi*-DHQ **24** arises by addition of the enolate onto the *si* face of the C-2 carbonyl whereas DHQ **4** arises by addition of the enolate onto the *re* face of the C-2 carbonyl. It is important to stress here that no epimer has ever been observed in the enzyme-catalysed formation of DHQ **4**; this supports that the enolate intermediate is not released from the enzyme active site prior to formation of DHQ **4**. Furthermore it suggests that the enzyme is responsible for ensuring the overall stereospecificity of the reaction by controlling the configuration of the transition state so as to form only one isomer of DHQ **4**.

This is consistent with the crystal structure findings that indicate enzyme-substrate interactions between the carboxylic acid at C-2 of DAH7P **3** and three protein residues containing amine functional groups which would prevent rotation about the C-2 and C-3  $\sigma$  bond.<sup>8</sup>

### 1.9 Further studies involving the role of the enzyme during ring closure

Parker and co-workers investigated the effects of two fluorinated analogues of DAH7P on the reaction catalysed by *E. coli* DHQS.<sup>27</sup> One analogue contained a fluorine in the equatorial position at C-3 of DAH7P [(3*R*)-3-fluoro-DAH7P **25**] and the other analogue contained a fluorine in the axial position at C-3 of DAH7P [(3*S*)-3-fluoro-DAH7P **28**]. Incubation of (3*R*)-3-fluoro-DAH7P **25** with DHQS proceeded to (6*R*)-6-fluoro-dehydroquininate **27** as the sole product (see figure 1.10). These results were no different to that of the enzymatic catalysis of DAH7P **3** to DHQ **4**.

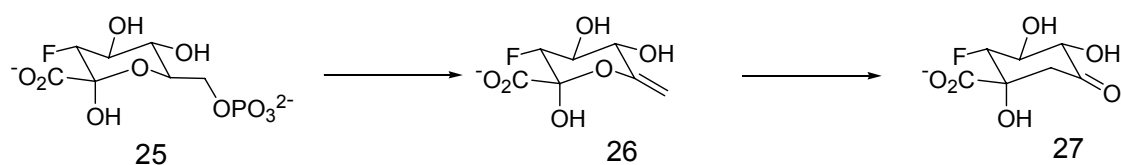


Figure 1.10. Formation of (6*R*)-6-fluoro-dehydroquininate from (3*R*)-3-fluoro-DAH7P in the presence of *E. coli* DHQS

Contrary to what was seen with (3*R*)-3-fluoro-DAH7P **25**, incubation of (3*S*)-3-fluoro-DAH7P **28** in the presence of *E. coli* DHQS produced (6*S*)-6-fluoro-dehydroquininate **30** and (6*S*)-1-*epi*-6-fluoro-dehydroquininate **31** in a percent ratio of 66% and 33% respectively (see figure 1.11). This outcome closely resembled that seen in the non-enzymatic conversion of the modified enol pyranose **22** to 1-*epi*-DHQ **24** and DHQ **4**.

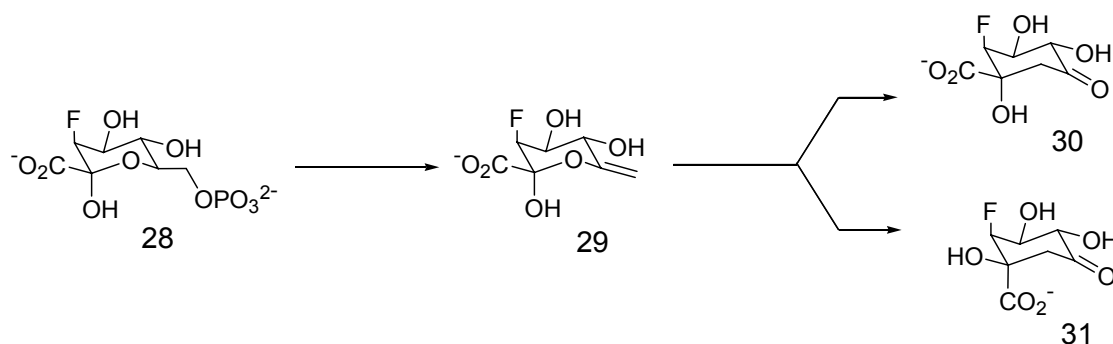


Figure 1.11. Formation of (6*S*)-1-*epi*-6-fluoro-dehydroquinone and (6*S*)-6-fluoro-dehydroquinone from (3*S*)-3-fluoro-DAH7P in the presence of *E. coli* DHQS

Although these results showed that the presence of a fluorine in (3*S*)-3-fluoro-DAH7P **28** leads to the formation of an epimeric product, it is unlikely that the formation of (6*S*)-1-*epi*-6-fluorodehydroquinone **31** occurred on the enzyme. This is consistent with the absence of epimer formation during the enzyme-catalysed formation of DHQ **4** from DAH7P **3**. It is, however, likely that at least some of the (3*S*)-3-fluoro-enol pyranose **29** dissociates from the enzyme and subsequently undergoes ring opening and carbocycle formation in solution, without control of the enzyme, to form the epimeric product or a mixture of (6*S*)-6-fluorodehydroquinone **30** and (6*S*)-1-*epi*-6-fluorodehydroquinone **31**.

The dissociation of the (3*S*)-3-fluoro-enol pyranose **29** from *E. coli* DHQS is likely due to an electronic effect from the fluorine. A comparison of reaction rates between DAH7P, (3*S*)-3-fluoro-DAH7P **28**, and (3*R*)-3-fluoro-DAH7P **25**, showed that (3*S*)-3-fluoro-DAH7P **28** reacted 200 times slower than DAH7P **3** and 100 times slower than (3*R*)-3-fluoro-DAH7P **25** with *E. coli* DHQS. (3*R*)-3-Fluoro-DAH7P **25** reacted at half the rate of DAH7P **3**. These results could suggest that the fluorine at C-3 of DAH7P may stabilise the fluoro-enol pyranose (**29** or **26**), increasing its life time.<sup>28</sup> This more stable fluoro enol pyranose could then be released from the enzyme whereupon cyclisation occurs in solution without the stereochemical constraints imposed by the enzyme.

With regard to (3*R*)-3-fluoro-DAH7P **25**, the data do not tell us if (6*R*)-6-fluoro-dehydroquinone **27** was formed on or off the enzyme just as it is not known for certain

if the 66% of (6*S*)-6-fluoro-dehydroquinone **30** from (3*S*)-3-fluoro-DAH7P **28** was formed on the enzyme or off. It is possible that the *E. coli* DHQS is capable of tolerating the fluoro substituent in the equatorial position at C-3 of DAH7P and the forward reaction is not slowed as much as seen with (3*S*)-3-fluoro-DAH7P **28**. On the other hand, it is also possible that the (3*R*)-3-fluoro-enol pyranose **26** dissociates from the enzyme but the favoured solution transition state leads exclusively to (6*R*)-6-fluoro-dehydroquinone **27**.

Parker and co-workers raised another issue pertaining to the chemical influence of fluorine during the ring opening and cyclisation steps. The geometry of the fluorine group at C-3 of fluoro-DAH7P, depending whether it is axial or equatorial, could have a significant influence on the transition states of the internal aldol reaction. For example, the predicted chair-like transition state for the enzyme-catalysed aldol reaction involving (3*R*)-3-fluoro-DAH7P **25** has the fluoro substituent on C-3 pointing away from the direction of attack of the enolate nucleophile; this predicted transition state would be favoured based on the Felkin-Anh model because the fluorine is orthogonal to the carbonyl at C-2 (see figure 1.12, A).<sup>29</sup> On the other hand, the predicted transition state for the enzyme-catalysed reaction involving (3*S*)-3-fluoro-DAH7P **28** has the fluoro substituent on C-3 pointing towards the direction of attack of the nucleophile; this predicted transition state would not be favoured based on the Felkin-Anh model because the fluorine is not orthogonal to the carbonyl at C-2 (see figure 1.12, B). Therefore, ring opening and carbocycle formation involving (3*S*)-3-fluoro-DAH7P **28** is not favoured unless there is a conformational change in the ring.

One possible configuration involves a ring flip, use of the other face of the enolate, and rotation about C2 and C3 resulting in attack of the *si* face of the C-2 carbonyl resulting in the formation of the epimeric product (see figure 1.12, C). It is likely that this conformational change would require release of the (3*S*)-3-fluoro-enol pyranose **29** from the enzyme. Therefore, the combination of an electronic effect from fluorine causing the stabilisation of the (3*S*)-3-fluoro-enol pyranose **29** and an unfavourable transition state for the internal aldol reaction may explain the release of the (3*S*)-3-fluoro-enol pyranose from the enzyme.

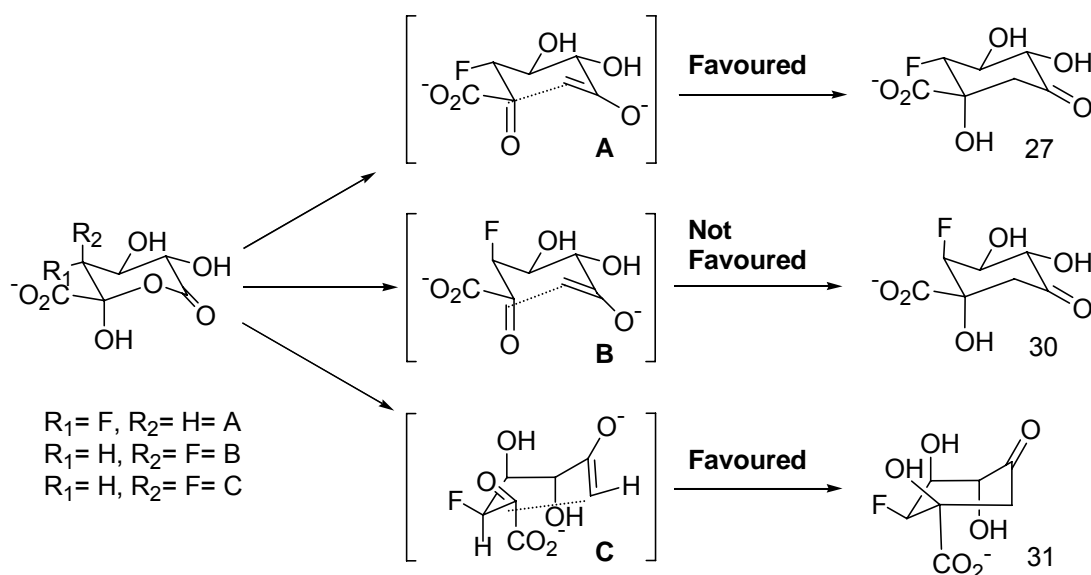


Figure 1.12. Proposed transition-state conformations of the fluoro enolate intermediates during cyclisation.

Once the fluoro-enol pyranose is off the enzyme it is essentially free from the conformational and configurational constraints of the enzyme. The (3*R*)-3-fluoro-enolate intermediate from (3*R*)-3-fluoro-DAH7P **25** can form (6*R*)-6-fluoro-DHQ **27** through a chair conformation which would be favourable by a Felkin-Anh model. Similarly, the (3*S*)-3-fluoro-enolate intermediate from (3*S*)-3-fluoro-DAH7P **28** can

form 1-*epi*-(6*S*)-6-fluoro-DHQ **31** through an alternative chair conformation which would be favourable by a Felkin-Anh model using the other face of the enolate.

Although *E. coli* DHQS has the ability to exert stereochemical control during ring closure, this study demonstrates how easily this control can be disrupted. Furthermore, this study raises questions with regard to the extent of dissociate dissociation of the enol pyranose from the enzyme and the implications this has on the role of the enzyme during the cyclisation step.

### **1.10 Purpose of the study**

Despite the numerous investigations into this mechanism of DHQS, two areas of interest have arisen out of this review and each area forms an objective of the study. The first area deals with the role of the enzyme during the cyclisation step of DHQS in the presence of fluorinated analogues of DAH7P. The objectives here are to: 1) determine the extent to which the stereochemical control of DHQS can be disrupted across different sources of DHQS; 2) determine if either of the enol pyranoses with fluorine in the axial or equatorial position fully dissociates from the enzyme; 3) investigate the effect of fluorine on the acyclic form of the enol pyranose in order to determine whether the formation of the epimeric product arises from a stereoelectronic effect.

The second area deals with the tolerance of DHQS for substituents in the axial or equatorial C-3 position of DAH7P. The objective here is to replace the fluoro group on DAH7P with the bulkier hydroxyl group and monitor the effects on the DHQS-catalysed reaction.

It is, therefore, the aim of this project to examine closely the biosynthetic mechanism of DHQS using the combination of chemical and biological techniques. Modified versions of DAH7P and a proposed intermediate of the reaction will be produced and examined as potential substrates for both the enzyme-catalysed and nonenzyme-catalysed cyclisation steps.

## 1.11 Thesis objectives

- To investigate the effects 3-fluoro substituted analogues of DAH7P on enzyme-catalysis of DHQS by:
  - comparing similarities and differences in behaviour across three sources of DHQS;
  - determine whether (3*S*)-3-fluoro-DAH7P and (3*R*)-3-fluoro-DAH7P cyclise on or off the enzyme;
  - determine the structural and kinetic differences between *Escherichia coli* DHQS, Kiwifruit DHQS and *Pyrococcus furiosus* DHQS.
- To investigate the bulk tolerance at C-3 of DAH7P by:
  - synthesising modified analogues of DAH7P containing a hydroxyl group at C-3;
  - monitoring the kinetic effects of these C-3 hydroxyl analogues on DHQS.

## **2. Expression and purification of DHQS and DHQase from *Escherichia coli* and *Pyrococcus furiosus*. Characterisation of DHQS from *Escherichia coli*, *Pyrococcus furiosus*, and Kiwifruit**

### **2.1 Introduction**

In order to study the enzymatic reactions in detail, sufficient quantities of purified enzyme were required. In this chapter the expression, purification, and characterisation of DHQS and DHQase (EC 4.2.1.10) from *E. coli* and *Pyrococcus furiosus* is discussed. Although DHQase was not the primary focus of this study, it was required for the coupled assay of DHQS activity. Purified Kiwifruit DHQS was provided by HortResearch (Auckland). The characterisation and activity of Kiwifruit DHQS are discussed in this chapter.

Initial attempts to purify *E. coli* DHQS following the published method were unsuccessful.<sup>30</sup> A modified protocol for the purification of *E. coli* DHQS is herein reported. In addition, new procedures for the purification of DHQase from both *E. coli* and *P. furiosus* are described. The purification of DHQS from *P. furiosus* closely resembles the procedure for the purification of DAH7PS from *P. furiosus*, as described by Schofield and co-workers.<sup>31</sup>

### **2.2 Expression of *E. coli* DHQS**

*E. coli* RB791 cells, transformed with the plasmid encoding the *E. coli* DHQS gene, were obtained from Prof. John R. Coggins (University of Glasgow). The expression and purification method described by Frost and co-workers was followed.<sup>30</sup> RB791

(pJB14) cells were grown overnight at 37°C in tubes containing Luria Bertani (LB) media supplemented with ampicillin and used to inoculate a larger flask. The culture in the larger flask was monitored by recording the optical density at 600 nm (OD<sub>600</sub>), and protein synthesis was induced with IPTG when the OD<sub>600</sub> reached ~0.6. The cells were harvested by centrifugation six hours after induction, and the cell pellets stored at -80°C until required. To obtain crude lysate, the harvested cells were thawed, resuspended in potassium phosphate buffer, and broken open by French press. To assess for soluble and insoluble protein, the crude lysate was centrifuged and the supernatant (soluble protein) removed. The remaining pellet (insoluble protein) was resuspended in a 1:1 mixture of 6 M urea and 20% SDS.

### 2.2.1 SDS-PAGE analysis of protein fractions from lysed cells

Fractions from crude lysate, soluble protein, and insoluble protein were analysed by gel electrophoresis (see figure 2.1).

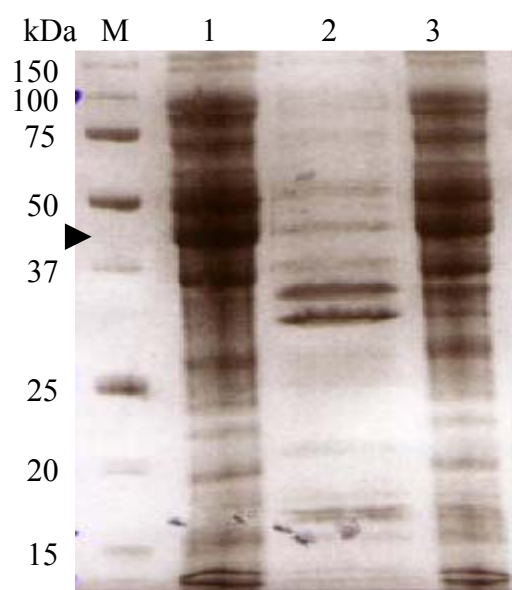


Figure 2.1. SDS-PAGE of crude *E. coli* DHQS. Markers (Lane M); crude lysate (Lane 1); insoluble protein (Lane 2); soluble protein (Lane 3). Arrow is pointing to the band of recombinant DHQS.

The published molecular weight of DHQS from *E. coli* (strain MM294) was calculated from the amino acid sequence at 40 kDa.<sup>30</sup> Examination of the gel shown in figure 9 showed a dark band between the 37 and 50 kDa region of soluble protein. A faint band is visible in the same region of insoluble protein which could be due to insoluble protein or incomplete cell lysis. This data suggests that most of the overexpressed DHQS protein is soluble.

### 2.2.2 Enzyme activity

To assess the activity of DHQS, a coupled enzyme continuous assay was performed using UV spectroscopy to monitor the reaction. Since neither the substrate (DAH7P) nor the product (DHQ) of DHQS is UV detectable, a second enzyme DHQase is coupled with DHQS in order to generate dehydroshikimate which can be detected spectrophotometrically at 234 nm ( $\epsilon = 1.2 \times 10^4 \text{ M}^{-1} \text{ cm}^{-1}$ ). When DHQase is used in excess in the presence of DHQS, it serves as a quantitative measure for the activity of DHQS.

DHQS from the crude lysate of induced cells was assayed to determine if the enzyme was active. The absorbance at 234 nm was observed to increase with time indicating that DHQS was active (see figure 2.2).

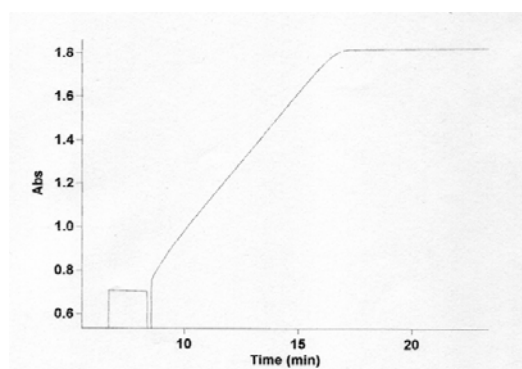


Figure 2.2. Enzyme activity of the crude lysate from induced cells.

A crude lysate fraction prepared from uninduced cells (no IPTG) was also assayed. A minor increase in absorbance was observed which could be attributed either to leaky expression of the plasmid (~10% activity) or to background activity (see figure 2.3). These results confirmed that the recombinant protein from cells induced with IPTG was active.

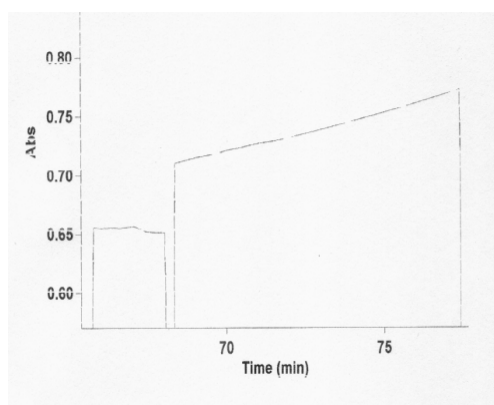


Figure 2.3. Enzyme activity of the crude lysate from uninduced cells.

### 2.3 Purification of *E. coli* DHQS

The initial purification protocol involved low-pressure liquid chromatography on a hydroxylapatite column followed by anion exchange via a Source Q column and final purification on a size-exclusion column.

A sample of soluble protein was filtered, diluted, and loaded onto the hydroxyapatite column. A linear gradient from low to high phosphate buffer concentration was applied to remove protein from the column. SDS-PAGE analysis showed that all of the soluble protein passed through the column during loading. Furthermore, only small amounts of protein with masses ranging between 50 to 100 kDa interacted with the column. Attempts to regenerate the column, decrease the slope of the linear gradient, and dilute the soluble protein a further three-fold did not improve the

chromatography. In order to circumvent this drawback, the published purification protocol was adjusted so that the first purification step involving hydroxyapatite was replaced with an ammonium sulfate (AS) precipitation.

The soluble crude protein was subjected to ammonium sulfate precipitation at 4°C. Four cut-off fractions were collected; 0-30%, 30-50%, 50-70%, and 70-100%. A small amount of each fraction was resuspended and checked for activity. Fraction 30-50% was the only fraction that showed significant activity for DHQS. The AS fractionation step was later refined so that the fraction collected was between 35-55%. The AS protein fraction containing DHQS was then resuspended and loaded on to a size-exclusion column to remove the excess ammonium sulfate. The desalted protein fractions were pooled, concentrated, diluted with loading buffer, and loaded onto an anion-exchange column (Source Q™). The protein eluted with 110 mM NaCl. Fractions that showed DHQS activity were examined by SDS-PAGE. Clean fractions were spiked with NAD<sup>+</sup> and CoCl<sub>2</sub>, pooled, and concentrated. Results showed that the activity of the enzyme improved after each purification step (see table 1).

Table 1.

Purification of DHQS from *E. coli*

Step	Total protein (mg)	Specific activity (U mg <sup>-1</sup> )	Yield (%)	Purity
Total crude	240	3	100	1.0
Soluble crude	217	4	90	1.4
AS cut 35-55%	49	10	21	3.3
Desalted	42	11	17	3.4
Anion exchange	26	14	11	4.4

The concentrated protein obtained from anion-exchange chromatography was then filtered and loaded onto a size-exclusion column for the final purification step. Active fractions were pooled, concentrated, divided into 0.5 mL aliquots, and stored at  $-80^{\circ}\text{C}$ . SDS-PAGE of each step shows the gradual purification of *E. coli* DHQS (see figure 2.4).

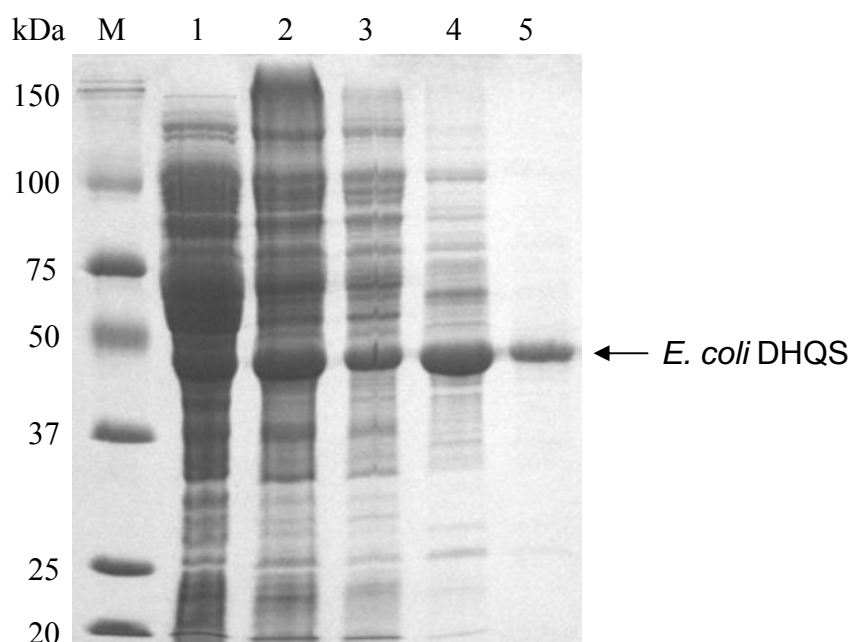


Figure 2.4. SDS-PAGE of the purification of *E. coli* DHQS. Markers (Lane M); soluble protein (Lane 1); AS cut 35-55% (Lane 2); AS cut 35-55%/ desalted (Lane 3); Source Q (Lane 4); size-exclusion chromatography (Lane 5).

## 2.4 Expression of *P. furiosus* DHQS

*E. coli* BL21(DE3) Rosetta cells, transformed with the plasmid pT7-7 containing the *P. furiosus* DHQS gene, were grown overnight at  $37^{\circ}\text{C}$  in tubes containing LB media supplemented with ampicillin and chloramphenicol. These cells were used to inoculate a larger flask. When the  $\text{OD}_{600}$  reached  $\sim 0.6$  the culture was induced with IPTG. The cells were harvested by centrifugation thirteen hours after induction and the pellets stored at  $-80^{\circ}\text{C}$  until required.

## 2.5 *P. furiosus* DHQS purification trials

In order to purify *P. furiosus* DHQS efficiently, advantage was taken of the thermostability of *P. furiosus* DHQS. The rationale was to heat-denature most of the host protein while retaining the thermally stable DHQS. The protocol involved cell disruption by sonication at 30°C, followed by a heat treatment for 20 minutes at 70°C. The remaining soluble protein was then purified either by size-exclusion or by anion-exchange chromatography.<sup>31</sup>

Initial attempts to obtain soluble protein were unsuccessful. Cells were resuspended in 50 mM bis-tris-propane buffer containing 2 mM DTT, 0.25 mM CoCl<sub>2</sub>, 0.5 mM NAD<sup>+</sup>, pH 6.5 buffer and sonicated at 30°C. The crude lysate was then heat-treated and cooled. After centrifugation the supernatant (soluble heat-treated protein) was removed and the remaining pellet (insoluble heat-treated protein) was resuspended. Gel electrophoresis showed that most of the DHQS protein was insoluble prior to the heat-treatment step, suggesting that the enzyme had possibly misfolded during expression or had precipitated during lysis (see figure 2.5). The calculated molecular weight of *P. furiosus* DHQS based on the published amino-acid sequence was 37,397 Da.<sup>32</sup> The mass of the protein based on gel electrophoresis was greater than the expected molecular weight.

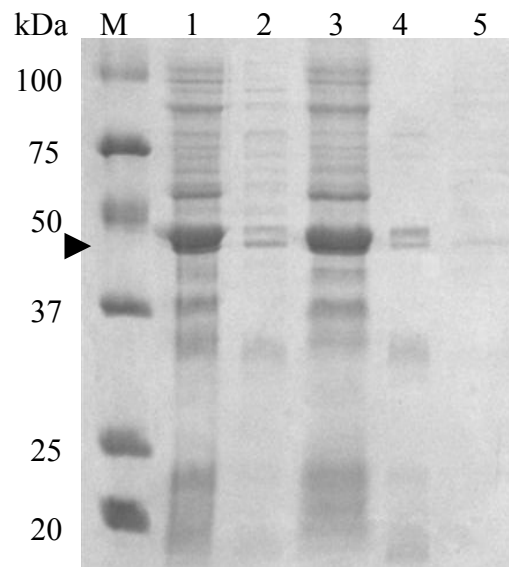


Figure 2.5. SDS-PAGE of *P. furiosus* DHQS original lysis conditions. Markers (Lane M); crude lysate (Lane 1); soluble protein (Lane 2); insoluble protein (Lane 3); soluble heat-treated protein (Lane 4); insoluble heat-treated protein (Lane 5). Arrow is pointing to the band of recombinant DHQS.

To address possible misfolding during expression, various modifications were done to the growing conditions. These included reducing the growth temperature to 25°C, and reducing the expression temperature to 25°C. None of these modifications resulted in significant improvements in protein solubility.

## 2.6 Expression of *P. furiosus* DHQS using Rosetta-gami B™ cells

It was decided to use Rosetta-gami B™ cells in an attempt to facilitate protein folding during expression. The pT7-7 plasmid was isolated and used to clone Rosetta-gami B cells™. A sample of pT7-7 plasmid treated with BamH1 restriction enzyme was loaded on Agarose gel and checked (see figure 2.6). The open pT7-7 plasmid was determined to be ~3.8 to 4 kb in length.

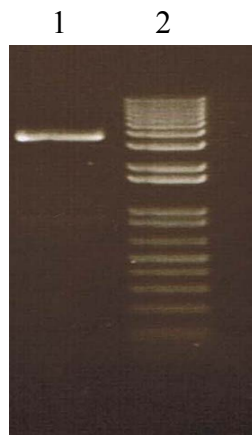


Figure 2.6. Agarose gel of pT7-7 plasmid. Open pT7-7 plasmid (Lane 1); DNA ladder (Lane 2).

Rosetta-gami B<sup>TM</sup> cells, transformed with the plasmid pT7-7 containing the *P. furiosus* DHQS gene, were grown overnight at 37°C in tubes containing LB media supplemented with ampicillin, chloramphenicol, and kanamycin. These cells were then used to inoculate a larger flask. When the OD<sub>600</sub> reached 0.5, the culture was induced with IPTG, allowed to shake overnight, and the cells were harvested by centrifugation. Cell pellets were then resuspended in lysis buffer, ruptured by sonication, and heat treated. Again there was no significant improvement in the solubility of the protein (see figure 2.7).

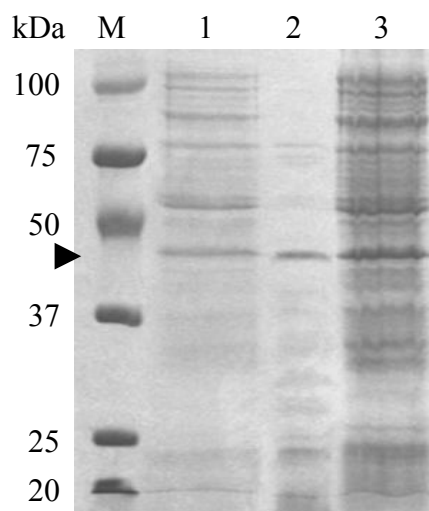


Figure 2.7. SDS-PAGE of *P. furiosus* DHQS from Rosetta-gami B. Markers (Lane M); total crude (Lane 1); soluble heat-treated (Lane 2); insoluble heat-treated (Lane 3). Arrow is pointing to the band of recombinant DHQS.

Another attempt was made using the same growth conditions except that this time the induction time was reduced to just 5 hours. It was thought that the expression of the *P. furiosus* DHQS may be toxic to the Rosetta-gami B™ cells. Thus, by reducing the expression time, despite less protein being produced, most of the expressed protein might remain in the cell where it could fold properly. As before, there was no significant improvement in solubility. Furthermore, there was an overall decrease in the amount of protein overexpressed (see figure 2.8).

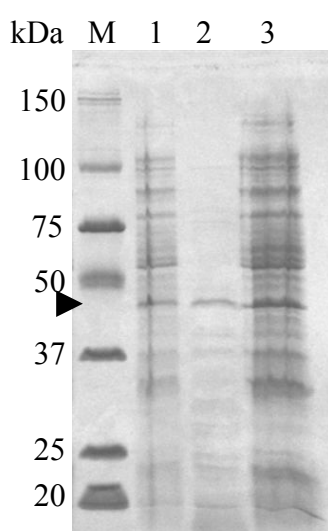


Figure 2.8. SDS-PAGE of *P. furiosus* DHQS from Rosetta-gami B post 5 hours induction (Lysis bufer: 50 mM BTP, 2 mM DTT, 200mM KCl, and 0.5 mM NAD<sup>+</sup>). Markers (Lane M); total crude (Lane 1); soluble heat-treated (Lane 2); insoluble heat-treated (Lane 3). Arrow is pointing to the band of recombinant DHQS.

A beneficial feature of Rosetta-gami B™ cells is that expression can be fine tuned by adjusting the concentration of IPTG.<sup>33</sup> Two lots of cells were grown using the conditions previously described except that each lot was induced with varying amounts of IPTG (100  $\mu$ M and 10  $\mu$ M respectively). SDS-PAGE results did not show any improvement in the production of soluble protein.

## 2.7 *P. furiosus* DHQS lysis trials

Given that there was no noticeable improvement using Rossetta-gami B™ cells, attention was redirected back to Rossetta cells and focus was placed on the lysis conditions and lysis buffer. An attempt was made to open the cells using lysozyme and osmotic shock. A new buffer was prepared containing 50 mM bis-tris-propane, 1% streptomycin, 2 mM DTT, 0.5 mM NAD<sup>+</sup>, 100 mM KCl, pH 6.5 buffer. Streptomycin was introduced into the buffer in order to precipitate out DNA. It was not used in previous buffers because sonication was the method used for lysis which subsequently breaks down DNA. Cell pellets were treated with 1 M sucrose, dispersed with gentle vortexing, and placed on ice. After centrifugation, cell pellets were resuspended in the new lysis buffer, treated with lysozyme for 1 hour, spun down and the supernatant containing soluble crude protein was collected. Unfortunately, it appeared that this method was unsuccessful in rupturing the cells as there was no visible protein band for the enzyme when assayed on gel electrophoresis.

Another attempt involved the use of the French press for cell lysis. Unfortunately, the lysis using the French press did not show significant improvements in protein solubility either (see figure 2.9).

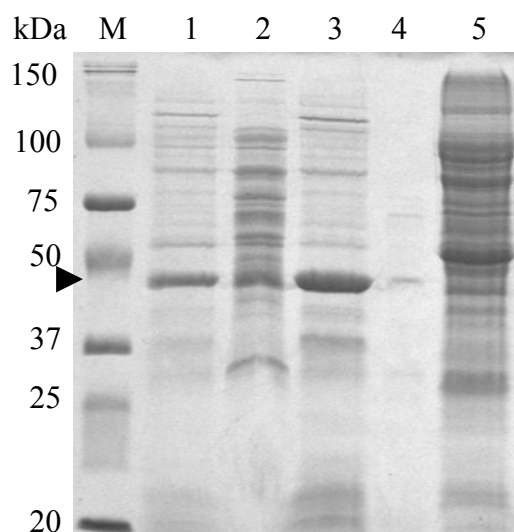


Figure 2.9. SDS-PAGE of *P. furiosus* DHQS from French press lysis Markers (Lane M); total crude (Lane 1); soluble crude (Lane 2); insoluble crude (Lane 3); soluble heat-treated (Lane 4); insoluble heat-treated (Lane 5). Arrow is pointing to band of recombinant DHQS. Arrow is pointing to the band of recombinant DHQS.

## 2.8 Final purification of *P. furiosus* DHQS

Finally it was decided to try lysing the cells using the original method. This involved sonication using 50 mM bis-tris-propane, 2 mM DTT, 0.5 mM  $\text{NAD}^+$ , 200 mM KCl, pH 6.5 as the lysis buffer. While a significant proportion of DHQS remained insoluble, the use of a higher concentration of salt proved to be the best method to prevent formation of insoluble protein (see figure 2.10).

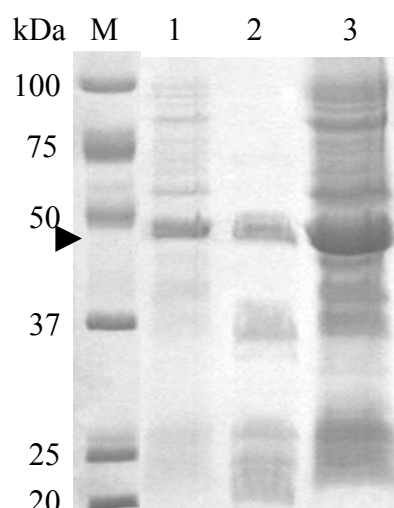


Figure 2.10. SDS-PAGE of *P. furiosus* DHQS final lysis conditions (Lysis buffer: 50 mM BTP, 2 mM DTT, 1 mM EDTA, and 200mM KCl, pH 6.5). Markers (Lane M); total crude (Lane 1); soluble heat-treated (Lane 2); insoluble heat-treated (Lane 3). Arrow is pointing to the band of recombinant DHQS.

The soluble heat-treated protein was then purified on an anion exchange column, eluting at 90 mM NaCl. Fractions that showed DHQS activity were analysed by SDS-PAGE. Clean fractions were spiked with  $\text{NAD}^+$ , pooled, and concentrated. Results showed that the specific activity of the enzyme improved after each purification step (see table 2).

Table 2.

Purification of DHQS from *P. furiosus*

Step	Total protein (mg)	Specific activity (U $\text{mg}^{-1}$ )	Yield (%)	Purity
Total crude	46	0.2	100	1
Heat treated	6.7	1.9	72	11
Anion exchange	3.2	3.2	59	19

## 2.9 Expression and purification of *E. coli* DHQase

*E. coli* AB2848/pKD201 cells, transformed with the plasmid pJKK12 which contains an inserted *E. coli* DHQase gene, were grown overnight in tubes containing LB media supplemented with ampicillin. These cells were then used to inoculate a larger flask. When the OD<sub>600</sub> reached ~0.5 the culture was induced with IPTG. The cells were harvested by centrifugation eight hours after induction and the pellets stored at -80°C until required. To obtain crude lysate, the harvested cells were thawed, resuspended in lysis buffer, and broken open by sonication. The soluble protein was filtered, loaded onto an anion exchange column, and eluted with 200 mM NaCl. Fractions were assayed for activity and analysed by SDS-PAGE (see figure 2.11).

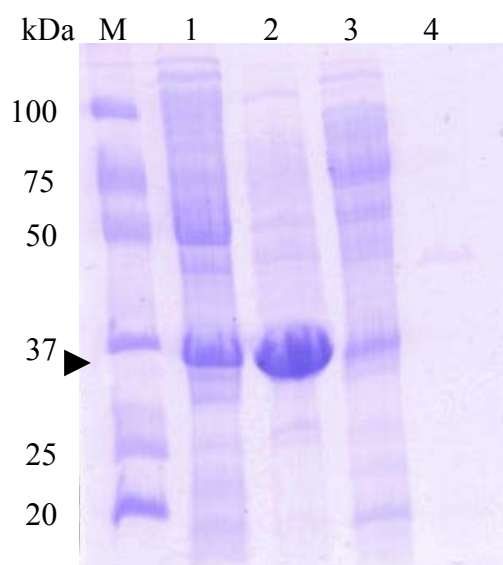


Figure 2.11. SDS-PAGE of Source Q fractions of *E. coli* DHQase. Markers (Lane M); soluble crude (Lane 1); fractions 26-29 (Lane 2); fractions 30-35 (Lane 3); fractions 67-68 (Lane 4). Arrow is pointing to the band of recombinant DHQase.

Clean fractions that showed activity were pooled, concentrated, divided into 500  $\mu$ L aliquots, and stored at -80°C.

## 2.10 Expression and purification of *P. furiosus* DHQase

*E. coli* BL21(DE3) Rosetta cells, transformed with the plasmid pT7-7 which contains an inserted *P. furiosus* DHQase gene, were grown overnight at 37°C in tubes containing LB media supplemented with ampicillin and chloramphenicol. These cells were then used to inoculate a larger flask. When the OD<sub>600</sub> reached ~0.6 the culture was induced with IPTG. The cells were harvested by centrifugation after six hours of induction and the pellets stored at -80°C until required. Cell pellets were then resuspended in lysis buffer, ruptured by sonication, and heat treated (see figure 2.12).

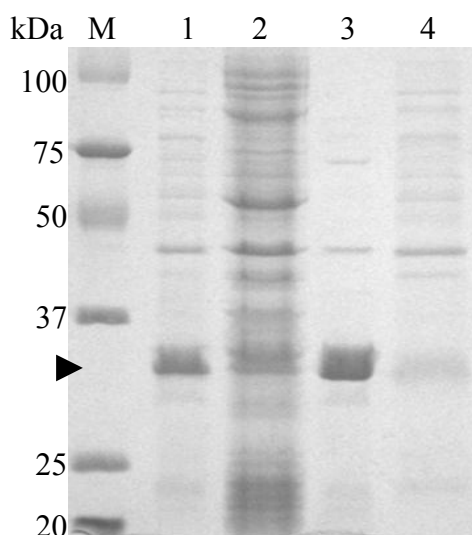


Figure 2.12. SDS-PAGE of *P. furiosus* DHQase final lysis conditions (Lysis buffer: 50 mM BTP, 2 mM DTT, 200mM KCl, 1 mM EDTA, pH 7.5). Markers (Lane M); soluble crude (Lane 1); insoluble crude (Lane 2); soluble heat-treated (Lane 3); insoluble heat-treated (Lane 4). Arrow is pointing to the band of recombinant DHQase.

The soluble heat-treated protein was then loaded onto a size-exclusion column and eluted with BTP buffer. Clean fractions that showed activity were pooled, concentrated, divided into 500  $\mu$ L aliquots, and stored at -80°C.

## 2.11 Characterisation of *E. coli* DHQS, *P. furiosus* DHQS, and Kiwifruit DHQS

The DNA sequence of the ORF encoding for each source of DHQS was used to translate the amino-acid sequence and determine the theoretical isoelectric points (*pI*) and molecular weights (see table 3).

Table 3.

Calculated molecular weights and *pI* for *E. coli* DHQS, *P. furiosus* DHQS, and Kiwifruit DHQS

	<i>E. coli</i> DHQS	Kiwifruit DHQS	<i>P. furiosus</i> DHQS
DNA base pairs	1086	1239	1005
Amino acid residues	362	413	335
<i>pI</i>	5.72	5.92	6.87
Molecular weight (Daltons)	38880.99	45166.64	37384.07

Amino-acid sequence alignments between *P. furiosus* DHQS and DHQS from various other sources showed the following sequence identities: 38% with *E. coli* DHQS, 38% with *Staphylococcus aureus* DHQS, 44% with *Thermus thermophilus* DHQS, 45% with *Sulfolobus solfataricus* DHQS, 38% with *Thermotoga maritima* DHQS, 36% with *Neisseria meningitidis* DHQS, 40% with *Streptococcus pneumonia* DHQS, 40% with *Mycobacterium tuberculosis* DHQS, and 31% with *Aspergillus nidulans* DHQS.

The thermal stability of *P. furiosus* DHQS and *E. coli* DHQS in water was examined using circular dichroism spectroscopy by monitoring the changes in the secondary structure at wavelengths in the far-UV. As expected, *P. furiosus* DHQS was significantly more thermally stable than *E. coli* DHQS. Loss of secondary structure can be seen at 90 and 30°C for *P. furiosus* DHQS and *E. coli* DHQS respectively (see figure 2.13). It is important to note here that the optimal growth temperature for *P. furiosus* is 100°C.

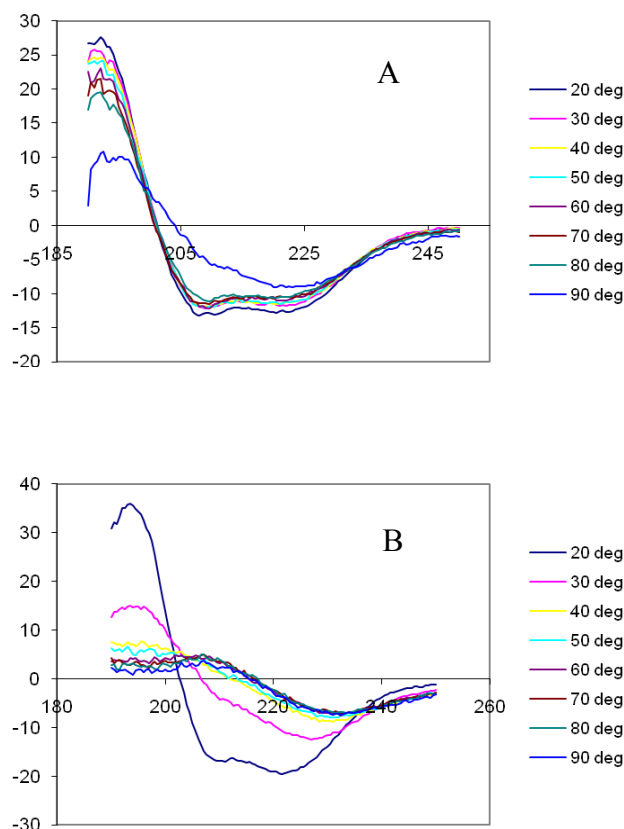


Figure 2.13. Thermal stability determination using circular dichroism (CD). A: CD spectrum of *P. furiosus* DHQS at increasing temperatures; B: CD spectrum of *E. coli* DHQS at increasing temperatures.

A fluorescence-based thermal stability assay was used to determine the thermal stability of DHQS and to confirm the results seen with circular dichroism spectroscopy. This assay distinguishes folded and unfolded proteins through exposure to a hydrophobic fluorescence probe.<sup>34</sup> When the quenched probe is exposed to the hydrophobic interior of an unfolded protein a decrease in quenching results in an increase in fluorescence that can be recorded as a function of temperature. Thermally induced unfolding of protein can be measured in terms of the midpoint of the folded versus unfolded transition states ( $T_m$ ). In the case of *P. furiosus* DHQS, the  $T_m$  was found to be 90.2°C, whereas the  $T_m$  for *E. coli* DHQS was 46.4°C (see figure 2.14).

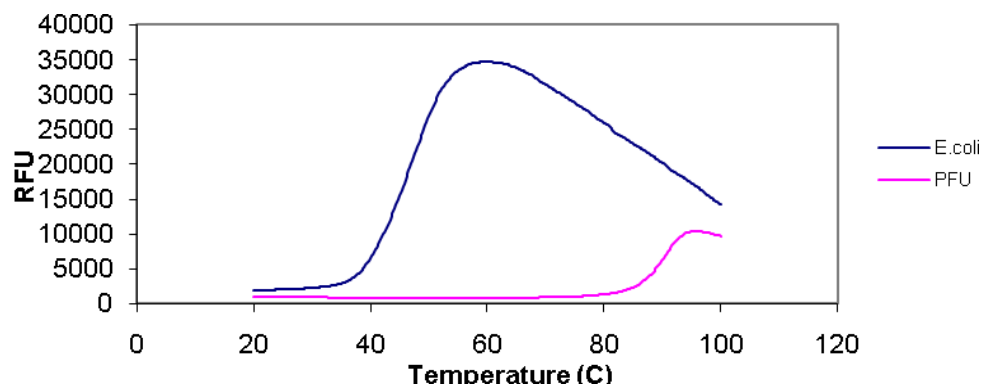
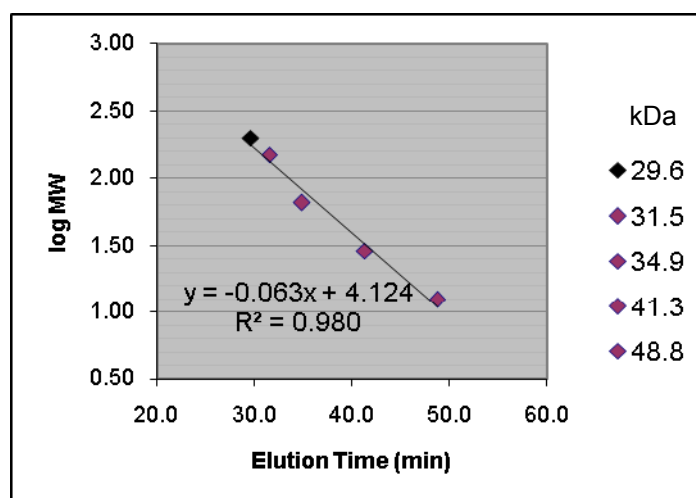


Figure 2.14. Fluorescence-based thermal stability assay of *P. furiosus* DHQS and *E. coli* DHQS.

Using size-exclusion chromatography and molecular-mass standards the apparent molecular masses of each enzyme were determined. The purified enzymes appeared to exist as dimers and only one protein peak per enzyme was obtained from the chromatography. The apparent molecular masses were 72 kDa, 76 kDa, and 89 kDa for *P. furiosus* DHQS, *E. coli* DHQS, and Kiwifruit DHQS respectively (see figure 2.15). These values were in excellent agreement with those of 37,384.07, 38,880.99, and 45166.64 based on the ORF coding for *P. furiosus* DHQS, *E. coli* DHQS, and Kiwifruit DHQS monomers respectively.



	<i>P. furiosus</i>	<i>E. coli</i>	Kiwifruit
MW	72.0	76.0	89.4 kDa
MW ratio	1.9	2.0	2.0
Exact mass	37.4	38.9	45.2 kDa

Figure 2.15. Molecular mass determination of *P. furiosus*, *E. coli*, and Kiwifruit DHQS; Standard log curve of molecular weight versus time.

The relative molecular mass of the purified recombinant enzymes, as determined by electrospray ionisation mass spectrometry, were  $37,397.36 \pm 1.41$  for the *P. furiosus* DHQS monomer,  $38,888.69 \pm 0.06$  for the *E. coli* DHQS monomer, and  $45,189.61 \pm 0.062$  for the His-tagged Kiwifruit DHQS monomer (see figures 2.16, 2.17, and 2.18).

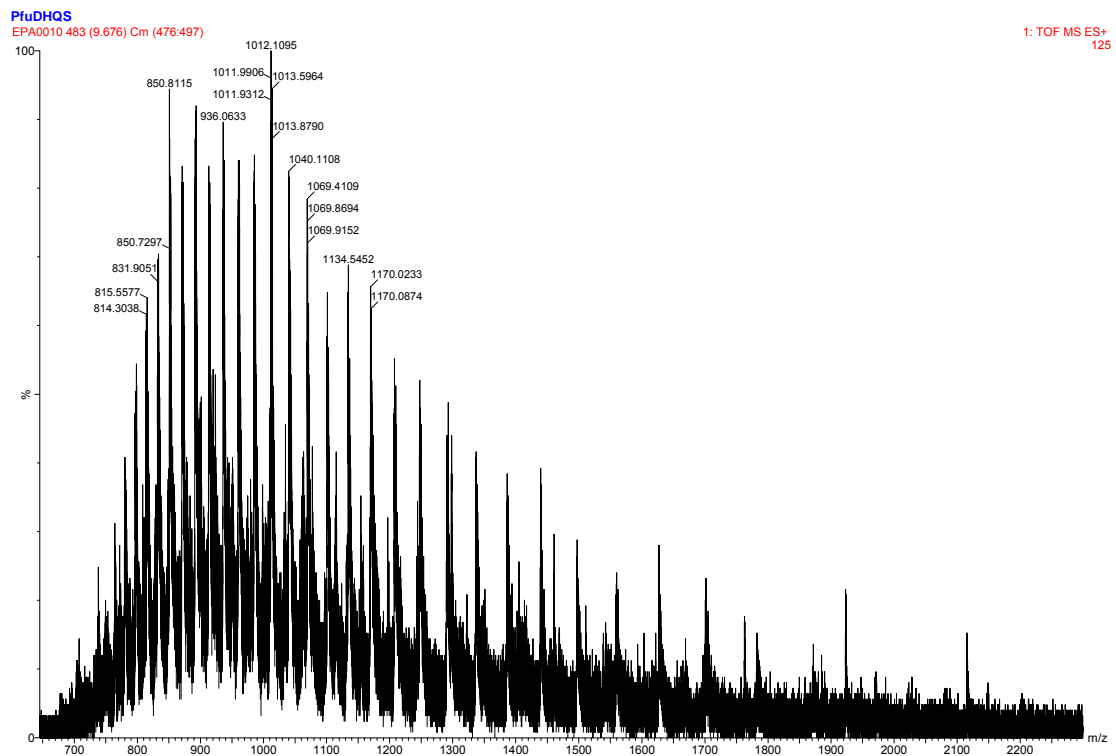
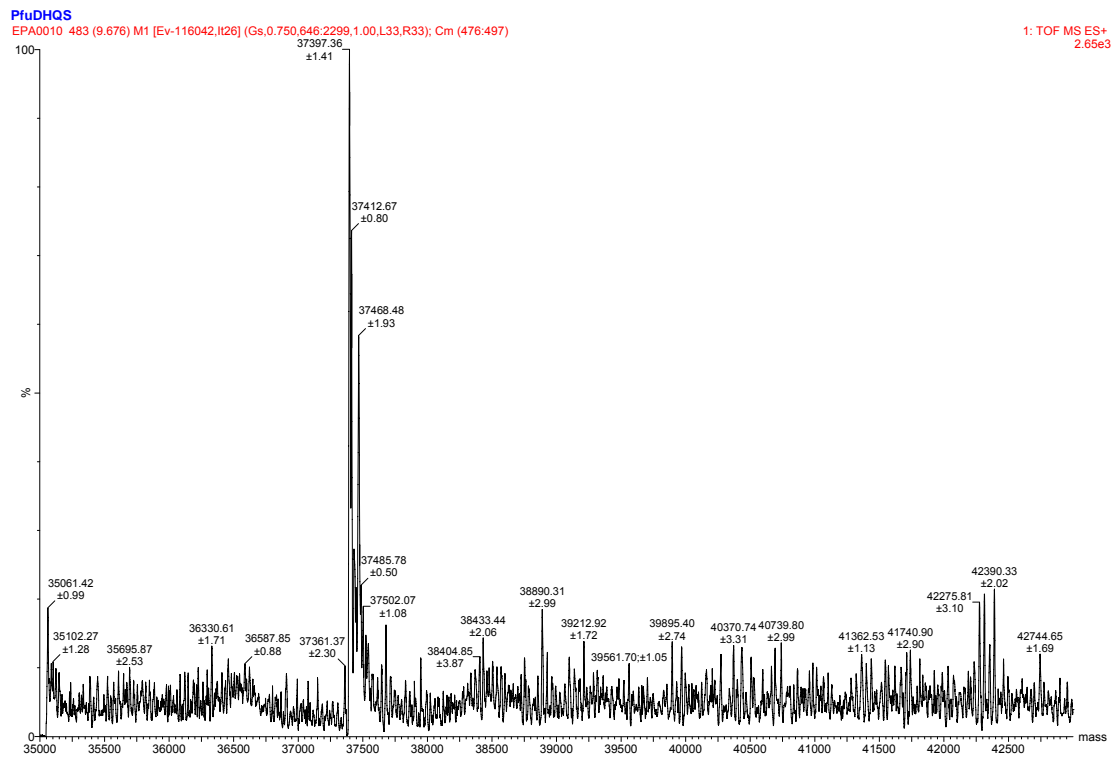


Figure 2.16. Molecular weight of *P. furiosus* DHQS based on ESI-MS.

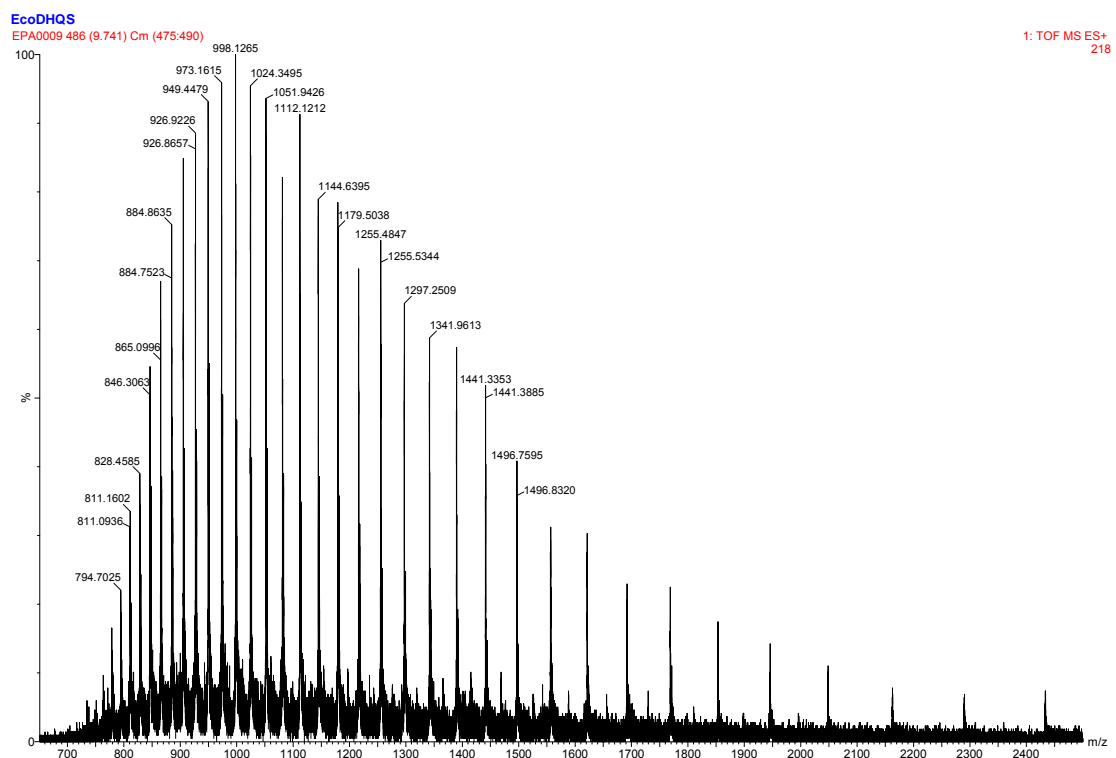
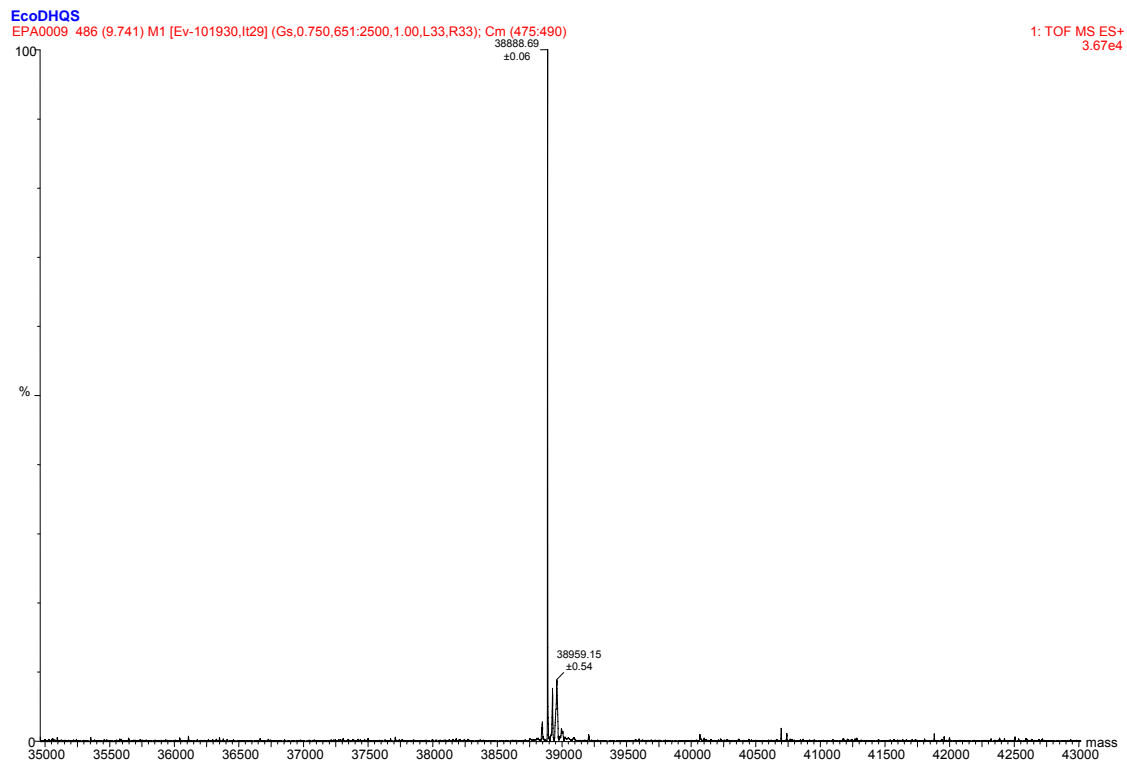


Figure 2.17. Molecular weight of *E. coli* DHQS based on ESI-MS.

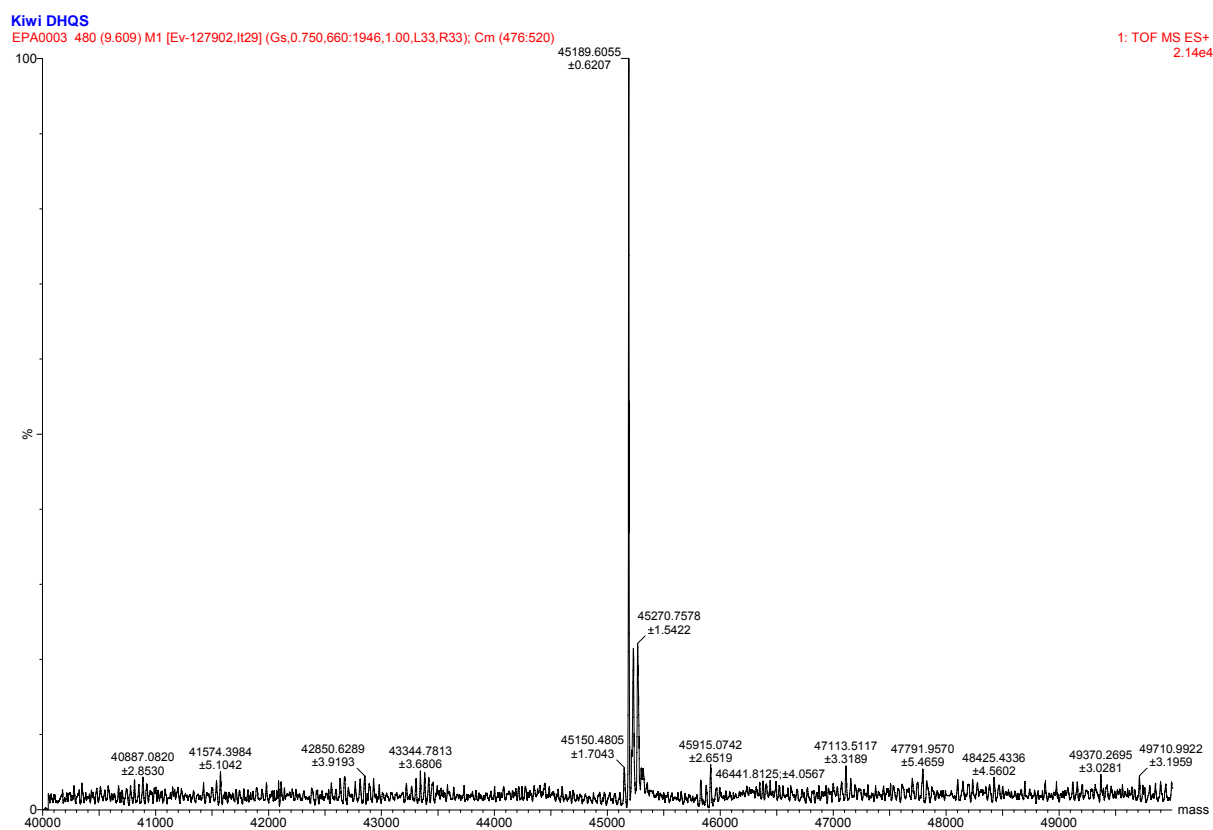
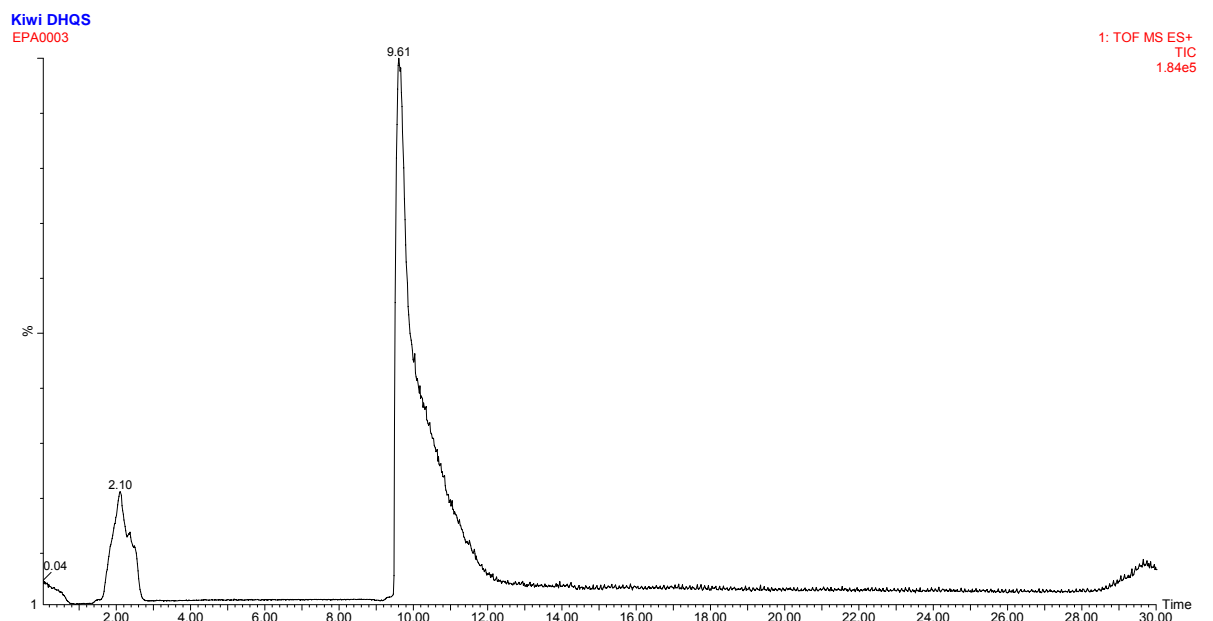


Figure 2.18. Molecular weight of kiwifruit DHQS based on ESI-MS.

To assess the kinetic activity of DHQS, *in vitro* experiments were performed spectroscopically using a coupled-enzyme continuous assay. Since the substrates and products of DHQS cannot be measured spectroscopically, DHQase was coupled with

DHQS to generate a UV-active compound, dehydroshikimate. When dehydroquinase is used in excess in the presence of DHQS, its activity serves as a quantitative measure for the activity of DHQS. *E. coli* DHQS and Kiwifruit DHQS were assayed at 25°C. *P. furiosus* DHQS was assayed at 60°C.

### **2.12 Metal dependency of *P. furiosus* DHQS and Kiwifruit DHQS**

To measure metal dependency of *P. furiosus* DHQS and Kiwifruit DHQS, a range of divalent metal salts were tested for their ability to restore activity to EDTA-treated DHQS. The activity of *P. furiosus* DHQS treated with 1 mM EDTA and assayed in the absence of metal ion was less than 0.5% of the EDTA-treated enzyme assayed in the presence of  $\text{Co}^{2+}$ . Similarly, the activity of Kiwifruit DHQS treated with 1 mM EDTA assayed in the absence of metal ion was 1% of the EDTA-treated enzyme assayed in the presence of  $\text{Co}^{2+}$  (see table 4). The residual activity may be due to the inability of EDTA to produce 100% metal-free enzyme or may represent the true residual activity of the apoenzyme.

Table 4.

Activation of EDTA-treated DHQS by various divalent metal ions

Divalent metal ion	Concentration (mM)	DHQS Activity (%)	
		<i>P. furiosus</i>	Kiwifruit
Co	0.1	100	100
Cd	0.1	121	10
Zn	0.1	86	24
Mn	0.1	50	17
Ni	0.1	4	3
Fe	0.1	3	110
Cu	0.1	2	19
Ca	0.1	2	1
Hg	0.1	2	1
Mg	0.1	2	2
Ba	0.1	1	1
Cr	0.1	1	3
No metal/ no EDTA	0	1	12
No metal/ EDTA Treated	0	0.1	1

$\text{Cd}^{2+}$  and  $\text{Co}^{2+}$  significantly activated the EDTA-treated *P. furiosus* DHQS compared to  $\text{Zn}^{2+}$ . In the case of EDTA-Kiwifruit DHQS,  $\text{Fe}^{2+}$  and  $\text{Co}^{2+}$  significantly activated the enzyme compared to  $\text{Zn}^{2+}$ .

The effect of temperature on *P. furiosus* DHQS activity showed an initial rise in activity proportional to the rise in temperature. However, the activity appeared to taper off above 75°C (see figure 2.19).

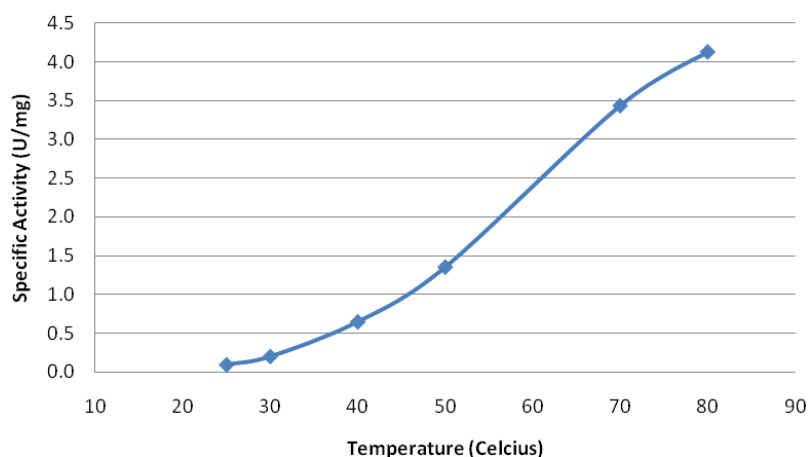


Figure 2.19. Effects of temperature on specific activity of purified *P. furiosus* DHQS.

*P. furiosus* DHQS was active between pH 6.5 and 8.5 with an optimal activity at pH 6.7 at 60°C (see figure 2.20).

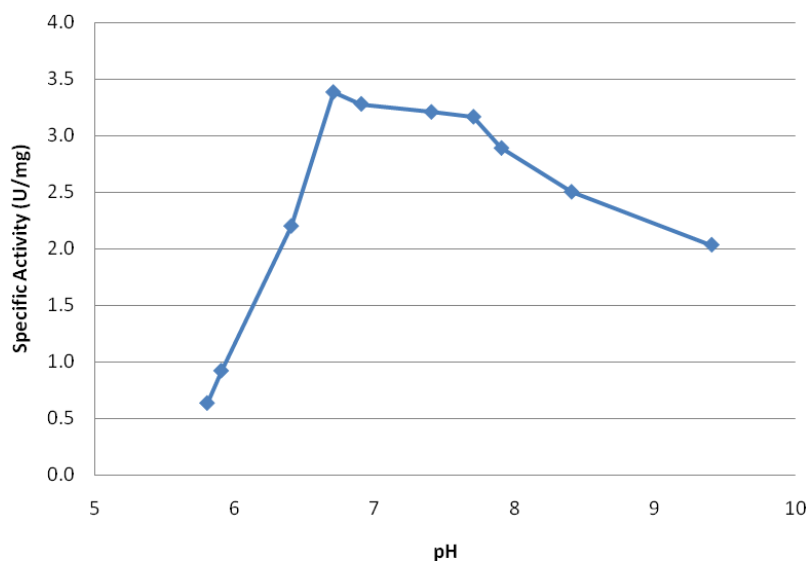


Figure 2.20. Effects of pH on the activity of purified *P. furiosus* DHQS.

A model of *P. furiosus* DHQS was created using homology modelling software (PRIME 1.5) and the crystal structure of *Staphylococcus aureus* DHQS as a template (see figure 2.21). *Staphylococcus aureus* DHQS was chosen because it gave the best

folding compared to that of *A. nidulans* DHQS. The *P. furiosus* DHQS model shares structural similarities with *Staphylococcus aureus* DHQS, specifically the N-terminal Rossmann-fold domain and the C-terminal  $\alpha$ -helical domain.

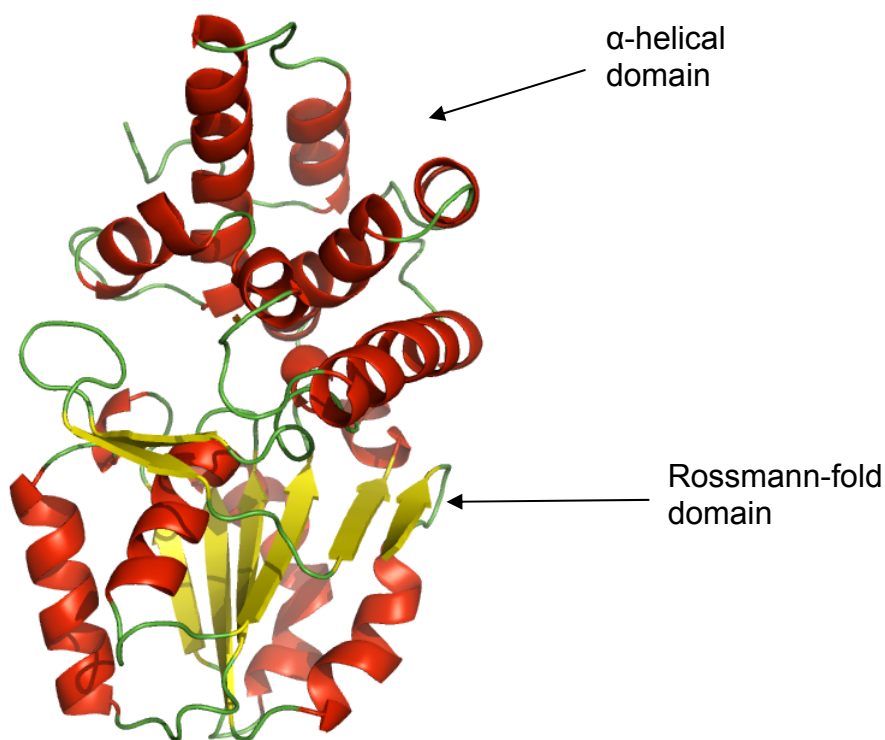


Figure 2.21. Model of *P. furiosus* DHQS

Using the crystal structure of DHQS from *Aspergillus nidulans* (*A. nidulans*), a list of amino acids involved in the binding pocket of the carboxylate on DAH7P and three other amino acids that are presumed to be involved in the cyclisation step of the mechanism of DHQS was generated.<sup>8</sup> The amino acids from *A. nidulans* DHQS are Arg264, Lys250, Asn268, and Lys152. DHQS from *Aspergillus nidulans*, *Thermus thermophilus*, *Staphylococcus aureus*, and the homology model of *P. furiosus* were superimposed and the amino acids corresponding to the selected amino acids from *A. nidulans* DHQS were compared (see table 5).

Table 5.

Conserved amino acids of the DAH7P carboxylate-binding site

	<i>A. nidulans</i>	<i>S. aureus</i>	<i>T. thermophilus</i>	<i>P. furiosus</i>
Arg	264	235	224	220
Lys	250	221	210	206
Asn	268	239	228	224
Lys	152	136	131	127
Asp	146	130	125	121
Lys	197	181	176	171

The superimposed amino acids showed close overlap (see figure 2.22). Two other amino acids that were not mentioned by Carpenter and co-workers in their analysis of the crystal structure of *A. nidulans* DHQS but which are in close proximity to the substrate are Asp146 and Lys197. In the homology model of the *P. furiosus* enzyme the equivalent residue to Asp146, Asp121, adopts a slightly different position to Asp146 (see figure 2.23). This may be due to the imprecision of the model, rather than indicating any distinct difference with this enzyme.

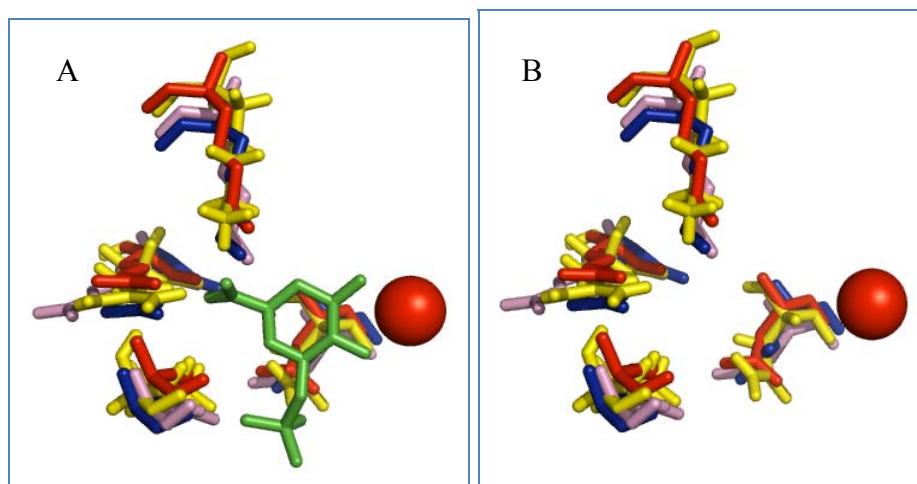


Figure 2.22. Overlapping conserved amino acids of the DAH7P carboxylate-binding site. Blue: *A. nidulans* amino acids, Red: *S. aureus* amino acids, Pink: *T. thermophilus*, Yellow: *P. furiosus* amino acids, Green: carbaphosphonate, Orange: Zn. A) Overlap with carbaphosphonate; B) Overlap without carbaphosphonate.

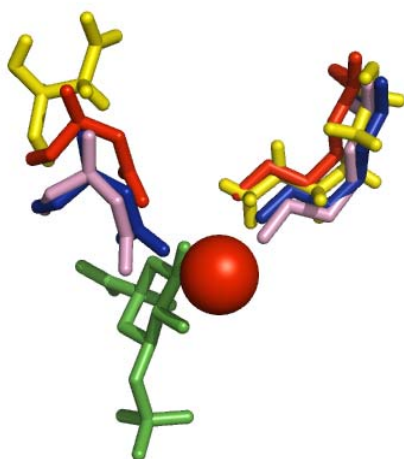


Figure 2.23. Overlapping Asp146 and Lys197 of *A. nidulans* DHQS with *P. furiosus* DHQS. Blue: *A. nidulans* amino acids, Red: *S. aureus* amino acids, Pink: *T. thermophilus*, Yellow: *P. furiosus* amino acids (hydrogens shown), Green: carbaphosphonate, Orange: Zn.

### 2.13 Tagged versus untagged Kiwifruit DHQS experiment

Purified Kiwifruit DHQS was a gift from Hort Research (Auckland). The enzyme was cloned with a His tag that included a protease cleavage site for the removal of the tag. In addition to adding extra weight to the enzyme, it was also necessary to know if the added residues were affecting the activity of the enzyme. Therefore, the activity of tagged versus untagged Kiwifruit DHQS was compared.

To obtain a clear and unbiased comparison between tagged versus untagged enzyme, the assay below was designed and executed in order to normalise both enzymes from the effects that could be caused by the His tag removal procedure. Five test samples were prepared as shown in table 6. Control A was prepared to see if the EKmax™ protease enzyme produced any band on gel electrophoresis. Control B at 37°C and 25°C were prepared to assess if the His-tagged Kiwifruit DHQS enzyme lost activity due over the time course of the digest. Trials at 37°C and 25°C were prepared to

assess which incubation temperature was most efficient in removing the His tag. The optimal temperature for the protease enzyme is 37°C. A temperature of 25°C was chosen as an alternative incubation temperature for the His tag removal procedure for the stability of Kiwifruit DHQS. Control C was the original unaltered His-tagged DHQS kept on ice.

Table 6.

Experimental conditions for His tag removal assay

	Control A No DHQS incubation (37°C)	Control B No EKmax incubation (25°C)	Control B No EKmax incubation (37°C)	Trial incubation (37°C)	Trial incubation (25°C)	Control C no treatment
Kiwifruit DHQS	✗	✓	✓	✓	✓	✓
EKmax enzyme	✓	✗	✗	✓	✓	✗

With the exception of Control C, each sample was washed with buffer, treated accordingly with protease or water, and incubated. The samples were assayed on SDS-PAGE to check for changes in protein mass (see figure 2.24).

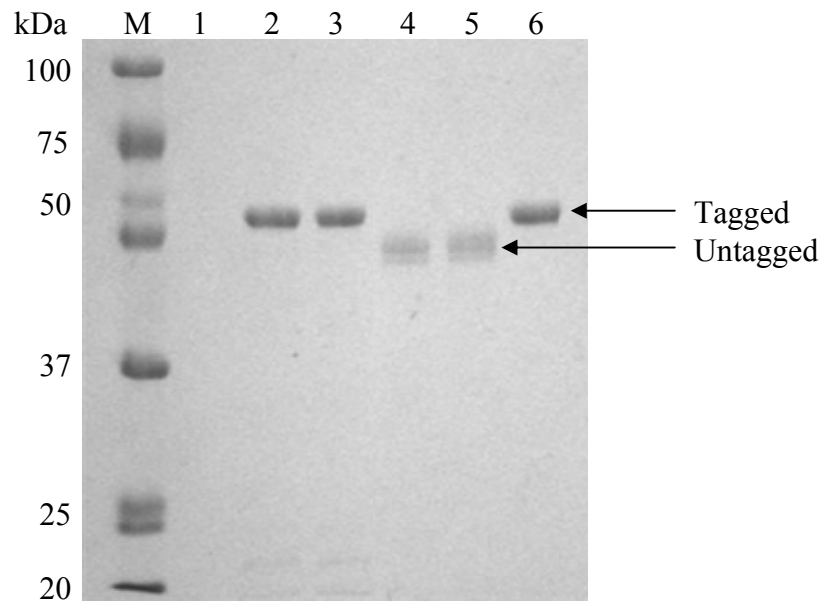


Figure 2.24. SDS-PAGE of tagged versus untagged Kiwifruit DHQS. Markers (Lane M); control A, no DHQS (Lane 1); control B, 37°C (Lane 2); control B, 25°C (Lane 3); Trial 37°C (Lane 4); Trial 25°C (Lane 5); control C (Lane 6).

Enzyme activity assays for each of the sample and the controls were done to check for differences in enzyme function (see Table 7).

Table 7.

Enzyme activity of Kiwifruit DHQS: tagged versus untagged

<b>Samples</b>	<b>Abs/min</b>
Control C	0.053
Control B	0.052
Trial (37°C)	0.048
Trial (25°C)	0.055

Results show that the His-tag was successfully removed at either 25°C or 37°C. This can be seen by the loss of mass for each of the protease-treated test samples on SDS-PAGE. The tag-removal procedure at either 25°C or 37°C had no major change in the activity of the enzyme, although the activity was slightly better for the test sample that

was incubated at 25°C. There was no significant difference in activity between tagged versus untagged Kiwifruit DHQS.

## 2.14 Discussion

Circular dichroism spectroscopy results showed that *P. furiosus* DHQS was stable up to 90 °C in water. It is likely that the stability could have been improved had a buffer with a high ionic strength been used. Using this technique *E. coli* DHQS in water was observed to unfold at an unexpectedly low temperature of 30 °C (the optimal growth temperature for *E. coli* is 37 °C). In contrast, the stability for *E. coli* DHQS in the fluorescence-based thermal stability assay was greater than that seen during the CD thermal stability assay (46.4 °C versus 30 °C respectively). It is possible that the phosphate buffer used in the fluorescence-based thermal stability assay increased the stability of *E. coli* DHQS.

No significant difference in activity was observed between tagged and untagged Kiwifruit DHQS, which could indicate that the extra amino acids of the His tag and the protease recognition site do not prevent the enzyme from folding correctly nor interfere with the mechanism at the active site.

Of the four DHQS crystal structures available in the RCSB protein data bank, those from *Aspergillus nidulans* and *Thermus thermophilus* assemble as homodimers, whereas that from *Staphylococcus aureus* is a monomer.<sup>8-10</sup> In contrast, the DHQS crystal structure from *Heliobacter pylori* assembles as a hexamer composed of three dimers.<sup>11</sup>

*Aspergillus nidulans* DHQS and *E. coli* DHQS occur naturally as part of a pentafunctional domain and trifunctional domain, respectively. However, when *Aspergillus nidulans* DHQS and *E. coli* DHQS are expressed as monofunctional domains, they have been shown to be monomeric.<sup>30,35</sup> Lumsden and Coggins showed that the DHQS domain from the *Neurospora crassa* pentafunctional AROM protein is dimeric.<sup>36</sup> Work by Yamamoto showed that the native DHQS from *Phaseolus mungo* had an apparent molecular weight, estimated by size exclusion chromatography, of 67 kDa. However, using SDS-gel electrophoresis, the minimum molecular weight of the enzyme was 43 kDa.<sup>20</sup> Contrary to the literature findings, the DHQS from *E. coli* in this thesis was found to be dimeric as well as the DHQSs from *P. furiosus* and Kiwifruit.

A comparison of metal dependency from other sources of DHQS reported in the literature showed that cobalt was the predominant activating metal in all screens with the exception of DHQS from *Neurospora crassa*, which showed a preference for zinc only.<sup>13,18,19,21,35</sup> Zinc restored the activity of *E. coli* DHQS to 53% of the level observed with cobalt. In addition to zinc, other metals such as nickel, cadmium, and manganese restored the activity of *E. coli* DHQS to 23%, 12%, and 10% of the level observed with cobalt, respectively.<sup>13</sup> Cobalt restored the activity of *A. nidulans* DHQS to 125% of the level observed with zinc. Iron and nickel restored the activity of *A. nidulans* DHQS to 18%, and 16% of the level observed with zinc, respectively.<sup>35</sup> Manganese and cobalt were the only divalent metals that activated DHQS from *Bacillus subtilis*.<sup>19</sup> Cobalt and copper activated DHQS from *Phaseolus mungo* whereas only cobalt activated *Sorghum bicolor*.<sup>21</sup> Cadmium restored the activity of *P. furiosus* DHQS to 121% of the level observed with cobalt and iron restored the

activity of Kiwifruit DHQS to 110% of the level observed with cobalt. Both of these metals ( $\text{Cd}^{2+}$  and  $\text{Fe}^{2+}$ ) have not been shown to activate other DHQS enzymes to this level.

### **2.15 Summary**

DHQS and DHQase from *E. coli* and *P. furiosus* have been successfully expressed and purified. Modifications of the purification methods described by Frost and co-workers, and by Schofield and co-workers did not have a negative impact on the specific activity of the enzymes. DHQSs from *E. coli*, Kiwifruit, and *P. furiosus* have been characterised successfully.

### 3. Chemo-enzymatic preparation of DAH7P, (3*S*)-3-fluoro-DAH7P, and (3*R*)-3-fluoro-DAH7P

#### 3.1 Introduction

In order to make DAH7P, (3*S*)-3-fluoro-DAH7P, and (3*R*)-3-fluoro-DAH7P efficiently, it was decided to take advantage of DAH7PS (the first enzyme in the shikimate pathway) and make our targets chemo-enzymatically. This involved incubation of E4P with either PEP or 3-fluoro-PEP in the presence of DAH7PS to make the target compounds. In this chapter the synthesis and isolation of (*Z*)-3-fluoro-PEP and (*E*)-3-fluoro-PEP, the preparation of E4P, and the enzymatic preparations of DAH7P, (3*S*)-3-fluoro-DAH7P, and (3*R*)-3-fluoro-DAH7P are discussed.

#### 3.2 Preparation of E4P

Erythrose 4-phosphate (E4P) **2** was prepared by a modification of the procedure of Baxter, Perlin, and Simpson.<sup>37</sup> The procedure involved oxidation of D-glucose 6-phosphate (G6P) **32** with lead tetraacetate to form crude E4P **2** in 61 % yield (see figure 3.1).

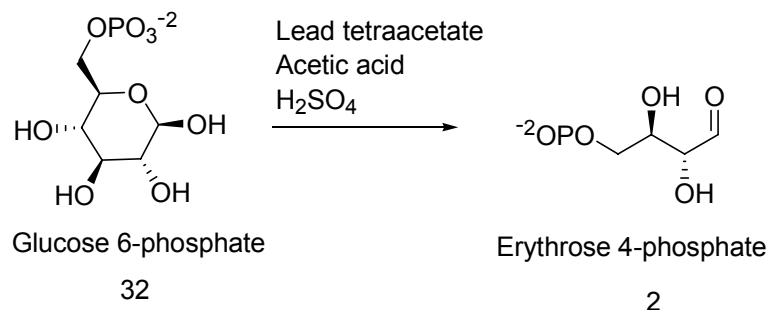


Figure 3.1. Synthesis of E4P.

### 3.2.1 Characterisation of E4P

E4P **2** was characterised indirectly by coupling with PEP **1** in the presence of *E. coli* DAH7PS to form DAH7P **3**. This reaction could be monitored by the loss of PEP **1** at 232 nm. The loss of PEP **1** implied that E4P **2** was successfully synthesised from G6P **32**. If PEP **1** is in excess, the concentration of PEP required to complete the above reaction is the same as the concentration of E4P **2**. The amount of PEP **1** required was determined by monitoring the total change in absorbance of PEP consumed and converting this amount into concentration using the extinction coefficient of PEP.

### 3.3 Preparation of (Z)-3-fluoro-PEP and (E)-3-fluoro-PEP

(Z)-3-Fluoro-PEP and (E)-3-fluoro-PEP were prepared by the procedures reported by Bergmann and Shahak, and later modified by Stubbe and Kenyon.<sup>38,39</sup> Synthesis of 3-fluoro-PEP involved coupling of diethyl oxalate **33** with ethyl fluoroacetate to form diethyl fluorooxalate **34** in 77% yield. This compound was then brominated to form diethyl bromofluorooxalate **35** in 97% yield (see figure 3.2).

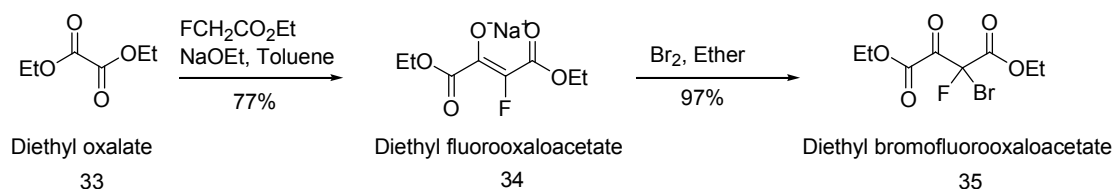


Figure 3.2. Initial two steps towards the synthesis of 3-fluoro-PEP.

The next step involved a hydrolysis and decarboxylation with concentrated HCl to form bromofluoropyruvic acid **36** in 63% yield. The final step involved formation of

the enol phosphate ether with trimethyl phosphite, followed by hydrolysis of the phosphate ethers with water to form the enol phosphate. Cyclohexylamine was added to form the 3-fluoroPEP salt.  $^{19}\text{F}$  NMR analysis indicated the presence of a 9:1 ratio of *Z* and *E* isomers (see figure 3.3).

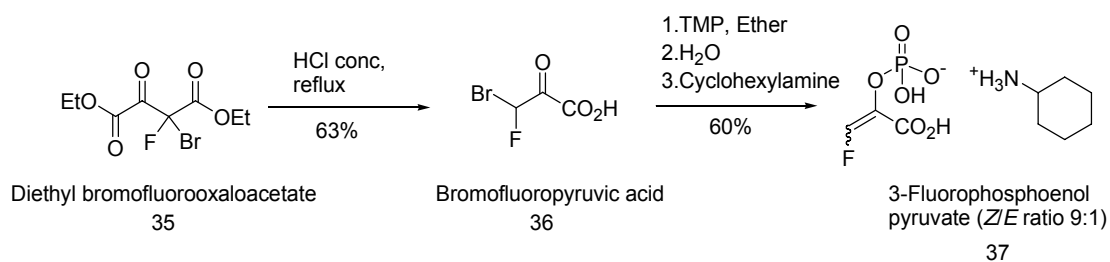


Figure 3.3. Final two steps towards the synthesis of 3-fluoro-PEP.

To form a mixture of 3-fluoro-PEP with a higher percentage of (*E*)-3-fluoro-PEP, the 9:1 mixture of (*Z/E*)-3-fluoro-PEP **37** was photoisomerised by exposure to ultraviolet light at neutral pH. The reaction was then monitored by  $^{19}\text{F}$  NMR spectroscopy. After four days of irradiation a solution of 58:42 (*Z/E*)-3-fluoro-PEP was obtained.

### 3.3.1 Characterisation of (*Z*)-3-fluoro-PEP and (*E*)-3-fluoro-PEP

$^{19}\text{F}$  NMR analysis of (*Z/E*)-3-fluoro-PEP **37** shows the chemical shift of fluorine for (*Z*)-3-fluoro-PEP **38** at -141.1 ppm and that of (*E*)-3-fluoro-PEP **39** at -152.7 ppm (see figure 3.4).

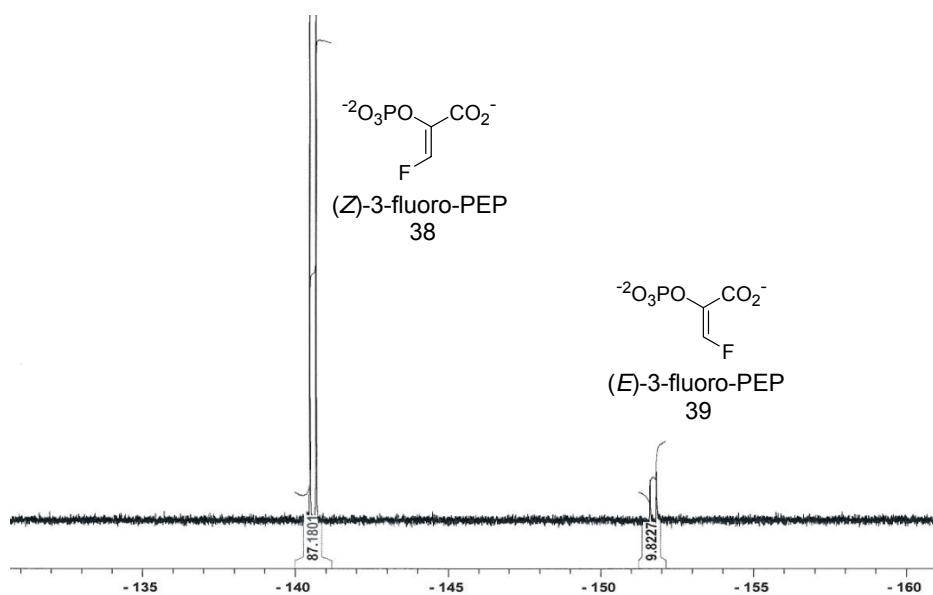


Figure 3.4.  $^{19}\text{F}$  NMR of 9:1 mixture of (*Z/E*)-3-fluoro-PEP.

Photoisomerisation of a mixture of 9:1 (*Z/E*)-3-fluoro-PEP resulted in a 58:42 mixture of (*Z/E*)-3-fluoro-PEP (see figure 3.5).

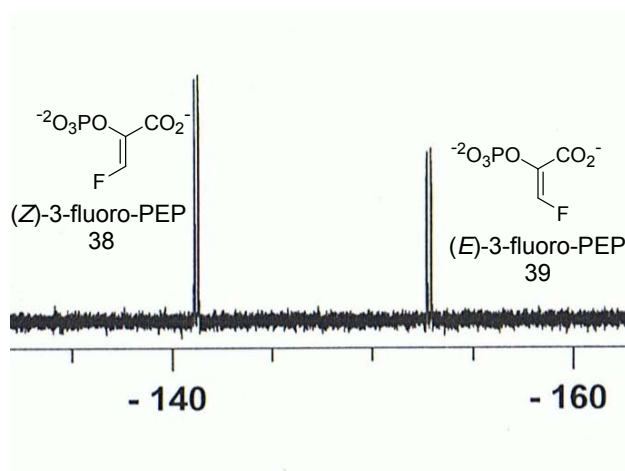


Figure 3.5.  $^{19}\text{F}$  NMR of 58:42 mixture of (*Z/E*)-3-fluoro-PEP

### 3.4 Preparation and isolation of DAH7P

DAH7P **3** was prepared by incubating PEP **1** and crude E4P **2** in the presence of DAH7PS (see figure 3.6). The reaction was monitored by tracking the disappearance of PEP **1** via UV spectrophotometry. The reaction mixture was filtered to remove the enzyme, the supernatant was loaded onto an anion-exchange column, and the fractions containing DAH7P **3** were isolated. DAH7P **3** eluted at 150 mM of ammonium bicarbonate.

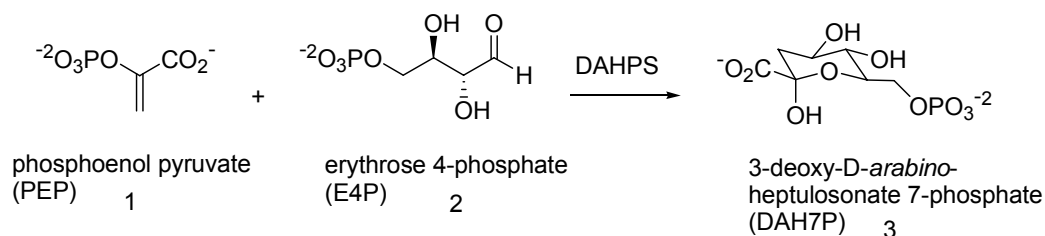


Figure 3.6. Enzymatic synthesis of DAH7P from PEP and E4P in the presence of DAH7PS.

#### 3.4.1 Characterisation of DAH7P

Purified DAH7P **3** was characterised indirectly by enzymatic analysis involving the conversion of DAH7P **3** to dehydroshikimate (DHS, **5**). The formation of DHS **5** ( $\epsilon = 1.2 \times 10^4 \text{ M}^{-1} \text{ cm}^{-1}$  at 25°C) was monitored spectroscopically at 234 nm. The extinction coefficient of DHS **5** was found to be temperature dependent under *P. furiosus* DHQS assay conditions (see figure 3.7). The extinction coefficient decreased slightly above 60°C. An extinction coefficient of  $1.2 \times 10^4 \text{ M}^{-1} \text{ cm}^{-1}$  was used in all calculations of activities at 60°C, the temperature at which all assays with *P. furiosus* DHQS were performed.

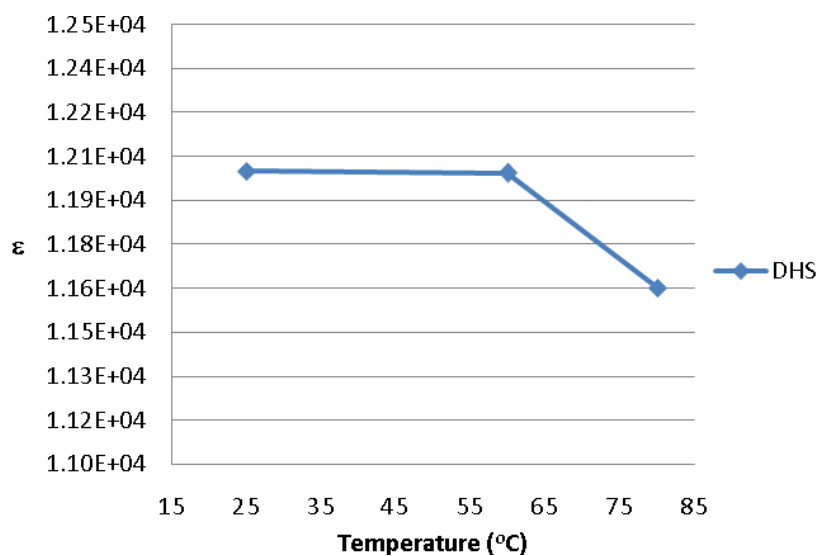


Figure 3.7. Extinction coefficient of DHS versus temperature.

The extinction coefficient of DHS **5** was examined further at 60°C and was found also to be pH dependent (see figure 3.8). The extinction coefficient began to decrease above a pH of 7.4. The extinction coefficient of DHS at pH 6.7 was  $1.2 \times 10^4 \text{ M}^{-1} \text{ cm}^{-1}$  and dropped to  $1.1 \times 10^4 \text{ M}^{-1} \text{ cm}^{-1}$  at pH 8.7.

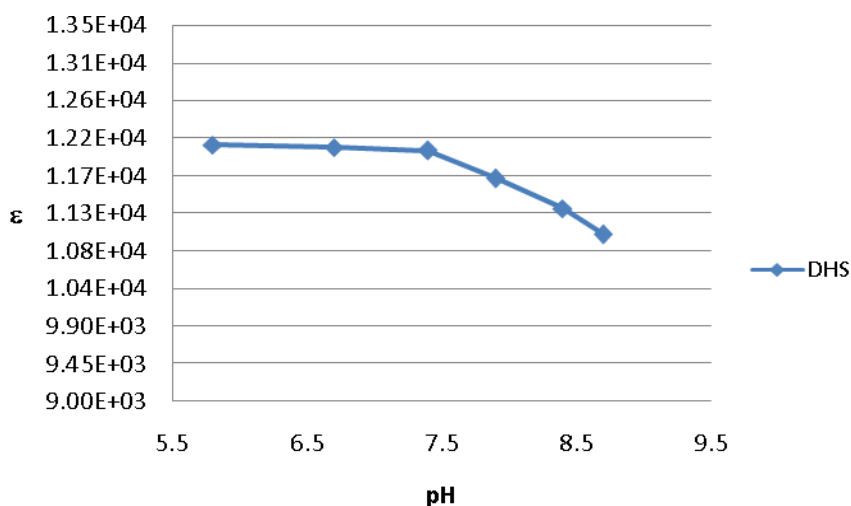


Figure 3.8. Extinction coefficient of DHS versus pH.

One of the challenges of examining thermostable enzymes *in vitro* is the stability of the substrates at elevated temperature. The stability of DAH7P **3** at 60°C was

examined. This was done by incubating fixed amounts of DAH7P **3** at 60°C from 0 to 30 minutes and monitoring the total change in absorbance generated by the enzymatic conversion of DAH7P **3** to DHS **5** using DHQS. Results showed that DAH7P **3** was stable at 60°C over 30 minutes (see figure 3.9).

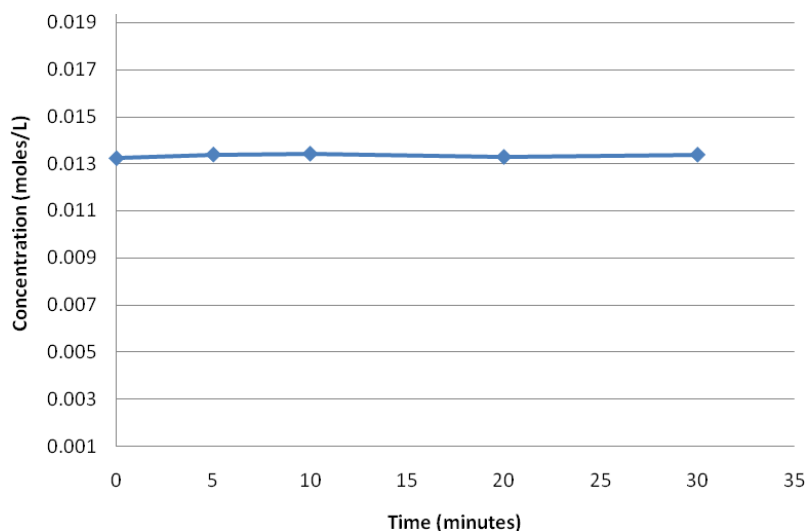


Figure 3.9. Concentration of DAH7P versus time at 60°C.

### 3.5 Preparation and isolation of (3S)-3-fluoro-DAH7P and (3R)-3-fluoro-DAH7P

Formation of 3-fluoro-DAH7P involved incubating E4P **2** with a mixture of (*Z*)-3-fluoro-PEP **38** and (*E*)-3-fluoro-PEP **39** in the presence of *E. coli* DAH7PS to obtain a mixture of diastereomers, (3*S*)-3-fluoro-DAH7P **28** and (3*R*)-3-fluoro-DAH7P **25** respectively (see figure 3.10). Since the two diastereomers separate by anion exchange they can be independently isolated and characterised.

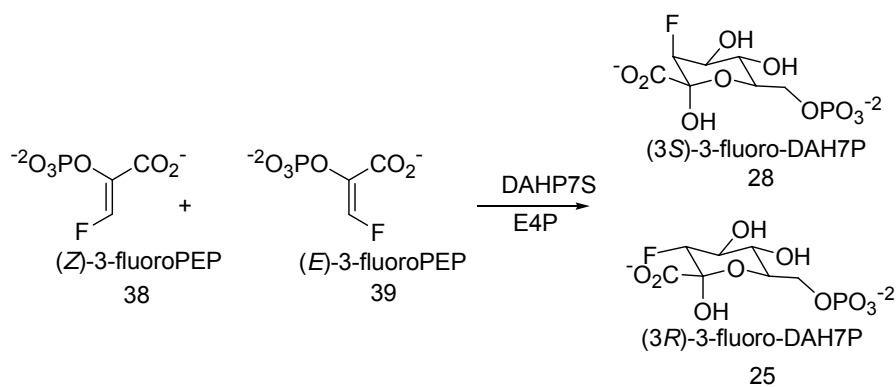


Figure 3.10. Enzymatic synthesis of (3*S*)-3-fluoro-DAH7P and (3*R*)-3-fluoro-DAH7P from 3-fluoro-PEP and E4P in the presence of DAHP7S.

The formation of 3-fluoro-DAH7P was monitored by  $^{19}\text{F}$  NMR spectroscopy. Both the disappearance of 3-fluoro-PEP and the appearance of fluoro-DAH7P were monitored.

A 9:1 mixture of (*Z/E*)-3-fluoroPEP **37** and E4P **2** were incubated in the presence of *E. coli* DAHP7S and monitored by  $^{19}\text{F}$  NMR spectroscopy (see figure 3.11).

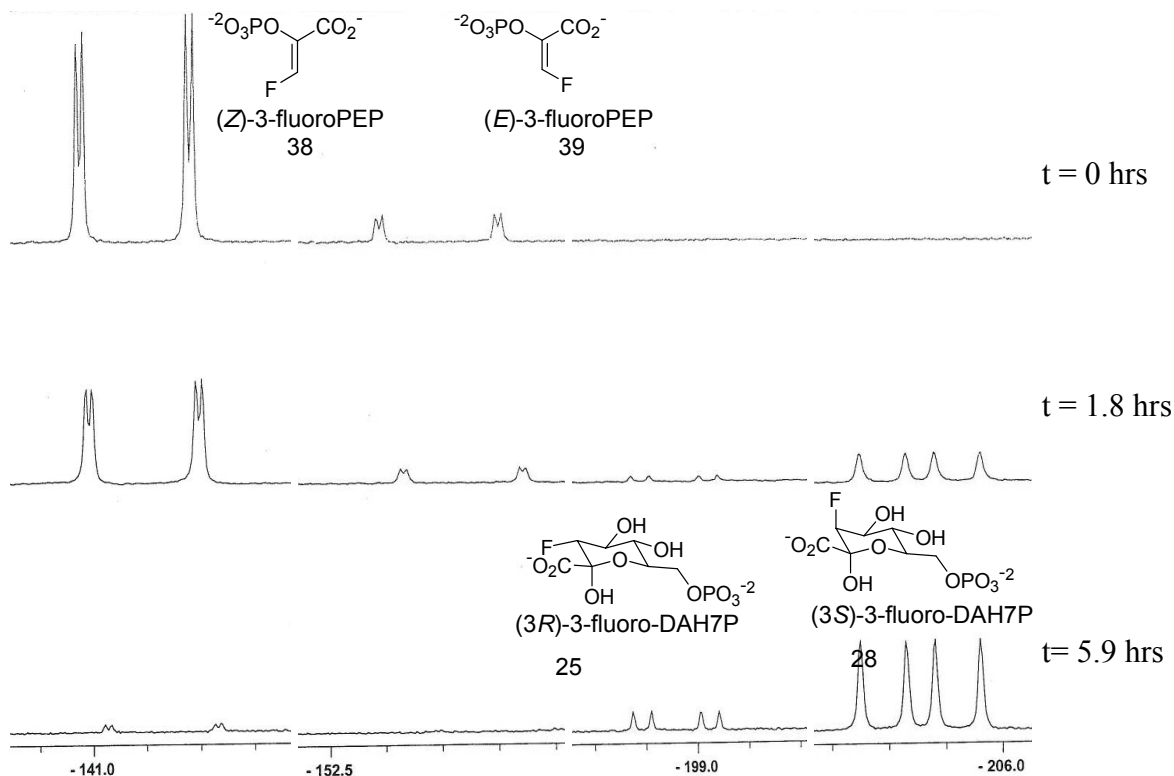


Figure 3.11.  $^{19}\text{F}$  NMR spectrum showing the formation of (3*S*)-3-fluoro-DAH7P and (3*R*)-3-fluoro-DAH7P from a 9:1 mixture of (*Z/E*)-3-fluoroPEP.

The reaction carried out by DAH7PS is stereospecific. Therefore, in the presence of E4P **2**, (*Z*)-3-fluoroPEP **38** is converted to (3*S*)-3-fluoro-DAH7P **28** and (*E*)-3-fluoroPEP **39** is converted to (3*R*)-3-fluoro-DAH7P **25**. (3*S*)-3-fluoro-DAH7P **28** and (3*R*)-3-fluoro-DAH7P **25** can be distinguished by the the chemical shift of the fluorine and the splitting pattern between fluorine and the adjacent proton. The chemical shift of the fluorine on (3*S*)-3-fluoro-DAH7P **28** is -205.8 ppm and the chemical shift of the fluorine on (3*R*)-3-fluoro-DAH7P **25** is -198.9 ppm. The coupling constant between the axial fluorine at C-3 and the axial proton at C-2 for (3*S*)-3-fluoro-DAH7P **28** is ~30 Hz, whereas the coupling constant between the equatorial fluorine at C-3 and the axial proton at C-2 for (3*R*)-3-fluoro-DAH7P **25** is

only ~13.4 Hz (see figure 3.12).<sup>27</sup>

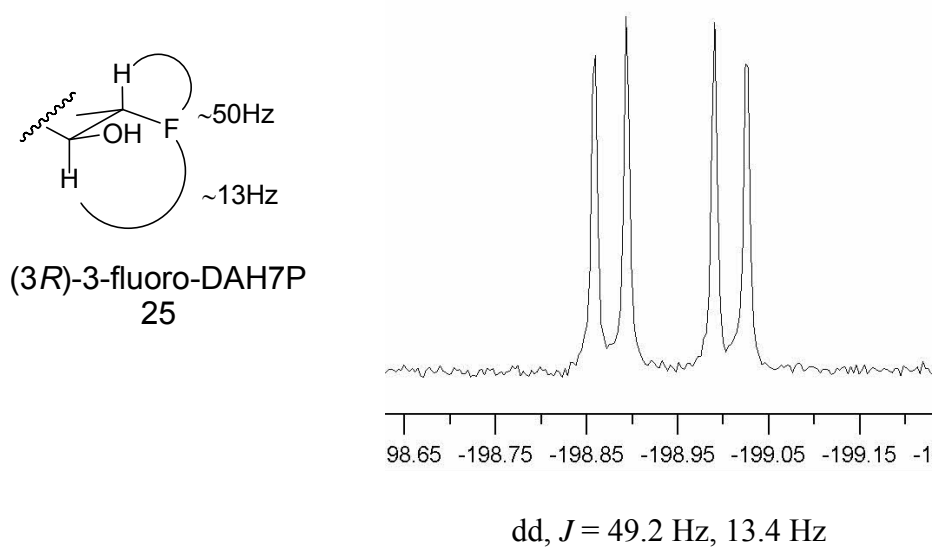
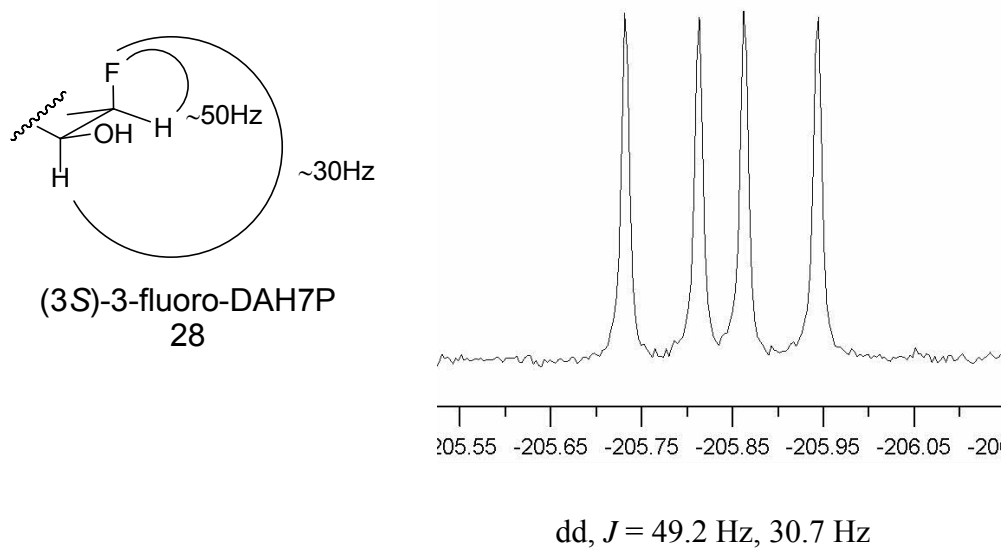


Figure 3.12. Coupling constants and chemical shifts of (3*S*)-3-fluoro-DAH7P and (3*R*)-3-fluoro-DAH7P

Analysis of the products at the end of the reaction showed the production of a 9:1 mixture of (3*S*)-3-fluoro-DAH7P **28** to (3*R*)-3-fluoro-DAH7P **25**. Since this preparation resulted in a larger production of (3*S*)-3-fluoro-DAH7P **28** than (3*R*)-3-

fluoro-DAH7P **25**, a separate preparation was done to obtain (3*R*)-3-fluoro-DAH7P **25** in higher yields.

A 58:42 mixture of (*Z/E*)-3-fluoroPEP and E4P were incubated in the presence of *E. coli* DAH7PS and monitored by  $^{19}\text{F}$  NMR spectroscopy (see figure 3.13).

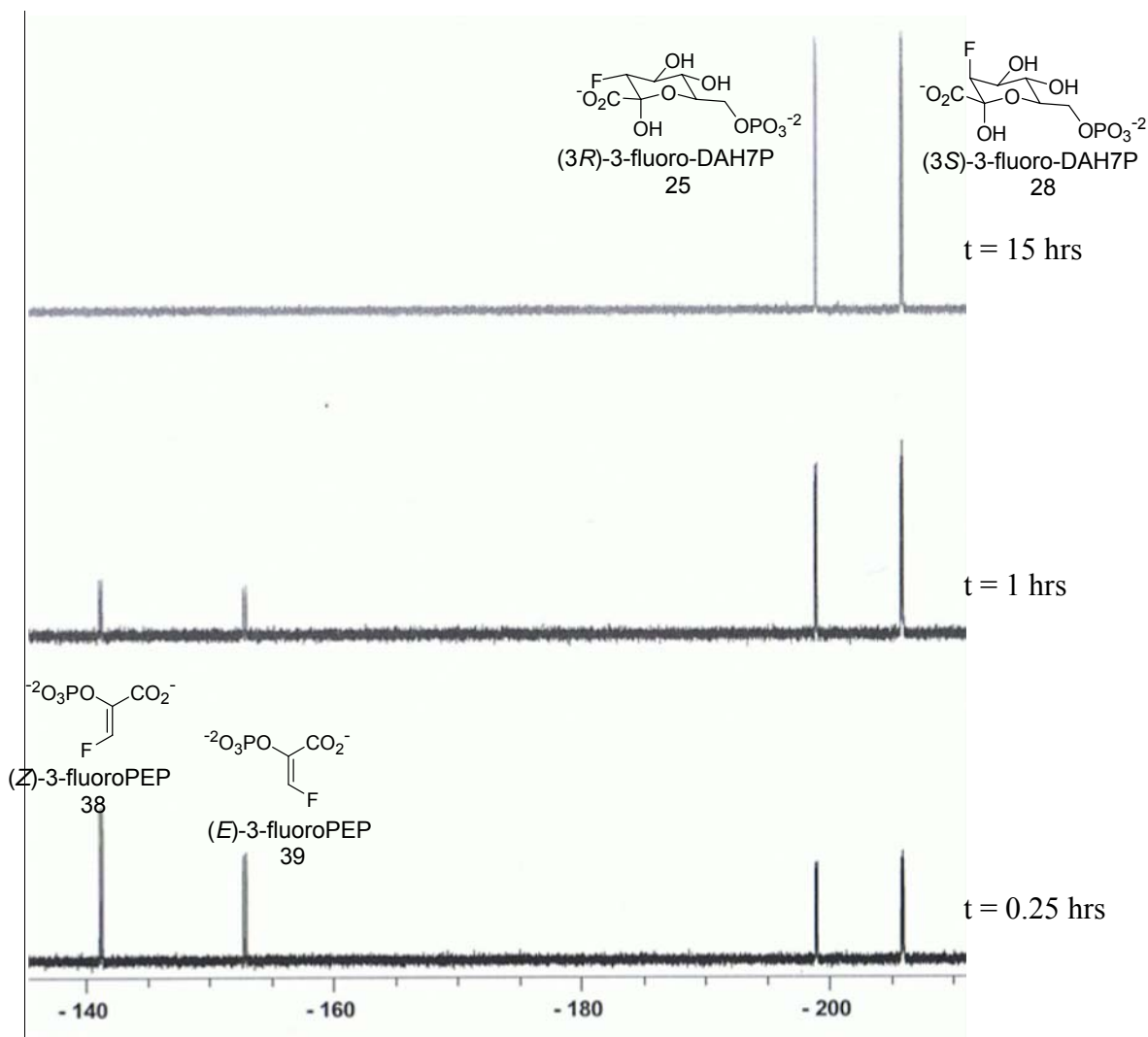


Figure 3.13.  $^{19}\text{F}$  NMR spectra showing the formation of (3*S*)-3-fluoro-DAH7P and (3*R*)-3-fluoro-DAH7P from a 58:42 mixture of (*Z/E*)-3-fluoroPEP.

Analysis of the products at the end of the reaction showed the production of a 58:42 mixture of (3*S*)-3-fluoro-DAH7P **28** to (3*R*)-3-fluoro-DAH7P **25**.

### 3.5.1 Characterisation of (3*S*)-3-fluoro-DAH7P, and (3*R*)-3-fluoro-DAH7P

Electrospray negative-ionisation mass spectrometry found a  $m/z$  of 305.01 for (3*S*)-3-fluoro-DAH7P **28**. The calculated mass was 305.01.  $^{19}\text{F}$  NMR spectroscopy shows successful isolation of the *S* and *R* isomers of 3-fluoro-DAH7P (see figure 3.14).<sup>27</sup>

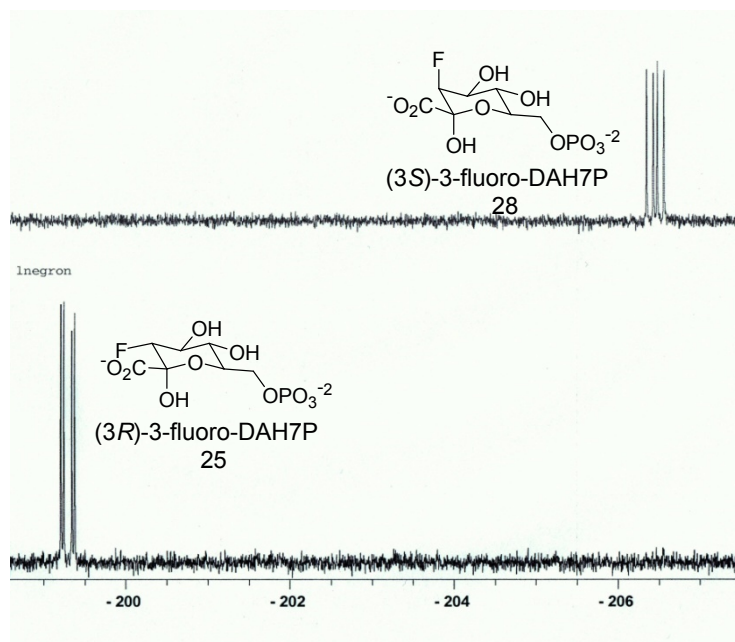


Figure 3.14.  $^{19}\text{F}$  NMR spectra of *S* and *R* isomers of 3-fluoroDAH7P after isolation by anion-exchange chromatography.

### 3.6 Substrate concentration

All substrate concentrations were determined by the Lanzetta assay.<sup>40</sup> The Lanzetta assay is a colourimetric method for the detection of nanomolar concentrations of inorganic phosphate. Determination of substrate concentrations involved generating a standard curve using potassium phosphate, reacting the standards and substrate samples with the Lanzetta reagent, and reading the absorbance at 660 nm. Glucose 6-phosphate (G6P, **32**) was used to test the reliability of the assay. A control of 20 mg/mL (w/v) of G6P **32** was prepared and diluted 100-fold. The final concentration of G6P **32** as determined by the Lanzetta assay was 0.7 mM or 0.24 mg/mL which

closely matches the concentration based on the weight of G6P **32** used. The concentrations of DAH7P **3**, (3*S*)-3-fluoro-DAH7P **28**, and (3*R*)-3-fluoro-DAH7P **25** determined by the Lanzetta assay were used for the determination of  $K_M$  and  $k_{cat}$  in chapter 4.

### 3.7 Summary

Chemo-enzymatic synthesis allowed for a facile and efficient method for the preparation of DAH7P **3**, (3*S*)-3-fluoro-DAH7P **28**, and (3*R*)-3-fluoro-DAH7P **25**. The diastereomers separated cleanly by anion-exchange chromatography. Synthesis of mixtures of (3*Z*)-3-fluoro-PEP **38** and (3*E*)-3-fluoro-PEP **39** allowed for the generation of both the *S* and *R* isomers of 3-fluoro-DAH7P. Photoisomerisation of the mixtures of 3-fluoro-PEP produced an increased percentage of (3*E*)-3-fluoro-PEP **39** and subsequently allowed the efficient isolation of (3*R*)-3-fluoro-DAH7P **25**.

There was some effect on DHS **5** stability at temperatures higher than 60°C, as judge by a 3% decrease in the extinction coefficient between 60°C and 80°C. Similarly, there was only a small effect on DHS **5** stability above pH 7.4 with a small decrease in the extinction coefficient between pH 7.4 and 7.9. DAH7P **3** was stable for at least 30 minutes at 60°C, which was more than adequate for all kinetic assays given that the incubation time for the duration of each assay was no more than 10 minutes at a time.

## 4. Interaction of (3*S*)-3-fluoro-DAH7P and (3*R*)-3-fluoro-DAH7P with DHQS enzymes

### 4.1 Introduction

The aim of this thesis was to assess how (3*S*)-3-fluoro-DAH7P **28** and (3*R*)-3-fluoro-DAH7P **25** interact with DHQS enzymes from a variety of sources. Three experimental tools were utilised for the assessment of the interaction of the 3-fluoro-DAH7P analogues with DHQS. <sup>19</sup>F NMR spectroscopy was used for the identification and quantification of products produced by each enzyme. This was a great advantage because it allowed the assays to be carried out in minimal deuterated water and avoided the complex spectra that would have otherwise been generated by <sup>1</sup>H NMR spectroscopy. Secondly, enzyme kinetic assays provided insight to the rate of activity for each enzyme during the catalysis of (3*S*)-3-fluoro-DAH7P **28** and (3*R*)-3-fluoro-DAH7P **25**. A comparison of the changes in rate of activity for each enzyme while processing (3*S*)-3-fluoro-DAH7P **28**, (3*R*)-3-fluoro-DAH7P **25** and DAH7P **3** was important to assess the stereoelectronic effects from the 3-fluoro substitution on DAH7P. Finally, UV spectrophotometry was used to measure the concentration of (6*S*)-6-fluoro-DHQ **30** produced and compare these findings with the partitioning results seen with <sup>19</sup>F NMR spectroscopy.

## 4.2 Partitioning results from $^{19}\text{F}$ NMR spectroscopy

Determining the partitioning of the products formed from (3*R*)-3-fluoro-DAH7P **25** and (3*S*)-3-fluoro-DAH7P **28** in the presence of different sources of DHQS involved monitoring the fluorine signal of the starting materials and the products by  $^{19}\text{F}$  NMR spectroscopy. The products were confirmed by comparing the splitting pattern and coupling constants between fluorine and the adjacent proton with that of the starting materials. The coupling constant between the equatorial fluorine at C-3 and the equatorial proton at C-4 for (3*R*)-3-fluoro-DAH7P **25** is  $\sim 13.4$  Hz. Similarly the coupling constant between the axial fluorine at C-2 and the equatorial proton at C-3 for (6*R*)-6-fluoro-DHQ **27** is  $\sim 12$  Hz. The coupling constant between the fluorine and the proton sharing the same carbon is  $\sim 50$  Hz for both (3*R*)-3-fluoro-DAH7P **25** and (6*R*)-6-fluoro-DHQ **27** (see figure 4.1). The additional splitting pattern seen in (6*R*)-6-fluoro-DHQ **27** is likely due to long range coupling ( $^4J$ ) between the C-2 fluorine and the C-6 equatorial proton.



The coupling constant between the axial fluorine at C-3 and the axial proton at C-4 for (3*S*)-3-fluoro-DAH7P **28** is ~30 Hz. Similarly the coupling constant between the axial fluorine at C-2 and the axial proton at C-3 for (6*S*)-6-fluoro-DHQ **30** is ~30 Hz and that of 1-*epi*-(6*S*)-6-fluoro-DHQ **31** is ~30 Hz. The coupling constant between the fluorine and the proton sharing the same carbon is ~50 Hz for (3*S*)-3-fluoro-DAH7P **28**, (6*S*)-6-fluoro-DHQ **30**, and 1-*epi*-(6*S*)-6-fluoro-DHQ **31** (see figure 4.2).

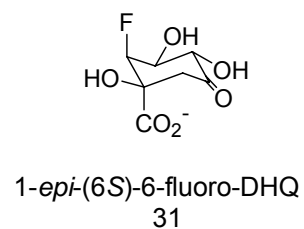
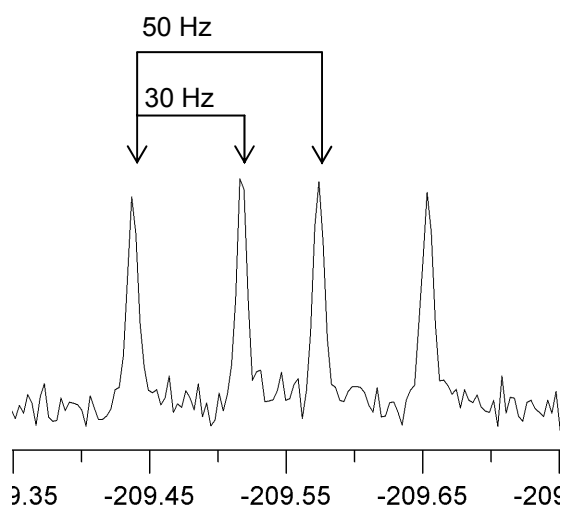
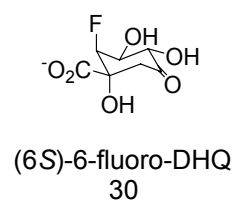
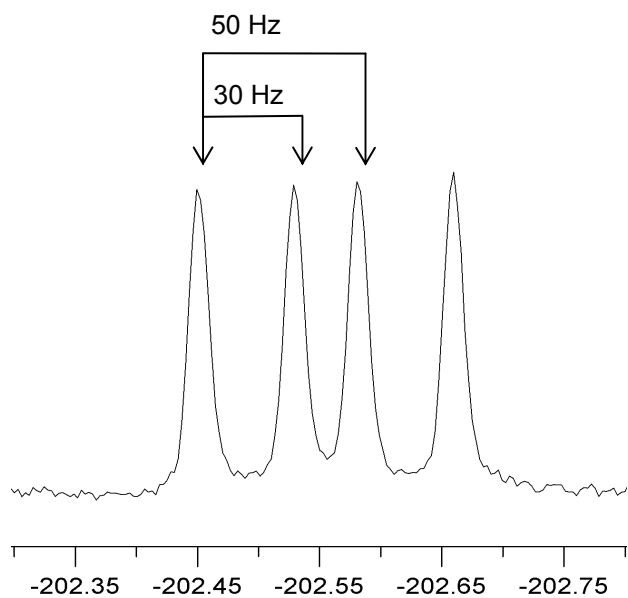
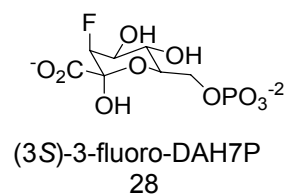
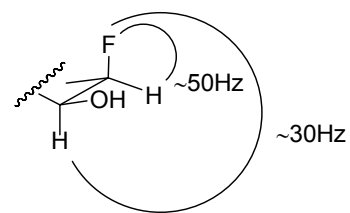
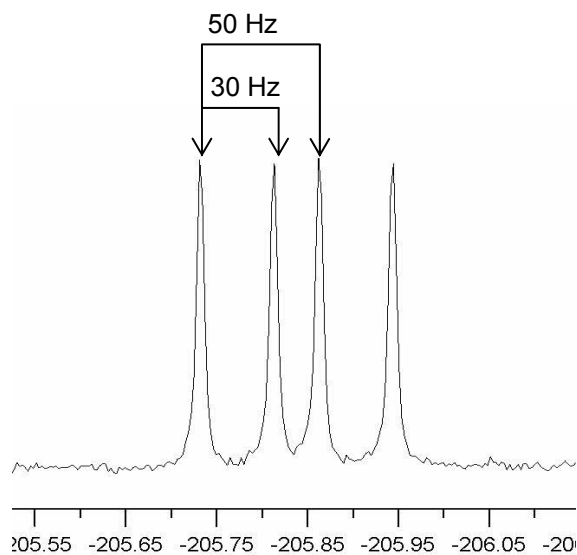


Figure 4.2.  $^{19}\text{F}$  NMR spectra showing coupling constants for (3*S*)-3-fluoro-DAH7P, (6*S*)-6-fluoro-DHQ, and 1-*epi*-(6*S*)-6-fluoro-DHQ.

Of the two fluoro-DHQ products formed by DHQS in the presence of (3*S*)-3-fluoro-DAH7P **28**, only (6*S*)-6-fluoro-DHQ **30** is a substrate for DHQase. Therefore, in the presence of DHQase, (6*S*)-6-fluoro-DHQ **30** is converted to (6*S*)-6-fluoro-DHS **40** while 1-*epi*-(6*S*)-6-fluoro-DHQ **31** remains untouched. To distinguish between (6*S*)-6-fluoro-DHQ **30** and 1-*epi*-(6*S*)-6-fluoro-DHQ **31** by  $^{19}\text{F}$  NMR, the signal from the compound that disappeared in the presence of DHQase was assigned (6*S*)-6-fluoro-DHQ **30** and the remaining signal was assigned 1-*epi*-(6*S*)-6-fluoro-DHQ **31** (see figure 4.3).

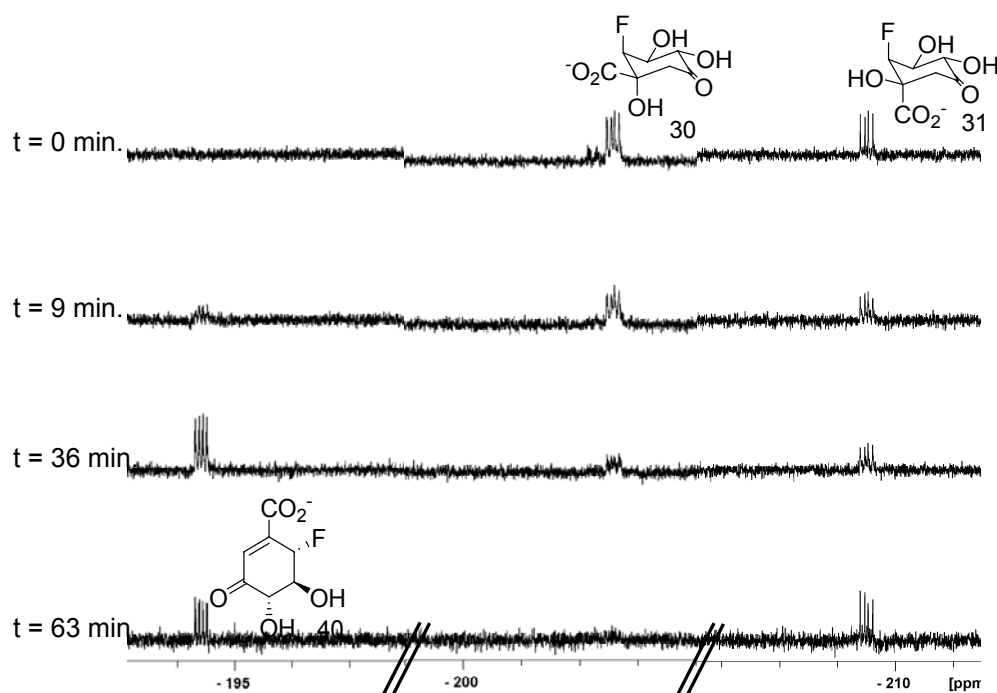


Figure 4.3. Time-course  $^{19}\text{F}$  NMR spectra showing conversion of (6*S*)-6-fluoro-DHQ to (6*S*)-6-fluoro-DHS.

Incubation of (3*R*)-3-fluoro-DAH7P **25** with DHQS from each source of DHQS resulted in the rapid formation of (6*R*)-6-fluoro-DHQ **27** as the sole isomer. The chemical shift of the fluorine signal of (3*R*)-3-fluoro-DAH7P **25** is -198.9 ppm and

the chemical shift of the fluorine signal from (6*R*)-6-fluoro-DHQ **27** is -202.2 ppm (see figure 4.4).

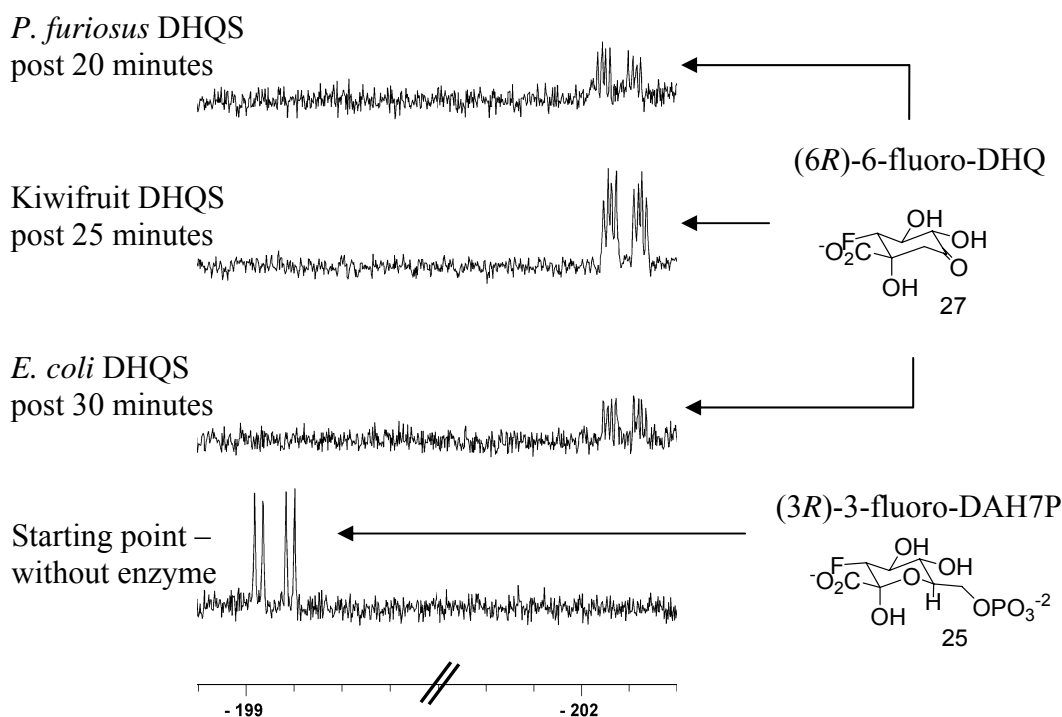


Figure 4.4.  $^{19}\text{F}$  NMR spectra showing formation of (6*R*)-6-fluoro-DHQ by *P. furiosus*, Kiwifruit, and *E. coli* DHQS. Conditions: [(3*R*)-3-fluoro-DAH7P] = 45 mM, [ $\text{Zn}^{2+}$ ] = 50  $\mu\text{M}$ , [ $\text{NAD}^+$ ] = 30  $\mu\text{M}$ , [DHQS] = 0.4 mg/mL, pH = 7, temperature = 25°C.

Incubation of *E. coli* DHQS with (3*S*)-3-fluoro-DAH7P **28** resulted in the formation of 1-*epi*-(6*S*)-6-fluoro-DHQ **31** and (6*S*)-6-fluoro-DHQ **30** at 31 and 68 percent respectively (see figure 4.5). This ratio of products for *E. coli* DHQS is consistent with the observed results by Parker and co-workers.<sup>27</sup> These products are diastereomers of each other and their fluorine signals have distinct chemical shifts. The chemical shift of the fluorine in 1-*epi*-(6*S*)-6-fluoro-DHQ **31** is -209.5 ppm and the fluorine signal of (6*S*)-6-fluoro-DHQ **30** is -202.6 ppm.

This reaction of (3*S*)-3-fluoro-DAH7P **28** did not go to completion and hence the fluorine signal of the starting material can be seen at -205.9 ppm in the final spectrum (~87% complete). Over the time that the reaction was monitored, the ratio of the two products was the same. It is suspected that the reason why the reaction did not go to completion was likely due to loss of enzyme activity over the time period of the assay.

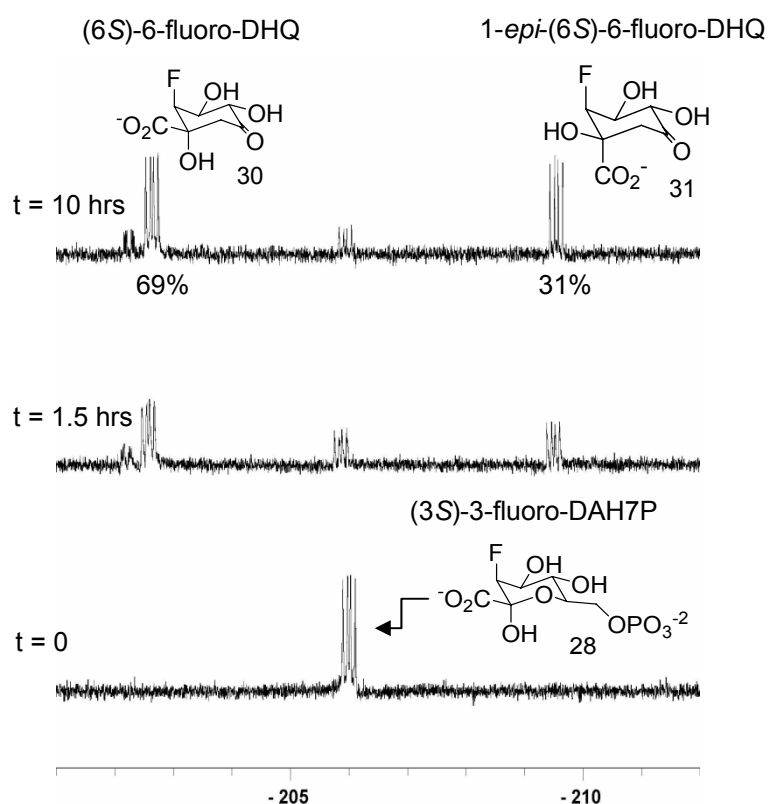


Figure 4.5.  $^{19}\text{F}$  NMR spectra showing partitioning of (3*S*)-3-fluoro-DAH7P to (6*S*)-6-fluoro-DHQ and 1-*epi*-(6*S*)-6-fluoro-DHQ by *E. coli* DHQS. Conditions: [(3*S*)-3-fluoro-DAH7P] = 45 mM, [ $\text{Zn}^{2+}$ ] = 50  $\mu\text{M}$ , [ $\text{NAD}^+$ ] = 30  $\mu\text{M}$ , [DHQS] = 0.4 mg/mL, pH = 7, temperature = 25°C.

Incubation of Kiwifruit DHQS with (3*S*)-3-fluoro-DAH7P **28** resulted in the formation of 1-*epi*-(6*S*)-6-fluoro-DHQ **31** and (6*S*)-6-fluoro-DHQ **30** at 7 and 93 percent respectively (see figure 4.6). In contrast to what was seen with DHQS from a bacterial source, Kiwifruit DHQS produces 24 percent less of 1-*epi*-(6*S*)-6-fluoro-

DHQ **31** than what was observed with *E. coli* DHQS. The reaction went to ~40% completion.

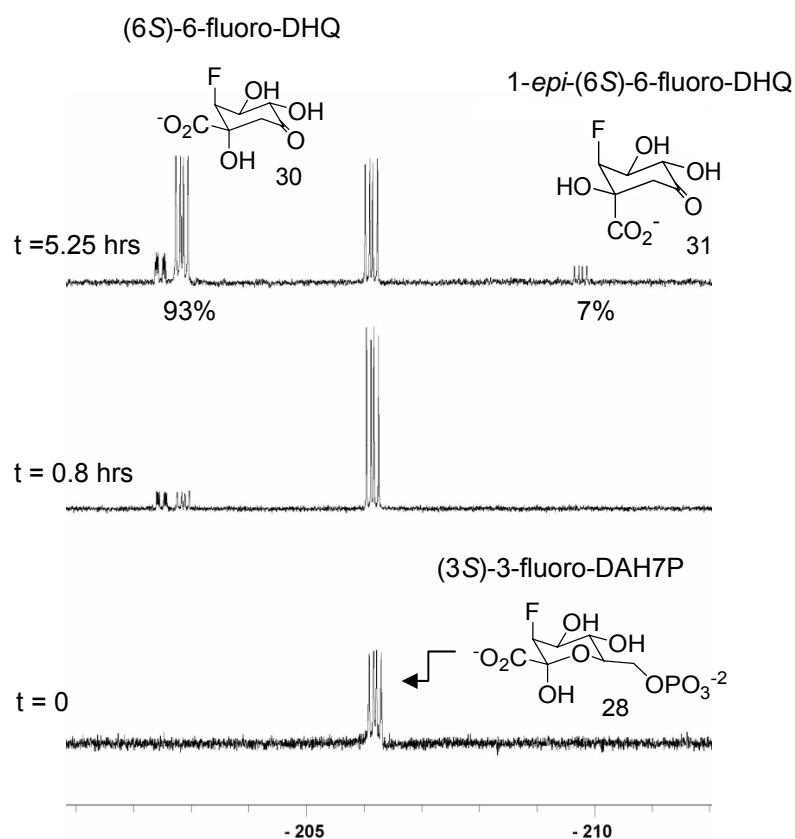


Figure 4.6.  $^{19}\text{F}$  NMR spectra showing partitioning of (3*S*)-3-fluoro-DAH7P to (6*S*)-6-fluoro-DHQ and 1-*epi*-(6*S*)-6-fluoro-DHQ by Kiwifruit DHQS. Conditions: [(3*S*)-3-fluoro-DAH7P] = 45 mM, [ $\text{Zn}^{2+}$ ] = 50  $\mu\text{M}$ , [ $\text{NAD}^+$ ] = 30  $\mu\text{M}$ , [DHQS] = 0.4 mg/mL, pH = 7, temperature = 25°C.

Contrary to what was observed with *E. coli* DHQS and Kiwifruit DHQS, incubation of *P. furiosus* DHQS with (3*S*)-3-fluoro-DAH7P **28** resulted in the formation of (6*S*)-6-fluoro-DHQ **30** exclusively; no 1-*epi*-(6*S*)-6-fluoro-DHQ **31** was observed (see figure 4.7). The reaction went to ~40% completion.



in the partitioning experiment at 50°C is due to *P. furiosus* DHQS and not a factor of decomposition (see figure 4.8).

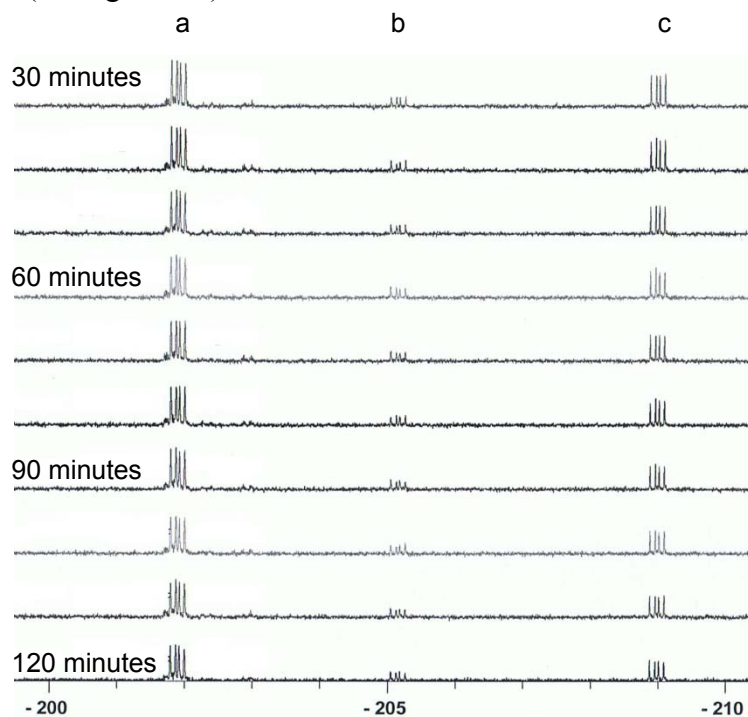


Figure 4.8.  $^{19}\text{F}$  NMR spectra showing stability of 1-*epi*-(6*S*)-6-fluoro-DHQ at 50°C; a). (6*S*)-6-fluoro-DHQ, b). (3*S*)-3-fluoro-DAH7P, c). 1-*epi*-(6*S*)-6-fluoro-DHQ. Conditions: [(6*S*)-6-fluoro-DHQ] = ~31 mM, [1-*epi*-(6*S*)-6-fluoro-DHQ] = ~14 mM, pH = 7, temperature = 50°C.

These results indicate that there are large differences in the proportion of epimer to non-epimer formed for each source of DHQS when incubated with (3*S*)-3-fluoro-DAH7P **28** (see table 8).

Table 8.

$^{19}\text{F}$  NMR partitioning results for *E. coli* DHQS, Kiwifruit DHQS, and *P. furiosus* DHQS incubated with (3*S*)-3-fluoro-DAH7P

Enzyme	Products formed				Ratio of products
	(6 <i>S</i> )-6-fluoro-DHQ		1- <i>epi</i> -(6 <i>S</i> )-6-fluoro-DHQ		
	% formed	Yield (mmol)	% formed	Yield (mmol)	
<i>E. coli</i> DHQS	69%	0.027	31%	0.012	2:1
Kiwifruit DHQS	93%	0.017	7%	0.0013	13:1
<i>P. furiosus</i> DHQS	100%	0.018	0%	0.0	---

### 4.3 Kinetic experiments

Steady-state kinetics for *E. coli* DHQS, Kiwifruit DHQS, and *P. furiosus* DHQS were determined using DAH7P **3**, (3*S*)-3-fluoro-DAH7P **28**, and (3*R*)-3-fluoro-DAH7P **25**. The data were fitted to Michaelis-Menten and Lineweaver-Burk plots to determine the  $K_M$  and  $k_{cat}$  values (see figures 4.9, 4.10, and 4.11).

Overall, the affinities for (3*S*)-3-fluoro-DAH7P **28** of all three DHQS enzymes were lower than those for DAH7P **3** and (3*R*)-3-fluoro-DAH7P **25**. However, when comparing across the three enzymes, the affinity of (3*S*)-3-fluoro-DAH7P **28** was greatest for *P. furiosus* DHQS. The affinity of (3*R*)-3-fluoro-DAH7P **25** for each of the enzymes was similar to that of DAH7P **3**. The specificity constant of (3*S*)-3-fluoro-DAH7P **28** for each of the each of the enzymes was reduced compared to that of DAH7P and (3*R*)-3-fluoro-DAH7P **25**. Similarly, the specificity constant of (3*R*)-3-fluoro-DAH7P **25** for *E. coli* and kiwifruit DHQS was also reduced when compared to that of DAH7P **3**. In contrast, the specificity constant of (3*R*)-3-fluoro-DAH7P **25** for *P. furiosus* DHQS was greater than that of DAH7P **3** (see table 9).

Table 9.

Steady-state kinetics for *E. coli* DHQS, Kiwifruit DHQS, and *P. furiosus* DHQS

Enzyme	Substrate	$K_M$ ( $\mu\text{M}$ )	$k_{\text{cat}}$ ( $\text{sec}^{-1}$ )	$k_{\text{cat}}/K_M$ ( $\mu\text{M}^{-1} \text{sec}^{-1}$ )
<i>E. coli</i> DHQS	DAH7P	$6.3 \pm 0.2$	$16.0 \pm 0.2$	2.5
	(3 <i>S</i> )-3-fluoro-DAH7P	$64 \pm 4$	$12.0 \pm 0.2$	0.2
	(3 <i>R</i> )-3-fluoro-DAH7P	$3.6 \pm 0.1$	$2.500 \pm 0.004$	0.7
Kiwifruit DHQS	DAH7P	$3.2 \pm 0.2$	$0.500 \pm 0.004$	0.2
	(3 <i>S</i> )-3-fluoro-DAH7P	$64 \pm 2$	$0.900 \pm 0.006$	0.01
	(3 <i>R</i> )-3-fluoro-DAH7P	$8.7 \pm 0.5$	$0.300 \pm 0.001$	0.04
<i>P. furiosus</i> DHQS	DAH7P	$3.7 \pm 0.2$	$3.00 \pm 0.06$	0.8
	(3 <i>S</i> )-3-fluoro-DAH7P	$29 \pm 1$	$1.30 \pm 0.01$	0.04
	(3 <i>R</i> )-3-fluoro-DAH7P	$2.0 \pm 0.2$	$3.30 \pm 0.01$	1.6

Figure 4.9.

Michaelis-Menten and Lineweaver-Burk plots for: a) DAH7P, b) (3*S*)-3-fluoro-DAH7P, and c) (3*R*)-3-fluoro-DAH7P incubated with *E. coli* DHQS.

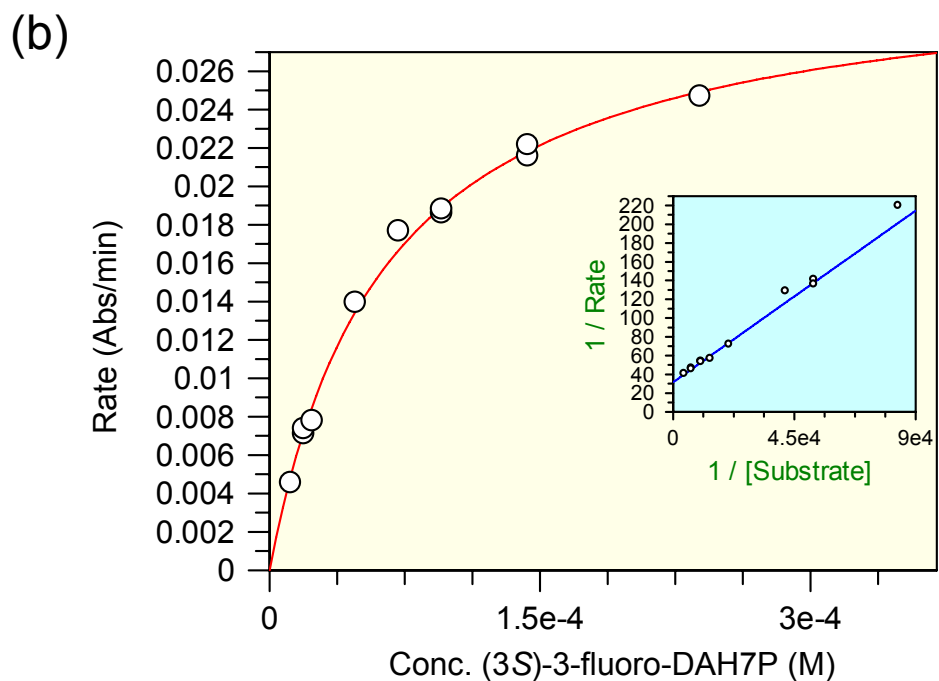
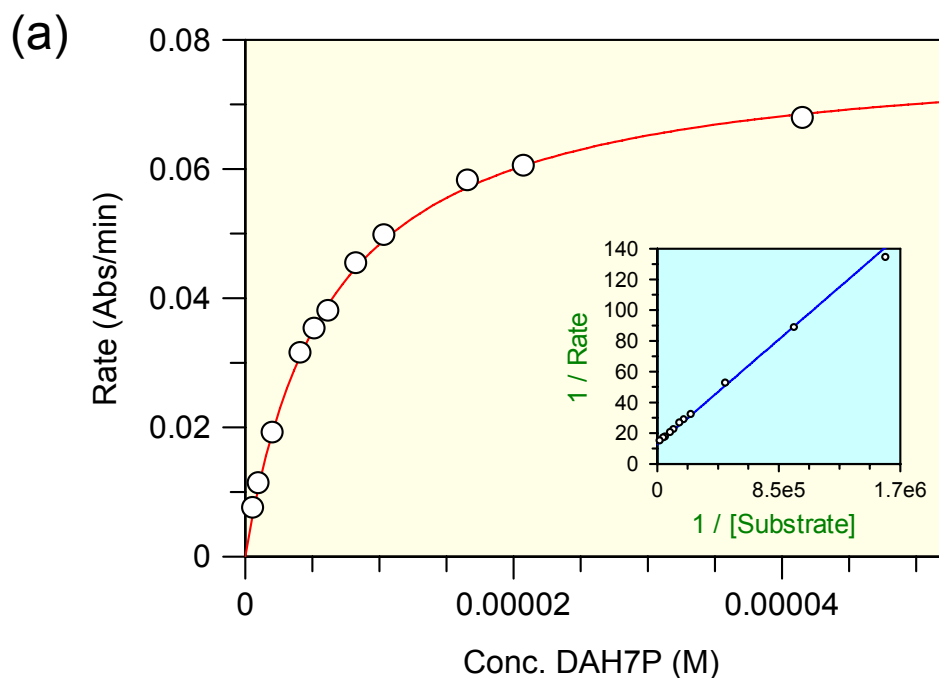
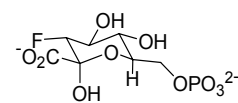
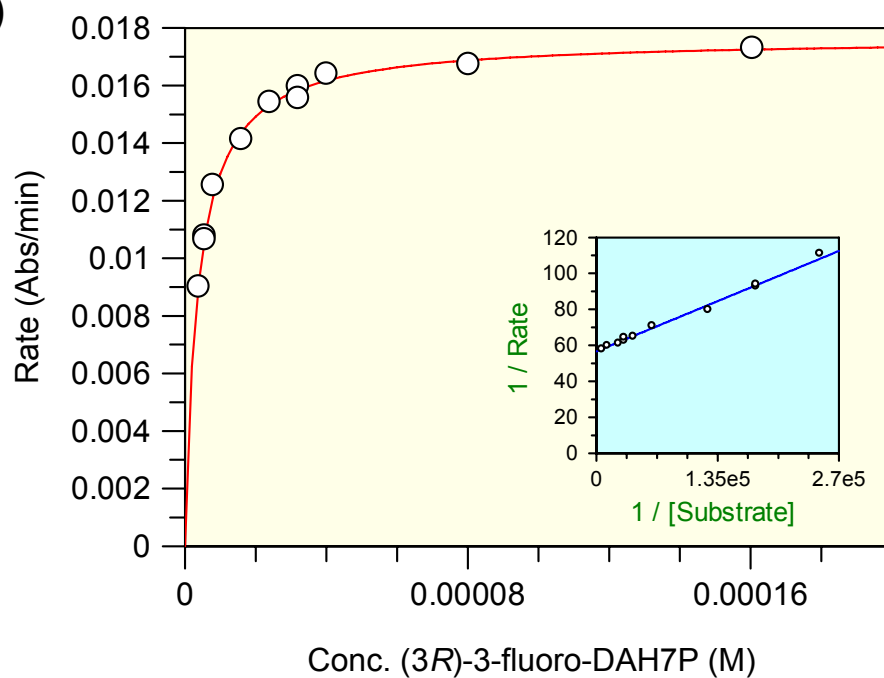


Figure 4.9. (continued)

Michaelis-Menten and Lineweaver-Burk plots for: a) DAH7P, b) (3*S*)-3-fluoro-DAH7P, and c) (3*R*)-3-fluoro-DAH7P incubated with *E. coli* DHQS.

(c)

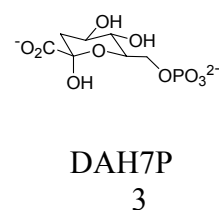
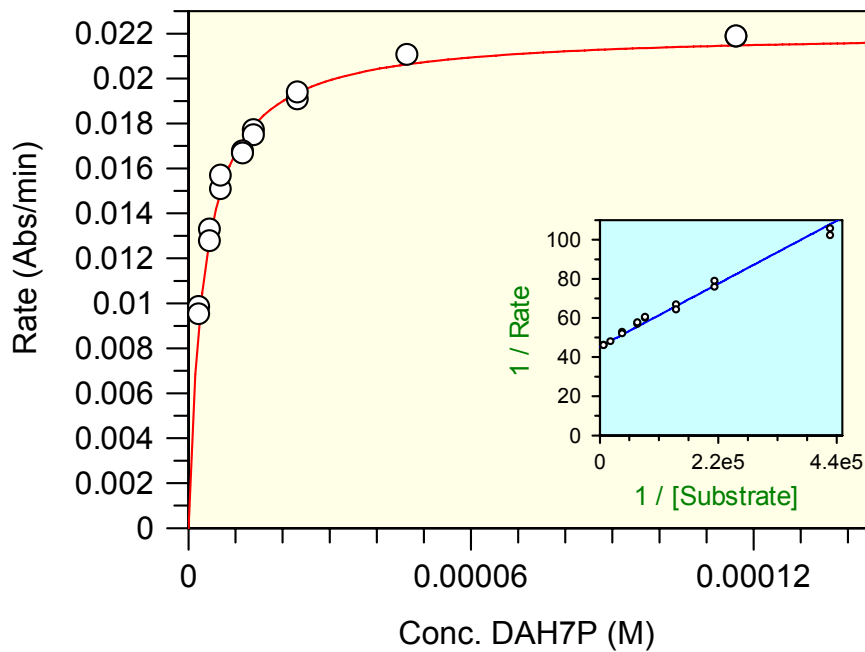


(3*R*)-3-fluoro-DAH7P  
25

Figure 4.10.

Michaelis-Menten and Lineweaver-Burk plots for: a) DAH7P, b) (3*S*)-3-fluoro-DAH7P, and c) (3*R*)-3-fluoro-DAH7P incubated with Kiwifruit DHQS.

(a)



(b)

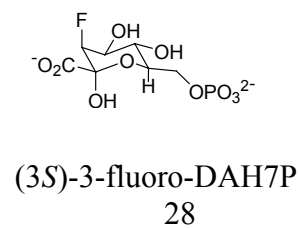
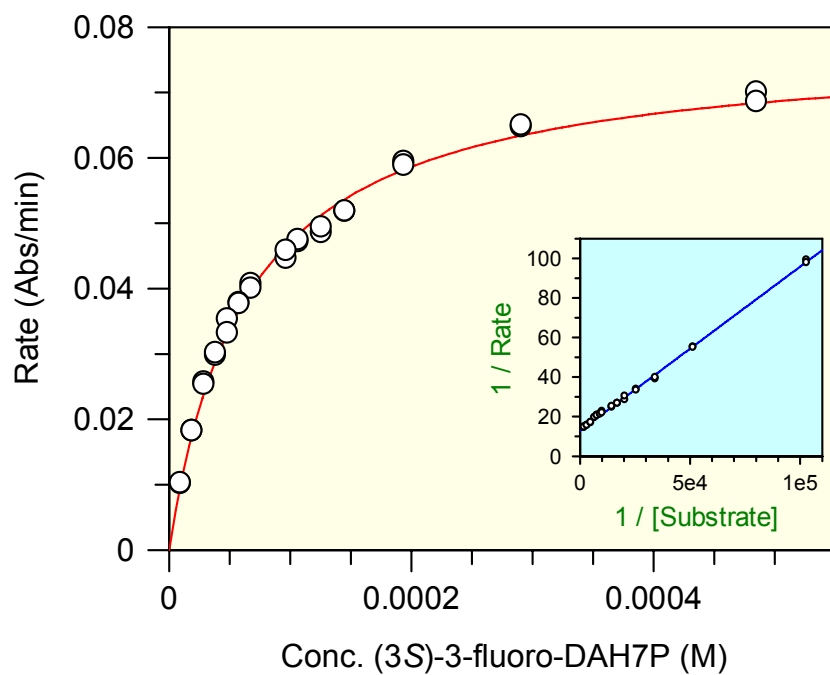
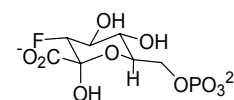
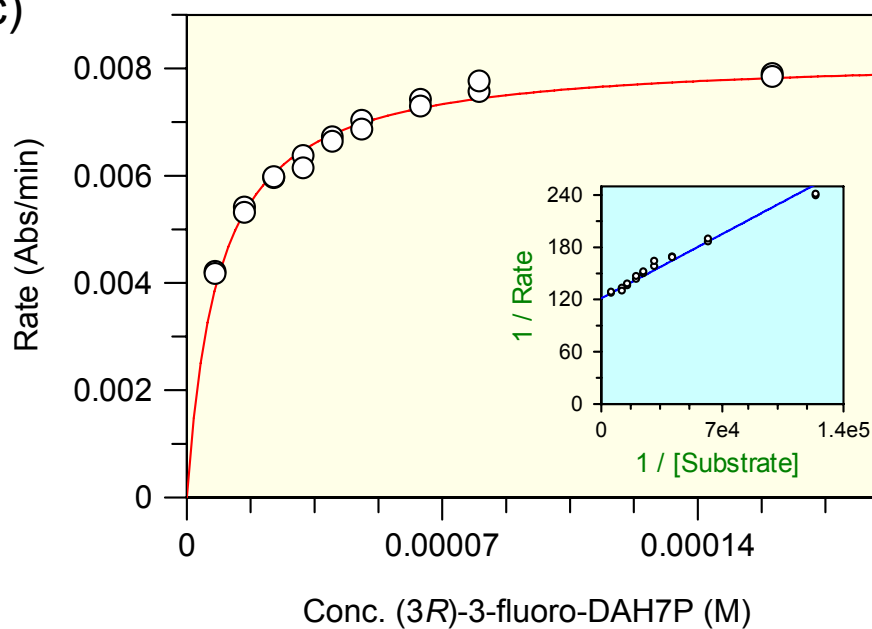


Figure 4.10. (continued)

Michaelis-Menten and Lineweaver-Burk plots for: a) DAH7P, b) (3*S*)-3-fluoro-DAH7P, and c) (3*R*)-3-fluoro-DAH7P incubated with Kiwifruit DHQS.

(c)

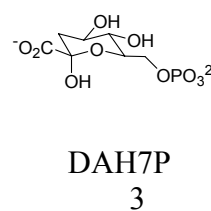
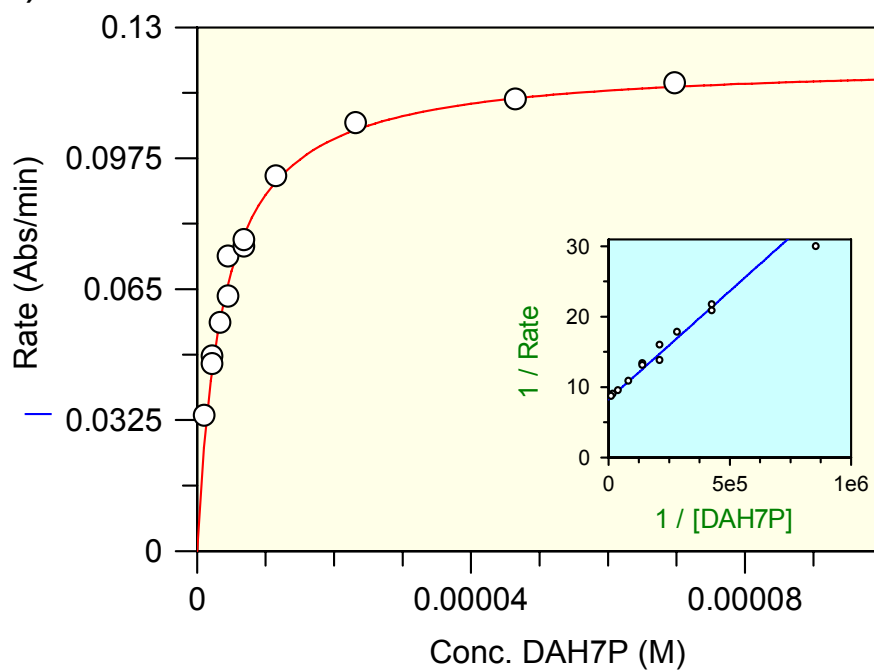


(3*R*)-3-fluoro-DAH7P  
25

Figure 4.11.

Michaelis-Menten and Lineweaver-Burk plots for: a) DAH7P, b) (3*S*)-3-fluoro-DAH7P, and c) (3*R*)-3-fluoro-DAH7P incubated with *P. furiosus* DHQS.

(a)



(b)

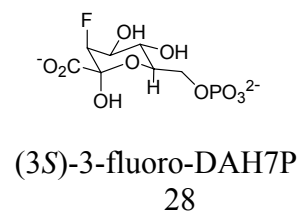
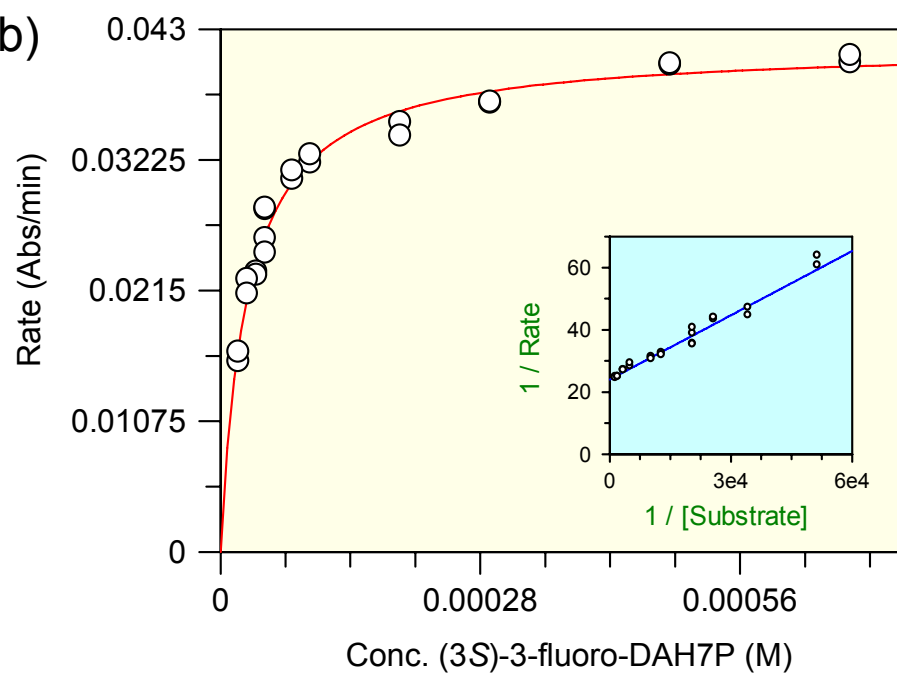
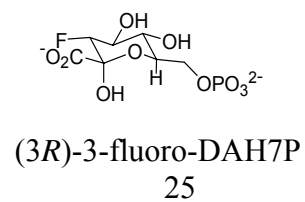
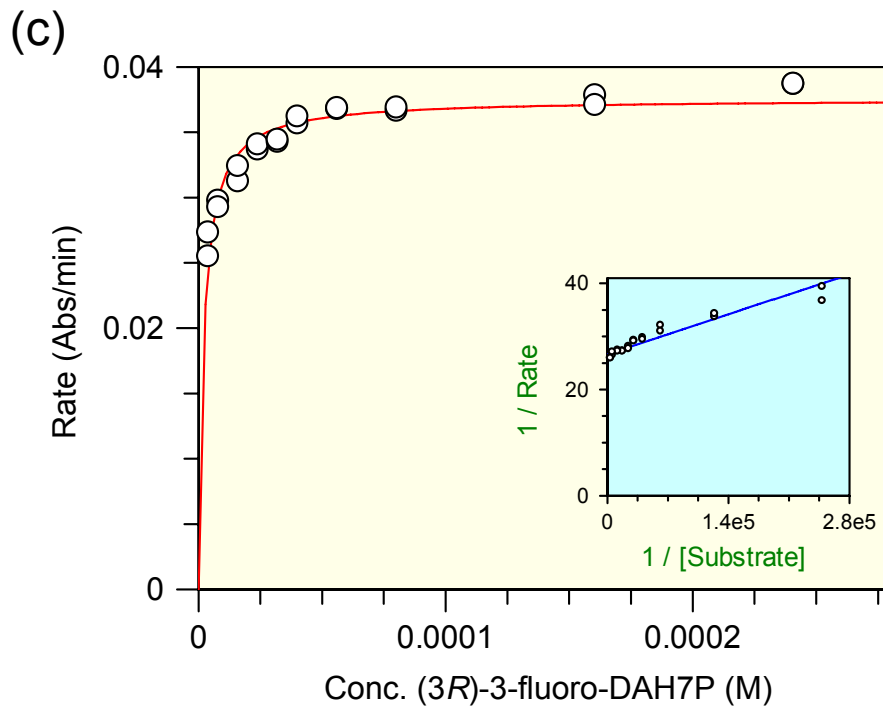


Figure 4.11. (continued)

Michaelis-Menten and Lineweaver-Burk plots for: a) DAH7P, b) (3*S*)-3-fluoro-DAH7P, and c) (3*R*)-3-fluoro-DAH7P incubated with *P. furiosus* DHQS.



### 4.3.1 Issues pertaining to the kinetic results

There appears to be a discrepancy with the kinetics assay using *E. coli* DHQS and DAH7P **3**. A comparison of the findings in this thesis with that of Parker and co-workers, showed similar trends in the  $k_{\text{cat}}$  and  $K_M$  although Parker's results had indicated greater differences between (3*S*)-3-fluoro-DAH7P **28** and (3*R*)-3-fluoro-DAH7P **25** in the kinetics of *E. coli* DHQS. The results in this thesis showed that the  $k_{\text{cat}}$  of *E. coli* DHQS for DAH7P **3** was only slightly greater than that of (3*S*)-3-fluoro-DAH7P **28**. Parker's results showed a 50-fold difference in the  $k_{\text{cat}}$  between DAH7P **3** and (3*S*)-3-fluoro-DAH7P **28** in the presence of *E. coli* DHQS ( $k_{\text{cat}}$  50 s<sup>-1</sup> and 0.9 s<sup>-1</sup> respectively).

In order to check that the assay was working correctly, several trials were done. It was thought originally that the *E. coli* DHQase may be limiting the rate of formation of DHS rather than the *E. coli* DHQS. Attempts were made to increase the concentration of *E. coli* DHQase in order to circumvent this problem. However, using high concentrations of *E. coli* DHQase resulted in high background noise. *E. coli* DHQase was further purified in order to raise the signal-to-noise ratio. Despite the increased concentration of *E. coli* DHQase the results were still showing small differences in the  $k_{\text{cat}}$  values for DAH7P **3** and (3*S*)-3-fluoro-DAH7P **28** for *E. coli* DHQS.

All the reagents and the buffer required for the reaction were prepared again. However, this too had no significant effect on the results. In order to determine if something was interfering with the production of DHS **5**, the extinction coefficient of DHS was determined using *E. coli* DHQS and compared with the published extinction coefficient of DHS **5** ( $\epsilon = 1.2 \times 10^4 \text{ M}^{-1} \text{ cm}^{-1}$ ). This was done by measuring the total

absorbance of DHS **5** generated by the coupled enzyme assay in the presence of a known amount of DAH7P **3**. The extinction coefficient of DHS **5** was back-calculated using Beer's Law. The recalculated extinction coefficient of DHS **5** was found to be  $9880 \text{ M}^{-1} \text{ cm}^{-1}$ , which could suggest that not all of the substrate was converted to the final product by the enzyme.

It was suspected that  $\text{NAD}^+$ , which was added to the enzyme for stability during the purification protocol, was causing an inhibitory effect on the enzyme.  $\text{NAD}^+$  decomposes over time and is likely to inhibit DHQS.<sup>41,42</sup> Despite this finding, the kinetic results for Kiwifruit DHQS experienced a similar fate to *E. coli* DHQS, despite the enzyme being washed with buffer to remove residual  $\text{NAD}^+$ . Therefore, it is possible that an unknown contaminant was affecting the kinetic results for *E. coli* DHQS and Kiwifruit DHQS.

#### **4.4 Partitioning experiments using UV spectroscopy**

As a comparison to the  $^{19}\text{F}$  NMR spectroscopic partitioning results, the amounts of (6*S*)-6-fluoro-DHQ **30** formed from (3*S*)-3-fluoro-DAH7P **28** in the presence of each source of DHQS was measured. A coupled enzyme assay that incorporates DHQase was used to convert (6*S*)-6-fluoro-DHQ **30** to (6*S*)-6-fluoro-dehydroshikimate **40** ((6*S*)-6-fluoro-DHS) and measure the total change in absorbance using UV spectrophotometry. In this assay only (6*S*)-6-fluoro-DHS **40** can be measured because 1-*epi*-(6*S*)-6-fluoro-DHQ **31** is not a substrate for DHQase (see figure 4.12).

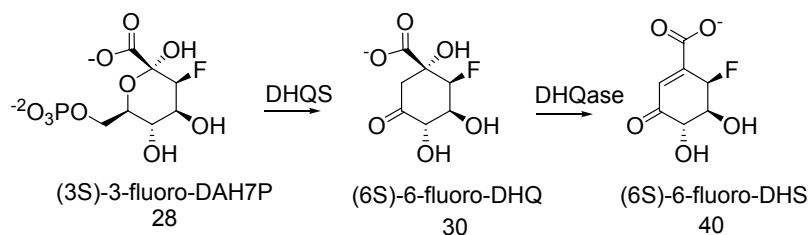


Figure 4.12. Schematic of the formation of (6S)-6-fluoro-DHS from (3S)-3-fluoro-DAH7P using DHQS and DHQase

Unfortunately, initial trials with *E. coli* DHQS and Kiwifruit DHQS resulted in a biphasic curve that made it difficult to determine when the reaction had gone to completion. Furthermore, it was unclear if the secondary curve was being formed by a contaminant that was likely contributing to the total absorbance. Given the discrepancy in the assay it was decided not to use the results from these experiments.

#### 4.4.1 Stability of (6S)-6-fluoro-DHS

One possible explanation for the difficulties encountered with this partitioning experiment could have been due to the stability of (6S)-6-fluoro-DHS **40**. To test this, (6S)-6-fluoro-DHQ **30** was placed in an NMR tube in the presence of *E. coli* DHQase and the formation of (6S)-6-fluoro-DHS **40** was monitored. After 30 minutes most of the dehydroquinone starting material was converted to (6S)-6-fluoro-DHS **40**. The chemical shift of the fluorine in (6S)-6-fluoro-DHS **40** is -193.6 ppm (see figure 4.13).

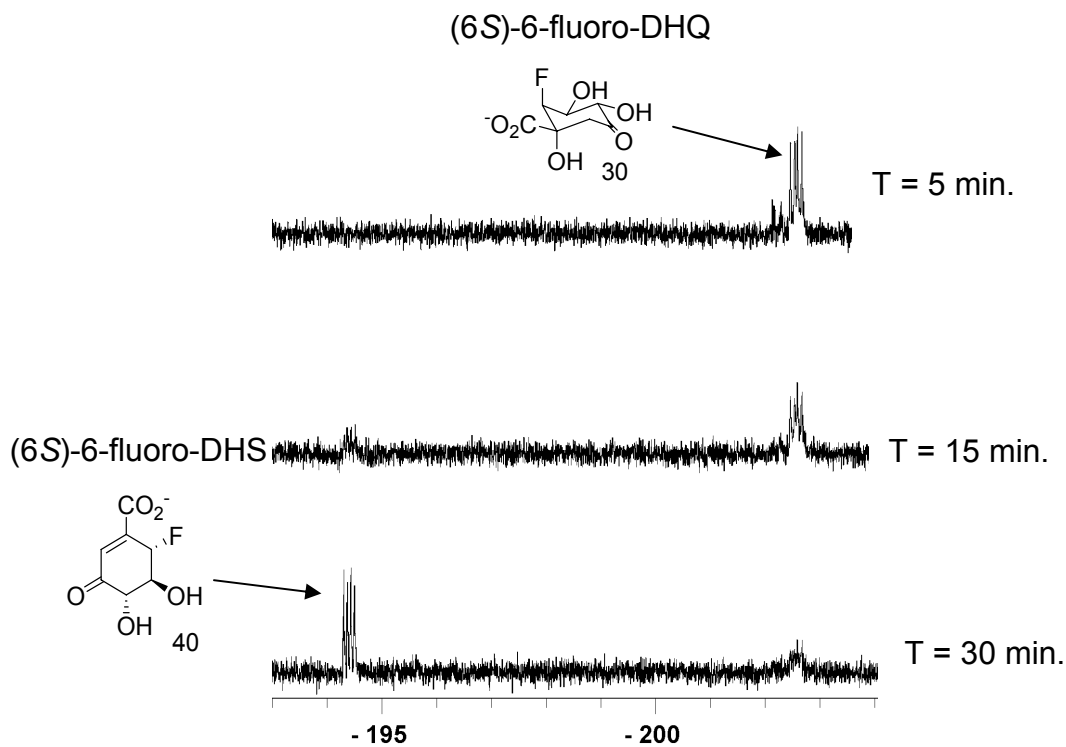


Figure 4.13.  $^{19}\text{F}$  NMR spectrum showing formation of (6*S*)-6-fluoro-DHS from (6*S*)-6-fluoro-DHQ using *E. coli* DHQase. Conditions: [(6*S*)-6-fluoro-DHQ] = ~31 mM, [DHQase] = 0.4 mg/mL, pH = 7, temperature = 25°C.

The product can be confirmed by comparing the coupling constants of (6*S*)-6-fluoro-DHS **40** with those of (6*S*)-6-fluoro-DHQ **30**. The coupling constant between the fluorine and the proton sharing the same carbon is ~50 Hz for (6*S*)-6-fluoro-DHQ **30** and (6*S*)-6-fluoro-DHS **40** (see figure 4.14).

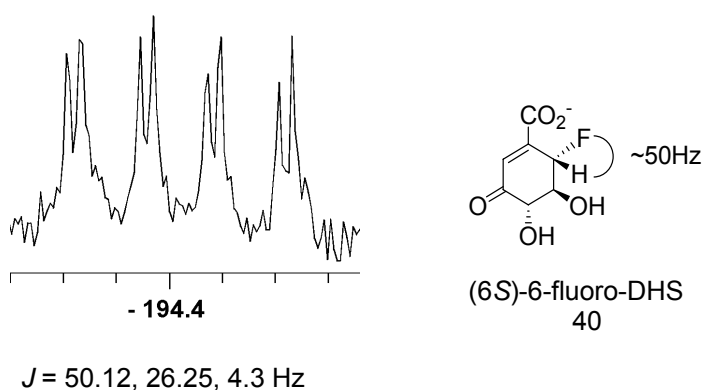


Figure 4.14.  $^{19}\text{F}$  NMR spectrum showing coupling pattern of (6*S*)-6-fluoro-DHS.

The enzyme was removed and the product was allowed to sit in the NMR tube for several days at room temperature. It was found that most of (6*S*)-6-fluoro-DHS **40** decomposes after five days (less than 5 % remaining).  $^{19}\text{F}$  NMR spectroscopy showed a gradual disappearance of the fluorine signal from (6*S*)-6-fluoro-DHS **40** (see figure 4.15).

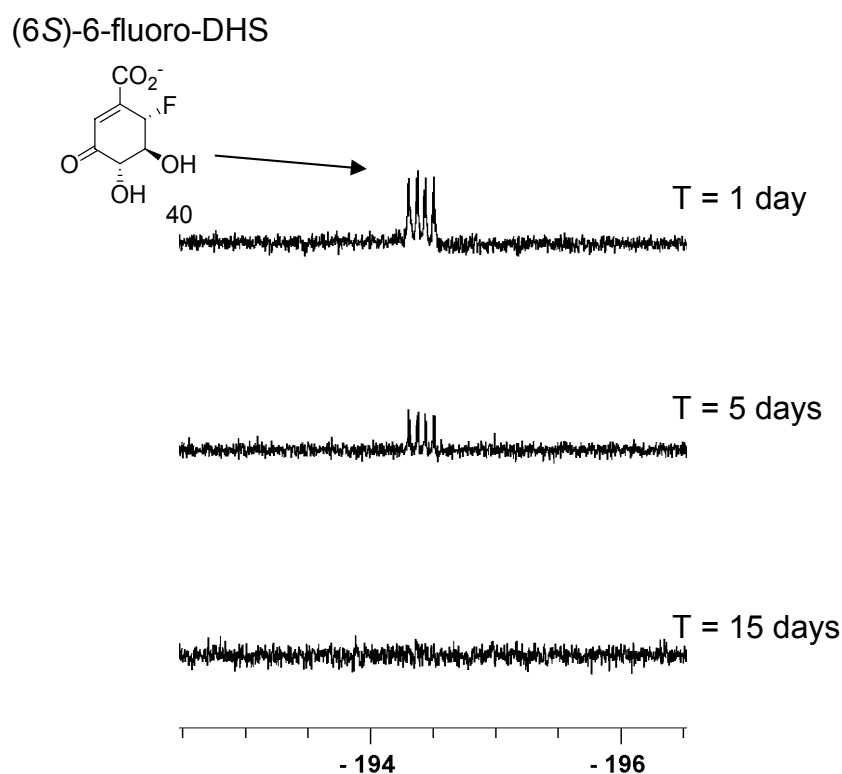


Figure 4.15. Time-course  $^{19}\text{F}$  NMR spectra monitoring the degradation of (6*S*)-6-fluoro-dehydroshikimate over 15 days. Conditions: [(6*S*)-6-fluoro-DHS] = ~31 mM, pH = 7, temperature = 25°C.

Closer inspection of the breakdown product via  $^1\text{H}$  NMR spectroscopy showed the presence of a substituted benzene similar to 1,2,4-benzenetriol (see figure 4.16). Both benzene compounds share the same splitting pattern; however, the chemical shifts of the proton peaks are different.

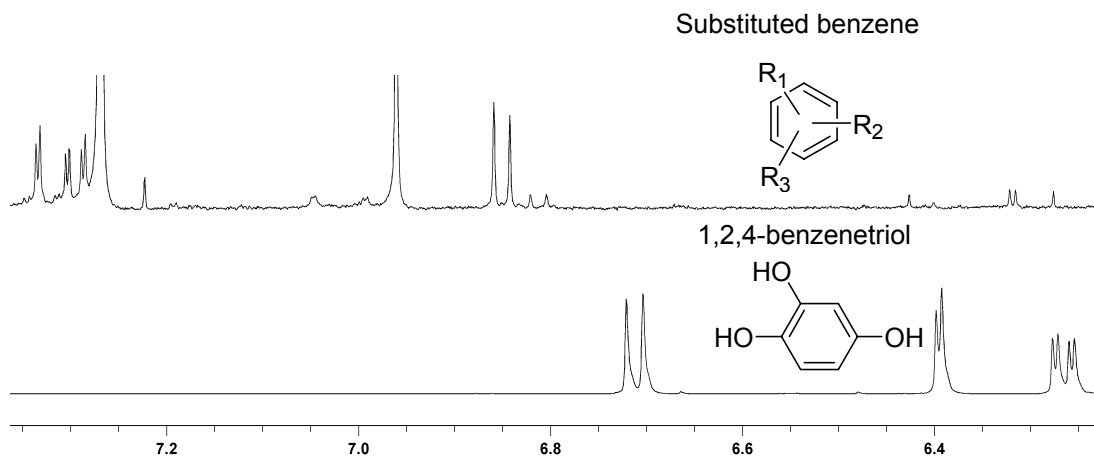


Figure 4.16. Proton NMR spectra of a substituted benzene and 1,2,4-benzenetriol.

Despite these differences, the lack of formation of a fluorine product from the degradation of (6*S*)-6-fluoro-DHS **40**, and the appearance of an aromatic breakdown product could explain the biphasic curve seen during the UV partitioning assay as explained in section 4.4 (see figure 4.17).

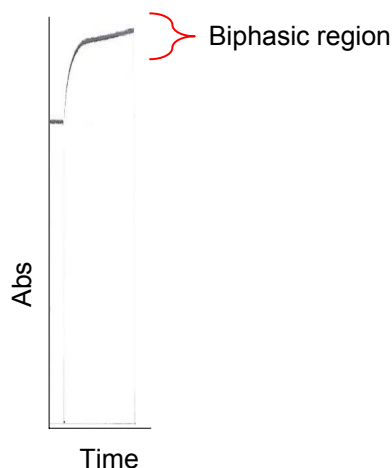


Figure 4.17. (3*S*)-3-Fluoro-DAH7P UV partitioning experiment showing the biphasic curve. [(3*S*)-3-fluoro-DAH7P] = 100  $\mu\text{M}$ , [ $\text{Zn}^{2+}$ ] = 100  $\mu\text{M}$ , [ $\text{NAD}^+$ ] = 29  $\mu\text{M}$ , [DHQS] = 0.03  $\mu\text{M}$ , [DHQase] = 1  $\mu\text{M}$ , pH = 7, temperature = 25°C at 230 nm.

It is suspected that a small amount of the aromatic breakdown product is being formed during the coupled enzyme assay. Since substituted aromatics such as quinines have

large extinction coefficients, even a very low concentration of a substituted benzene by-product would be sufficient to alter the UV signal resulting in a biphasic curve during the partitioning experiment.

#### 4.5 Discussion

The observed partitioning results for *E. coli* DHQS, Kiwifruit DHQS and *P. furiosus* DHQS when incubated with (3*R*)-3-fluoro-DAH7P **25** showed the formation of (6*R*)-6-fluoro-DHQ **27** as the sole product in all the three cases (see figure 4.18).

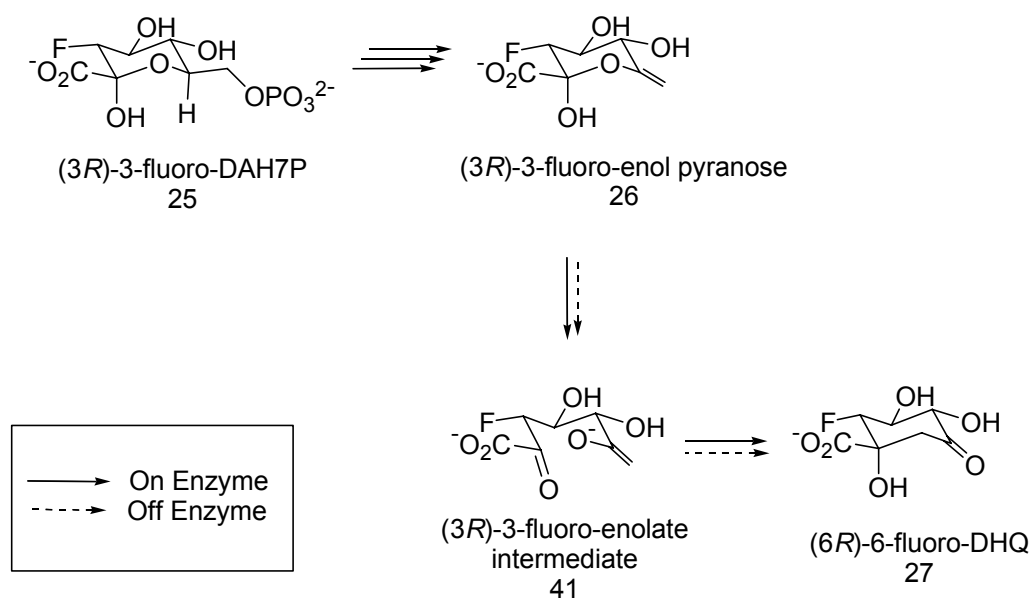


Figure 4.18. Schematic of product formed from (3*R*)-3-fluoro-DAH7P in the presence of *E. coli* DHQS, Kiwifruit DHQS and *P. furiosus* DHQS

Steady-state kinetics showed that all three sources of DHQS have a similar affinity for (3*R*)-3-fluoro-DAH7P **25** as they do for DAH7P **3**. It is likely that the equatorial fluorine on (3*R*)-3-fluoro-DAH7P **25** is having little effect on the binding of the substrate to the enzyme. Based on the Felkin-Anh model, the predicted transition-state for the enzyme-catalysed cyclisation of the (3*R*)-3-fluoro-enolate intermediate **41**

places the fluoro substituent on C-3 pointing away from the direction of attack of the internal nucleophile at C-7. This conformation is electronically favourable because the fluorine is placed orthogonal to the carbonyl and anti to the direction of attack (see figure 4.19).

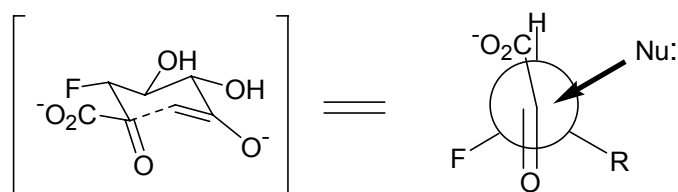


Figure 4.19. Proposed transition-state conformation of the on-enzyme cyclisation of the (3*R*)-3-fluoro-enolate intermediate. Newman projection showing fluorine pointing away from the angle of attack of the incoming nucleophile.

These results could suggest that (6*R*)-6-fluoro-DHQ **27** is formed on the enzyme. However, an alternative pathway to the formation of (6*R*)-6-fluoro-DHQ **27** is also possible if the (3*R*)-3-fluoro-enol pyranose **26** is released into solution. It has been suggested that the solution transition-state conformation for the cyclisation of the (3*R*)-3-fluoro-enolate intermediate **41** is favoured by the Felkin-Anh model, and subsequently the exclusive formation of (6*R*)-6-fluoro-DHQ **27** can occur in solution.<sup>22,27</sup> Therefore, the observed results with (3*R*)-3-fluoro-DAH7P **25** cannot report on whether there is leakage (full or partial) from the enzyme given the likelihood that the lowest energy solution transition-state is the same as the predicted enzymatic transition-state (see figure 4.20).

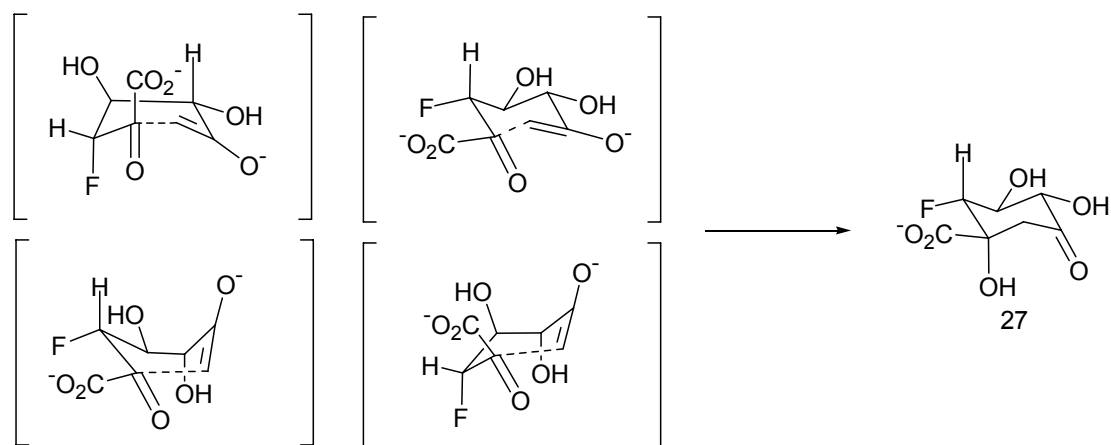


Figure 4.20. Possible transition-state conformations of the off-enzyme cyclisation of the open ring (3*R*)-3-fluoro-enolate intermediate

The initial observation of the partitioning results for *E. coli* DHQS when incubated with (3*S*)-3-fluoro-DAH7P **28** lead to the explanation that the (3*S*)-3-fluoro-enol pyranose **29** was dissociating completely from the enzyme and subsequently cyclising in solution to form the two carbacycle products. An alternate explanation of the partitioning results is that there is partial leakage of the (3*S*)-3-fluoro-enol pyranose **29** from the enzyme as opposed to complete dissociation and subsequently only the released intermediate leads to the formation of the epimerised carbacycle. Given the constraints that the enzymatic template imposes on the substrate, only (6*S*)-6-fluoro-DHQ **30** and not 1-*epi*-(6*S*)-6-fluoro-DHQ **31** would be expected to form on the enzyme. Therefore, two possible explanations are that the (3*S*)-3-fluoro-enol pyranose **29** is fully released and cyclisation in solution gives rise to (6*S*)-6-fluoro-DHQ **30** and 1-*epi*-(6*S*)-6-fluoro-DHQ **31** or there is partial leakage of the (3*S*)-3-fluoro-enol pyranose and cyclisation in solution gives rise to 1-*epi*-(6*S*)-6-fluoro-DHQ **31**. The results in this thesis attempt to provide evidence in support of the partial leakage of intermediate from the enzyme.

The strategy was to test the fate of (3*S*)-3-fluoro-DAH7P **28** across three phylogenetically distinct sources of DHQS and observe the ratio of products formed to cast light on the molecular mechanisms. If the product ratio of the *E. coli* DHQS catalysed reaction arises because of complete release of the intermediate from the enzyme, then we would expect to see no difference in the ratio of products formed across all three enzymes as a result of the cyclisation occurring in solution. However, the results showed that the ratio of products formed across all three sources of DHQS were in fact very different (see figure 4.21). Both partitioning assays for *E. coli* DHQS and Kiwifruit DHQS were done in similar environments and at the same temperature; however, the observed results showed different ratios of diastereomers formed for each enzyme. More interesting is the result from *P. furiosus* DHQS where only one product was formed. In this case all conditions were the same except that the reaction was done at a higher temperature (50°C).

Based on the observations of the partitioning assays, it is unlikely that both diastereomers are formed in solution. In fact, the best explanation for the differences in the amount of epimer produced is that the enzyme was involved in the formation of at least one of the products, this being (6*S*)-6-fluoro-DHQ **30**. Therefore, the differences in the ratio of products formed from (3*S*)-3-fluoro-DAH7P **28** when comparing *E. coli* DHQS, Kiwifruit DHQS, and *P. furiosus* DHQS strongly suggest that the cyclisation occurs in part on the enzyme and that the epimeric product arises only by an abortive reaction pathway where the (3*S*)-3-fluoro-enol pyranose **29** is prematurely released and allowed to cyclise free in solution.

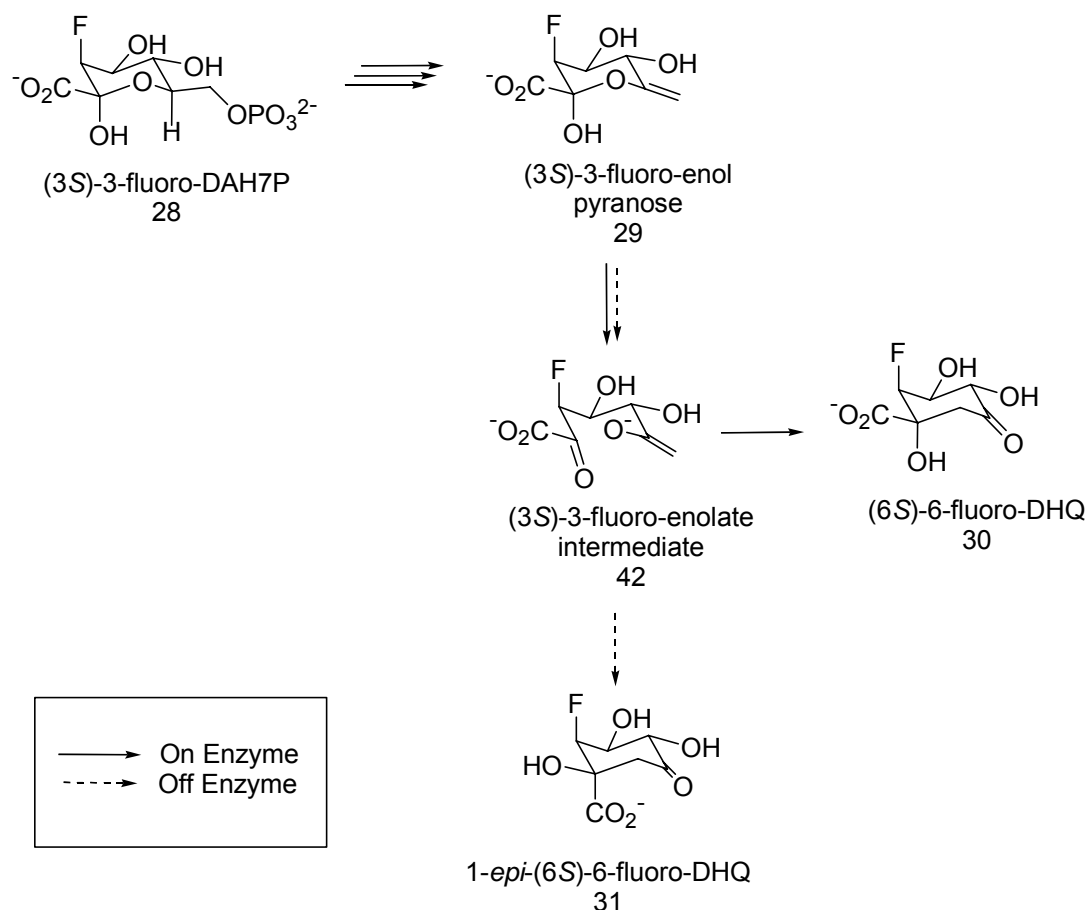


Figure 4.21. Schematic of products formed from (3*S*)-3-fluoro-DAH7P in the presence of *E. coli* DHQS and Kiwifruit DHQS.

The dissociation of the (3*S*)-3-fluoro-enol pyranose **29** from the enzyme could be indicative of an electronic effect from the fluoro group at C-3 resulting in the stabilisation of this intermediate.<sup>28</sup> An increase in the stabilisation of the (3*S*)-3-fluoro-enol pyranose **29** would allow release of this intermediate from the enzyme to compete with the on-going on-enzyme reaction. This stabilising effect would be expected for the fluoro-enol pyranose from both (3*S*)-3-fluoro-DAH7P **28** and (3*R*)-3-fluoro-DAH7P **25**. No epimeric product from the reaction with the (3*R*)-3-fluoro-DAH7P **25** is formed, but this may occur because the transition-state favoured for the solution reaction and on-enzyme transition-state have the same configuration.

Steady-state kinetics showed that all three sources of DHQS have a diminished affinity for (3*S*)-3-fluoro-DAH7P **28**. Specificity constant results also show that the DHQSs have a preference for (3*R*)-3-fluoro-DAH7P **25** over (3*S*)-3-fluoro-DAH7P **28**. This strongly suggests that fluorine in an axial position has more impact on the enzyme-catalysed reaction than when it is in an equatorial position.

Another factor that could explain the dissociation observed in *E. coli* DHQS and Kiwifruit DHQS is the unfavourable transition-state likely to be demanded by the enzyme during cyclisation for (3*S*)-3-fluoro-DAH7P **28**. Based on the Felkin-Anh model, the predicted transition-state for the enzyme-catalysed cyclisation of the (3*S*)-3-fluoro-enolate intermediate **42** places the fluoro substituent on C-3 pointing towards the direction of attack of the internal nucleophile at C-7. It is more favourable electronically to place the fluorine orthogonal to the carbonyl and *anti* to the direction of attack of the internal nucleophile (see figure 4.22). It is possible that the rate of carbacycle formation under these conditions becomes comparable to the rate of release of the intermediate from the enzyme. The combination of an unfavourable transition-state conformation and the stabilisation of the (3*S*)-3-fluoro-enol pyranose **29** could subsequently lead to partial leakage of the fluoro-enol pyranose and cyclisation of the (3*S*)-3-fluoro-enolate intermediate **42** in solution.

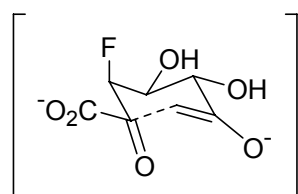


Figure 4.22. Predicted transition-state conformation of the (3*S*)-3-fluoro-enolate intermediate on the enzyme

Although we do not have proof that the leaked (3*S*)-3-fluoro-enol pyranose **29** from (3*S*)-3-fluoro-DAH7P **28** leads exclusively to the epimeric product it is suspected that the position of fluorine influences the likely transition-state in carbacycle formation leading to the production of the epimeric product. It is important to emphasise that once released from the enzyme, the transition-state of the (3*S*)-3-fluoro-enolate intermediate **42** is no longer under the constraints that the enzyme imposes. In solution the (3*S*)-3-fluoro-enolate intermediate **42** is free to adopt alternative conformations. However, the axial position of the fluorine on (3*S*)-3-fluoro-DAH7P **28** influences the predicted transition-state and possibly the product formed from the cyclisation of (3*S*)-3-fluoro-enolate intermediate **42**.

If we assume that the predicted transition-state for the non-enzymatic cyclisation of the (3*S*)-3-fluoro-enolate intermediate **42** involves the fluoro substituent on C-3 pointing away from the direction of attack of the nucleophile so that the transition-state would be favoured based on the Felkin-Anh model, a conformational change in the ring would involve a ring flip, and use of the other face of the enolate, and rotation about C2 and C3 and attack of the other face of the C-2 carbonyl in order to form the epimeric product (see figure 4.23).

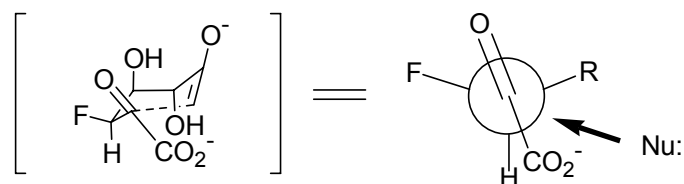


Figure 4.23. Proposed transition-state conformation of the (3*S*)-3-fluoro-enolate intermediate off the enzyme. Newman projection showing fluorine pointing away from the angle of attack of the incoming nucleophile.

Possible solution transition-state conformations for the (3*S*)-3-fluoro-enolate intermediate **42** include boat and chair configurations (see figure 4.24).

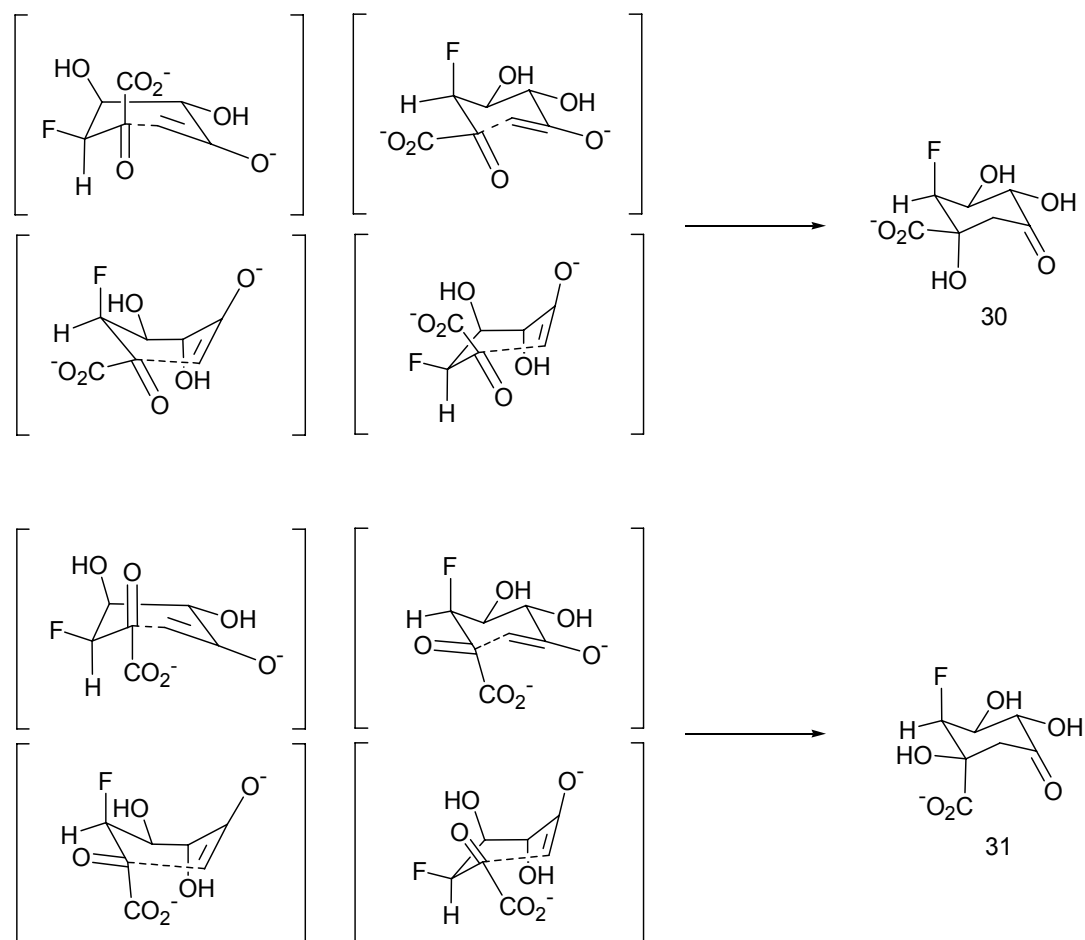


Figure 4.24. Possible transition-state conformations of the off-enzyme cyclisation of the open ring (3*S*)-3-fluoro-enolate intermediate

<sup>19</sup>F NMR partitioning results showed that the amount of 1-*epi*-(6*S*)-6-fluoro-DHQ **31** formed decreased when comparing *E. coli* DHQS and Kiwifruit DHQS. Both enzymes produced the epimeric product; however, it appears that Kiwifruit DHQS was able to prevent the release of the (3*S*)-3-fluoro-enol pyranose **29** more so than *E. coli* DHQS. *P. furiosus* DHQS, on the other hand, resulted in the complete conversion of (3*S*)-3-fluoro-DAH7P **28** to (6*S*)-6-fluoro-DHQ **30**, completely preventing the release of the (3*S*)-3-fluoro-enol pyranose **29**. This observation is

consistent with (6*S*)-6-fluoro-DHQ **30** forming exclusively on-enzyme and the epimer forming off-enzyme following enol pyranose release. With regard to *P. furiosus* DHQS, it could be argued that the partitioning results observed could be due to the assay being done at a suboptimal temperature (<100°C). A suboptimal assay temperature would have resulted in a slower, less active enzyme, more rigid protein structure and hence, it is possible that this may have slowed the release of any intermediate from the enzyme.

The enzymes diverge when comparing their affinity for (3*S*)-3-fluoro-DAH7P **28** against each other. *E. coli* DHQS and Kiwifruit DHQS show a lower affinity for (3*S*)-3-fluoro-DAH7P **28** than does *P. furiosus* DHQS. The differences in affinity for (3*S*)-3-fluoro-DAH7P **28** could explain why *P. furiosus* DHQS does not produce 1-*epi*-(6*S*)-6-fluoro-DHQ **31**, unlike *E. coli* DHQS and Kiwifruit DHQS.

#### 4.6 Summary

Results from the partitioning assay with (3*S*)-3-fluoro-DAH7P **28** suggest that there is partial leakage of the (3*S*)-3-fluoro-enol pyranose **29** from *E. coli* DHQS and Kiwifruit DHQS. It is also suggested that the (3*S*)-3-fluoro-enolate intermediate **42** undergoes cyclisation in solution free from the constraints of the enzyme to form 1-*epi*-(6*S*)-6-fluoro-DHQ **31**.

## 5. Approaches to the synthesis of the modified DAH7P analogues

### 5.1 Methodology

In order to examine the conformation of the transition states leading to the formation of 1-*epi*-(6*S*)-6-fluoro-DHQ **31** and (6*S*)-6-fluoro-DHQ **30**, two compounds (7*R*)-[7-<sup>2</sup>H]-(3*S*)-3-fluoro-DAH7P **43** and (7*R*)-[7-<sup>2</sup>H]-(3*R*)-3-fluoro-DAH7P **44** were proposed for synthesis. These compounds each incorporate a deuterium at C-7 and a fluorine at C-3. To determine the effects of a hydroxyl substituent in the axial and equatorial position at C-3 of DAH7P, a third compound, *gluco*-heptulosonate 7-phosphate (GH7P) was proposed for synthesis. Common precursors to all the proposed compounds are 2-keto-*gluco*-heptulosonic acid **45** and 2-keto-*manno*-heptulosonic acid **46**.

A retrosynthetic analysis suggests that 2-keto-*gluco*-heptulosonic acid **45** and 2-keto-*manno*-heptulosonic acid **46** are best obtained from glucose **47** and mannose **48**, respectively (see figure 5.1).

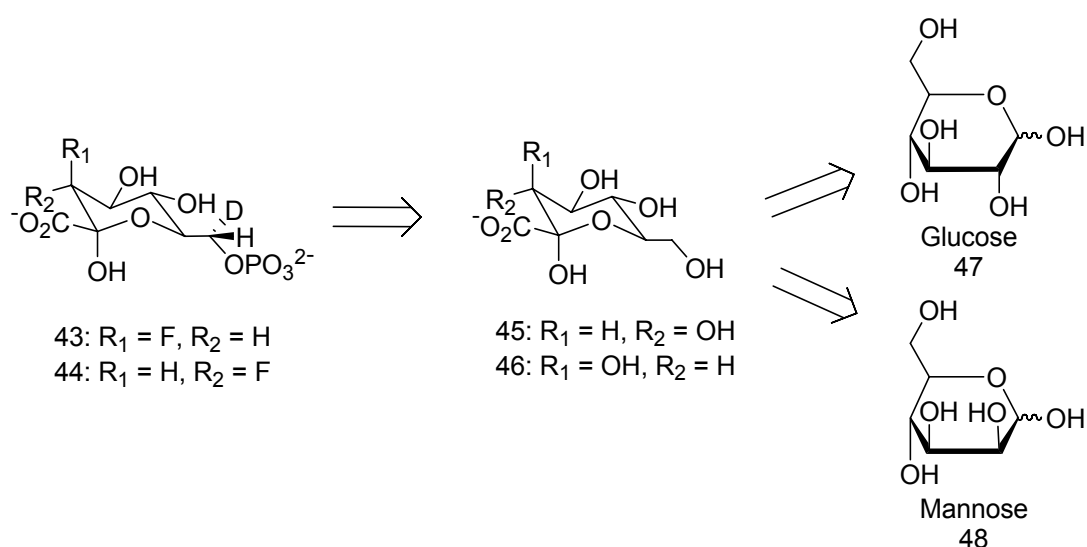


Figure 5.1. Retrosynthesis of compounds **45** and **43** from glucose **47**, and **46** and **44** from mannose **48**.

By fluorinating 2-keto-*gluco*-heptulosonic acid **45** or 2-keto-*manno*-heptulosonic acid **46** with dimethylaminosulfur trifluoride (DAST), inversion of configuration at C-3 would be expected, leading to the correct stereochemistry of the final product.<sup>43,44</sup> If a compound with the fluoro group in the axial position at C-3 is desired [(7*R*)-[7-<sup>2</sup>H]-(3*S*)-3-fluoro-DAH7P **43**], then the starting material would have to be glucose. On the other hand, if the fluoro group in the equatorial position at C-3 is desired [(7*R*)-[7-<sup>2</sup>H]-(3*R*)-3-fluoro-DAH7P **44**], then the starting material would be mannose.

An alternative approach would be to synthetically modify 2-keto-*gluco*-heptulosonic acid **45** to 3-deoxy-D-*arabino*-heptulosonic acid (DAH, **49**) and then electrophilically fluorinate with Selectfluor. By fluorinating with Selectfluor it is expected a mixture of diastereomers would form (fluorinated heptulosonates **43** and **44**) which may be separated chromatographically (see figure 5.2).

The next section will discuss proposed methods for the synthesis of 2-keto-*gluco*-heptulosonic acid **45** and attempts to fluorinate precursors of 2-keto-*gluco*-heptulosonic acid **45** by nucleophilic and electrophilic fluorination.

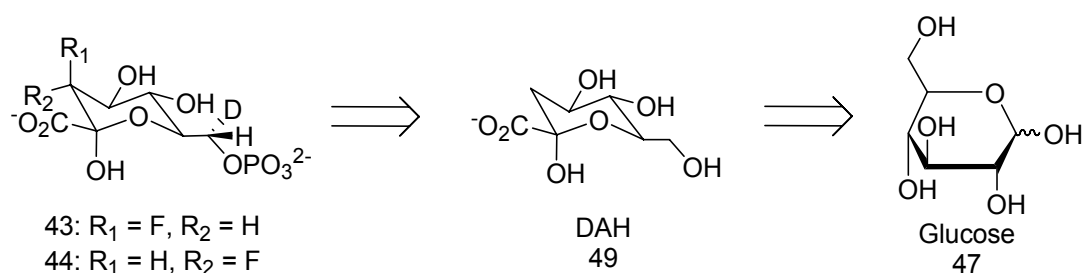


Figure 5.2. Retrosynthesis of compounds **43** and **44** from glucose **47**.

## 5.2 Methodology and synthesis of 7-carbon phosphate sugars

Pre-established synthetic schemes (published schemes) for 7-carbon sugars were assessed based on ease of synthesis and flexibility. Modified versions of these published schemes were designed (proposed schemes) and the synthesis executed. In this section the results of these executed synthetic schemes are reported.

### 5.2.1 Synthesis of 3-deoxy-D-arabino-heptulosonate 7-phosphate by Frost and Knowles

Frost and Knowles prepared DAH7P **3** through a eight-step synthesis starting with 2-deoxy-glucose **50** (see figure 5.3).<sup>45</sup>

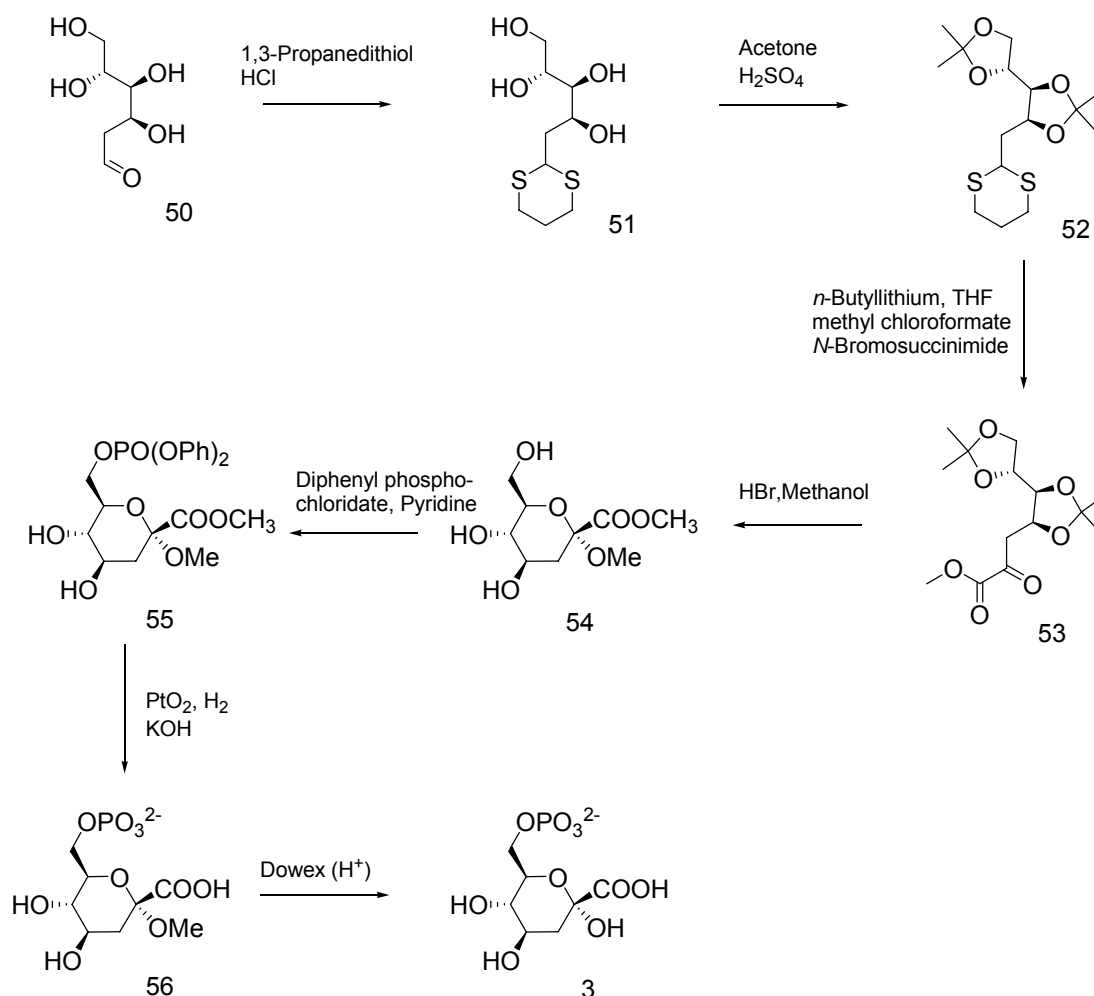


Figure 5.3. Synthetic scheme for DAH7P by Frost and Knowles.<sup>45</sup>

The first two steps involved the formation of a dithioacetal **51** followed by acetal protection of the hydroxyl on C-3, C-4, C-5, and C-6 of 2-deoxy-glucose. Step three involved a one-carbon extension through the formation of an  $\alpha$ -keto ester **53**. Steps four and five involved removal of the acetal protecting groups followed by a phosphorylation at C-6 of heptulosonate **54** to form protected DAH7P **55**. The final three steps (six, seven, and eight) involved deprotection of the phosphate, removal of the methyl ester at C-1, and removal of the methyl ether at C-2 to form DAH7P **3**.

### 5.2.2 Proposed scheme for the synthesis of 2-keto-*gluco*-heptulosonic acid modified from the synthesis of DAH7P

By modifying some steps from the published synthesis of DAH7P **3**, a scheme for the synthesis of 2-keto-*gluco*-heptulosonic acid was proposed (see figure 5.4). In order to obtain a hydroxyl group at C-3, it was necessary to start with gluconolactone instead of 2-deoxy-glucose. The proposed scheme involves acetal protection of the C-3, C-4, C-5, and C-6 hydroxyl groups of gluconolactone **57**, esterification at C-1, and benzylation of the C-2 hydroxyl to form methyl ester **59** (steps a and b). Steps c and d, involve reduction of the methyl ester **59** to a primary alcohol **60**, followed by oxidation of alcohol **60** to an aldehyde **61**. In step e, the aldehyde is converted to a dithioacetal **62**. Dithioacetal **62** then undergoes a one-carbon extension using *n*-butyllithium, methyl chloroformate, and *N*-bromosuccinimide in steps f, g, and h respectively, to form the  $\alpha$ -keto ester **63**. Step i involves removal of the benzyl group on  $\alpha$ -keto ester **63**, exposing the C-3 hydroxyl to give alcohol **64**. The final step (step j) involves deprotection of the acetonide protecting groups and cyclisation of the  $\alpha$ -keto ester to give heptulosonate **65**.

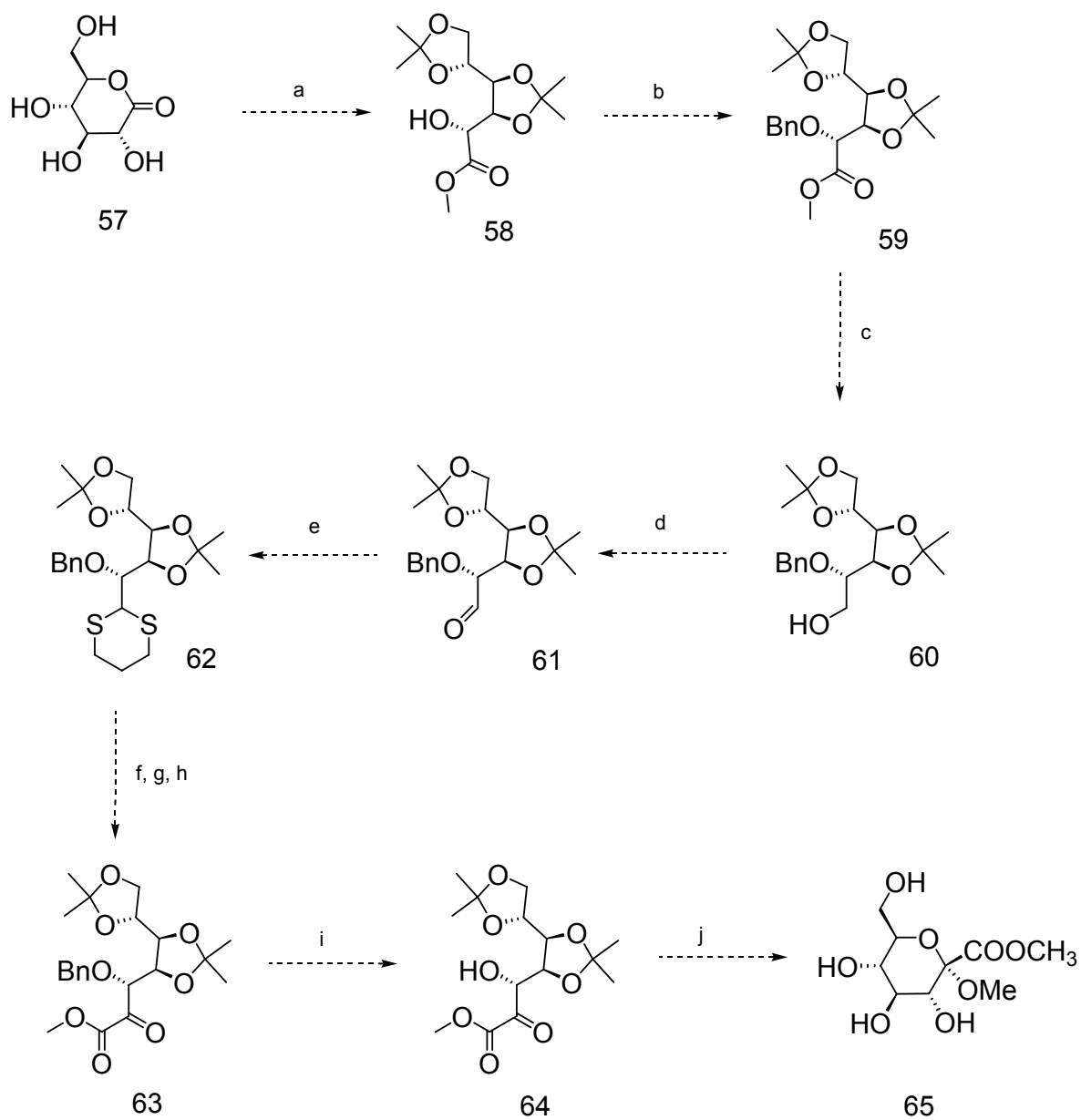


Figure 5.4. Proposed scheme for the synthesis of 2-keto-glucoheptulosonic acid modified from the synthesis of DAH7P (see figure 5.3).

### 5.2.3 Attempted synthesis of 2-keto-*gluco*-heptulosonic acid using a scheme modified from the synthesis of DAH7P

Acetal protection and methyl esterification of gluconolactone **57** with 2,2-dimethoxypropane, *p*Ts, methanol, and acetone gave acetal **58** in 71% yield (see figure 5.5). Benzylation of acetal **58** with benzyl bromide, silver (I) oxide, and potassium iodide in dichloromethane (DCM) initially gave benzylated acetal **59** in poor yield. The yield in this benzylation reaction was improved from 40% to 65% by adjusting the order in which the reagents were added to the reaction. It appears that adding silver (I) oxide last to the reaction mixture prevents the loss of the acetonide protecting groups and subsequently fewer by-products are formed.

Reduction of benzylated acetal **59** with lithium aluminum hydride in tetrahydrofuran (THF) gave alcohol **60** in 81% yield. For the oxidation of the alcohol to the aldehyde, a change from the proposed scheme was made. Both Swern and Dess-Martin oxidation procedures were investigated. <sup>1</sup>H NMR analysis of aldehyde **61** formed by Swern oxidation showed the presence of two diastereomers. It is likely that the acidic proton on the carbon adjacent to the newly formed aldehyde readily epimerises in the presence of a strong base. In the Swern oxidation, triethylamine (TEA) is used to quench the reaction and is thought to result in the formation of the two products. <sup>1</sup>H NMR analysis of aldehyde **61** formed by Dess-Martin oxidation showed the formation of a single aldehyde product. Use of freshly made 1,1,1-tris(acetyloxy)-1,1-dihydro-1,2-benziodoxol-3-(1H)-one (periodinane) in DCM resulted in the formation of aldehyde **61** in 62% yield.

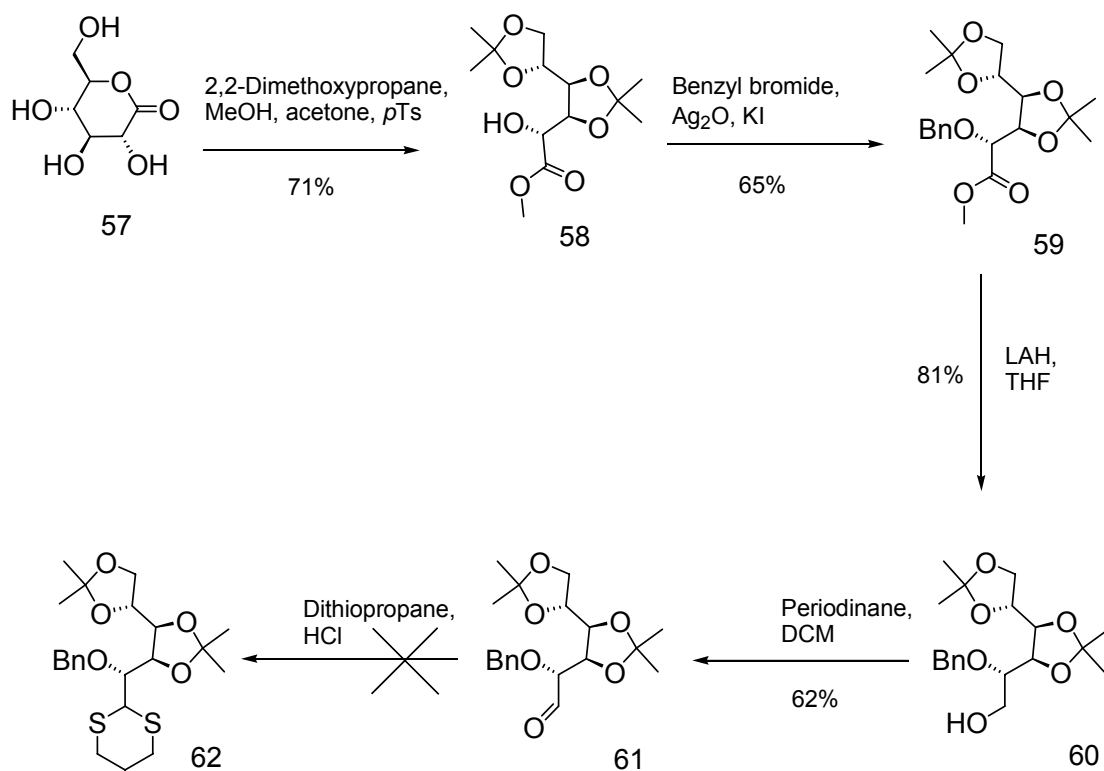


Figure 5.5. Attempted synthesis of 2-keto-*gluco*-heptulosonic acid using a scheme modified from the synthesis of DAH7P.

Although the next step in the synthesis involving the formation of the dithioacetal was not tried, it is likely that the reaction conditions would not have been compatible with the isopropyl acetal protecting groups. The use of hydrochloric acid would have likely resulted in the loss of the acetal protecting groups. Acetonide protecting groups can be removed with acetic acid which is a milder acid compared to hydrochloric acid.<sup>46</sup> Due to the oversight when designing this first scheme, a second scheme was sought.

#### 5.2.4 Synthesis of 3-deoxy-D-*arabino*-heptulosonic acid by Liu and co-workers

Liu and co-workers prepared 3-deoxy-D-*arabino*-hept-2-ulosonic acid (DAH, **49**), a non-phosphorylated form of DAH7P.<sup>47</sup> This method forms DAH **49** in a total of nine steps (see figure 5.6). The first step involved acetal protection of the hydroxyl on C-3, C-4, C-5, and C-6 of gluconolactone **57** and esterification of the C-1 aldehyde to form acetal **58**. The second step involved dehydroxylation at C-2 to form deoxy acetal **66**. The next two steps (three and four) involved reduction of the methyl ester at C-2 followed by oxidation of the C-1 hydroxyl to aldehyde **68**. Steps five, six, and seven involved a one-carbon extension through the formation of dibromoalkene **69** which is then converted to terminal alkyne **70** and finally to bromoalkyne **71**. Steps eight and nine involved the oxidation of the bromoalkyne to  $\alpha$ -keto-ester **72** followed by removal of the acetal protecting groups to form heptulosonate **73**.

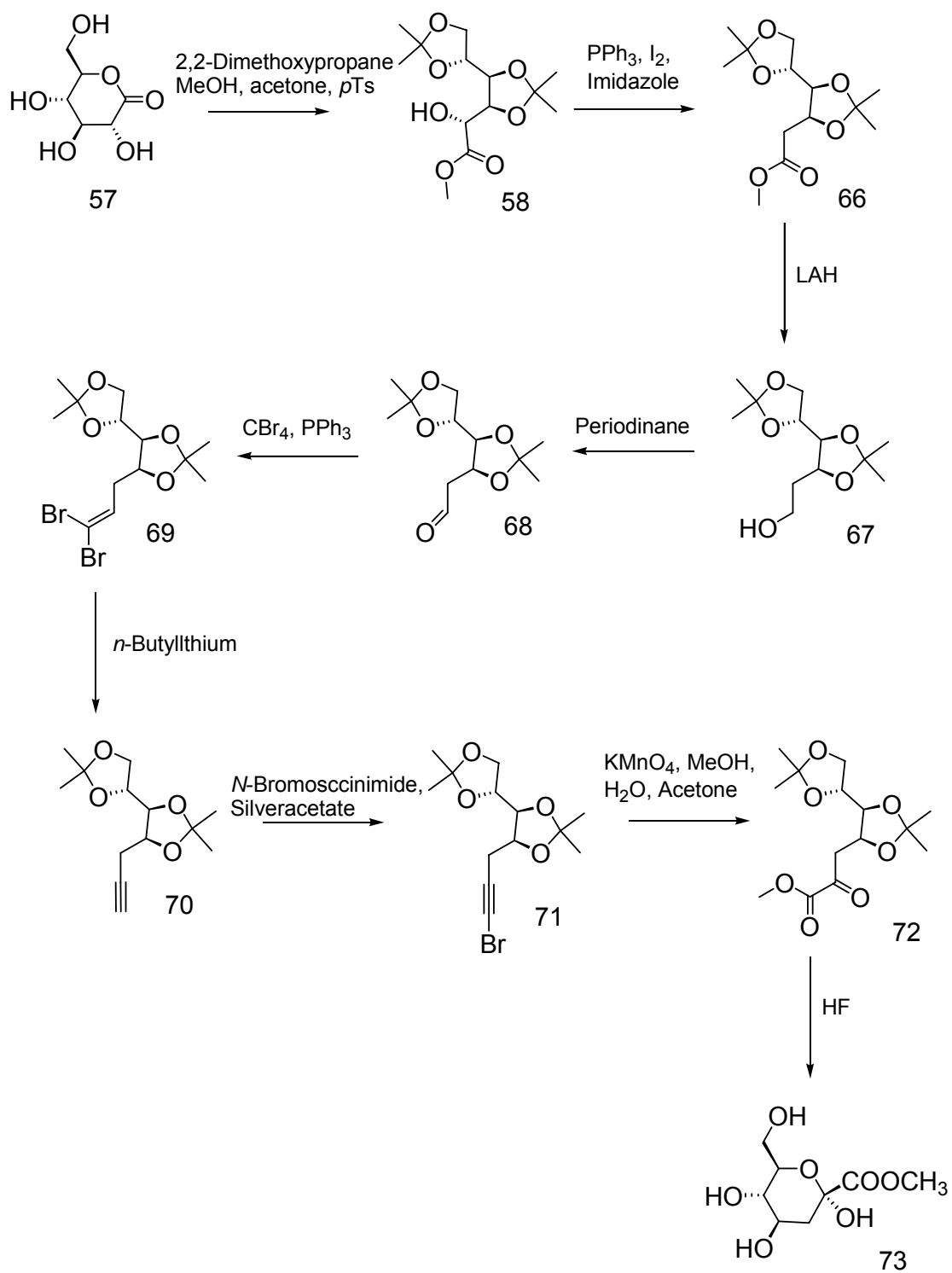


Figure 5.6. Synthetic scheme for DAH by Liu and co-workers.<sup>47</sup>

### 5.2.5 Proposed scheme for the synthesis of 2-keto-*gluco*-heptulosonic acid modified from the synthesis of DAH

The published synthetic route for DAH **49** was modified to accommodate the first four steps from the first scheme (figure 5.5), thus conserving the efforts made up to this point.<sup>47</sup> The main changes from the published synthesis of DAH **49** were to omit the dehydroxylation step and bypass the formation of the terminal alkyne (see figure 5.7). In this second scheme, steps a, b, c, and d, starting with gluconolactone up to the formation of the aldehyde **61**, are identical to those of the first scheme. Step e involves a one-carbon homologation of aldehyde **61** to form the dibromoalkene **74**. Dibromoalkene **74** is then converted to the monobromoalkyne **75** in step f. Step f bypasses having to form the terminal alkyne from the published DAH scheme and therefore shortens the proposed scheme by one step. Monobromoalkyne **75** undergoes oxidation (step g) to form the  $\alpha$ -keto ester **63**. In step h the benzyl group on  $\alpha$ -keto ester **62** is removed to form alcohol **64**. The final step (step i) involves deprotection of the acetonide protecting groups and cyclisation to give heptulosonate **76**.

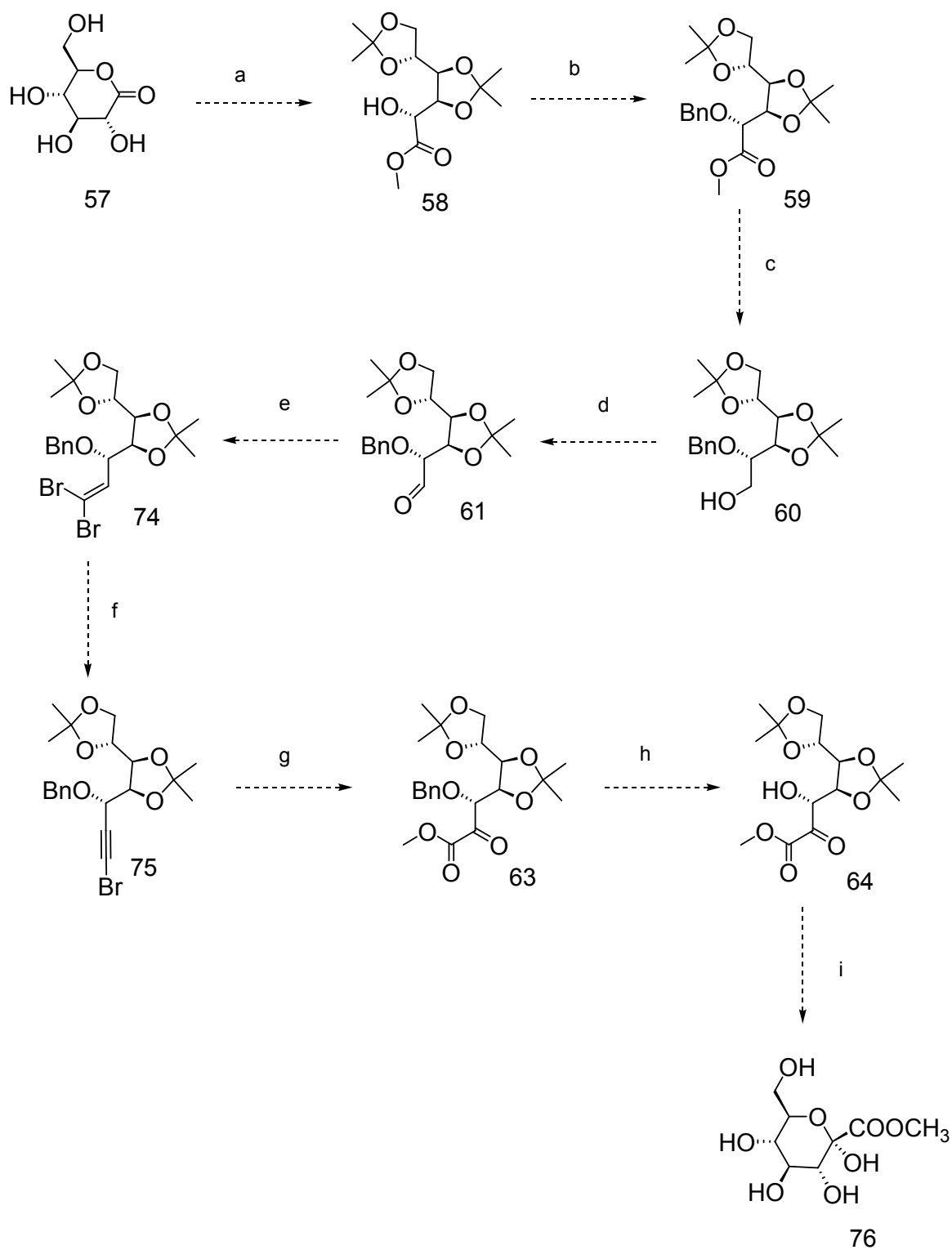


Figure 5.7. Proposed scheme for the synthesis of 2-keto-glucoheptulosonic acid modified from the synthesis of DAH (see figure 5.6).

### 5.2.6 Attempted synthesis of 2-keto-*gluco*-heptulosonic acid using a scheme modified from the synthesis of DAH

Aldehyde **61** was brominated with carbon tetrabromide and triphenyl phosphine in DCM to give dibromoalkene **74** in 86% yield (see figure 5.8).

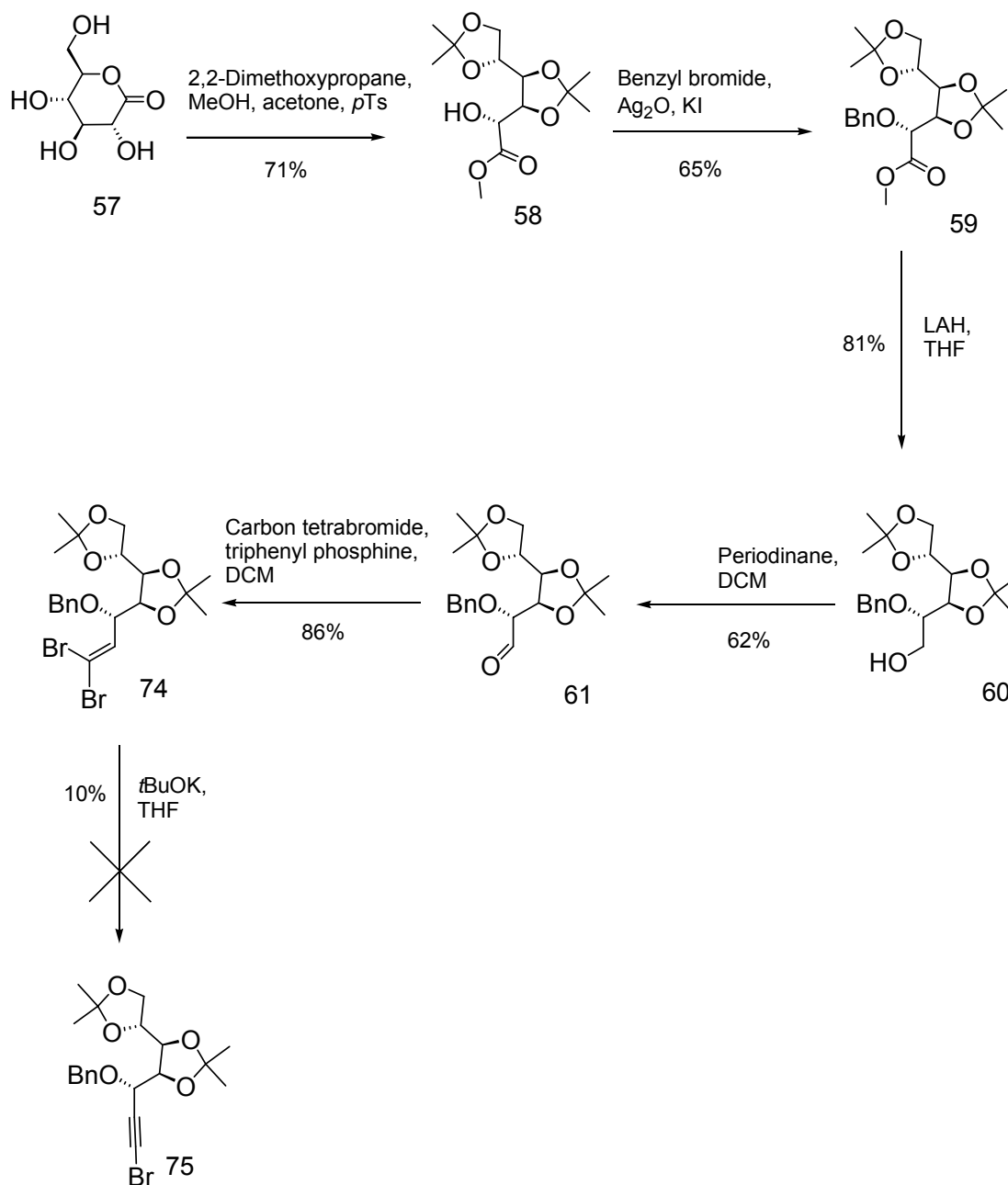


Figure 5.8. Attempted synthesis of 2-keto-*gluco*-heptulosonic acid using a scheme modified from the synthesis of DAH.

Unfortunately, attempts to form monobromoalkyne **75** in step f gave a poor yield at best. Several bases were used to abstract the C-6 proton on the alkene. All the bases resulted in no reaction except for potassium *t*-butoxide (*t*-Bu). Two equivalents of *t*-Bu in THF gave a 10% yield of monobromoalkyne **75** (see table 10).

Table 10.

Reaction condition for the synthesis of monobromoalkyne

Reaction Conditions	Ref	Results
4 eq. TBAF, THF	<sup>48</sup>	No Reaction <sup>†</sup>
4 eq. TBAF, 1-3 eq. 1M KOH, THF	<sup>48</sup>	No Reaction <sup>†</sup>
2.1 eq. NaH, THF	<sup>49</sup>	No Reaction <sup>†</sup>
4.2 eq. NaH, THF	<sup>49</sup>	No Reaction <sup>†</sup>
2 eq. NaOCH <sub>3</sub> , MeOH	<sup>50</sup>	No Reaction <sup>†</sup>
2 eq. <i>t</i> -Bu, THF, 21°C	<sup>51</sup>	10% Yield
4 eq. <i>t</i> -Bu, THF, 21°C	<sup>51</sup>	Some evidence <sup>††</sup>

<sup>†</sup> Results based on TLC, <sup>††</sup> TLC showed multiple spots

### 5.2.7 Revision to the scheme for the synthesis of 2-keto-*gluco*-heptulosonic acid modified from the synthesis of DAH

Given the poor success of the monobromoalkyne step from the second scheme (figure 5.7) for the synthesis of 2-keto-*gluco*-heptulosonic acid **45**, it was decided to follow the published synthesis of DAH **49** more closely. The synthesis of 2-keto-*gluco*-heptulosonic acid **45** was essentially kept the same with the exception of two additional steps (see figure 5.9). These involved converting the dibromoalkene to a non-brominated alkyne **77** followed by a bromination to form the monobromoalkyne **75**. The remaining steps were left unchanged.

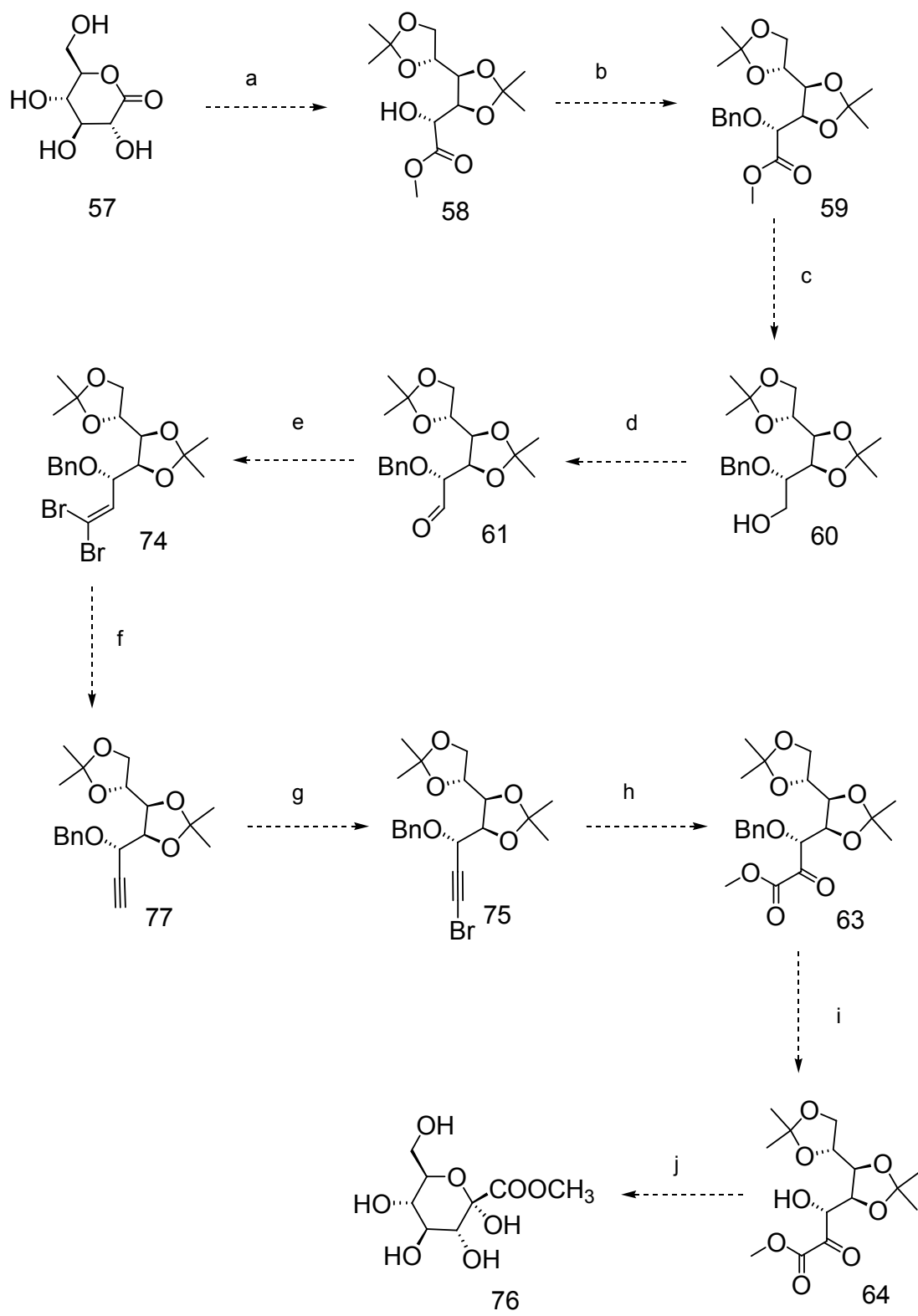


Figure 5.9. Revision to the scheme for the synthesis of 2-keto-*gluco*-heptulosonic acid modified from the synthesis of DAH.

### 5.2.8 Attempted synthesis of 2-keto-*gluco*-heptulosonic acid using a revised scheme modified from the synthesis of DAH

Starting from the sixth step, dibromoalkene **74** was treated with *n*-butyllithium (*n*BuLi) in THF at -10°C to yield alkyne **77** in 53% yield (see figure 5.10). Alkyne **77** was brominated with *N*-bromosuccinimide (NBS) and silver acetate (AgOAc) in acetone giving monobromoalkyne **75** in 68% yield. Monobromoalkyne **75** was treated with potassium permanganate (KMnO<sub>4</sub>), sodium bicarbonate (NaHCO<sub>3</sub>) and magnesium sulfate (MgSO<sub>4</sub>) in methanol and water to make  $\alpha$ -keto ester **63** (step h). However, this gave poor yields due to the insolubility of monobromoalkyne **75** in the KMnO<sub>4</sub>/NaHCO<sub>3</sub> solution. In a second attempt at step h, acetone was added as co-solvent in order to improve the solubility of monobromoalkyne **75**. This modification successfully gave the  $\alpha$ -keto ester **63**. The crude yield of the  $\alpha$ -keto ester **63** was 95% with only impurities on the baseline of a thin layer chromatography plate (TLC). Keto ester **63** was not purified at this point.

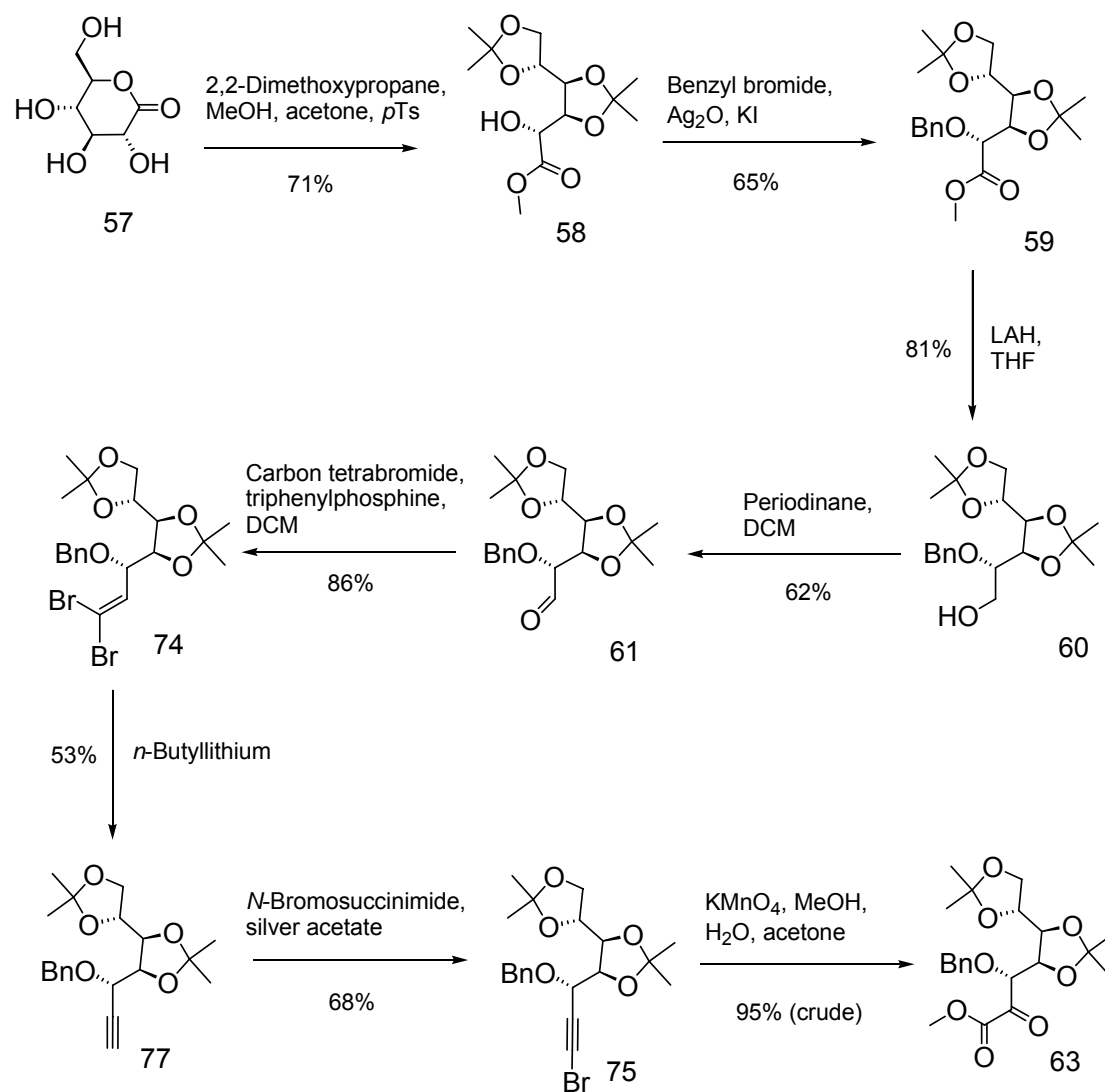


Figure 5.10. Attempted synthesis of 2-keto-*gluco*-heptulosonic acid using a revised scheme modified from the synthesis of DAH.

### 5.2.9 Optimisation of the revised scheme for the synthesis of 2-keto-*gluco*-heptulosonic acid originally based on the synthesis of DAH

Despite the initial success of the previous scheme it was decided to optimise the synthesis of 2-keto-*gluco*-heptulosonic acid **45** by reducing the total number of steps up to the formation of the  $\alpha$ -keto ester. The optimised scheme was essentially the same as the previous with the exception that four steps were replaced by one (see figure 5.11). The optimisation involved converting the benzylated acetal **59** to alkyne **77** (step c). The remaining steps d through g (g through j from the previous scheme) were left unchanged.

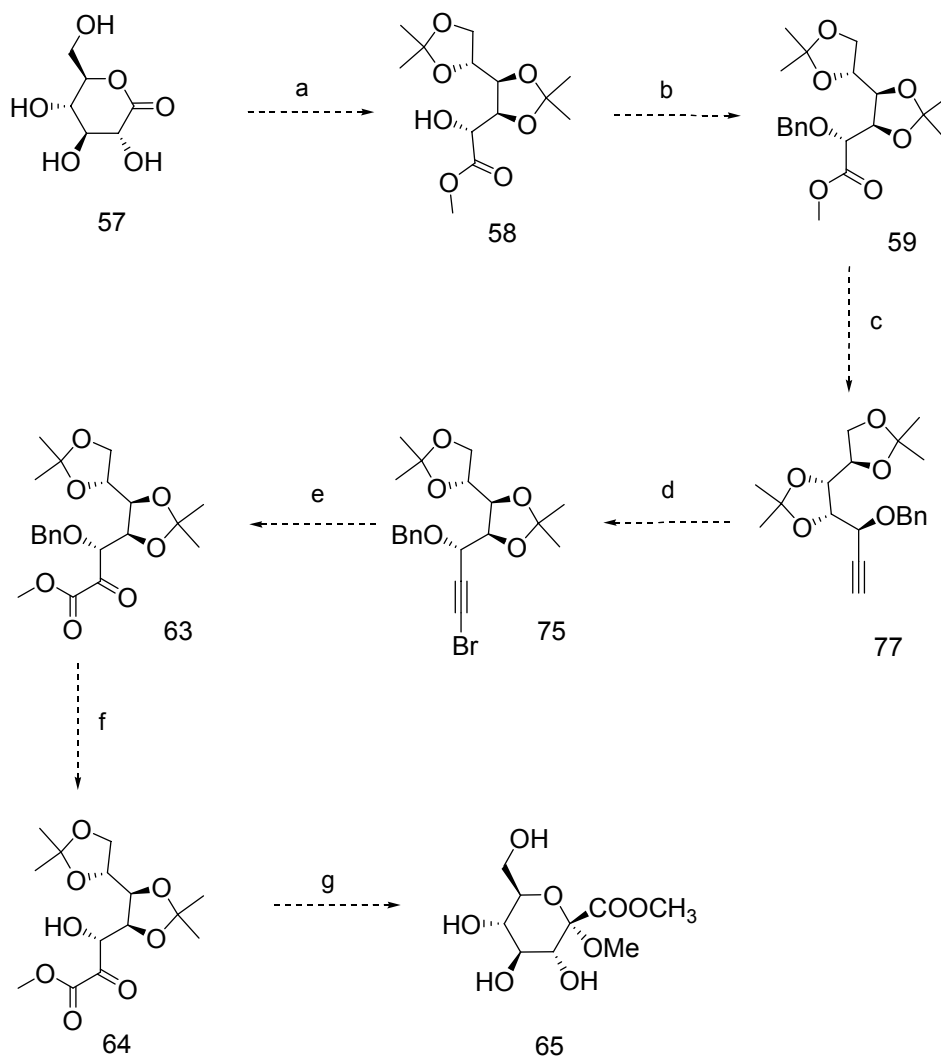


Figure 5.11. Optimised scheme for the synthesis of 2-keto-*gluco*-heptulosonic acid originally based on the synthesis of DAH.

### 5.2.10 Attempted synthesis of 2-keto-*gluco*-heptulosonic acid using an optimised scheme originally based on the synthesis of DAH

Benzylated acetal **59** was treated with DIBAL followed by Bestmann's reagent [Dimethyl (Diazomethyl)phosphonate] in DCM at  $-78^{\circ}\text{C}$  to yield alkyne **77** in 70% yield (see figure 5.12). The next two compounds, monobromoalkyne **75** and  $\alpha$ -keto ester **63** were synthesised as previously mentioned to give 68% and 95% yield respectively. At this stage, it was decided to test several fluorination methods at various stages of the proposed scheme therefore no further synthesis was carried out (see section 5.3.2).

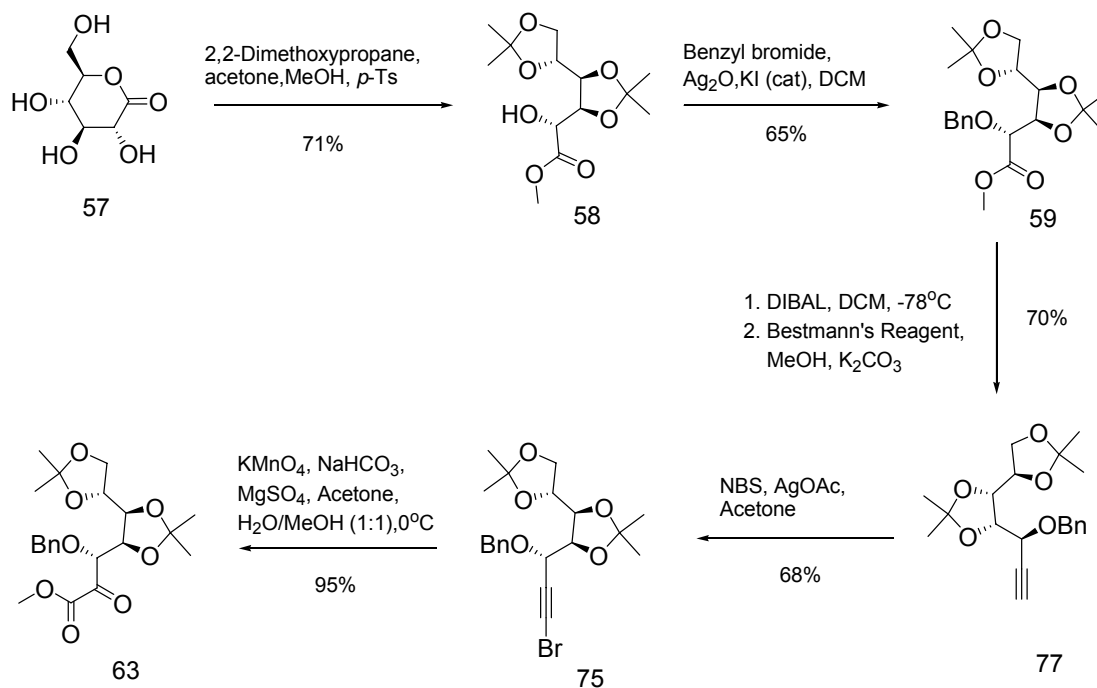


Figure 5.12. Attempted synthesis of 2-keto-*gluco*-heptulosonic acid.

### 5.3 Other syntheses

From the development of the schemes for the synthesis of 2-keto-*gluco*-heptulosonic acid **45** several other ideas emerged. One such idea was to synthesise *gluco*-

heptulosonate 7-phosphate (GH7P, **82**). GH7P **82** differs from (3*R*)-3-fluoro-DAH7P by only one functional group, this being a hydroxyl. The scheme from section 5.2.9 (see figure 5.11) can be easily modified to make GH7P **82**. Previous results from Le Marechal et al. suggest that GH7P **82** is a competitive inhibitor of DHQS.<sup>52</sup> Incorporation of this substrate to our study would be of great interest and provide insight to the steric properties of the enzyme. The second idea was to take advantage of electrophilic and nucleophilic fluorination in order to introduce fluorine to our target compounds. The scheme from section 5.2.9 provides various advanced intermediates that can be fluorinated directly or after slight modification. The third idea was to synthesise 4-[<sup>2</sup>H]-D-erythrose 4-phosphate (*dE4P*), which could then be incubated with DAH7PS in the presence of F-PEP to make (7*R*)-[7-<sup>2</sup>H]-(3*S*)-3-fluoro-DAH7P **43**.

### 5.3.1 Proposed scheme for the synthesis of GH7P

Keto ester **63** provides an ideal starting point for the synthesis of GH7P **82** because no further alteration to the stereochemistry of the core structure is required. After cyclisation the advanced intermediate is phosphorylated and deprotected to form GH7P **82** (see figure 5.13).

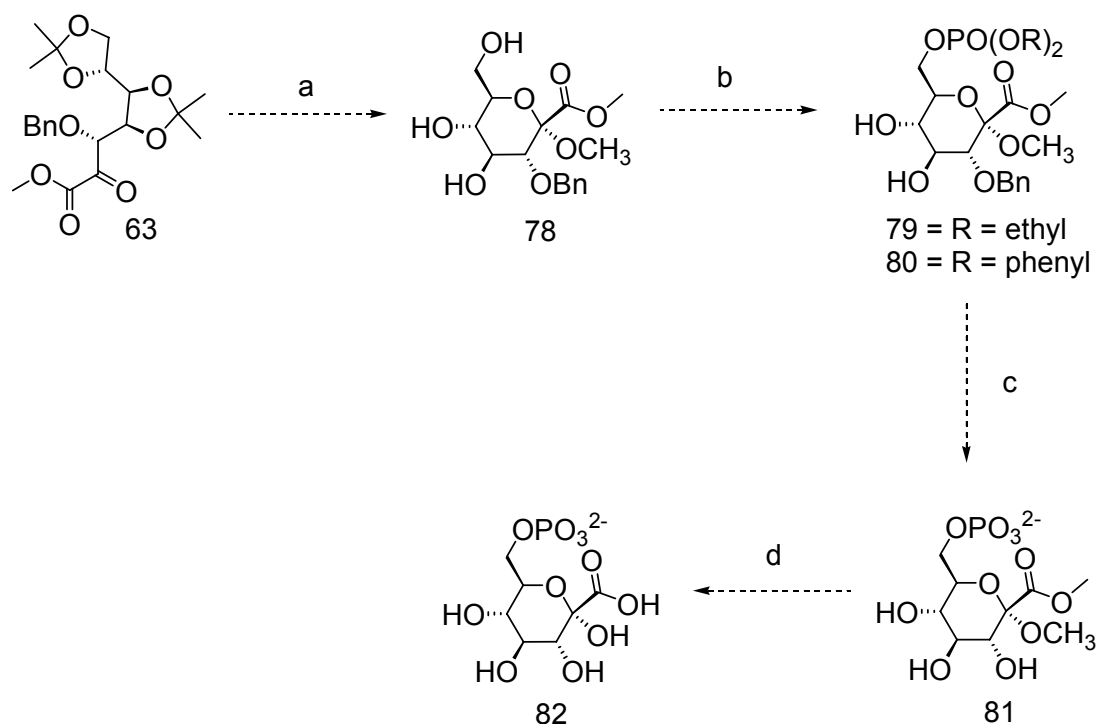


Figure 5.13. Proposed scheme for the synthesis of GH7P.

### 5.3.1.1 Attempted synthesis of GH7P

Several different methods were tried for the phosphorylation of the cyclised advanced intermediate prior to the design of the proposed synthetic scheme for GH7P **82**. Keto ester **63** was refluxed with *p*Ts in methanol to give what was thought to be heptulosonate **78** in 43% yield. Initially, heptulosonate **78** was tritylated at C-7 with the aim of selectively protecting the C-4 and C-5 hydroxyl groups. The advantage of this was to selectively phosphorylate C-7 without phosphorylating the hydroxyl on C-4 and C-5. However, the tritylation of heptulosonate **78** produced insufficient amounts of product. It was then thought that the primary alcohol would favour phosphorylation over the two other secondary alcohols at C-4 and C-5, hence, not requiring further hydroxyl protection. Heptulosonate **78** was then phosphorylated with diethyl phosphorochloridate but this resulted in phosphorylated heptulosonate **79** in yields

below 10%. In addition to the low yield, the downstream deprotection of the ethyl ethers on the phosphate complicated the synthetic scheme and was therefore abandoned. Attempts to phosphorylate heptulosonate **78** with diphenyl phosphorochloridate to form phosphorylated heptulosonate **80** were initially unsuccessful.

After close investigation of the synthesis of heptulosonate **78**, it was found that either the *p*Ts was deprotecting the methyl ether at C-2 or the base used to neutralise the *p*Ts was deprotecting the methyl ester at C-1. In an attempt to circumvent this problem, keto ester **63** was treated with concentrated HCl in methanol at room temperature and the acid neutralised with Amberlite to give heptulosonate **83** in 81% yield. Unfortunately, heptulosonate **83** was missing the methyl ether at C-2, however, it was decided to continue with this compound despite the loss of the protecting group. Heptulosonate **83** was finally phosphorylated with diphenyl phosphorochloridate in DCM containing imidazole to give phosphorylated heptulosonate **84** in 27% yield (see figure 5.14).

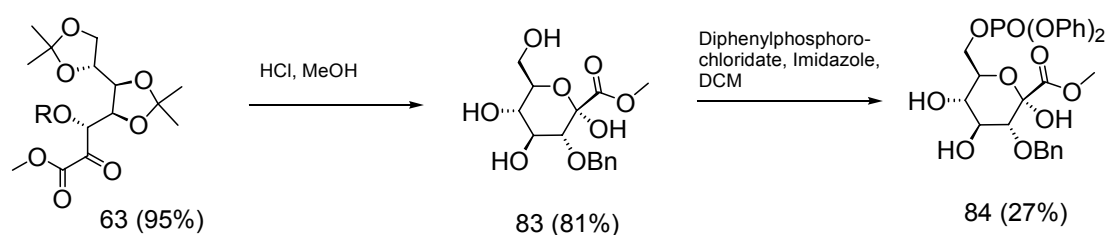


Figure 5.14. Attempted synthesis of GH7P.

### 5.3.2 Fluorination of advanced intermediates

One of the more challenging parts of the proposed synthetic schemes discussed in section 5.2 is the introduction of fluorine onto C-3 of 2-keto-*gluco*-heptulosonic acid.

Introduction of the fluorine at the beginning of the scheme is likely to make the proton at C-2 acidic. This could lead to epimerisation at C-2 during the formation of alkyne **77** (see figure 5.12). The same problem can occur if fluorine is introduced after the formation of the  $\alpha$ -keto ester **63** (see figure 5.12). A safer approach could be to introduce the fluorine after cyclisation of the seven-carbon intermediate, heptulosonate **83** (see figure 5.14). The main concern here would be the potential for multiple fluorinations and low yields of the desired mono-fluorinated targets (7*R*)-[7-<sup>2</sup>H]-(3*S*)-3-fluoro-DAH7P **43** and (7*R*)-[7-<sup>2</sup>H]-(3*R*)-3-fluoro-DAH7P **44**. Both nucleophilic and electrophilic fluorinations were attempted at different stages of the synthesis of 2-keto-*gluco*-heptulosonic acid **45** in order to introduce fluorine at C-3.

#### 5.3.2.1 Nucleophilic fluorination

Nucleophilic fluorination involves attack of a “F<sup>-</sup> species” (nucleophile) on to an electrophile containing a leaving group. A commonly used fluorinating agent for the nucleophilic fluorination of monosaccharides is diethylaminosulfur trifluoride; DAST. In the presence of monosaccharides, DAST couples to a hydroxyl group on the sugar by way of an O-S bond forming a good leaving group. During this step a fluoride ion is released which then attacks the electrophilic carbon rapidly displacing the leaving group.<sup>53</sup> Furthermore, substitution of the hydroxyl with fluorine when using DAST occurs with inversion of configuration. This is an ideal reagent for introducing fluorine stereospecifically into optically active sugars.<sup>43,44</sup>

### 5.3.2.2 Nucleophilic fluorinations of alcohol **58**

Alcohol **58** was chosen for an investigation of nucleophilic fluorination because it only required one synthetic step to prepare and hence was available in bulk quantities. Alcohol **58** was also the obvious choice given that the only unprotected hydroxyl was on C-2 which is exactly where we wanted to introduce the fluorine. The proposed synthesis involved fluorinating alcohol **58** with DAST to obtain methyl 3,4:5,6-di-*O*-isopropylidene-2-deoxy-2-fluoro-D-gluconate **85** (see figure 5.15).

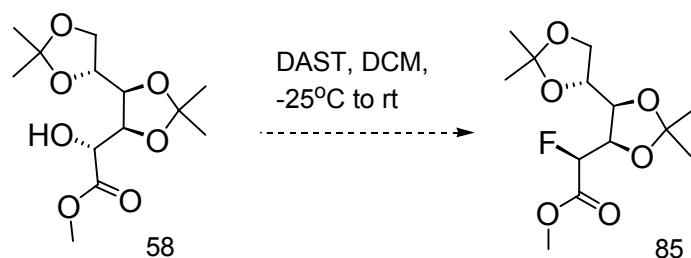


Figure 5.15. Proposed scheme for the synthesis of methyl 3,4:5,6-di-*O*-isopropylidene-2-deoxy-2-fluoro-D-gluconate

Another approach was to fluorinate a selectively acetyl protected form of heptulosonate **83** (see figure 5.16). This would involve the cyclisation of  $\alpha$ -keto ester **63** and acetylation of the C-4, C-5, and C-7 hydroxyls in a one-pot reaction to form acetylated heptulosonate **86**. The next step would involve removal of the benzyl protecting group at C-3 forming alcohol **87** followed by DAST fluorination to form fluoro-heptulosonate **88**.

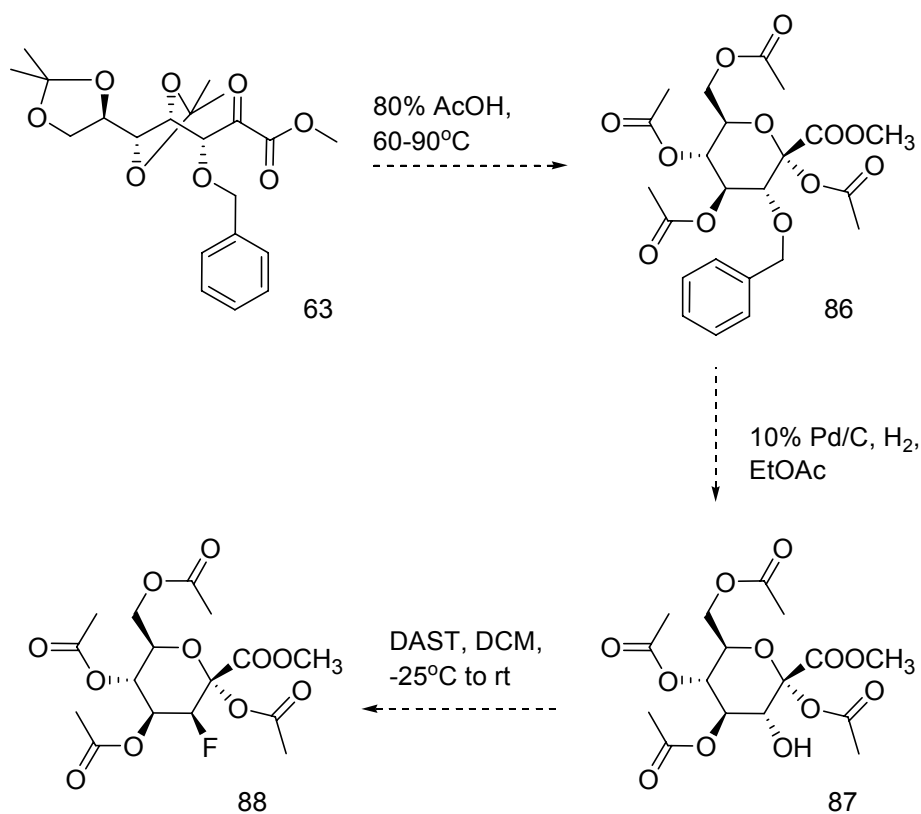


Figure 5.16. Proposed scheme for the synthesis of fluoroheptulosonate **88**

### 5.3.2.3 Nucleophilic fluorination results for the synthesis of mono-fluoro product **85**

Alcohol **58** was treated with 1.5 equivalents of DAST at -25°C and allowed to warm to room temperature. Silica gel TLC using 1:3 ethyl acetate/hexane showed the starting material at  $R_f$  0.4 plus two products at  $R_{fs}$  0.5 and 0.6. An attempt was made to separate the products via column chromatography but the purification was unsuccessful. Upon use of a less polar mobile phase it was revealed that the initial two product spot on TLC contained multiple products eluting closely to one another. <sup>19</sup>F NMR spectroscopy did show a mono-fluoro product **85** but at only 10% yield with impurities. It was thought that decreasing the reaction temperature could possibly lead

to the generation of a mono-fluoro product. Alcohol **58** was treated with 1.5 equivalents of DAST at -25°C and allowed to warm to 0°C. TLC showed little to no conversion after five hours. The reaction was then allowed to stir overnight at room temperature. As before two products at  $R_{f's}$  0.5 and 0.6, plus the starting material were visible on TLC. Separation of the products via column chromatography was again unsuccessful. A third attempt involved treating alcohol **58** with 3 equivalents of DAST at 25°C and allowing the reaction to warm to room temperature. TLC showed two products above above the starting material and one product below the starting material. No further attempts were made to synthesise methyl 3,4:5,6-di-*O*-isopropylidene-2-deoxy-2-fluoro-D-gluconate.

It was decided to try the fluorination on a cyclised starting material. The idea was to fluorinate a compound with less movement. Ketoester **63** was acetylated with 80% (w/v) acetic acid in water at 60°C to 90°C. After the removal of excess acetic acid the residue was treated with acetic anhydride, triethylamine (TEA), and 4-dimethylaminopyridine (DMAP) in DCM to give acetylated heptulosonate **86** in 90% yield. Acetylated heptulosonate **86** was dissolved in ethanol and treated with 10% Pd/C under hydrogen gas to give heptulosonate **87** in 95% yield. Heptulosonate **87** was dissolved in anhydrous DCM and treated with DAST to give fluoro-heptulosonate **88** in 10% yield. Fluoro-heptulosonate **88** appeared to be a mono-fluoro product by  $^{19}\text{F}$  NMR .

#### 5.3.2.4 Electrophilic fluorination

Electrophilic fluorination reactions are also a possible route for the introduction of fluorine onto 2-keto-*gluco*-heptulosonic acid **45** or 2-keto-*manno*-heptulosonic acid

**46.** Electrophilic fluorination involves attack on a fluorine “F<sup>+</sup> species” (electrophile) by a nucleophile.<sup>54</sup> This type of reaction could be done on the  $\alpha$ -keto intermediate, ketoester **63** (figure 5.12). Deprotonation at C-3 of ketoester **63** leads to the formation of deoxygluconate. Treatment of deoxygluconate with a bulky base leads to the formation of the nucleophilic enolate (between C-2 and C-3) thus providing the site for electrophilic fluorination. Recently, a new class of electrophilic fluorinating reagents with the general structure R<sub>2</sub>N-F or R<sub>3</sub>N<sup>+</sup>-F have begun to gain popularity.<sup>55</sup> These have become popular because they are safer than F<sub>2</sub> gas, stable at room temperature, and easy to handle. An example of a R<sub>2</sub>N-F fluorinating agent is Selectfluor™, 1-chloromethyl-4-fluoro-1,4-diazoniabicyclo[2.2.2]octane bis(tetrafluoroborate).<sup>56</sup> Mechanisms of the reactions of R<sub>2</sub>NF fluorinating reagents with organic compounds are not well understood; however, a possible mechanism involves the displacement of the R<sub>2</sub>N group during the attack on fluorine by the nucleophile.<sup>54,55</sup>

#### **5.3.2.5 Electrophilic fluorination of methyl 3,4:5,6-di-*O*-isopropylidene-2-deoxy-D-gluconate**

The proposed synthesis involved removing the C-2 hydroxyl from ester **58** with triphenyl phosphine and iodine to form methyl 3,4:5,6-di-*O*-isopropylidene-2-deoxy-D-gluconate (deoxygluconate) **66**. Deoxygluconate **66** could then be fluorinated with Selectfluor™ to obtain methyl 3,4:5,6-di-*O*-isopropylidene-2-deoxy-2-fluoro-D-gluconate **89** (see figure 5.17).

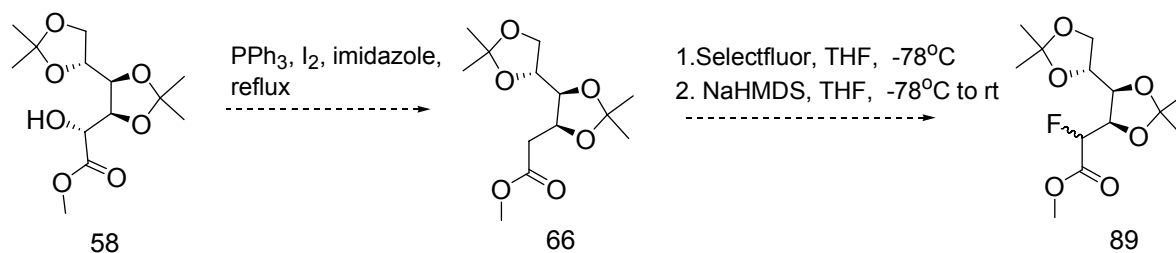


Figure 5.17. Proposed scheme for the fluorination of methyl 3,4:5,6-di-*O*-isopropylidene-2-deoxy-D-gluconate.

### 5.3.2.6 Electrophilic fluorination results

Alcohol **58** was treated with triphenyl phosphine, iodine and imidazole in toluene to give deoxygluconate **66** in 75% yield. Unfortunately, the synthesis of methyl 3,4:5,6-di-*O*-isopropylidene-2-deoxy-2-fluoro-D-gluconate **89** was not successful. Initial attempts to fluorinate deoxygluconate **66** by electrophilic fluorination led to the elimination of the C4 hydroxyl without any evidence of the fluorination of deoxygluconate **66**. The  $^1\text{H}$  NMR spectrum showed the formation of alkene **90**, evidenced by the alkene protons at 6.9 and 6.2 ppm. This reaction is likely to be generated by way of a E1cB process (see figure 5.18).

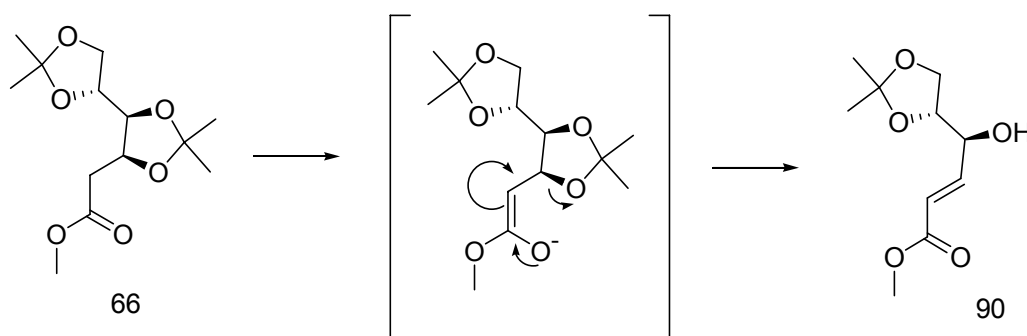


Figure 5.18. Elimination product from the electrophilic fluorination of methyl 3,4:5,6-di-*O*-isopropylidene-2-deoxy-D-gluconate.

Several conditions were tried in order to circumvent this elimination product. The first attempt involved maintaining the reaction below room temperature, which resulted in slowing the rate of the overall reaction but did not yield any target material. The second attempt involved the use of a silyl group prior to adding the fluorinating agent so as to derivatise the enolate as the silyl enol ether **91** (see figure 5.19).

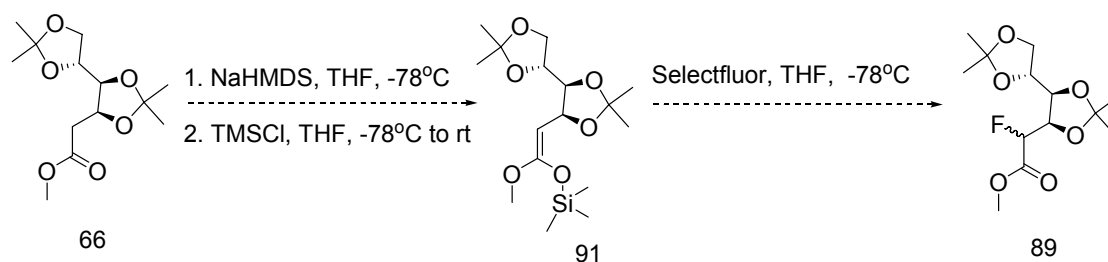


Figure 5.19. Proposed fluorination of methyl 3,4:5,6-di-*O*-isopropylidene-2-deoxy-D-gluconate by way of a silyl enol ether.

Treatment of deoxygluconate **66** with NaHMDS followed by addition of TMSCl at -78°C appeared to have produced the silylated product based on TLC ( $R_f$  0.5). However, treatment of the silylated product with Selectfluor and NaHMDS resulted in the silylated alkene **92** (see figure 5.20).

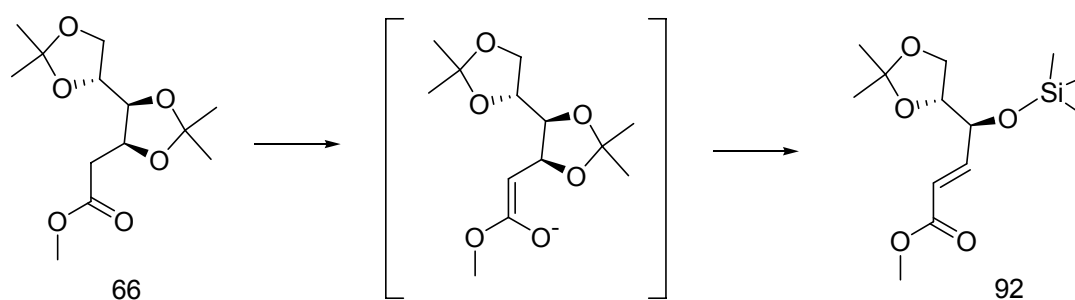


Figure 5.20. Elimination product from the silylation of methyl 3,4:5,6-di-*O*-isopropylidene-2-deoxy-D-gluconate

A third attempt involved reversing the order of addition of the reagents so that the fluorination agent was present in high concentration prior to forming the enolate. This

also resulted in the production of the elimination product, possibly because the fluorinating agent was insoluble in tetrahydrofuran. Changing the solvent to DMF created problems due to the low temperature required to form the enolate. To prevent the solvent from freezing, a one-to-one mixture of THF and DMF was tried. This improved the solubility of the fluorinating agent but no improvement to the synthesis was observed.

### 5.3.3 Synthesis of 4-[<sup>2</sup>H]-D-erythrose 4-phosphate

An alternative method to prepare (7*R*)-[7-<sup>2</sup>H]-(3*S*)-3-fluoro-DAH7P **43** and (7*R*)-[7-<sup>2</sup>H]-(3*R*)-3-fluoro-DAH7P **44** could be by utilising a chemo-enzymatic approach. This would involve incubating 4-[<sup>2</sup>H]-D-erythrose 4-phosphate **93** and (*Z/E*)-3-fluoro-PEP with DAH7PS to form a mixture of heptulosonates **43** and **44** (see figure 5.21).

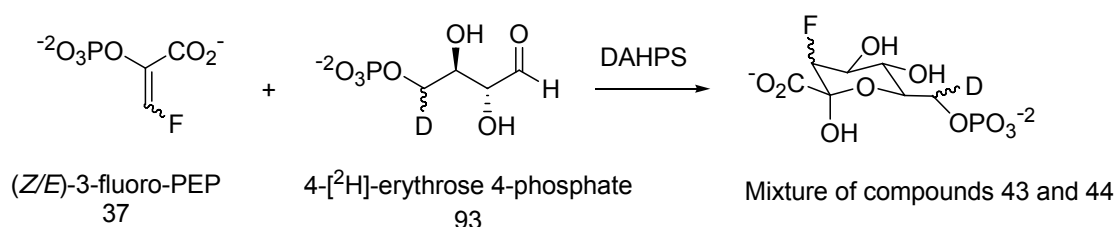


Figure 5.21. Enzymatic preparation of heptulosonates **43** and **44**

The proposed scheme for the synthesis of 4-[<sup>2</sup>H]-D-erythrose 4-phosphate **93** involved using 2,3-*O*-isopropylidene-erythronolactone **94** as the starting material. The lactone is converted to a methyl ester **95** followed by reduction to aldehyde **96**, introduction of a deuterium at C-4, phosphorylation of the C-4 hydroxyl, and a series of deprotections to form 4-[<sup>2</sup>H]-D-erythrose 4-phosphate **93** (see figure 5.22).

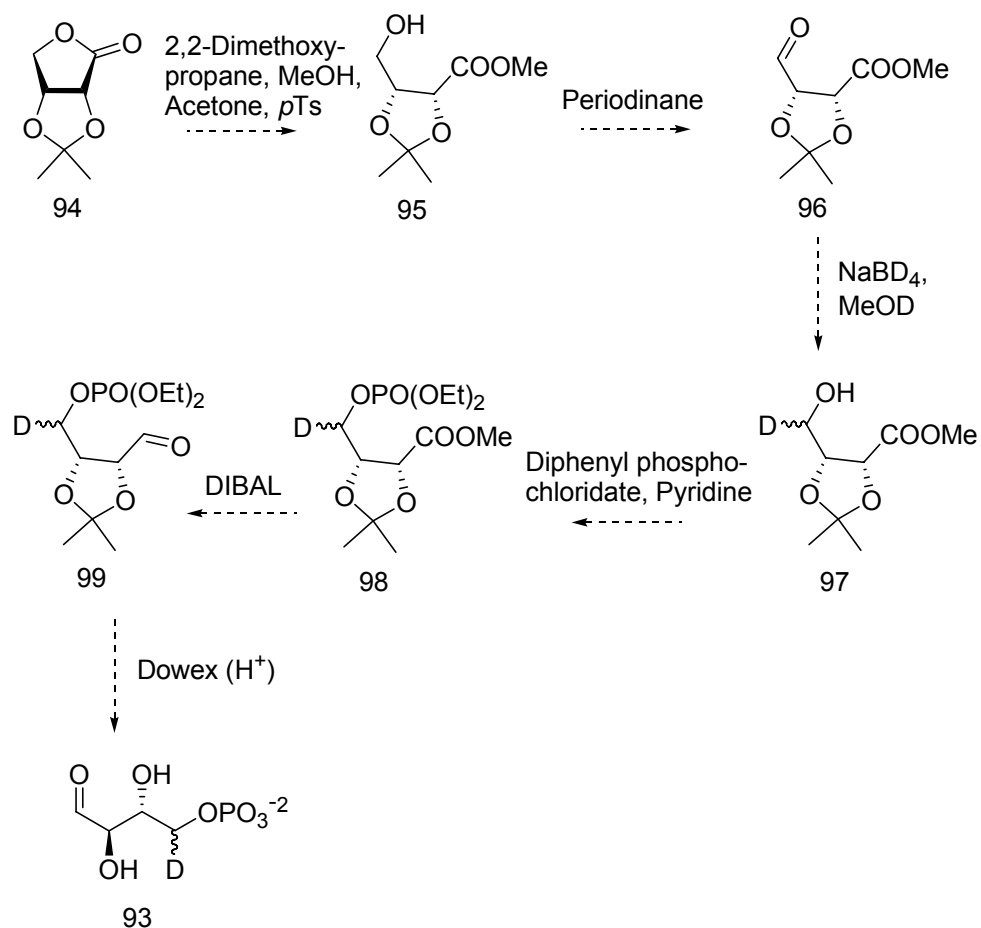


Figure 5.22. Proposed synthesis of 4-[<sup>2</sup>H]-D-erythrose-4-phosphate by way of 2,3-*O*-isopropylidene-erythrone

Another scheme was to start with erythrone **100**, benzyl protect C-2 and C-3, and introduce a thioester or an isopropylacetone at C-1. To C-4 would be introduced a deuterium followed by phosphorylation of the C-4 hydroxyl (see figure 5.23).

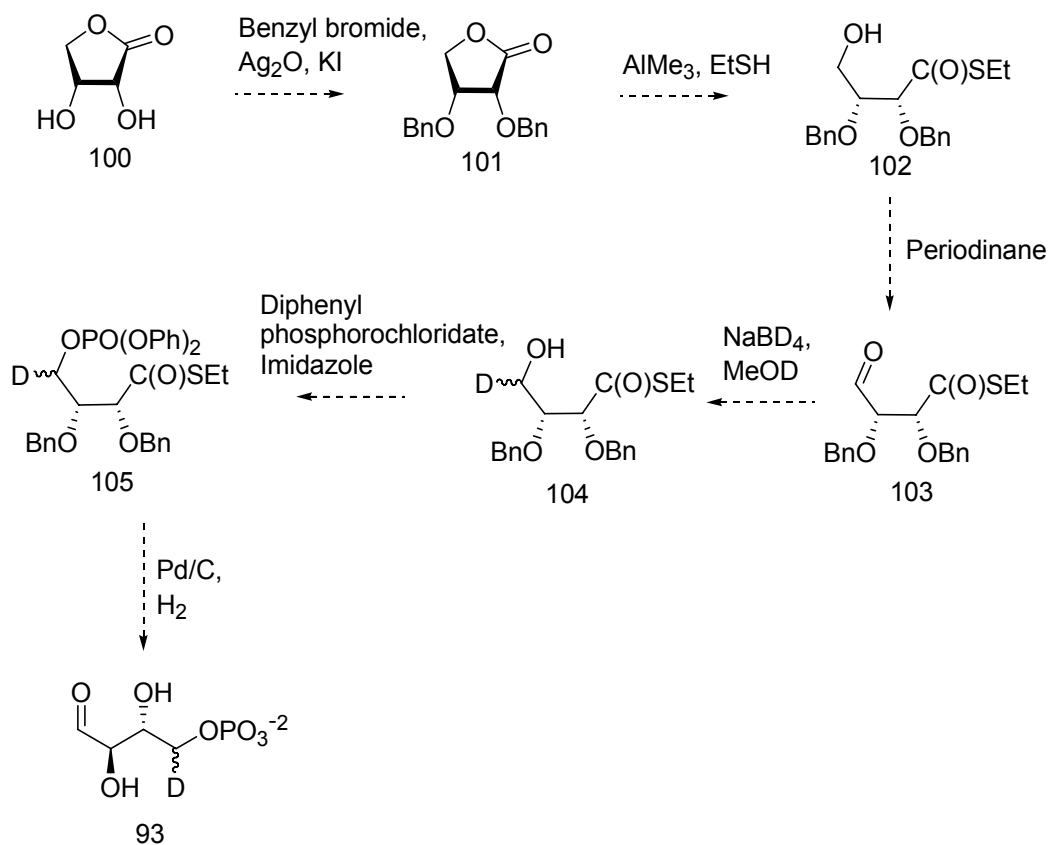


Figure 5.23. Proposed synthesis of 4-[ $^2\text{H}$ ]-D-erythrose-4-phosphate by way of erythronolactone

### 5.3.3.1 4-[ $^2\text{H}$ ]-D-erythrose 4-phosphate results

Initial attempts to form methyl ester **95** were unsuccessful with only a miniscule amount of unknown product being produced based on TLC (insufficient for NMR analysis). Upon closer inspection of 2,3-*O*-isopropylidene-erythronolactone **94** it was found that this starting material was lacking the expected acetal protecting group. No further reactions using this method were done.

Using the second method, erythronolactone **100** was protected using benzyl bromide in the presence of potassium iodide and silver (I) oxide to form benzyl protected lactone **101** in 56% yield. Given the difficulty of deprotecting thioesters it was decided to try protecting the C-1 lactone as an isopropylidene acetal. To benzyl protected lactone

**101** was added DIBAL to reduce the C-1 lactone, followed by dimethylpropanediol in the presence of trimethylsilylchloride to form alcohol **106** in 26% yield. Oxidation of alcohol **106** with periodinane to form aldehyde **107** was unsuccessful (see figure 5.24).

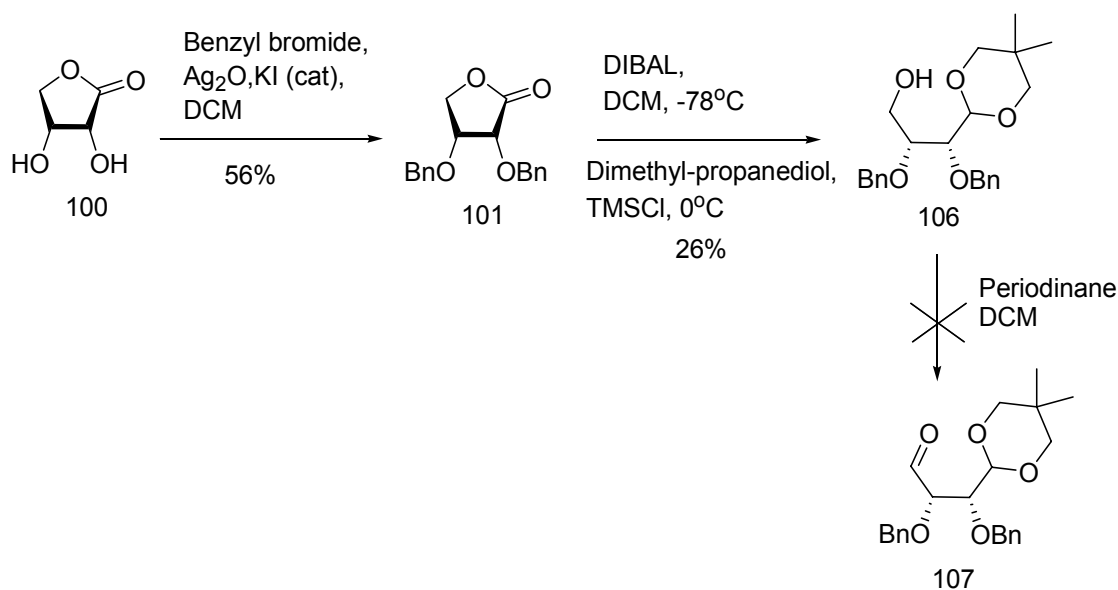


Figure 5.24. Results for the synthesis of 4- $^{2}\text{H}$ -D-erythrose-4-phosphate by way of erythronolactone

Upon closer inspection it was discovered that alcohol **106** was incorrectly characterised. Treatment of the reduced form of benzyl protected lactone **101** with dimethylpropanediol actually resulted in ether **108** (see figure 5.25).

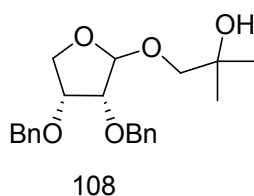


Figure 5.25. Product formed from the acetonide protection of the lactone

As an alternative, benzyl protected lactone **101** was treated with ethanethiol in the presence of trimethylaluminum to form the thioester **102** in 54% yield. Thioester **102**

was then oxidised with periodinane to form aldehyde **103** in 42% yield (see figure 5.26).

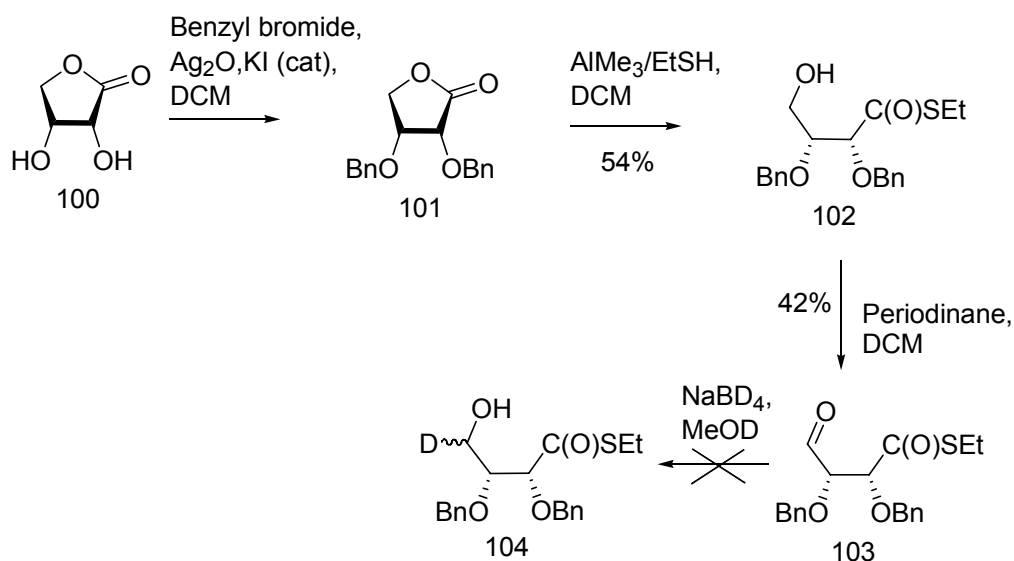


Figure 5.26. Results for the modified synthesis of 4-[<sup>2</sup>H]-D-erythrose 4-phosphate by way of erythrulose

Aldehyde **103** was treated sodium borodeuteride to form deuterated product **104**. However, <sup>1</sup>H NMR analysis of deuterated product **104** showed the formation of an over-reduced product **109** whereby the thioester was subsequently removed (see figure 5.27).

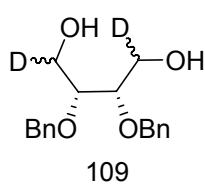


Figure 5.27. Over-reduced product **109**; loss of thioester after reduction with sodium borodeuteride

It was decided to stop at this point given that there was insufficient time to investigate the synthesis of 4-[<sup>2</sup>H]-D-erythrose 4-phosphate any further.

## 5.4 Summary

Of the four proposed schemes from section 5.2 for the synthesis of 2-keto-*gluco*-heptulosonic acid **45**, the fourth scheme (figure 5.12) was the most successful. Although the synthesis of GH7P **82** had some complications due to the loss of the methyl ether at C-2 of heptulosonate **78**, it is still likely to form GH7P **82** if the synthesis is carried to completion using heptulosonate **83**. Nucleophilic fluorination of a closed-ring advanced intermediate of 2-keto-*gluco*-heptulosonic acid **45** would be the best approach to synthesising (7*R*)-[7-<sup>2</sup>H]-(3*S*)-3-fluoro-DAH7P **43** and (7*R*)-[7-<sup>2</sup>H]-(3*R*)-3-fluoro-DAH7P **44**. Both electrophilic and nucleophilic fluorinations of an open-ring advanced intermediate of 2-keto-*gluco*-heptulosonic acid **45** were unsuccessful.

## 6. Overall conclusions and future work

The aim of this research was, firstly, to determine the extent to which the stereochemical control of DHQS is maintained across different sources of DHQS; and, secondly, to determine if either of the enol pyranose with fluorine in the axial or equatorial position fully dissociates from the enzyme resulting in the formation of products occurring off the enzyme. Finally, this research investigated the effect of fluorine on the enolate intermediate in order to determine whether the formation of the epimeric product arises from a stereoelectronic effect.

Two fluorinated analogues of DAH7P were prepared and used to examine the enzyme-catalysed cyclisation steps across three phylogenetically distinct sources of DHQS. These sources were *Escherichia coli*, Kiwifruit, and *Pyrococcus furiosus*. *E. coli* DHQS was purified by ammonium sulfate precipitation and a combination of anion exchange and size exclusion chromatography. *P. furiosus* DHQS was purified by heat denaturation and anion exchange chromatography. The modified DAH7P substrates were (3*S*)-3-fluoro-DAH7P **28** and (3*R*)-3-fluoro-DAH7P **25**. (3*S*)-3-Fluoro-DAH7P **28** contains a fluorine in the axial position and (3*R*)-3-fluoro-DAH7P **25** contains a fluorine in the equatorial position. <sup>19</sup>F NMR spectroscopy was used to determine the partitioning of products formed for each enzyme and steady-state kinetics was used to determine the activity of the enzymes in the presence of each modified substrate.

All three enzymes processed (3*R*)-3-fluoro-DAH7P **25** in the exact same manner, each producing (6*R*)-6-fluoro-DHQ **27** as the sole product (see figure 6.1).

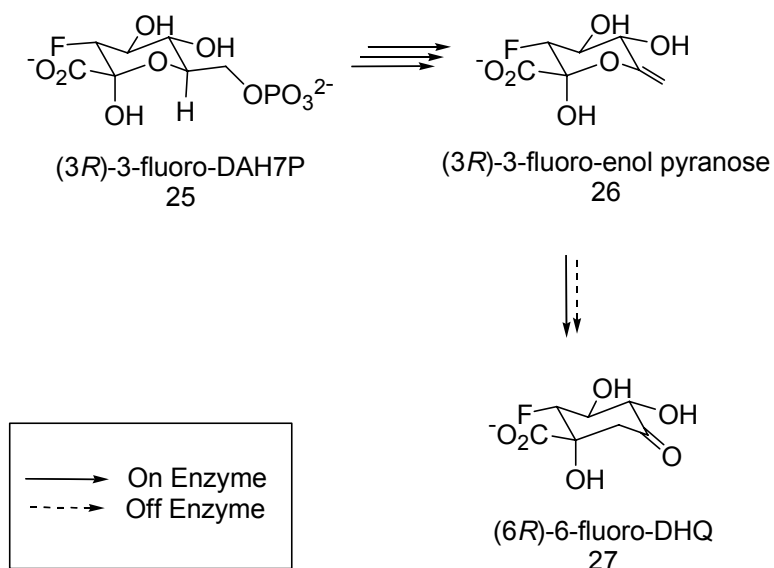


Figure 6.1. Schematic of product formed from (3R)-3-fluoro-DAH7P in the presence of *E. coli* DHQS, Kiwifruit DHQS and *P. furiosus* DHQS

The data from (3R)-3-fluoro-DAH7P **25** do not provide much insight to the cyclisation step of DHQS. The products from (3R)-3-fluoro-DAH7P **25** could have been formed exclusively on or off the enzyme. This is primarily due to the possible transition-state conformations that would favour the formation of (6R)-6-fluoro-DHQ **27**, based on a Felkin-Anh model, as the sole product whether it be on or off the enzyme.

In contrast to the (3R)-3-fluoro-DAH7P **25** results, all three enzymes processed (3S)-3-fluoro-DAH7P **28** in different ways, each producing different ratios of products (see table 11). *E. coli* DHQS produced a 2:1 ratio of (6S)-6-fluoro-DHQ **30** to 1-*epi*-(6S)-6-fluoro-DHQ **31**. Kiwifruit DHQS produced a 13:1 ratio of (6S)-6-fluoro-DHQ **30** to 1-*epi*-(6S)-6-fluoro-DHQ **31**. *P. furiosus* DHQS produced (6S)-6-fluoro-DHQ **30** as the sole product. It should be noted that the assay for *P. furiosus* DHQS was done at an elevated temperature but not at the temperature the enzyme prefers to work at.

Table 11.

$^{19}\text{F}$  NMR partitioning results for *E. coli* DHQS, Kiwifruit DHQS, and *P. furiosus* DHQS incubated with (3*S*)-3-fluoro-DAH7P

Enzyme	Products formed		
	(6 <i>S</i> )-6-fluoro-DHQ	1- <i>epi</i> -(6 <i>S</i> )-6-fluoro-DHQ	Ratio of products
<i>E. coli</i> DHQS	69%	31%	2:1
Kiwifruit DHQS	93%	7%	13:1
<i>P. furiosus</i> DHQS	100%	0%	---

It is possible that both diastereomers were formed in solution by way of an abortive pathway after the third step of the mechanism (see figure 6.2).

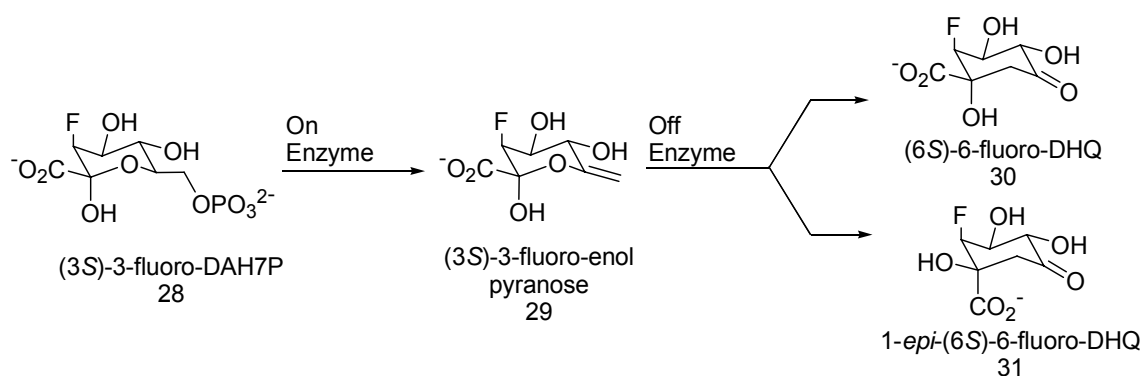


Figure 6.2. Formation of (6*S*)-1-*epi*-6-fluoro-dehydroquinate and (6*S*)-6-fluoro-dehydroquinate from (3*S*)-3-fluoro-DAH7P in the presence of *E. coli* DHQS.

During the internal aldol reaction, the formation of the non-epimeric product involves attack of the *re* face of the carbonyl, whereas formation of the epimeric product involves attack of the *si* face of the carbonyl. Based on the observations of the partitioning assays reported in this thesis, it is unlikely that both diastereomers are formed on the enzyme from (3*S*)-3-fluoro-enol pyranose **29**, as there are significant differences in the ratio of products formed by the different enzymes.

The best explanation for the differences in the amount of epimer produced by the different enzymes is that the enzyme is involved in the formation of at least one of the products, this being (6*S*)-6-fluoro-DHQ **30** (see figure 6.3).

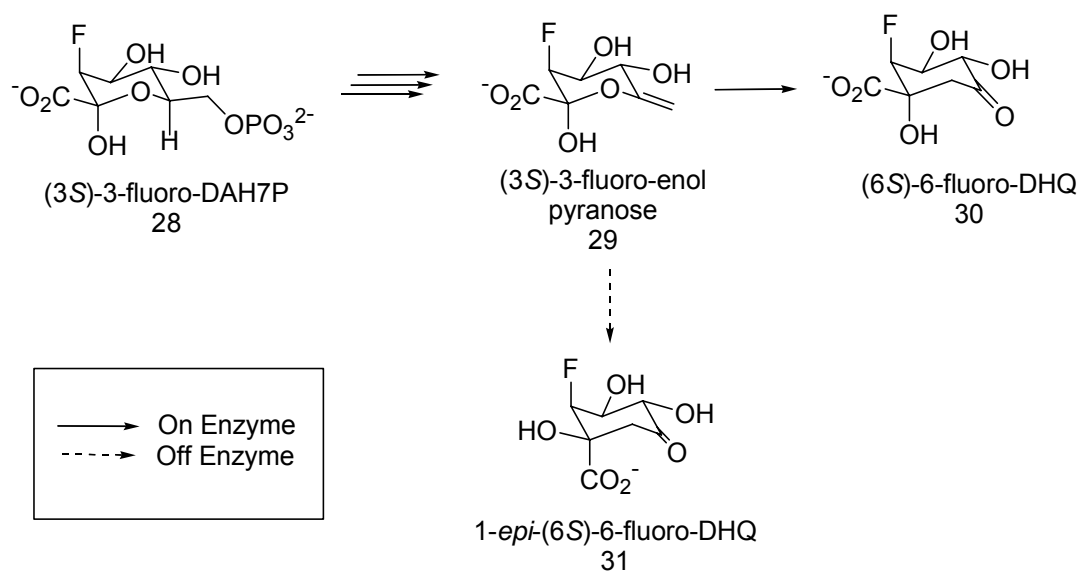


Figure 6.3. Schematic of products formed from (3*S*)-3-fluoro-DAH7P in the presence of *E. coli* DHQS and Kiwifruit DHQS.

The ability of (3*S*)-3-fluoro-enol pyranose **29** to dissociate at least partially from the enzyme could be indicative of an electronic effect from the fluoro group at C-3 resulting in the stabilisation of this intermediate and a decrease in the rate of ring opening (see figure 6.4).<sup>28</sup>

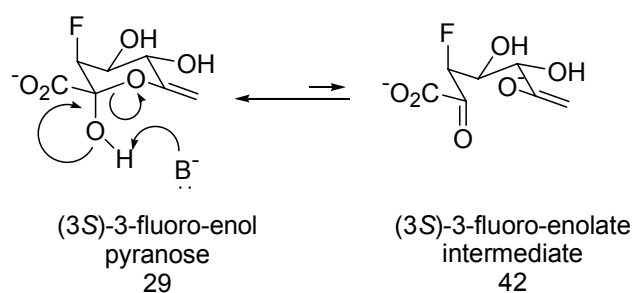


Figure 6.4. Schematic of the stabilising effect of fluorine on (3*S*)-3-fluoro-enol pyranose.

This is supported by the steady-state kinetics results for all three DHQSs, which show a decrease in affinity for (3*S*)-3-fluoro-DAH7P **28** compared to DAH7P **3**. There is also a decrease in affinity for (3*S*)-3-fluoro-DAH7P **28** compared to (3*R*)-3-fluoro-DAH7P **25** across all three sources of DHQS. The stabilisation of the (3*S*)-3-fluoro-enol pyranose **29** is further supported by a decrease in the specificity constant for (3*S*)-3-fluoro-DAH7P **28** compared to DAH7P **3** across all three enzymes. Once in solution, the (3*S*)-3-fluoro-enolate intermediate **42** could undergo a conformational change in the ring leading to the formation of the epimeric product (see figure 6.5). However, it is also possible that the fluoro-enol pyranose is no more stabilised in either case and perhaps all that is being observed is that the C-3 fluorine plays a critical role stereoelectronically in the ring closing step.

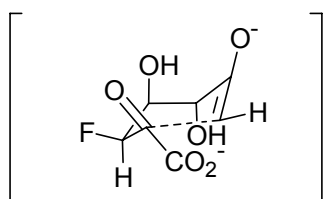
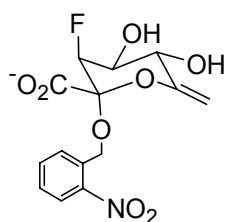


Figure 6.5. Predicted transition-state conformation of the (3*S*)-3-fluoro-enolate intermediate off the enzyme

These studies have illuminated the role of the enzyme in guiding the correct stereochemistry of the product. By derailing the enzyme through the introduction of fluorine in DAH7P, it is possible to create a breakdown in the enzyme-substrate interactions of DHQS. This breakdown is demonstrated by the formation of two products and can be explained by partial leakage of a substrate intermediate whereby cyclisation occurs in solution. In addition, enzyme catalysis showed a slowing of reaction rates when either fluorinated substrate was used, suggesting that the fluoro at C-3 is stabilising the enol pyranose. An increase in the stabilisation of the fluoro-enol pyranose would allow release of this intermediate from the enzyme to compete with

the on-going on-enzyme reaction. With regard to the partitioning results, the amount of 1-*epi*-(6*S*)-6-fluoro-DHQ **31** formed was much less for Kiwifruit DHQS than for *E. coli* DHQS. Most notable were the results seen with *P. furiosus* DHQS, which showed no formation of 1-*epi*-(6*S*)-6-fluoro-DHQ **31**. This could be because differences in the amino acid composition and structural composition of the enzymes result in variations in stereochemical control of the overall reaction with (3*S*)-3-fluoro-DAH7P **28**. It is also possible that the results seen with *P. furiosus* DHQS are due to the suboptimal temperature at which the reaction was performed. The information provided from this study illustrates the important molecular interplay between the enzyme and substrate.

It is still unknown if the (3*S*)-3-fluoro-enolate intermediate **42** cyclises in solution to form exclusively 1-*epi*-(6*S*)-6-fluoro-DHQ **31** as the sole product or whether there is partitioning in solution also to generate (6*S*)-6-fluoro-DHQ **30**. This question could be addressed by monitoring the cyclisation of the (3*S*)-3-fluoro-enolate intermediate **42** in solution and determining the ratio of 1-*epi*-(6*S*)-6-fluoro-DHQ **31** and (6*S*)-6-fluoro-DHQ **30** formed. The synthesis of a modified (3*S*)-3-fluoro-enol pyranose **107** would be of great benefit to complete the cyclisation story of DHQS (see figure 6.6). The modified (3*S*)-3-fluoro-enol pyranose **110** would contain a nitro-benzyl protecting group which could be removed by UV irradiation thereby allowing for ring opening followed by spontaneous cyclisation.



110

Figure 6.6. Schematic of modified (3*S*)-3-fluoro-enol pyranose **110**.

Bartlett and Satake (1988) showed that the ring opening of the enol pyranose **13** and intramolecular aldol reaction steps can occur spontaneously in solution to form DHQ **4** without the assistance of the enzyme. However, this spontaneous reaction also results in the formation of 2-4% 1-*epi*-DHQ **24** (see figure 6.7).

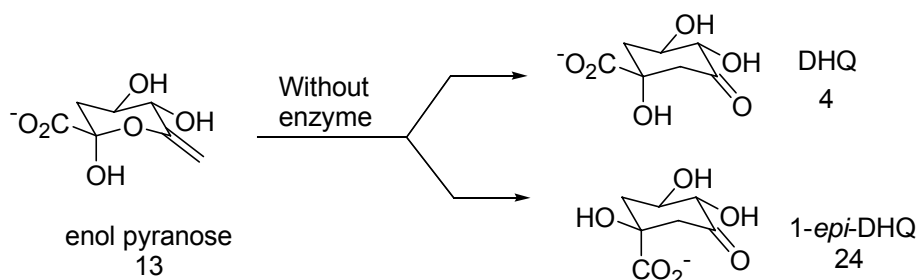


Figure 6.7. Partitioning of enol pyranose from DAH7P in the absence of DHQS.

In the same manner, the modified (3*S*)-3-fluoro-enol pyranose **110** could be used to monitor the spontaneous cyclisation of this fluorinated analogue in order to determine the ratio of products formed in solution from the (3*S*)-3-fluoro-enolate intermediate **42**.

Further work needs to be done to incorporate fluorine into 2-keto-*gluco*-heptulosonic acid **45**. The fluorinated 2-keto-*gluco*-heptulosonic acid analogue **111** can then be converted to the modified (3*S*)-3-fluoro-enol pyranose **110** by adapting the synthetic scheme published by Bartlett and Satake (see figure 6.8).<sup>25</sup>

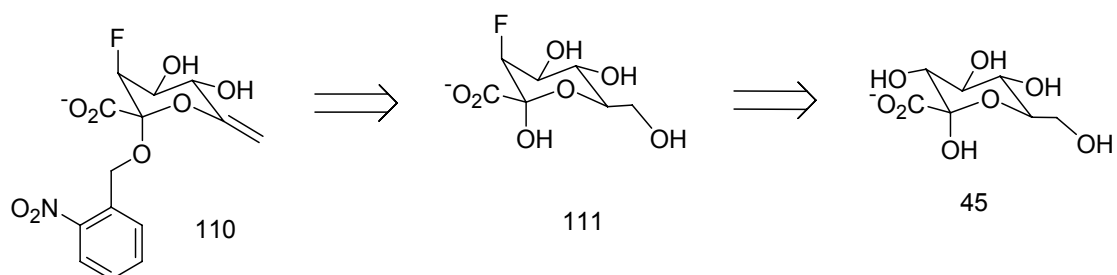


Figure 6.8. Retrosynthesis of the modified (3*S*)-3-fluoro-enol pyranose **110**.

Of the two fluorination techniques available, it appears that nucleophilic fluorination would be the most promising given the partial success seen with the formation of monofluoro products **85** and **88**, albeit both at 10% yields only (refer to section 5.3.2.3 in previous chapter). None of the electrophilic fluorinations attempted in this study were remotely successful.

Assessment of *gluco*-heptulosonate 7-phosphate (GH7P) **82** as a substrate or inhibitor for DHQS would provide some insight to the steric limitations of the enzyme at the binding site. GH7P **82** is similar to 3-fluoro-DAH7P except that a hydroxyl would be present in place of fluorine. The C-3 hydroxyl could provide the opportunity to understand both the electronic effect of the C3 substitution and the effect of introducing a H-bond donor or acceptor in this position (see figure 6.9).

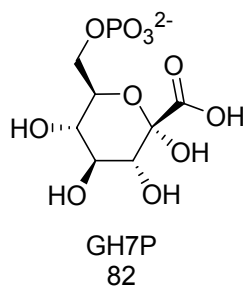


Figure 6.9. Schematic of GH7P.

However, a real-time method to monitor the reaction and products formed from GH7P **82** would have to be developed. It is unlikely that the quinate product of GH7P **82** would be UV active. It is also unknown whether the quinate product of GH7P **82** is a substrate for DHQase. Two alternative methods would be to assay the products formed after the reaction using <sup>1</sup>H NMR spectroscopy and monitoring the rate of release of phosphate during the reaction using the Lanzetta assay.

In addition to the elucidation of the cyclisation steps of DHQS, this research also developed new methods for the purification of DHQS and DHQase from *P. furiosus*. *P. furiosus* DHQS and DHQase were expressed, purified, and characterised successfully. In addition, DHQS and DHQase from *E. coli* were both expressed, purified, and characterised using modifications to the previously reported protocols from Frost and co-workers.<sup>30</sup> Finally, in this study the characterisation of Kiwifruit DHQS was reported for the first time.

One characterisation result of interest is that DHQs from *E. coli*, *P. furiosus*, and Kiwifruit all exist as homodimers under the conditions examined. Frost and co-workers reported recombinant *E. coli* DHQS was monomeric. The differences in quaternary structures of the two *E. coli* DHQs could be due to the different methods for molecular-weight determination or to the modifications made to the purification protocol for *E. coli* DHQS in this study, which likely preserved the protein as a dimer.

Homology modelling of *P. furiosus* DHQS showed potentially close structural similarity and conservation of active-site amino acids compared to *S. aureus* DHQS, *T. thermophilus* DHQS, and *A. nidulans* DHQS. However, the active site Asp121 from *P. furiosus* DHQS may not overlap with equivalent Asp146 from *A. nidulans* DHQS. It is possible that the Asp121 from *P. furiosus* DHQS can be rotated to a similar conformation to Asp146 from *A. nidulans* DHQS which is similar to that found in the enzymes from *S. aureus* and *T. thermophilus*. Given the differences in the partitioning experiment with *P. furiosus* DHQS and the preliminary differences seen with the homology model of *P. furiosus* DHQS, a crystal structure of this enzyme

would help provide answers as to why the enzyme interacts differently with (3*S*)-3-fluoro-DAH7P **28** compared to *E. coli* DHQS.

## **7. Experimental**

### **7.1 General methods**

#### **Synthetic reactions**

Air- and moisture-sensitive reactions were carried out under an atmosphere of nitrogen or argon unless otherwise stated. All glassware was dried in a heated drying closet or with a heat gun.

#### **Chromatography**

Analytical thin-layer chromatography was performed on Merck Silica Gel 60 F<sub>254</sub> aluminium sheets. Spots on silica sheets were visualised under UV light (254nm) and by charring with basic potassium permanganate. Flash chromatography was performed on Scharlau Silica Gel 60, 230-400 mesh.

#### **Solvents**

All organic solvents were distilled prior to use unless otherwise stated. Dichloromethane was distilled from calcium hydride, tetrahydrofuran from sodium wire and benzophenone. Ethyl acetate and hexane were distilled to remove non-volatile contaminants prior to use in flash column chromatography. All other solvents were used as supplied from commercial sources. Milli-Q water was used for all biochemical work.

## **NMR**

One- and two-dimensional NMR spectra were recorded on a Bruker Avance<sup>®</sup> 400 MHz or 500 MHz NMR spectrometer in deuterated solvents as indicated.

**pH measurements** were made using a Sartorius Professional Meter. The pH of solutions was adjusted using 10 M NaOH and ~12 M HCl.

## **Fast protein liquid chromatography (FPLC)**

FPLC was performed at 4 °C using a BioLogic Duo-Flow FPLC system (Bio-Rad) with detection at 280 and 214 nm or at room temperature on an AKTA FPLC (Pharmacia).

## **Electrospray ionisation mass spectrometry (ESI MS)**

The molecular weight of protein samples was determined by ESI MS on a Micromass LCT TOF instrument, equipped with an electrospray ionisation (ESI) probe. This system was controlled by MassLynx (version 4.0) software. Protein and small molecule samples (10 µg/mL) were prepared in 50% acetonitrile and water and directly injected at 20 µL/mL. Samples were analysed with a cone voltage of 25 V and a probe voltage of 3,200 V.

**Sonication** was performed on a VirTis VirSonic digital 475 ultrasonic cell disrupter fitted with an 1/8 inch probe at ~60 Watts.

**Centrifugation** was performed in one of three centrifuges: a SORVALL Evolution RC centrifuge, a SORVALL Heraeus multifuge<sup>™</sup> 1S/1S-R or a MiniSpin<sup>™</sup> centrifuge

(Eppendorf). All centrifugations were done at 4 °C with the exception of the MiniSpin centrifuge which was done at 21 °C.

### **Reagents**

All reagents were of the highest grade available and purchased from Sigma-Aldrich or Merck unless otherwise stated. Media was purchased from Invitrogen.

**UV-Visible spectrophotometry** was performed on a Varian Cary 1 UV spectrophotometer at 25 °C unless otherwise specified using 1 cm quartz cells. Temperature was controlled with a thermostated water bath. Initial rates were calculated using the least-squares gradient facility over the first 10% of the reactions progress curve.

## 7.2 General biological methods

### Buffers for FPLC

Buffers for anion exchange chromatography were prepared for each enzyme as follows:

#### *P. furiosus* DHQS

Buffer A: 50 mM 1,3-bis(tris(hydroxymethyl)amino)propane (BTP) with 10  $\mu$ M EDTA, pH 7.8

Buffer B: 50 mM BTP, 10  $\mu$ M EDTA with 1M NaCl, pH 7.8

#### *E. coli* DHQS

Buffer A: 10 mM  $\beta$ -glycerophosphate, pH 6.6

Buffer B: 10 mM  $\beta$ -glycerophosphate with 1 M NaCl, pH 6.6

#### *E. coli* DHQase

Buffer A: 50 mM BTP with 10  $\mu$ M EDTA, pH 7.5

Buffer B: 50 mM BTP, 10  $\mu$ M EDTA with 1M NaCl, pH 7.5

Buffers for size exclusion chromatography were prepared for each enzyme as follows:

#### *P. furiosus* DHQase

10 mM BTP, 10  $\mu$ M EDTA, 50 mM KCl, pH 6.8

#### *E. coli* DHQS

10 mM  $\beta$ -glycerophosphate, 0.15 M NaCl, pH 6.6

### Amino acid sequence alignments

Amino acid sequence alignments were performed by copying and pasting the desired primary sequences into ClustalW (EMBL-EBI) (<http://www.ebi.ac.uk/ClustalW>) and performing a multiple sequence alignment.

### **Lanzetta phosphate assay<sup>40,57</sup>**

The Lanzetta reagent was composed of a 3:1:0.1 mixture of malachite green (0.045%), ammonium molybdate (4.2%), and Triton X100 (1.5%). This reagent was made up fresh, stirred for 0.5 hours and filtered through a 0.45  $\mu\text{m}$  filter and protected from light. A standard curve was generated using five solutions of  $\text{KH}_2\text{PO}_4$  ranging from zero to 51  $\mu\text{g/mL}$ . Samples containing 10  $\mu\text{L}$  of substrate, 10  $\mu\text{L}$  of 10x buffer, 78  $\mu\text{L}$  of water, 1  $\mu\text{L}$  of shrimp alkaline phosphatase (1000 U, Roche<sup>TM</sup>), and 1  $\mu\text{L}$  of 500 mM  $\text{MgCl}_2$  (final volume of 100  $\mu\text{L}$ ) were incubated at 37 °C for 1.5 hours. To each standard (100  $\mu\text{L}$ ) and sample (100  $\mu\text{L}$ ) was added 750  $\mu\text{L}$  of Lanzetta reagent and the mixture was allowed to react. After 20 minutes the absorbance for each sample and standard was recorded at 660 nm. A solution of milli-Q water and reagent provided the blank.

### **Gel electrophoresis**

Polyacrylamide gel electrophoresis (PAGE) in the presence of sodium dodecylsulfate (SDS) was performed by the method of Laemmli with a 4% (w/v) stacking gel and a 12% (w/v) running gel, using a Mini Protean III cell (BioRad). Samples were prepared in a loading buffer containing SDS, boiled, and loaded within 10 minutes. Low range SDS-PAGE molecular weight standards (BioRad) were used. After electrophoresis gels were stained for protein using Coomassie Brilliant Blue R 250 (Park Scientific).

### **Determination of protein concentration<sup>58</sup>**

Protein concentrations were determined by the method of Bradford, using bovine serum albumin as a standard. Bradford reagent (Bio-Rad) was diluted 5-fold with Milli-Q water and filtered (0.2  $\mu\text{m}$ ). The BSA protein standards were made from dilution of a stock (Bio-Rad, 20 mg/mL). The assays were performed by thoroughly mixing 100  $\mu\text{L}$  of protein standard solution or sample with 1 mL of Bradford reagent. Absorbance readings (595 nm) were then taken of all the standards and samples and the concentration (mg/mL) was determined using the Cary UV software.

### **Enzyme assays – general conditions**

*In vitro* experiments were performed spectroscopically using a coupled enzyme continuous assay to determine the activity of DHQS. In the presence of excess DHQase, the measurement of dehydroshikimate served as a quantitative measure for the activity of DHQS. The appearance of dehydroshikimate was monitored spectrophotometrically at 234 nm ( $\epsilon = 1.2 \times 10^4 \text{ M}^{-1} \text{ cm}^{-1}$  at 25 °C, pH 6.8). In the case of the fluorinated substrates, the appearance of (6*S*)-6-fluoro-DHS and (6*R*)-6-fluoro-DHS was monitored at 230 nm ( $\epsilon = 9.6 \times 10^3 \text{ M}^{-1} \text{ cm}^{-1}$  and  $3.4 \times 10^3 \text{ M}^{-1} \text{ cm}^{-1}$  respectively) at 25 °C pH 6.8.<sup>27</sup> Measurements were made in a 1 cm path length quartz cuvette maintained at the required temperature in a thermostated cuvette holder.

Assays were performed at 25 °C for *E. coli* DHQS and Kiwifruit DHQS, and 60 °C for *P. furiosus* DHQS. Initial rates of reaction were determined by a least-squares fit of the initial rate data. One unit (1 U) of enzyme activity is defined as the production of 1  $\mu\text{mol}$  of shikimate product per minute at 25 °C for *E. coli* DHQS and Kiwifruit DHQS, and at 60 °C for *P. furiosus* DHQS. Specific activity is defined as the

production of 1  $\mu\text{mol}$  of shikimate product per minute at 25 °C per mg of protein (U/mg).  $K_m$  and  $k_{\text{cat}}$  values were determined by fitting the data to the Michaelis-Menten equation using GraFit 5 (Erithacus Software Limited, 2006). Errors between measurements were no more than 10 %.

## **Media**

All *E. coli* cultures were grown in Luria Bertani (LB) broth unless otherwise stated. LB broth (Invitrogen) was made up (25 g/L) with Milli-Q water and sterilised by autoclaving at 121 °C and 15 psi for 20 minutes. Agar media for agar plates was prepared by adding 1.5 % agar (Oxoid) to the liquid media prior to autoclaving.

SOC media was used to incubate freshly transformed *E. coli*. SOC media consists of 20 g/L bacto-tryptone (Merck), 5 g/L bacto-yeast extract (Invitrogen), 0.5 g/L NaCl (Univar), 2.5 mM KCl (Merck), 10 mM  $\text{MgCl}_2$  (BDH) and 10 mM glucose (Invitrogen). All components were added to Milli-Q water, except glucose, and autoclaved. Solutions of glucose (100 mM) and  $\text{MgCl}_2$  (1 M) were filter-sterilised (0.2  $\mu\text{m}$ ) and added immediately prior to use.

### 7.3 Experimental for chapter 2

#### **Expression of *Escherichia coli* DHQS**

*E. coli* RB791 cells transformed with the plasmid pJB14 containing the *Escherichia coli* (*E. coli*) DHQS gene, were grown overnight at 37 °C in 5 mL tubes containing Luria Bertani (LB) media supplemented with ampicillin (100 µg/mL). Four mL of inoculum were added to a 250 mL flask containing 60 mL of LB with ampicillin (100 µg/mL), and allowed to shake at 37 °C. After one-hour growth, the culture was split into two portions and each 30 mL culture was used to inoculate 1 L of LB supplemented with ampicillin (100 µg/mL). After incubating for a further hour, 0.5 mL of culture were removed from each flask and the optical density at 600 nm (O.D.<sub>600</sub>) of each sample was assessed. When the O.D.<sub>600</sub> reached ~0.6, 1 mL of IPTG (final concentration 1 mM) was added to each 1 L flask and allowed to shake at 37 °C. After six hours of incubation, the cells were harvested.

#### **Expression of *Pyrococcus furiosus* DHQS**

*E. coli* BL21(DE3) Rosetta cells transformed with the plasmid pT7-7, containing the *Pyrococcus furiosus* (*P. furiosus*) DHQS gene, were grown overnight at 37 °C in two 5 mL tubes containing Luria Bertani (LB) media supplemented with ampicillin (100 µg/mL) and chloramphenicol (34 µg/mL). Ten mL of inoculum were added to a 1000 mL flask containing 500 mL of LB with ampicillin (100 µg/mL) and chloramphenicol (34 µg/mL), and allowed to shake at 37 °C. After incubating for three hours, 0.5 mL of culture was removed and the optical density assessed. When the O.D.<sub>600</sub> reached ~0.6, 1 mL of IPTG (final concentration 1 mM) was added and the culture was allowed to shake overnight at 37 °C. After 16 hours of incubation, the cells were harvested.

### **Expression of *Escherichia coli* DHQase**

*E. coli* AB2848/pKD201 cells transformed with the plasmid pJJK12 containing the *E. coli* DHQase gene, were grown overnight in 2 x 5 mL tubes containing Luria Bertani (LB) media supplemented with ampicillin (100 µg/mL). Ten mL of inoculum were added to a 2 L flask containing 1000 mL of LB with ampicillin (100 µg/mL), and allowed to shake at 37 °C. When the O.D.<sub>600</sub> reached 0.5, 1 mL of IPTG (final concentration 1 mM) was added to the 1 L flask and allowed to shake at 37 °C. After eight hours of incubation, the cells were harvested.

### **Expression of *Pyrococcus furiosus* DHQase**

*E. coli* BL21(DE3) Rosetta cells transformed with the plasmid pT7-7 containing the *P. furiosus* DHQase gene, were grown overnight at 37 °C in 2 x 5 mL tubes containing LB media supplemented with ampicillin (100 µg/mL) and chloramphenicol (34 µg/mL). Ten mL of inoculum were added to a 1 L flask containing 500 mL of LB media with ampicillin (100 µg/mL) and chloramphenicol (34 µg/mL), and allowed to shake at 37 °C. When the O.D.<sub>600</sub> reached 0.6, 0.5 mL of IPTG (final concentration 1 mM) was added to the 1 L flask and allowed to shake at 37 °C. After six hours of incubation, the cells were harvested.

## Harvesting and Lysis of Cells

The cells were harvested by centrifuging at 4000 *g* for 20 minutes at 4 °C. The cell pellets were then stored at -80 °C until lysis.

The cell pellets were re-suspended in the appropriate lysis buffer (on ice). Cells containing *E. coli* DHQS and *E. coli* DHQase were lysed by sonication on ice. Cells containing *P. furiosus* DHQS and *P. furiosus* DHQase were lysed by sonication at 30 °C. The cell debris were removed by centrifugation (10,000 *g* at 4 °C for 15 minutes).

## Lysis buffer

Lysis buffer for each enzyme was prepared as follows:

### *E. coli* DHQS

75 mM potassium phosphate with 100 mM NaCl and 1 mM DTT, pH 6.63.

### *E. coli* DHQase

50 mM BTP, 10 μM EDTA, pH 6.8.

### *P. furiosus* DHQS

50 mM BTP, 2 mM DTT, 0.5 mM NAD<sup>+</sup>, 200 mM KCl, pH 7.8.

### *P. furiosus* DHQase

50 mM BTP, 2 mM DTT, 1 mM EDTA, 200 mM KCl, pH 7.5.

The BTP buffer was made up with milli-Q water and treated with Chelex (1 hour at room temperature) prior to addition of additives.

### **Ammonium sulfate fractionation<sup>59</sup>**

*E. coli* DHQS was subjected to ammonium sulfate fractionation. To a 10 mL sample of soluble crude protein in 10 mM  $\beta$ -glycerophosphate pH 6.6 buffer, was added 1.7 g of ammonium sulfate to make a 30% solution of ammonium sulfate. The solution was stirred for 30 minutes at 4 °C and centrifuged at 10000 g for 20 minutes at 4 °C. The supernatant was removed and the remaining pellet was labelled “0-30% AS cut” and stored on ice. To the remaining supernatant was added 1.2 g of ammonium sulfate to make a 50% solution of ammonium sulfate and this was allowed to stir for 30 minutes at 4 °C. The solution was centrifuged and the supernatant removed. The remaining pellet was labelled “30-50% AS cut” and stored on ice. To the remaining supernatant was added 1.29 g of ammonium sulfate to make a 70% solution of ammonium sulfate and allowed to stir for 30 minutes at 4 °C. The solution was centrifuged and the supernatant removed. The remaining pellet was labelled “50-70% AS cut” and stored on ice. To the remaining supernatant was added 2.15 g of ammonium sulfate to make a 100% solution of ammonium sulfate and this was allowed to stir for 30 minutes at 4 °C. The solution was centrifuged and the supernatant removed. The remaining pellet was labelled “70-100% AS cut” and stored on ice. A small amount of each fraction was resuspended and checked for activity. The fraction with activity was resuspended in 10 mM  $\beta$ -glycerophosphate pH 6.6 buffer and this fraction subjected to desalting column chromatography.

### **Anion exchange chromatography**

Anion exchange chromatography was performed using a Source Q 15 column (Amersham Biosciences). Filtered lysate was diluted to 10 mL with buffer A and loaded onto the column. Enzyme was eluted using a NaCl gradient. Fractions containing protein and exhibiting activity were pooled and concentrated using a prewashed 20 mL Vivaspin 10000 MWCO concentrator (Vivascience). The concentrate was frozen in aliquots in liquid nitrogen and stored at -80 °C.

### **Size exclusion chromatography**

Filtered samples of semi-purified protein (400 µL) at concentrations of  $\leq 10$  mg/ mL were applied to the column (Superdex S200 HR 10/300 column (Amersham Biosciences) using a 500 µL loop. The system was run at 0.4 mL/ min. Fractions (0.5 mL) were collected for the entire run. Fractions containing protein and exhibiting activity were pooled and concentrated using a prewashed 20 mL Vivaspin 10000 MWCO concentrator (Vivascience). The concentrate was frozen in aliquots in liquid nitrogen and stored at -80 °C.

### **Storage of enzymes**

All enzyme preparations were stored as aliquots of volumes no greater than 250 µL, flash-frozen in liquid nitrogen and stored at -80 °C.

### **Desalting column chromatography**

Protein samples were diluted with 10 mM  $\beta$ -glycerophosphate, 0.5 mM NAD<sup>+</sup>, 0.25 mM CoCl<sub>2</sub>, pH 6.8 buffer and loaded on to a Hi Prep™ 26/10 desalting column with a Sephadex G-25 fine, crosslinked dextran matrix (Amersham Pharmacia). Protein

eluted as one broad peak after 8 to 10 minutes of isocratic flow. Protein fractions were pooled and concentrated using a prewashed 20 mL Vivaspin 10000 MWCO concentrator.

### **Agarose gel electrophoresis**

Agarose gels (0.8 % (w/v)) were prepared by adding 0.4 g agarose to 50 mL 1X TAE buffer (40 mM Tris.HCl, 20 mM acetic acid and 2 mM EDTA at pH 8.0) and heating until dissolved. The molten gel was allowed to cool to ~50 °C before adding 4 µL of SYBR-Safe DNA gel stain (Invitrogen) and pouring into gel tray. All gels were run using a Sub-Cell<sup>®</sup> GT Agarose Gel electrophoresis system (Bio-Rad) in 1X TAE buffer. A sample of the pT7-7 plasmid containing the gene for *P. furiosus* DHQS was treated with BamH1 restriction enzyme to open the plasmid prior to loading on Agarose gel. To 1.5 µL of open plasmid was added 1.5 µL of DNA loading buffer and 1.5 µL of 1x TEA and this mixture was loaded into the wells. Electrophoresis was performed at 80 volts for ~25 minutes in 1 x TEA buffer. The DNA on the gels was visualised by exposure to ultraviolet light (302 nm). Pictures of the gels were taken using an Alpha Imager gel documentation system (Alpha Innotech Corporation, USA).

### **DNA sequencing**

DNA sequencing services were provided by the Massey University Allan Wilson Center for Molecular Evolution and Ecology Genome Service. DNA sequencing was carried out on either an ABI Prism 377-64 sequencer or an ABI Prism 3730 capillary sequencer, using BIGDYE labeled dideoxy chain termination chemistries (Applied Biosystems).

### **Determination of native molecular weight**

The native molecular weight was determined by size exclusion chromatography. A standard curve was generated using cytochrome C (12.4 kDa, Sigma), carbonic anhydrase (29 kDa, Sigma), bovine serum albumin (66 kDa, Sigma), alcohol dehydrogenase (150 kDa, Sigma),  $\beta$ -amylase (200 kDa, Sigma). The molecular weight was estimated from a curve prepared by plotting the elution time versus the log of the molecular weight of the standards.

### **Determination of thermal stability using circular dichroism**

CD spectroscopic data were generated using a Jasco J-815 circular dichroism spectrophotometer. Spectra were collected at a concentration of 0.01 mg/mL of enzyme in water. Wavelength scans were collected at 20 °C using a 10 mm path-length cuvette, 1.0 nm bandwidth, 0.5 nm step size, and a 1 second averaging time. Temperature scans were monitored at 220 nm and data were collected at 0.5 °C intervals between 20–90 °C with a 1 second averaging time. Cuvettes were stoppered during temperature scans to prevent evaporation.

### **Fluorescence-based determination of thermal stability**

Fluorescence-based protein thermal stability assays were carried out as described previously. A 25- $\mu$ L aliquot of solution containing 0.5 mg/mL of protein, 50 mM  $\text{Na}_2\text{HPO}_4$  pH 8.0 and 10x Sypro Orange dye (Invitrogen) was added to the wells of a 96-well thin-wall PCR plate (Bio-Rad). The plates were sealed and heated in an iCycler iQ Real Time PCR Detection System (Bio-Rad) from 20 to 80 °C in increments of 0.5 °C, with 30 seconds dwell time. Fluorescence changes in the wells

of the plate were monitored simultaneously with a charge-coupled device (CCD) camera. The wavelengths for excitation and emission were 490 and 575 nm, respectively. Experiments were carried out in triplicate for each condition.

### **Effect of temperature on activity of *P. furiosus* DHQS**

Assays to determine the effect of temperature on activity contained 50 mM BTP buffer with 10  $\mu$ M EDTA adjusted to pH 6.7 at the temperature of use. The reaction mixture contained DAH7P (21  $\mu$ M), ZnCl<sub>2</sub> (100  $\mu$ M), and NAD<sup>+</sup> (29  $\mu$ M) in 50 mM BTP buffer with 10  $\mu$ M EDTA at pH 6.7 at the required temperature. The mixture was preincubated at the required temperature for 5 minutes followed by addition of 20  $\mu$ L of *P. furiosus* DHQase (4.1 mg/mL). After a further minute of incubation, the reaction was initiated by the addition of 10  $\mu$ L of *P. furiosus* DHQS (0.2 mg/mL). Specific activities at 40, 60, and 80 °C were calculated using the extinction coefficients for DAH7P determined at each temperature. Specific activities at 25, 30, 50, and 70 °C were calculated using predicted extinction coefficients of 1.2, 1.2, 1.1, and 1.0 x 10<sup>3</sup> M<sup>-1</sup> cm<sup>-1</sup>.

### **Effects of pH on activity of *P. furiosus* DHQS**

Assays to determine the effect of pH on activity contained 50 mM BTP buffer with 10  $\mu$ M EDTA adjusted to the pH of use at 60 °C. The reaction mixture contained DAH7P (21  $\mu$ M), ZnCl<sub>2</sub> (100  $\mu$ M), NAD<sup>+</sup> (29  $\mu$ M), 10  $\mu$ L *P. furiosus* DHQS (0.2 mg/ mL), and *P. furiosus* DHQase (excess) in 50 mM BTP buffer with 10  $\mu$ M EDTA at the required pH at 60 °C. Specific activities at pH 5.9, 6.4, 6.9, 7.4, 7.7, 7.9, 8.4, 8.7, and 8.9 were calculated using an extinction coefficient of 1.2 x 10<sup>4</sup> M<sup>-1</sup> cm<sup>-1</sup>

### **Divalent metal ion screen for *P. furiosus* DHQS**

Assays to determine the adventitious activity of *P. furiosus* DHQS in the absence of divalent metal, contained DAH7P (46  $\mu\text{M}$ ), and  $\text{NAD}^+$  (29  $\mu\text{M}$ ) in 50 mM BTP buffer with 10  $\mu\text{M}$  EDTA, pH 6.7<sub>60°C</sub> pre-treated with Chelex. Reaction mixtures and *P. furiosus* DHQS samples were pre-treated for 10 minutes with EDTA (100  $\mu\text{M}$  and 1 mM respectively). The EDTA-treated reaction mixture was preincubated at 60 °C for 5 minutes followed by addition of 2  $\mu\text{L}$  of *P. furiosus* DHQase (4.1 mg/mL). After a further minute of incubation, the reaction was initiated by the addition of 2  $\mu\text{L}$  of EDTA-treated *P. furiosus* DHQS (0.2 mg/mL). Divalent metal ion salts used in assays to restore activity to the EDTA-treated *P. furiosus* DHQS were dissolved in 50 mM BTP buffer, pH 6.7<sub>60°C</sub> pre-treated with Chelex. The metal salts used were:  $\text{CoCl}_2 \cdot 6\text{H}_2\text{O}$  (Sigma),  $\text{BaCl}_2 \cdot 2\text{H}_2\text{O}$  (BDH),  $\text{FeSO}_4 \cdot 7\text{H}_2\text{O}$  (Sigma),  $\text{MgSO}_4 \cdot \text{H}_2\text{O}$  (May and Baker),  $\text{CaCl}_2$  (Prolabo),  $\text{MnSO}_4 \cdot \text{H}_2\text{O}$  (Sigma),  $\text{CrCl}_2$  (Aldrich),  $\text{HgCl}_2$  (Aldrich),  $\text{CdCl}_2$  (May and Baker),  $\text{NiCl}_2 \cdot 6\text{H}_2\text{O}$  (May and Baker),  $\text{CuSO}_4 \cdot 5\text{H}_2\text{O}$  (May and Baker), and  $\text{ZnCl}_2$  (BDH).

### **Divalent metal ion screen for Kiwifruit DHQS**

Assays to determine the adventitious activity of Kiwifruit DHQS in the absence of divalent metal, contained DAH7P (46  $\mu\text{M}$ ), and  $\text{NAD}^+$  (29  $\mu\text{M}$ ) in 50 mM BTP buffer with 10  $\mu\text{M}$  EDTA, pH 6.8<sub>25°C</sub> pre-treated with Chelex. Reaction mixtures and Kiwifruit DHQS samples were pre-treated for 10 minutes with EDTA (100  $\mu\text{M}$  and 1 mM respectively). The EDTA-treated reaction mixture was preincubated at 25 °C for 1 minutes followed by addition of 10  $\mu\text{L}$  of *E. coli* DHQase (10 mg/mL). After a further minute of incubation, the reaction was initiated by the addition of 10  $\mu\text{L}$  of EDTA-treated Kiwifruit DHQS (0.56 mg/mL). Divalent metal salts used in assays to restore activity to the EDTA-treated Kiwifruit DHQS were dissolved in 50 mM BTP buffer, pH 6.8<sub>25°C</sub> pre-treated with Chelex. The metal salts used were:  $\text{CoCl}_2 \cdot 6\text{H}_2\text{O}$ ,  $\text{BaCl}_2 \cdot 2\text{H}_2\text{O}$ ,  $\text{FeSO}_4 \cdot 7\text{H}_2\text{O}$ ,  $\text{MgSO}_4 \cdot \text{H}_2\text{O}$ ,  $\text{CaCl}_2$ ,  $\text{MnSO}_4 \cdot \text{H}_2\text{O}$ ,  $\text{CrCl}_2$ ,  $\text{HgCl}_2$ ,  $\text{CdCl}_2$ ,  $\text{NiCl}_2 \cdot 6\text{H}_2\text{O}$ ,  $\text{CuSO}_4 \cdot 5\text{H}_2\text{O}$ , and  $\text{ZnCl}_2$ .

### **Tagged versus untagged Kiwifruit DHQS experiment**

From a 500  $\mu\text{L}$  sample of purified Kiwifruit DHQS were taken two 60  $\mu\text{L}$  aliquots and labelled 1 and 2. Sample 2 was spiked with  $\text{NAD}^+$  (29  $\mu\text{M}$ ), washed twice with 500  $\mu\text{L}$  of EKmax buffer and concentrated on a 10,000 MW cut-off concentrator. Sample 1 was spiked with  $\text{NAD}^+$  (29  $\mu\text{M}$ ). Nine samples were prepared as follows: Control A (37 °C) no DHQS, EKmax treatment; Control B (37 °C) unwashed DHQS, no EKmax enzyme; Control B (25 °C) unwashed DHQS, no EKmax enzyme; Trial 1 (37 °C) unwashed DHQS, EKmax treatment; Trial 1 (25 °C) unwashed DHQS, EKmax treatment; Trial 2 (37 °C) washed DHQS, EKmax treatment; Trial 2 (25 °C) washed DHQS, EKmax treatment; Control C washed DHQS, no EKmax treatment; and Control C unwashed DHQS, no EKmax treatment (see table below for details).

## Experimental conditions for His-Tag removal assay

	Control A (37 °C) No DHQS	Control B (37 °C) unwashed	Control B (25 °C) unwashed	Trial 1 (37 °C) unwashed	Trial 1 (25 °C) unwashed	Trial 2 (37 °C) washed	Trial 2 (25 °C) washed	Control C washed no treatment	Control C unwashed no treatment
Kiwifruit DHQS	0 µL	13 µL	13 µL	15 µL	15 µL	15 µL	15 µL	4 µL	4 µL
EKmax enzyme	1 µL	0 µL	0 µL	1 µL	1 µL	1 µL	1 µL	0 µL	0 µL
EKmax buffer 10X	3 µL	3 µL	3 µL	3 µL	3 µL	3 µL	3 µL	0 µL	0 µL
MilliQ water	26 µL	14 µL	14 µL	11 µL	11 µL	11 µL	11 µL	0 µL	0 µL
Total volume	30 µL	30 µL	30 µL	30 µL	30 µL	30 µL	30 µL	0 µL	0 µL

Each sample was incubated for 16 hours at either 25 °C or 37 °C; at all other times the samples were kept on ice. Samples were analysed on SDS-PAGE and assayed for activity.

### Homology modelling for *P. furiosus* DHQS

The in-silico *P. furiosus* DHQS homology model was created through the use of PRIME 1.5 protein-folding facility with the prepared crystal structure of *Staphylococcus aureus* (1XAG) as the template.<sup>60</sup> These structures were then minimised with MACROMODEL 9.1 using the OPLS2005 force field with a GB/SA water model over 500 iterations.<sup>61</sup>

## 7.4 Experimental for chapter 3

### Preparation of DAH7P

Phosphoenol pyruvate (PEP, 0.88 mM), D-erythrose-4-phosphate (E4P, 0.88 mM), and ZnCl<sub>2</sub> (100 μM) were incubated in the presence of *E. coli* 3-deoxy-D-arabino-heptulosonate 7-phosphate synthase (*E. coli* DAH7PS, 100 μL, 10 mg/mL) in 1.5 mL of 50 mM BTP buffer pH 6.8 at 25 °C. Upon completion, the reaction mixture was filtered through a 10kDa MWC concentrator in order to remove DAH7PS. The filtrate was loaded onto an anion exchange column and a linear gradient from 0 to 500 mM of ammonium bicarbonate was applied over a span of two hours. DAH7P eluted at 150 mM of ammonium bicarbonate. The purified fractions were pooled and concentrated via lyophilisation to obtain 5 mg of purified DAH7P.

### Preparation of (3*S*)-3-fluoro-DAH7P and (3*R*)-3-fluoro-DAH7P

ZnCl<sub>2</sub> (100 μM), E4P (23 mg), and a 9:1 mixture of (*Z/E*)-3-fluoro-PEP (23 mg) were dissolved in 10 mL of 50 mM BTP buffer pH 6.8 at 25 °C and allowed to incubate in the presence of 10 μL of *E. coli* DAH7PS (10 mg/mL) for one hour. Additional aliquots of *E. coli* DAH7PS were added until all of the (*Z/E*)-3-fluoro-PEP was consumed. The consumption of (*Z/E*)-3-fluoro-PEP was determined by monitoring the disappearance of the signal generated by this compound at 232 nm by UV spectroscopy. Upon completion, the reaction was filtered through a 10kDa MWC concentrator in order to remove DAH7PS. The filtrate containing a 9:1 mixture of (3*S*)-3-fluoro-DAH7P and (3*R*)-3-fluoro-DAH7P was loaded onto an anion exchange column and a linear gradient from 0 to 500 mM of ammonium bicarbonate was applied over a span of two hours. (3*S*)-3-fluoro-DAH7P eluted at 130 mM of ammonium bicarbonate. The purified fractions of (3*S*)-3-fluoro-DAH7P were pooled

and concentrated via lyophilisation to obtain 2 mg of purified (3*S*)-3-fluoro-DAH7P. Electrospray ionisation mass spectrometry found a mass of 305.0088 for (3*S*)-3-fluoro-DAH7P (calculated mass: 305.0074). To obtain (3*R*)-3-fluoro-DAH7P, the same reaction mixture was prepared except 23 mg of a 58:42 mixture of (*Z/E*)-fluoro-PEP was used. Upon completion of the enzymatic reaction, the filtrate was loaded onto an anion exchange column and a linear gradient from 0 to 500 mM of ammonium bicarbonate was applied over a span of two hours. (3*R*)-3-fluoro-DAH7P eluted at 170 mM of ammonium bicarbonate. The purified fractions of (3*R*)-3-fluoro-DAH7P were pooled and concentrated via lyophilisation to obtain 1 mg of purified (3*R*)-3-fluoro-DAH7P.

#### **Determination of substrate concentration**

Accurate concentrations of DAH7P, (3*S*)-3-fluoro-DAH7P, and (3*R*)-3-fluoro-DAH7P were determined by the Lanzetta assay (see general biological methods, section 7.2).

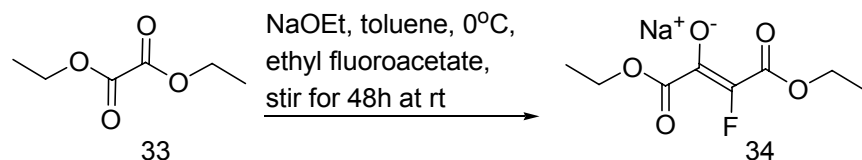
#### **Synthesis of D-erythrose-4-phosphate<sup>37</sup>**

D-Glucose 6-phosphate (0.34 g, 1 mmol) was moistened with 2 mL of water and 5 mL of glacial acetic acid. To the reaction mixture was added a 0.17 mL aliquot of 3 M sulfuric acid and a further 245 mL of glacial acetic acid. A mixture containing 3 M sulfuric acid (0.6 mL), glacial acetic acid (40 mL), and lead tetraacetate (1.7 mmol) was prepared before use and added dropwise to the D-glucose 6-phosphate reaction mixture over 30 minutes with vigorous stirring. The reaction mixture was then filtered through a Celite pad. The Celite was washed three times with 100 mL of water and the filtrate concentrated until the volume of the solution reached approximately 20 mL.

The concentrate was then extracted continuously with ether for 15 hours and the volume of the aqueous solution was reduced in vacuo to give a final volume of 50 mL. The solution of D-erythrose-4-phosphate was divided into 40 Eppendorf vials each containing 1.25 mL aliquots and stored at -20 °C.

## Synthesis of (Z/E)-3-fluoro-phosphoenol pyruvate cyclohexamine salt

### Diethyl fluorooxaloacetate sodium salt 34



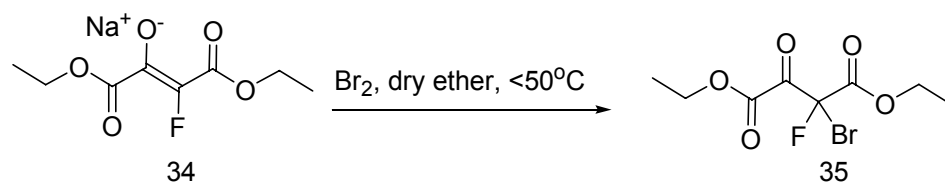
To a stirred solution of sodium ethoxide (2.59 g, 38 mmol) in dry toluene (19 mL) at 0 °C under nitrogen, was added diethyl oxalate (5.55 g, 38 mmol) over 10 minutes. To the mixture was then added ethyl fluoroacetate (4.03 g, 38 mmol) while maintaining the temperature at 0 °C. After stirring for 48 hours at room temperature, the reaction mixture was filtered and the solids rinsed with diethyl ether. The white solids were dried under vacuum to give diethyl fluorooxaloacetate (6.71 g, 77% yield).

<sup>1</sup>H NMR (400 MHz, D<sub>2</sub>O): δ 1.17 (3H, t, *J*: 7.1 Hz); 1.26 (3H, t, *J*: 7.1 Hz); 4.10 (2H, q, *J*: 7.1 Hz); 4.22 (2H, q, *J*: 7.1 Hz).

<sup>13</sup>C NMR (400 MHz, D<sub>2</sub>O): δ 13.1 (-CH<sub>3</sub>), 13.5 (-CH<sub>3</sub>), 61.1 (-CH<sub>2</sub>-), 63.0 (-CH<sub>2</sub>-), 133.0 (d, *J*<sub>FC</sub>: 225 Hz, (-CF-), 158.5 (d, *J*<sub>FCC</sub>: 56 Hz), 165.4 (d, *J*<sub>FCC</sub>: 108 Hz), 169.7 (d, *J*<sub>FCCC</sub>: 40 Hz).

*m/z* (+ve ESMS) 374.0981 (M+3Na, 100%, calculated mass: 374.0194)

### Diethyl bromofluorooxaloacetate 35



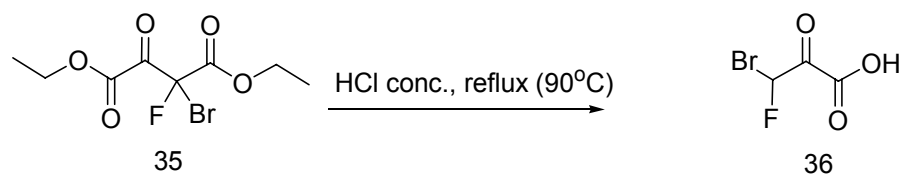
To a suspension of diethyl fluorooxaloacetate (3.68 g, 16.22 mmol) in 8.3 mL dry diethyl ether was added bromine (2.58 g, 16.22 mmol) drop-wise while maintaining the internal reaction temperature between 35 and 40 °C. When bromine colour persisted, the reaction was diluted with 75 mL of diethyl ether and washed with 9 mL of water followed by 9 mL of sodium sulfite. The combined aqueous portion was extracted with diethyl ether (2 x 40 mL). The organic extracts were combined, dried with magnesium sulfate and concentrated under vacuum to give diethyl bromofluorooxaloacetate as a brown oil (4.28 g, 93%).  $R_f$  (50% ethyl acetate/hexane): 0.67;  $^1\text{H NMR}$  (400 MHz,  $\text{CDCl}_3$ ):  $\delta$  1.37 (3H, t,  $J$ : 7.2 Hz); 1.42 (3H, t,  $J$ : 7.2 Hz); 4.36-4.47 (4H, m).

$^{13}\text{C NMR}$  (400 MHz,  $\text{CDCl}_3$ ) showed peaks corresponding to both the hydrate and keto form:  $\delta$  13.8 (- $\text{CH}_3$ ), 13.9 (- $\text{CH}_3$ ), 64.2 (- $\text{CH}_2$ -), 64.3 (- $\text{CH}_3$ ), 93.8 (d,  $J_{\text{FC}}$ : 25.8 Hz, - $\text{CBrF}$ -), 96.7 (d,  $J_{\text{FC}}$ : 275.3 Hz, - $\text{CBrF}$ -), 165.8 (COOEt), 166.0 (COOEt), 167.0.

$^{19}\text{F NMR}$  (400 MHz,  $\text{CDCl}_3$ ):  $\delta$  -128.7.

$m/z$  (+ve ESMS) 284.9762 (M+H, 100%, calculated mass: 284.9774).

### Bromofluoropyruvic acid 36

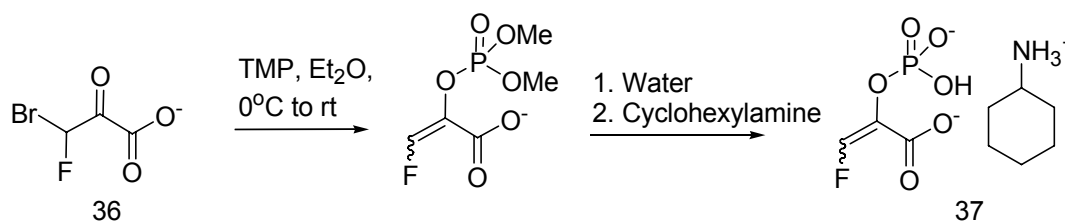


Diethyl bromofluorooxaloacetate (4.28 g, 15 mmol) was refluxed for 10 hours in 15 mL of concentrated HCl. Excess acid and low molecular weight impurities were removed from the crude mixture using vacuum distillation. The black residue was taken up in 75 mL of diethyl ether and extracted with 0.1 M sodium hydroxide (4 x 40 mL). The pale yellow aqueous solution was then adjusted to pH 1 with 10% hydrochloric acid. The aqueous acidic solution was extracted with ethyl acetate (8 x 50 mL) and concentrated under vacuum to give bromofluoropyruvic acid as a pale yellow oil (1.77 g, 64% yield).  $R_f$  (5% ethyl acetate/ethanol): 0.52;  $^1\text{H}$  NMR (400 MHz,  $\text{D}_2\text{O}$ ):  $\delta$  6.32 (1H, d,  $J_{\text{FCH}}$ : 48.7 Hz).

$^{13}\text{C}$  NMR (400 MHz,  $\text{D}_2\text{O}$ ):  $\delta$  93.0 (d,  $J$ : 23 Hz,  $-\text{C}(\text{OH})_2-$ ), 101.1 (C-F, d,  $J$ : 247 Hz,  $-\text{CHBrF}$ ), 171.1 ( $-\text{COOH}$ ).

$^{19}\text{F}$  NMR (400 MHz,  $\text{D}_2\text{O}$ ):  $\delta$  -150.5 (d,  $J_{\text{FCH}}$ : 48.8 Hz).

**(Z/E)-3-Fluoro-phosphoenol pyruvate cyclohexylammonium salt 37**



To a stirred solution of trimethyl phosphite (1.65 g, 13.3 mmol) at 0 °C, under argon, was added bromofluoropyruvic acid (1.63 g, 8.87 mmol) in 16.8 mL of dry ether. The reaction mixture was allowed to warm to room temperature with stirring for four hours followed by removal of diethyl ether under vacuum. To the residue was added 13.4 mL of water and the mixture was allowed to stir overnight at room temperature. After adding 1.1 mL of cyclohexylamine (0.932 g, 9.4 mmol), the aqueous mixture was concentrated under vacuum at 40 °C and placed under high vacuum overnight. The resulting residue was dissolved in 20 mL of methanol and diethyl ether (5 x 20 mL). The cloudy solution was allowed to re-crystallise at -20 °C overnight. The solution was filtered to give (Z/E)-3-fluoro-phosphoenol pyruvate cyclohexylammonium salt as white crystals (1.51 g, 60%).  $R_f$  (5% ethyl acetate/ethanol): 0.31;  $^1\text{H}$  NMR (400 MHz, D<sub>2</sub>O):  $\delta$  1.12-1.29 (5H, m), 1.48-1.57 (1H, m), 1.73-1.61 (2H, m), 1.79-1.9 (2H, m), 2.96-3.07 (1H, m), 7.58 (1H, *Z* isomer, dd,  $J$ : 73.0, 2.4 Hz), 7.43 (1H, *E* isomer, dd,  $J$ : 75.0, 3.3 Hz).  $^{19}\text{F}$  NMR (400 MHz, D<sub>2</sub>O):  $\delta$  -133.9 (*Z* isomer, dd,  $J$ : 74.0, 5.9 Hz), -146 (*E* isomer, dd,  $J$ : 78.7, 4.0 Hz).  $m/z$  (-ve ESMS) 184.9660 (M-H, 100%, calculated mass: 184.9651).

## 7.5 Experimental for chapter 4

### Steady state kinetics for *E. coli* DHQS with DAH7P

The standard assay reaction mixture contained DAH7P (0.5 to 42  $\mu\text{M}$ ),  $\text{ZnCl}_2$  (100  $\mu\text{M}$ ), and  $\text{NAD}^+$  (29  $\mu\text{M}$ ) in 50 mM BTP buffer with 10  $\mu\text{M}$  EDTA, pH 6.8 at 25 °C. The mixture was preincubated at 25 °C for 1 minute followed by addition of 20  $\mu\text{L}$  of *E. coli* DHQase (10 mg/mL). After a further minute of incubation, the reaction was initiated by the addition of 20  $\mu\text{L}$  of *E. coli* DHQS (7 nM). The final volume was 1000  $\mu\text{L}$ .

### Steady state kinetics for Kiwifruit DHQS with DAH7P

The standard assay reaction mixture contained DAH7P (5 to 500  $\mu\text{M}$ ),  $\text{ZnCl}_2$  (100  $\mu\text{M}$ ), and  $\text{NAD}^+$  (29  $\mu\text{M}$ ) in 50 mM BTP buffer with 10  $\mu\text{M}$  EDTA, pH 6.8 at 25 °C. The mixture was preincubated at 25 °C for 1 minute followed by addition of 20  $\mu\text{L}$  of *E. coli* DHQase (10 mg/mL). After a further minute of incubation, the reaction was initiated by the addition of 5  $\mu\text{L}$  of Kiwifruit DHQS (86 nM). The final volume was 1000  $\mu\text{L}$ .

### Steady state kinetics for *P. furiosus* DHQS with DAH7P

The standard assay reaction mixture contained DAH7P (1 to 70  $\mu\text{M}$ ),  $\text{ZnCl}_2$  (100  $\mu\text{M}$ ), and  $\text{NAD}^+$  (29  $\mu\text{M}$ ) in 50 mM BTP buffer with 10  $\mu\text{M}$  EDTA, pH 6.7 at 60 °C. The mixture was preincubated at 60 °C for 1 minute followed by addition of 20  $\mu\text{L}$  of *P. furiosus* DHQase (4.1 mg/mL). After a further minute of incubation, the reaction was initiated by the addition of 10  $\mu\text{L}$  of *P. furiosus* DHQS (56 nM). The final volume was 1000  $\mu\text{L}$ .

### **Steady state kinetics for *E. coli* DHQS with (3S)-3-fluoro-DAH7P**

The standard assay reaction mixture contained (3S)-3-fluoro-DAH7P (5 to 240  $\mu\text{M}$ ),  $\text{ZnCl}_2$  (100  $\mu\text{M}$ ), and  $\text{NAD}^+$  (29  $\mu\text{M}$ ) in 50 mM BTP buffer with 10  $\mu\text{M}$  EDTA, pH 6.8 at 25  $^\circ\text{C}$ . The mixture was preincubated at 25  $^\circ\text{C}$  for 1 minute followed by addition of 20  $\mu\text{L}$  of *E. coli* DHQase (10 mg/mL). After a further minute of incubation, the reaction was initiated by the addition of 20  $\mu\text{L}$  of *E. coli* DHQS (7 nM). The final volume was 1000  $\mu\text{L}$ .

### **Steady state kinetics for Kiwifruit DHQS with (3S)-3-fluoro-DAH7P**

The standard assay reaction mixture contained (3S)-3-fluoro-DAH7P (8 to 93  $\mu\text{M}$ ),  $\text{ZnCl}_2$  (100  $\mu\text{M}$ ), and  $\text{NAD}^+$  (29  $\mu\text{M}$ ) in 50 mM BTP buffer with 10  $\mu\text{M}$  EDTA, pH 6.8 at 25  $^\circ\text{C}$ . The mixture was preincubated at 25  $^\circ\text{C}$  for 1 minute followed by addition of 20  $\mu\text{L}$  of *E. coli* DHQase (10 mg/mL). After a further minute of incubation, the reaction was initiated by the addition of 10  $\mu\text{L}$  of Kiwifruit DHQS (86 nM). The final volume was 1000  $\mu\text{L}$ .

### **Steady state kinetics for *P. furiosus* DHQS with (3S)-3-fluoro-DAH7P**

The standard assay reaction mixture contained (3S)-3-fluoro-DAH7P (10 to 680  $\mu\text{M}$ ),  $\text{ZnCl}_2$  (100  $\mu\text{M}$ ), and  $\text{NAD}^+$  (29  $\mu\text{M}$ ) in 50 mM BTP buffer with 10  $\mu\text{M}$  EDTA, pH 6.7 at 60  $^\circ\text{C}$ . The mixture was preincubated at 60  $^\circ\text{C}$  for 1 minute followed by addition of 20  $\mu\text{L}$  of *P. furiosus* DHQase (4.1 mg/mL). After a further minute of incubation, the reaction was initiated by the addition of 10  $\mu\text{L}$  of *P. furiosus* DHQS (56 nM). The final volume was 1000  $\mu\text{L}$ .

### **Steady state kinetics for *E. coli* DHQS with (3*R*)-3-fluoro-DAH7P**

The standard assay reaction mixture contained (3*R*)-3-fluoro-DAH7P (2 to 160  $\mu\text{M}$ ),  $\text{ZnCl}_2$  (100  $\mu\text{M}$ ), and  $\text{NAD}^+$  (29  $\mu\text{M}$ ) in 50 mM BTP buffer with 10  $\mu\text{M}$  EDTA, pH 6.8 at 25 °C. The mixture was preincubated at 25 °C for 1 minute followed by addition of 20  $\mu\text{L}$  of *E. coli* DHQase (10 mg/mL). After a further minute of incubation, the reaction was initiated by the addition of 5  $\mu\text{L}$  of *E. coli* DHQS (35 nM). The final volume was 1000  $\mu\text{L}$ .

### **Steady state kinetics for Kiwifruit DHQS with (3*R*)-3-fluoro-DAH7P**

The standard assay reaction mixture contained (3*R*)-3-fluoro-DAH7P (4 to 160  $\mu\text{M}$ ),  $\text{ZnCl}_2$  (100  $\mu\text{M}$ ), and  $\text{NAD}^+$  (29  $\mu\text{M}$ ) in 50 mM BTP buffer with 10  $\mu\text{M}$  EDTA, pH 6.8 at 25 °C. The mixture was preincubated at 25 °C for 1 minute followed by addition of 20  $\mu\text{L}$  of *E. coli* DHQase (10 mg/mL). After a further minute of incubation, the reaction was initiated by the addition of 4  $\mu\text{L}$  of Kiwifruit DHQS (0.13  $\mu\text{M}$ ). The final volume was 1000  $\mu\text{L}$ .

### **Steady state kinetics for *P. furiosus* DHQS with (3*R*)-3-fluoro-DAH7P**

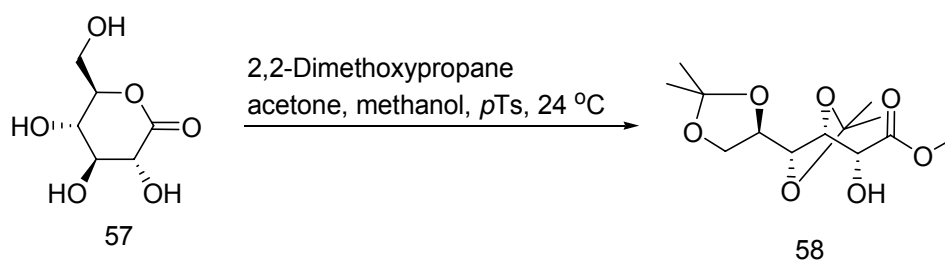
The standard assay reaction mixture contained (3*R*)-3-fluoro-DAH7P (4 to 241  $\mu\text{M}$ ),  $\text{ZnCl}_2$  (100  $\mu\text{M}$ ), and  $\text{NAD}^+$  (29  $\mu\text{M}$ ) in 50 mM BTP buffer with 10  $\mu\text{M}$  EDTA, pH 6.7 at 60 °C. The mixture was preincubated at 60 °C for 1 minute followed by addition of 20  $\mu\text{L}$  of *P. furiosus* DHQase (4.1 mg/mL). After a further minute of incubation, the reaction was initiated by the addition of 10  $\mu\text{L}$  of *P. furiosus* DHQS (56 nM). The final volume was 1000  $\mu\text{L}$ .

### **<sup>19</sup>F NMR spectroscopy monitoring of enzyme-substrate interactions**

To assess the interaction of the fluoro analogues with DHQS, reactions with substrate and enzyme were carried out in NMR tubes and monitored by <sup>19</sup>F NMR spectroscopy (400 MHz). In an NMR tube was added 45 mM (*Z/E*)-fluoroPEP, 47 mM E4P, 50 μM ZnCl<sub>2</sub>, 30 μM NAD<sup>+</sup>, and 20% D<sub>2</sub>O in 50 mM BTP buffer at pH 7 (final volume 550 μL). DAH7PS (0.4 mg/mL) was added to the NMR tube and the reaction was monitored overnight by <sup>19</sup>F NMR spectroscopy. DHQS (0.4 mg/mL) was then added to the NMR tube and the reaction was monitored for a further 12 hours by <sup>19</sup>F NMR spectroscopy. A multi-experiment protocol was setup whereby 120 experiments were performed at 1 experiment every 5 minutes.

## 7.6 Experimental for chapter 5

### Methyl 3,4:5,6-di-*O*-isopropylidene-D-gluconate **58**<sup>62</sup>

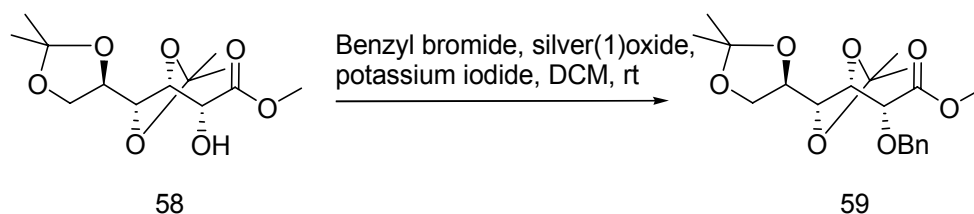


To a stirred solution of D-glucono-1,5-lactone **57** (6.235 g, 35 mmol) in acetone (3.5 mL) at 24 °C, was added 2,2-dimethoxypropane (8.894 g, 85.4 mmol), *p*-toluenesulfonic acid (0.072 g, 0.42 mmol), and methanol (25.9 mmol, 1.05 mL). After stirring for 25 hours, the solution was evaporated and the residue taken up in 200 mL dichloromethane. The dichloromethane solution was washed with saturated aqueous sodium bicarbonate (50 mL), water (50 mL), brine (50 mL), and dried over MgSO<sub>4</sub>. The dichloromethane solution was filtered and evaporated to give a pale yellow syrup. The pale yellow syrup was subjected to column chromatography (25% ethyl acetate/hexane) to give acetal **58** as a colourless, clear syrup (7.227 g, 71.1%). *R<sub>f</sub>* (33% ethyl acetate/hexane): 0.48; <sup>1</sup>H NMR (400 MHz, CDCl<sub>3</sub>): δ 1.37 (3H, s); 1.38 (3H, s); 1.41 (3H, s); 1.45 (3H, s); 3.03 (1H, d, *J*: 9.2 Hz); 3.86 (3H, s); 4.01 (1H, dd, *J*: 8.5, 4.1 Hz); 4.08 (1H, dd, *J*: 8.5, 5.8 Hz); 4.11 (1H, ddd, *J*: 14.4, 8.5, 4.1 Hz); 4.17 (1H, dd, *J*: 8.5, 5.8 Hz); 4.24 (1H, dd, *J*: 8.0, 1.5 Hz); 4.36 (1H, dd, *J*: 9.2, 1.5 Hz).

<sup>13</sup>C NMR (400 MHz, CDCl<sub>3</sub>): δ 25.3, 26.5, 26.7, 27.2, 52.7, 67.9, 69.5, 76.5, 77.3, 80.9, 109.9, 110.1, 173.0.

*m/z* (+ve ESMS) 291.1455 (M+H, 100%, calculated mass: 291.1444).

### Methyl 2-*O*-benzyl-3,4:5,6-di-*O*-isopropylidene-D-gluconate **59**<sup>63</sup>

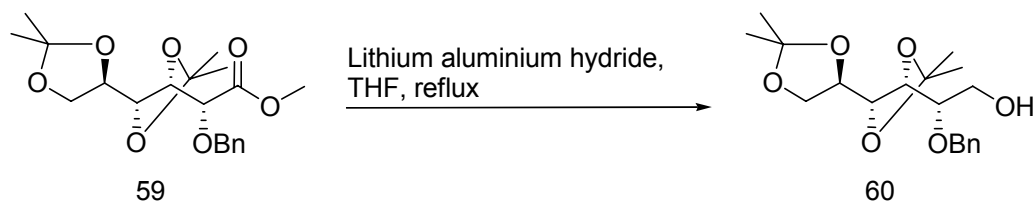


To a stirred solution of methyl 3,4:5,6-di-*O*-isopropylidene-D-gluconate **58** (5.36 g, 18.4 mmol) in dry dichloromethane (55.5 mL) was added potassium iodide (0.01 g, 0.055 mmol). The solution was cooled to 0 °C and benzyl bromide (3.47 g, 20.3 mmol) was added dropwise followed by silver (I) oxide (6.41 g, 27.7 mmol). The mixture was allowed to stir for five minutes at 0 °C before it was allowed to warm to room temperature. After 27 hours the reaction was diluted with 25 mL of dichloromethane and filtered through a pad of Celite. The Celite cake was rinsed with an additional 75 mL of dichloromethane and the filtrate was washed with saturated aqueous NaHCO<sub>3</sub> (50 mL), and brine (50 mL). The dichloromethane solution was dried over MgSO<sub>4</sub>, filtered, and evaporated to give a yellow syrup. The crude syrup was subjected to column chromatography (14% ethyl acetate/hexane) to give methyl ester **59** as a white solid (4.69 g, 66.8%). *R<sub>f</sub>* (20% ethyl acetate/hexane): 0.59; <sup>1</sup>H NMR (400 MHz, CDCl<sub>3</sub>): δ 1.27 (3H, s); 1.29 (3H, s); 1.33 (3H, s); 1.37 (3H, s); 3.78 (3H, s); 3.84 (1H, m); 4.02-4.03 (2H, m); 4.06-4.11 (1H, m); 4.12 (1H, d, *J*: 2.5 Hz); 4.32 (1H, dd, *J*: 6.9, 2.6 Hz); 4.40 (1H, d, *J*: 11.3 Hz); 4.84 (1H, d, *J*: 11.3 Hz); 7.24-7.36 (5H, m).

<sup>13</sup>C NMR (400 MHz, CDCl<sub>3</sub>): δ 25.6, 27.0, 27.0, 27.7, 52.6, 68.1, 73.5, 77.2, 77.5, 77.6, 81.1, 110.1, 110.8, 128.3, 128.4, 128.4, 128.8, 128.8, 137.6, 171.2.

*m/z* (+ve ESMS) 381.1926 (M+H, 100%, calculated mass: 381.1913).

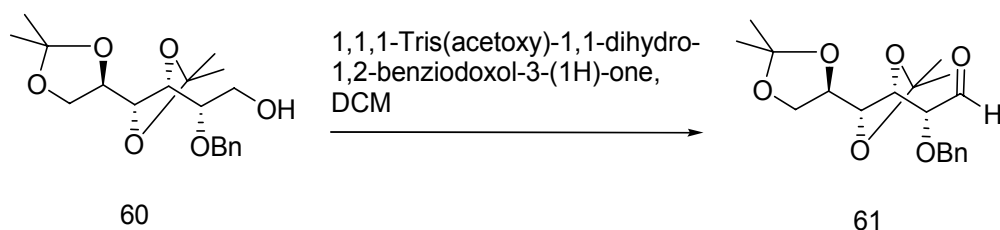
### 2-*O*-Benzyl-3,4:5,6-di-*O*-isopropylidene-D-gluconol **60**<sup>47</sup>



To dry tetrahydrofuran (10 mL) stirred at 0 °C was added lithium aluminium hydride powder (0.50 g) in small portions. A solution of methyl 2-*O*-benzyl-3,4:5,6-di-*O*-isopropylidene-D-gluconate **59** (1.33 g, 3.49 mmol) in dry tetrahydrofuran (10 mL) was slowly added to the lithium aluminium hydride solution. After refluxing for 20 hours, the reaction mixture was cooled to -10 °C and quenched sequentially with water (0.50 mL), 10% aqueous sodium hydroxide (0.50 mL), and water (1.49 mL). The quenched mixture was then diluted with 50 mL dichloromethane and filtered through a pad of Celite. The Celite cake was rinsed with an additional 100 mL of dichloromethane and the filtrate washed with water (2x 50 mL), and brine (50 mL). The dichloromethane solution was dried over MgSO<sub>4</sub>, filtered, and evaporated to give a white slurry residue. The residue was subjected to column chromatography (25% ethyl acetate/hexane to 33% ethyl acetate/hexane) to give alcohol **60** as a colourless, clear syrup (1.07 g, 87%). *R<sub>f</sub>* (33% ethyl acetate/hexane): 0.37; <sup>1</sup>H NMR (400 MHz, CDCl<sub>3</sub>): δ 1.31 (3H, s); 1.36 (6H, s); 1.38 (3H, s); 2.47 (1H, s); 3.57-3.63 (1H, m); 3.72-3.79 (1H, m); 3.81-3.91 (2H, m); 3.96-4.07 (2H, m); 4.08-4.10 (2H, m); 4.65 (1H, d, *J*: 11.8 Hz); 4.73 (1H, d, *J*: 11.8 Hz); 7.23-7.37 (5H, m).

<sup>13</sup>C NMR (400 MHz, CDCl<sub>3</sub>): δ 25.6, 26.8, 27.1, 27.6, 62.7, 68.3, 72.9, 77.6, 77.9, 78.4, 82.6, 110.2, 110.2, 128.1, 128.2, 128.2, 128.8, 128.8, 138.7.

## 2-*O*-Benzyl-3,4:5,6-di-*O*-isopropylidene-D-gluconal **61**<sup>64</sup>

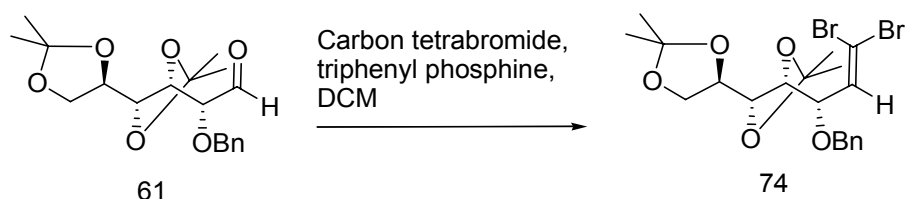


To a stirred solution of 1,1,1-tris(acetoxy)-1,1-dihydro-1,2-benziodoxol-3-(1H)-one (0.90 g, 2.1 mmol) in dry dichloromethane (6 mL) was added a solution of 2-*O*-benzyl-3,4:5,6-di-*O*-isopropylidene-D-gluconol **60** (0.50 g, 1.42 mmol) in dry dichloromethane (2 mL). After stirring at room temperature for 3 hours in darkness, the solution was diluted with 40 mL of dichloromethane and washed with saturated aqueous NaHCO<sub>3</sub> (10 mL), saturated aqueous sodium thiosulfate (10 mL), and brine (10 mL). The dichloromethane solution was dried over MgSO<sub>4</sub>, filtered, and evaporated to give a colourless residue. The residue was subjected to column chromatography (15% ethyl acetate/hexane) to give aldehyde **61** as a colourless, clear syrup (0.31 g, 62%). *R<sub>f</sub>* (20% ethyl acetate/hexane): 0.45; <sup>1</sup>H NMR (400 MHz, CDCl<sub>3</sub>): δ 1.29 (3H, s); 1.30 (3H, s); 1.32 (3H, s); 1.38 (3H, s); 3.83-3.89 (1H, m); 3.92-3.96 (1H, m); 4.01-4.04 (2H, m); 4.07-4.14 (1H, m); 4.24-4.30 (1H, m); 4.59 (1H, d, *J*: 11.8 Hz); 4.74 (1H, d, *J*: 11.8 Hz); 7.25-7.36 (5H, m); 9.70 (1H, d, *J*: 1.6 Hz).

<sup>13</sup>C NMR (400 MHz, CDCl<sub>3</sub>): δ 25.5, 26.9, 27.0, 27.5, 68.3, 73.9, 77.0, 77.5, 80.5, 83.0, 110.2, 110.8, 128.4, 128.6, 128.6, 129.0, 129.0, 137.4, 203.0.

*m/z* (-ve ESMS) 385.2294 (M+Cl, 100%, calculated mass: 385.1423).

**1,1-Dibromo-1,2-dideoxy-3-*O*-benzyl-4,5:6,7-di-*O*-isopropylidene-D-gluco-hept-1-enitol **74**<sup>65</sup>**

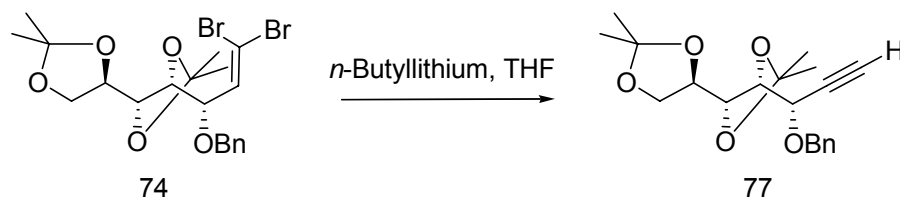


To a 0 °C, stirred solution of triphenyl phosphine (9.27 g, 35.3 mmol) in dry dichloromethane (5 mL) was added carbon tetrabromide (5.84 g, 17.6 mmol) in dry dichloromethane (5 mL) over a span of 20 minutes. The solution was allowed to warm to room temperature over 30 minutes and then cooled to 0 °C. To this was added a solution of 2-*O*-benzyl-3,4:5,6-di-*O*-isopropylidene-D-gluconal **61** (3.08 g, 8.79 mmol) in dry dichloromethane (55 mL). The mixture was allowed to warm to room temperature. After stirring for 2.5 hours, the mixture was cooled to 0 °C, diluted with 150 mL of hexane, stirred for one hour, and filtered through a pad of Celite. The Celite cake was washed with hexane (3x 25 mL) and the filtrate evaporated to give a clear, brown syrup. The syrup was subjected to column chromatography (10% ethyl acetate/hexane) to give alkene **74** as a clear, light brown syrup (3.81 g, 85.6%).  $R_f$  (20% ethyl acetate/hexane): 0.75;  $^1\text{H NMR}$  (400 MHz,  $\text{CDCl}_3$ ):  $\delta$  1.29 (3H, s); 1.30 (3H, s); 1.36 (6H, s); 3.82-3.88 (1H, m); 3.94-4.10 (4H, m); 4.23 (1H, dd,  $J$ : 9.0, 3.7 Hz); 4.42 (1H, d,  $J$ : 12.0 Hz); 4.65 (1H, d,  $J$ : 12.0 Hz); 6.56 (1H, d,  $J$ : 9.0 Hz); 7.23-7.36 (5H, m).

$^{13}\text{C NMR}$  (400 MHz,  $\text{CDCl}_3$ ):  $\delta$  25.6, 27.1, 27.2, 27.9, 67.9, 71.4, 77.5, 77.6, 78.9, 81.7, 110.0, 110.8, 128.2, 128.3, 128.3, 128.7, 128.7, 137.0, 138.1, 207.5.

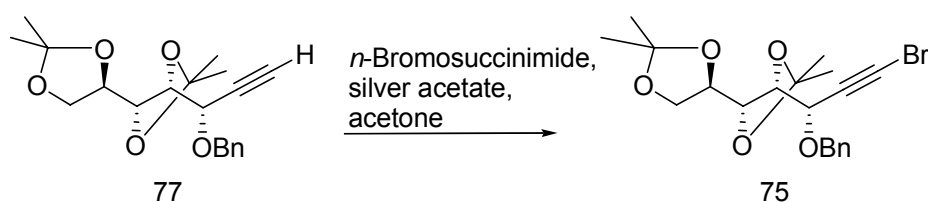
$m/z$  (+ve ESMS) 449.0570 ( $\text{M}+\text{Na}+\text{H}-\text{Br}$ , 100%, calculated mass: 449.0934).

**1,2-Dideoxy-3-*O*-benzyl-4,5:6,7-di-*O*-isopropylidene-D-*gluco*-hept-1-ynitol **77**<sup>65</sup>**



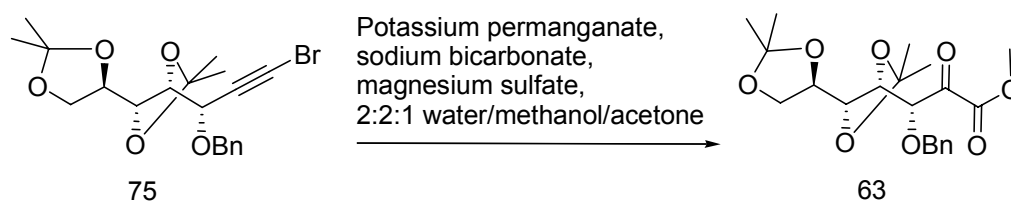
To a  $-10\text{ }^{\circ}\text{C}$ , stirred solution of 1,1-dibromo-1,2-dideoxy-3-*O*-benzyl-4,5:6,7-di-*O*-isopropylidene-D-*gluco*-hept-1-enitol **74** (1.519 g, 3 mmol) in dry tetrahydrofuran (28 mL) was added dropwise 1.48M *n*-butyllithium in THF (4 mL, 6 mmol). The solution was allowed to stir at  $-10\text{ }^{\circ}\text{C}$ ; after 50 minutes, the reaction was quenched with 15 mL saturated aqueous ammonium chloride and extracted with ethyl acetate (2x 50 mL). The ethyl acetate solution was washed with water (1x 25 mL) and brine (1x 25 mL), dried over  $\text{MgSO}_4$ , filtered, and evaporated to give a colourless residue. The residue was subjected to column chromatography (10% ethyl acetate/hexane) to give alkyne **77** as a colourless, clear syrup (0.552 g, 53%).  $R_f$  (20% ethyl acetate/hexane): 0.48;  $^1\text{H}$  NMR (400 MHz,  $\text{CDCl}_3$ ):  $\delta$  1.28 (3H, s); 1.29 (3H, s); 1.38 (3H, s); 1.39 (3H, s); 2.54 (1H, d,  $J$ : 2.2 Hz); 3.89-3.95 (1H, m); 4.01-4.17 (4H, m); 4.26 (1H, dd,  $J$ : 3.7, 2.2 Hz); 4.53 (1H, d,  $J$ : 11.8 Hz); 4.86 (1H, d,  $J$ : 11.8 Hz); 7.24-7.36 (5H, m).  $^{13}\text{C}$  NMR (400 MHz,  $\text{CDCl}_3$ ):  $\delta$  25.7, 26.9, 27.4, 28.0, 67.1, 68.7, 71.2, 76.2, 77.2, 77.7, 80.2, 81.5, 110.0, 111.0, 128.3, 128.6, 128.6, 128.8, 128.8, 137.6.  $m/z$  (+ve ESMS) 347.1863 ( $\text{M}+\text{H}$ , 100%, calculated mass: 347.1858).

**1-Bromo-1,2-dideoxy-3-*O*-benzyl-4,5:6,7-di-*O*-isopropylidene-D-*gluco*-hept-1-ynitol **75**<sup>66</sup>**



To a stirred solution of 1,2-dideoxy-3-*O*-benzyl-4,5:6,7-di-*O*-isopropylidene-D-*gluco*-hept-1-ynitol **77** (0.502 g, 1.45 mmol) in acetone (8 mL) was added *n*-bromosuccinimide (0.361 g, 2.03 mmol) and silver acetate (0.097 g, 0.58 mmol). The solution was allowed to stir at room temperature in darkness. After six hours, the solution was diluted with 75 mL of ethyl acetate and washed with water (25 mL) and brine (25 mL), dried over MgSO<sub>4</sub>, filtered, and evaporated to give a colourless residue. The residue was subjected to column chromatography (12% ethyl acetate/hexane) to give bromoalkyne **75** as a colourless, clear syrup (0.422 g, 68%). *R<sub>f</sub>* (10% ethyl acetate/hexane): 0.34; <sup>1</sup>H NMR (400 MHz, CDCl<sub>3</sub>): δ 1.29 (6H, s); 1.36 (3H, s); 1.38 (3H, s); 3.96-3.94 (1H, m); 4.01-4.16 (4H, m); 4.29 (1H, d, *J*: 3.9 Hz); 4.51 (1H, d, *J*: 11.9 Hz); 4.84 (1H, d, *J*: 11.9 Hz); 7.24-7.34 (5H, m). <sup>13</sup>C NMR (400 MHz, CDCl<sub>3</sub>): δ 23.0, 25.7, 26.9, 27.5, 28.0, 48.1, 67.1, 70.0, 71.5, 76.9, 78.0, 81.3, 110.0, 111.1, 128.3, 128.6, 128.6, 128.8, 128.8, 137.5.

**Methyl 3-*O*-benzyl-4,5:6,7-di-*O*-isopropylidene-D-*gluco*-hept-2-ulosonate **63**<sup>47,67</sup>**



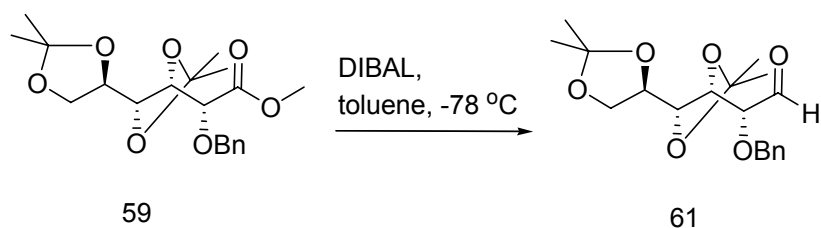
To a 0 °C, stirred solution of 1-bromo-1,2-dideoxy-3-*O*-benzyl-4,5:6,7-di-*O*-isopropylidene-D-*gluco*-hept-1-ynitol **75** (0.04 g, 0.1 mmol) in methanol (1.8 mL) and acetone (0.9 mL) was added a solution of sodium bicarbonate (0.01 g, 0.07 mmol) and magnesium sulfate (0.03 g, 0.236 mmol) in water (1.8 mL). After 10 minutes potassium permanganate (0.05 g, 0.295 mmol) was added in small portions. After three hours at 0 °C the mixture was poured into ice-water, filtered through a pad of Celite. The Celite cake was washed with ethyl acetate (3x 25 mL). The aqueous layer was extracted with ethyl acetate (2x 25 mL) and the organic layers were combined. The ethyl acetate solution was washed with brine (3x 25 mL), dried over MgSO<sub>4</sub>, filtered, and evaporated to give  $\alpha$ -keto ester **63** as a colourless residue (0.04 g, 95%).

$R_f$  (20% ethyl acetate/hexane): 0.32; <sup>1</sup>H NMR (400 MHz, CDCl<sub>3</sub>):  $\delta$  1.36 (3H, s); 1.37 (6H, s); 1.38 (3H, s); 3.86-3.92 (4H, m); 4.06-4.19 (3H, m); 4.51 (1H, d,  $J$ : 11.4 Hz); 4.55-4.60 (1H, m); 4.74-4.77 (1H, m); 4.80 (1H, d,  $J$ : 11.4 Hz); 7.30-7.40 (5H, m).

<sup>13</sup>C NMR (400 MHz, CDCl<sub>3</sub>):  $\delta$  25.2, 26.4, 26.4, 27.1, 52.9, 67.6, 73.6, 76.9, 77.0, 79.2, 81.4, 109.8, 110.6, 128.0, 128.0, 128.1, 128.5, 128.5, 137.0, 161.7, 191.4.

$m/z$  (+ve ESMS) 409.1882 (M+H, 100%, calculated mass: 409.1862).

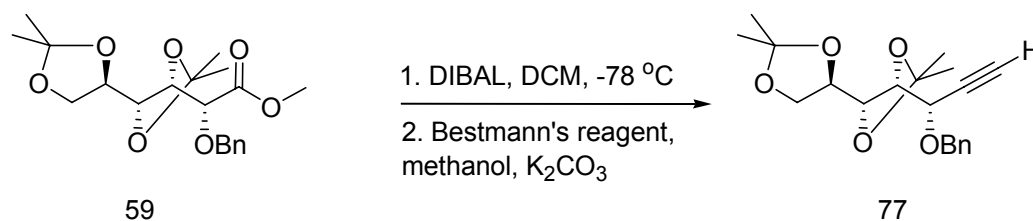
**2-*O*-Benzyl-3,4:5,6-di-*O*-isopropylidene-D-gluconal **61**<sup>68,69</sup>**



To a  $-78\text{ }^{\circ}\text{C}$ , stirred solution of methyl 2-*O*-benzyl-3,4:5,6-di-*O*-isopropylidene-D-gluconate **59** (1.0 g, 2.63 mmol) in dry toluene was added 1M DIBAL (7.9 mL) over 20 minutes. After two hours of stirring the reaction was quenched with methanol, Rochelle's salts, EtOAc and brine. The mixture was allowed to stir for one hour at room temperature. The aqueous layer was extracted with ethyl acetate (2x 25 mL) and the organic layers were combined. The residue was subjected to column chromatography (15% ethyl acetate/hexane) to give aldehyde **61** as a colourless, clear syrup (0.9 g, 95%).  $R_f$  (22% ethyl acetate/hexane): 0.45;  $^1\text{H}$  NMR (400 MHz,  $\text{CDCl}_3$ ): 1.30 (6H, s); 1.32 (3H, s); 1.38 (3H, s); 3.83-3.89 (1H, m); 3.92-3.96 (1H, m); 3.98-4.04 (2H, m); 4.07-4.15 (1H, m); 4.23-4.30 (1H, m); 4.58 (1H, d,  $J$ : 11.8 Hz); 4.74 (1H, d,  $J$ : 11.8 Hz); 7.25-7.37 (5H, m); 9.70 (1H, s).

$^{13}\text{C}$  NMR (400 MHz,  $\text{CDCl}_3$ ):  $\delta$  25.1, 26.5, 26.6, 27.1, 67.9, 73.5, 76.6, 77.1, 80.1, 82.6, 109.8, 110.4, 128.0, 128.0, 128.2, 128.5, 128.5, 137.0, 202.7.

**1,2-Dideoxy-3-*O*-benzyl-4,5:6,7-di-*O*-isopropylidene-D-gluco-hept-1-ynitol **77**<sup>68,70</sup>**



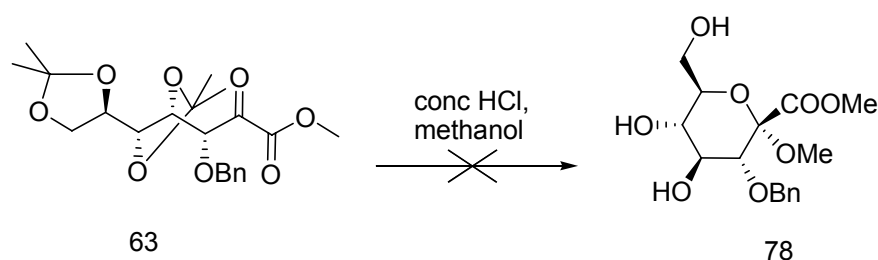
To a solution of dimethyl-2-oxopropylphosphonate (2.8 g, 16.7 mmol) in chloroform (41 mL) under N<sub>2</sub> at 0 °C was added 4-acetamidobenzenesulfonyl azide (4.0 g, 16.7 mmol) and K<sub>2</sub>CO<sub>3</sub> (2.4 g, 17 mmol) in one portion. The mixture was allowed to stir for 48 hours at <10 °C (solution A). To a stirred solution of methyl 2-*O*-benzyl-3,4:5,6-di-*O*-isopropylidene-D-gluconate **59** (1.9 g, 4.9 mmol) dissolved in dichloromethane (33 mL) at -78 °C under N<sub>2</sub> was added 14.7 mL of 1M DIBAL (allowing the solution to slide along the inside of the flask). The mixture was allowed to stir for 2 hours at -78 °C or until finished based on TLC. The excess DIBAL was quenched with 11 mL of methanol to give solution B. To solution B was added additional methanol (50 mL). To solution A was added additional K<sub>2</sub>CO<sub>3</sub> (1.1 g, 7.8 mmol) followed by the slow addition of solution B at 0 °C. This mixture (thick-yellow) was allowed to stir for 24 hours at <10 °C, until finished based on TLC. The reaction was quenched with aqueous NH<sub>4</sub>Cl (sat.), and extracted with chloroform, and the aqueous layer removed via a separatory funnel. The organic layer was then washed twice with aqueous NH<sub>4</sub>Cl (sat.) and twice with water. The aqueous layers were extracted with chloroform. The organic layers were combined, dried, and concentrated under vacuum. The residue was subjected to column chromatography (10% ethyl acetate/hexane) to give alkyne **77** as a colourless, clear syrup (0.5 g, 24%). R<sub>f</sub> (25% ethyl acetate/hexane): 0.74; <sup>1</sup>H NMR (400 MHz, CDCl<sub>3</sub>): δ 1.34 (3H, s); 1.35 (3H, s); 1.43 (3H, s); 1.44 (3H, s); 2.60 (1H, d, *J*: 2.2 Hz); 3.95-3.99 (1H, m);

4.08-4.15 (2H, m); 4.15-4.22 (2H, m); 4.32 (1H, dd,  $J$ : 3.7, 2.2 Hz); 4.58 (1H, d,  $J$ : 11.8 Hz); 4.92 (1H, d,  $J$ : 11.8 Hz); 7.29-7.41 (5H, m).

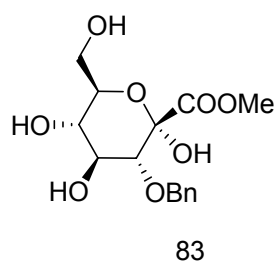
$^{13}\text{C}$  NMR (400 MHz,  $\text{CDCl}_3$ ):  $\delta$  25.3, 26.5, 27.0, 27.6, 66.7, 68.4, 70.9, 75.8, 76.9, 77.3, 79.9, 81.1, 109.6, 110.6, 127.9, 128.1, 128.1, 128.4, 128.4, 137.2.

## Attempted synthesis of methyl 2-*O*-methyl-3-*O*-benzyl-D-gluco-heptulosonate

**78**<sup>47</sup>



To a solution of methyl 3-*O*-benzyl-4,5:6,7-di-*O*-isopropylidene-D-gluco-hept-2-ulosonate **63** (0.09 g, 0.22 mmol) in anhydrous methanol cooled to 0 °C, was added 3% concentrated HCl. The reaction was allowed to warm to room temperature and stir for four days. The reaction was cooled back down to 0 °C and to this was added Amberlite resin IRA 400 (Cl<sup>-</sup>) charged with NaOH. After shaking for 4.5 hours, the resin was filtered off and the filtrate concentrated. The crude solid was subjected to column chromatography (10% methanol/dichloromethane) to give heptulosonate **83** as a white solid (0.06 g, 81%).

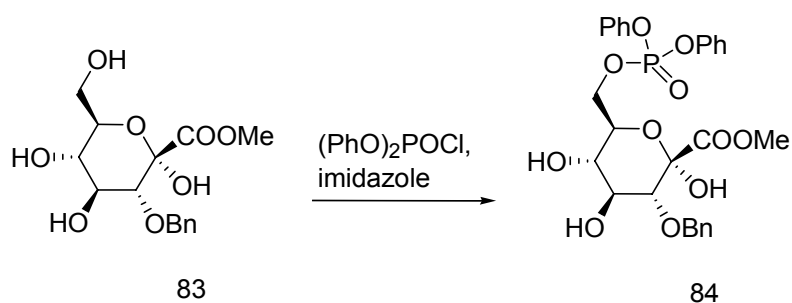


$R_f$  (1:6 methanol/dichloromethane): 0.45; <sup>1</sup>H NMR (400 MHz, CDCl<sub>3</sub>): δ 3.43 (1H, t,  $J$ : 9.0 Hz); 3.64 (3H, s); 3.67-3.73 (1H, m); 3.75 (1H, d,  $J$ : 9.5 Hz); 3.77-3.83 (2H, m); 3.88 (1H, t,  $J$ : 9.0 Hz); 4.62 (1H, d,  $J$ : 11.4 Hz); 4.89 (1H, d,  $J$ : 11.4 Hz); 7.29-7.37 (5H, m).

<sup>13</sup>C NMR (400 MHz, CDCl<sub>3</sub>): δ 51.8, 61.2, 70.5, 73.9, 74.4, 74.5, 80.6, 95.7, 127.2, 127.7, 127.7, 127.8, 127.8, 138.5, 169.9.

$m/z$  (-ve ESMS) 365.0955 (M+K-2H, 100%, calculated mass: 365.0644).

**Methyl 3-*O*-benzyl-7-*O*-diphenylphosphate-D-gluco-heptulosonate **84**<sup>45</sup>**



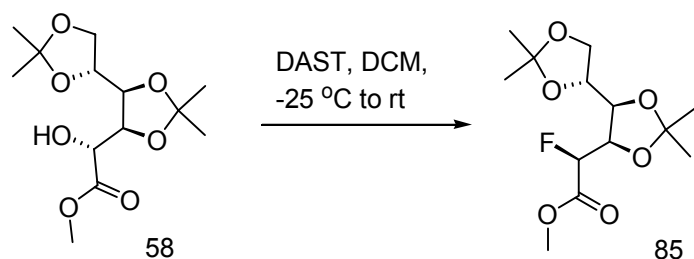
To a solution of imidazole (0.05 g, 0.7 mmol) and methyl 3-*O*-benzyl-D-gluco-heptulosonate **83** (0.06 g, 0.176 mmol) in anhydrous dichloromethane under argon at 0 °C was added diphenyl phosphorochloridate (0.05 g, 0.176 mmol). The reaction was allowed to warm to room temperature (approximately four hours) with stirring and monitored by TLC. The solvent was concentrated under vacuum and the residue subjected to column chromatography (15% methanol/chloroform) to give phosphorylated heptulosonate **84** as a white solid (0.03 g, 27%).  $R_f$  (15% methanol/chloroform): 0.45;  $^1\text{H}$  NMR (400 MHz,  $\text{CDCl}_3$ ):  $\delta$  3.46 (1H, t,  $J$ : 9.1 Hz); 3.64 (3H, s); 3.71-3.76 (1H, m); 3.76-3.79 (1H, m); 3.80-3.83 (1H, m); 3.83-3.86 (1H, m); 3.92 (1H, t,  $J$ : 9.1 Hz); 4.64 (1H, d,  $J$ : 11.1 Hz); 4.91 (1H, d,  $J$ : 11.1 Hz); 7.28-7.34 (5H, m); 7.64-7.75 (10H, m).

$^{13}\text{C}$  NMR (400 MHz,  $\text{CDCl}_3$ ):  $\delta$  51.8, 61.1, 70.5, 73.9, 74.5, 74.6, 80.7, 95.8, 121.2, 121.2, 121.2, 127.3, 127.8, 127.8, 127.8, 127.8, 127.9, 127.9, 127.9, 127.9, 134.9, 138.4, 141.1, 175.9, 178.5.

$^{31}\text{P}$  NMR (400 MHz,  $\text{CDCl}_3$ ):  $\delta$  102.3 (dd,  $J$ : 7.0, 12.0 Hz).

$m/z$  (-ve ESMS) 627.3527 ( $M$ +formic acid+Na-2H, 100%, calculated mass: 627.1249).

**Methyl 3,4:5,6-di-*O*-isopropylidene-2-deoxy-2-fluoro-D-gluconate **85****<sup>43,44</sup>

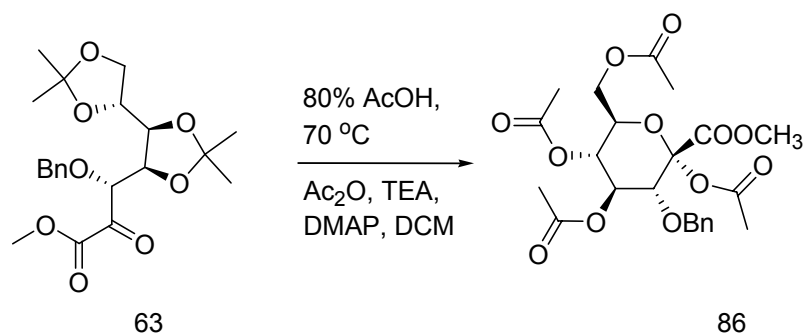


To a solution of methyl 3,4:5,6-di-*O*-isopropylidene-D-gluconate **58** (0.30 g, 1.03 mmol) in dichloromethane (3 mL) under N<sub>2</sub> at -25 °C was added DAST (0.24 g, 1.48 mmol) dropwise. After two hours of stirring at room temperature the reaction mixture was poured into a saturated solution of cold NaHCO<sub>3</sub> and extracted with dichloromethane. The organic layers were combined, dried over MgSO<sub>4</sub>, concentrated under vacuum, and the residue subjected to column chromatography (25% ethyl acetate/hexane) to give fluorinated methyl ester **85** as a yellow oil (0.03 g, 10%). *R<sub>f</sub>* (60% ethyl acetate/hexane): 0.89; <sup>1</sup>H NMR (400 MHz, CDCl<sub>3</sub>): δ 1.30 (3H, s); 1.37 (6H, s); 1.39 (3H, s); 3.77 (3H, s); 3.85 (1H, dd, *J*: 8.3, 8.3 Hz); 3.89-3.94 (1H, m); 3.94-4.06 (1H, m); 4.12 (1H, dd, *J*: 18.8, 8.3 Hz); 4.30-4.40 (1H, m); 5.16 (1H, dd, *J*: 48.3, 1.7 Hz).

<sup>19</sup>F NMR (400 MHz, CDCl<sub>3</sub>): δ -198.15 (dd, *J*: 22.8, 48.3 Hz).

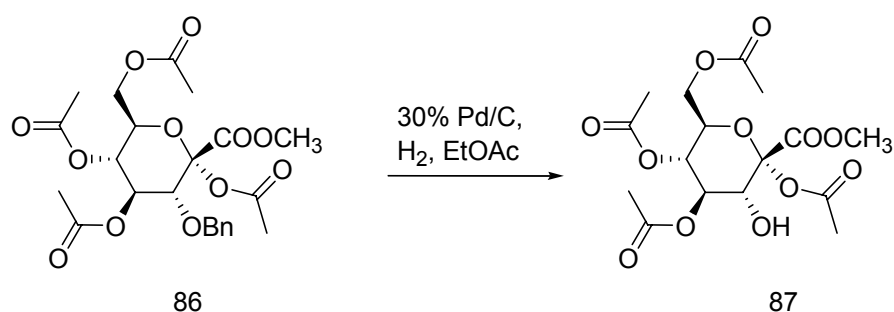
*m/z* (-ve ESMS) 351.21 (M+acetic acid-H, 40%, calculated mass: 351.1439).

### Methyl 2,4,5,7-tetra-*O*-acetyl-3-*O*-benzyl-D-gluco-heptulosonate **86**<sup>71</sup>



To a solution of methyl 3-*O*-benzyl-4,5:6,7-di-*O*-isopropylidene-D-gluco-hept-2-ulosonate **63** (0.04 g, 0.1 mmol) was added 80% acetic acid (3 mL) in water (w/v) and stirred at 70 °C. After two hours the reaction mixture was concentrated under vacuum with toluene. The residue was dissolved in dichloromethane (0.5 mL) under N<sub>2</sub> gas and to this was added triethylamine (0.1 g, 1 mmol), acetic anhydride (0.82 g, 0.8 mmol), and DMAP (0.01 g, 0.08 mmol). The reaction was allowed to stir at room temperature overnight. The reaction mixture was concentrated under vacuum and the residue dissolved in ethyl acetate. The solution was washed with water, 10% HCl, NaHCO<sub>3</sub> (sat.), and brine, dried over MgSO<sub>4</sub>, and concentrated under vacuum to give acetylated heptulosonate **86** (crude) as a white solid (0.04 g, 78%). R<sub>f</sub> (25% ethyl acetate/hexane): 0.1; <sup>1</sup>H NMR (400 MHz, CDCl<sub>3</sub>): δ 1.83 (3H, s); 1.97 (3H, s); 2.03 (3H, s); 2.18 (3H, s); 3.72 (3H, s); 3.90 (1H, d, *J*: 9.5 Hz); 3.88-3.95 (1H, m); 4.04 (1H, dd, *J*: 12.5, 2.2 Hz); 4.26 (1H, dd, *J*: 12.5, 4.7 Hz); 4.45 (1H, d, *J*: 11.6 Hz); 4.58 (1H, d, *J*: 11.6 Hz); 5.05 (1H, t, *J*: 9.5 Hz); 5.38 (1H, t, *J*: 9.5 Hz); 7.20-7.32 (5H, m). <sup>13</sup>C NMR (400 MHz, CDCl<sub>3</sub>): δ 20.6, 20.6, 20.7, 21.0, 53.3, 61.5, 67.9, 70.4, 72.3, 75.1, 78.4, 97.3, 128.1, 128.2, 128.2, 128.5, 128.5, 137.1, 165.8, 168.0, 169.5, 170.0, 170.7.

**Methyl 2,4,5,7-tetra-*O*-acetyl-D-*gluco*-heptulosonate **87**<sup>46</sup>**

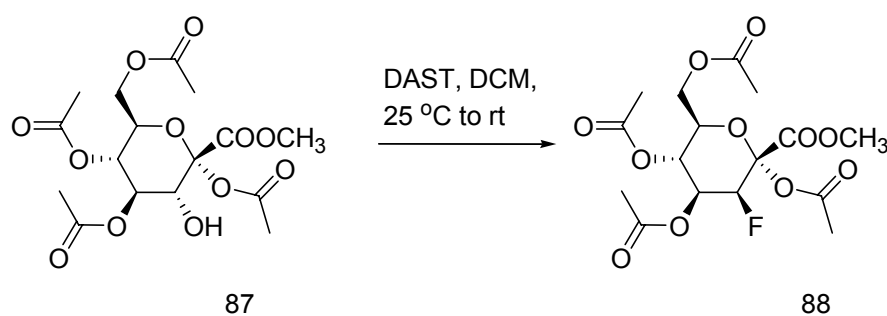


To a solution of methyl 2,4,5,7-tetra-*O*-acetyl-3-*O*-benzyl-D-*gluco*-heptulosonate **86** (0.03 g, 0.07 mmol) in ethyl acetate (0.15 mL) was added 10% palladium on carbon (0.01 g) and hydrogen gas. After stirring overnight at room temperature, the reaction mixture was filtered and concentrated under vacuum to give heptulosonate derivative **87** (crude) as a white solid (0.03 g). *R<sub>f</sub>* (50% ethyl acetate/hexane): 0.31; <sup>1</sup>H NMR (400 MHz, CDCl<sub>3</sub>): δ 2.06 (3H, s); 2.09 (3H, s); 2.10 (3H, s); 2.24 (3H, s); 3.86 (3H, s); 3.93 (1H, d, *J*: 9.8 Hz); 3.96-4.02 (1H, m); 4.11 (1H, dd, *J*: 12.6, 2.0 Hz); 4.32 (1H, dd, *J*: 12.6, 4.7 Hz); 5.15 (1H, t, *J*: 9.8 Hz); 5.33 (1H, t, *J*: 9.8 Hz).

<sup>13</sup>C NMR (400 MHz, CDCl<sub>3</sub>): δ 20.6, 20.7, 20.8, 20.9, 53.6, 61.5, 67.2, 70.8, 71.9, 72.6, 97.2, 165.9, 168.2, 169.4, 170.7, 170.9.

*m/z* (-ve ESMS) 347.0983 (M-H, 100%, calculated mass: 347.0978).

**Methyl 2,4,5,7-tetra-*O*-acetyl-3-deoxy-3-fluoro-D-*gluco*-heptulosonate **88****<sup>43,44</sup>

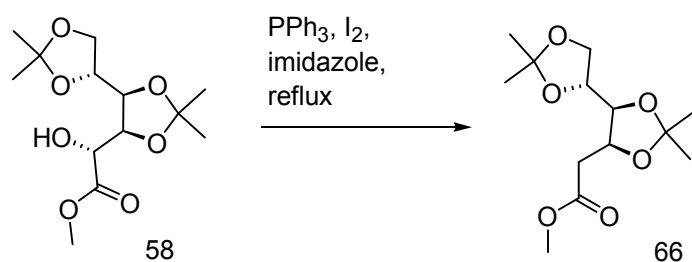


To a solution of methyl 2,4,5,7-tetra-*O*-acetyl-D-*gluco*-heptulosonate **87** (0.028 g, 0.07 mmol) in dichloromethane (0.2 mL) under N<sub>2</sub> at -25 °C was added DAST (0.020 g, 0.1 mmol) dropwise. After 24 hours of stirring at room temperature the reaction was poured into a saturated solution of cold NaHCO<sub>3</sub> and extracted with dichloromethane. The organic layers were combined, dried over MgSO<sub>4</sub>, and concentrated under vacuum to give fluorinated heptulosonate derivative **88** (crude) as a yellow oil (0.028 g, 100%). R<sub>f</sub> (50% ethyl acetate/hexane): 0.49; <sup>1</sup>H NMR (400 MHz, CDCl<sub>3</sub>): δ 2.00 (3H, s); 2.01 (3H, s); 2.04 (3H, s); 2.06 (3H, s); 3.85 (3H, s); 4.02-4.08 (1H, m); 4.18-4.20 (1H, m); 4.21-4.30 (1H, m); 4.36-4.42 (1H, m); 5.32 (1H, t, *J*: 6.9 Hz); 5.43 (1H, t, *J*: 6.9 Hz).

<sup>13</sup>C NMR (400 MHz, CDCl<sub>3</sub>): δ 20.4, 20.6, 20.6, 20.7, 53.4, 61.4, 67.0, 69.5, 71.5, 72.8, 93.9, 168.5, 169.3, 169.8, 170.0, 170.5.

<sup>19</sup>F NMR (400 MHz, CDCl<sub>3</sub>): δ -112.6 (d, *J*: 10.7 Hz).

### Methyl 3,4:5,6-di-*O*-isopropylidene-2-deoxy-D-gluconate **66**<sup>62</sup>

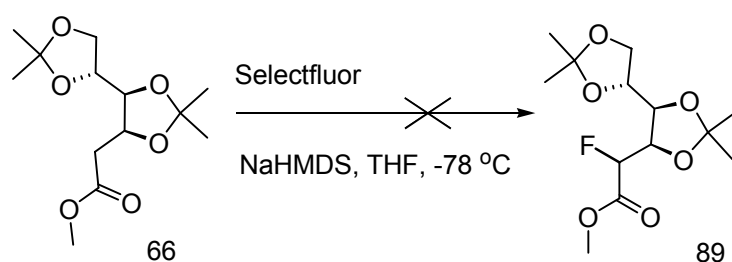


To a solution of triphenyl phosphine (0.98 g, 3.7 mol) in dry toluene (8.3 mL) under N<sub>2</sub> was added iodine (0.71 g, 2.8 mmol) and imidazole (0.25 g, 3.7 mmol) and stirred at room temperature for 10 minutes. To the mixture was then added a solution of methyl 3,4:5,6-di-*O*-isopropylidene-D-gluconate **58** (0.27 g, 0.93 mmol) in dry toluene (8.3 mL) and refluxed at 115 °C for six hours. The reaction was cooled, filtered, and concentrated under vacuum. The residue was subjected to column chromatography (10% ethyl acetate/hexane) to give gluconate **66** as a colourless, clear syrup (0.19 g, 75%). R<sub>f</sub> (25% ethyl acetate/hexane): 0.62; <sup>1</sup>H NMR (400 MHz, CDCl<sub>3</sub>): δ 1.27 (3H, s); 1.33 (6H, s); 1.34 (3H, s); 2.52 (1H, dd, *J*: 15.8, 8.8 Hz); 2.78 (1H, dd, *J*: 15.8, 3.2 Hz); 3.53 (1H, t, *J*: 8.3 Hz); 3.66 (3H, s); 3.89 (1H, dd, *J*: 8.3, 4.9 Hz); 3.94-4.02 (1H, m); 4.08 (1H, dd, *J*: 8.3, 6.2 Hz); 4.28 (1H, ddd, *J*: 16.4, 8.3, 3.2 Hz).

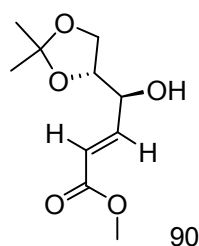
<sup>13</sup>C NMR (400 MHz, CDCl<sub>3</sub>): δ 25.2, 26.7, 26.9, 27.1, 38.3, 51.7, 67.8, 76.7, 76.9, 80.4, 109.5, 109.7, 171.1.

m/z (-ve ESMS) 297.2007 (M+Na, 100%, calculated mass: 297.1309).

**Attempted synthesis of methyl 3,4:5,6-di-*O*-isopropylidene-2-deoxy-2-fluoro-D-gluconate **89**<sup>72,73</sup>**



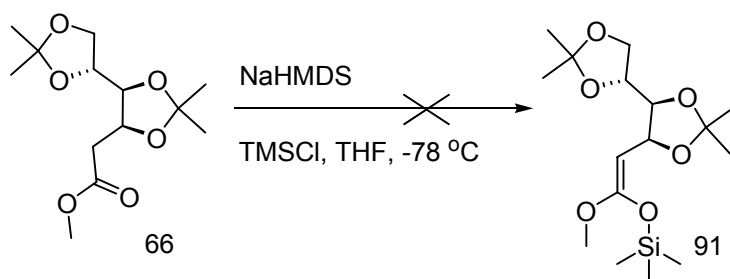
To a solution of methyl 3,4:5,6-di-*O*-isopropylidene-2-deoxy-D-gluconate **66** (0.09 g, 0.31 mmol) and Selectfluor (0.11 g, 0.31 mol) in dry tetrahydrofuran (14 mL) under argon at -78 °C was added NaHMDS (0.08 g, 0.41 mmol) dropwise. The reaction was allowed to stir for 3 hours at -78 °C, then for one hour at room temperature. The mixture was quenched with NH<sub>4</sub>Cl and diluted with diethyl ether. The mixture was washed with cold NaHCO<sub>3</sub> and brine. The aqueous layer was extracted again with ether, the organic layers were combined, dried over MgSO<sub>4</sub>, and concentrated under vacuum to give alkene **90** (crude) as a red oil (0.02 g, 25%).



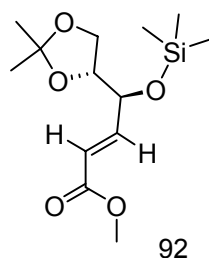
$R_f$  (33% ethyl acetate/hexane): 0.3; <sup>1</sup>H NMR (400 MHz, CDCl<sub>3</sub>): δ 1.37 (3H, s); 1.46 (3H, s); 3.75 (3H, s); 3.91 (1H, dd, *J*: 26.4, 8.5 Hz); 3.93 (1H, dd, *J*: 26.4, 8.5 Hz); 4.14-4.20 (1H, m); 4.49 (1H, ddd, *J*: 8.5, 4.3, 1.9 Hz); 6.19 (1H, dd, *J*: 15.7, 1.9 Hz); 6.92 (1H, dd, *J*: 15.7, 4.1 Hz).

<sup>13</sup>C NMR (400 MHz, CDCl<sub>3</sub>): δ 24.9, 26.4, 51.8, 64.6, 70.4, 77.3, 109.8, 121.7, 144.9, 166.6.

**Attempted synthesis of methyl 3,4:5,6-Di-*O*-isopropylidene-1-*O*-silyl-2-deoxy-D-*gluco*-enolate **91**<sup>72</sup>**



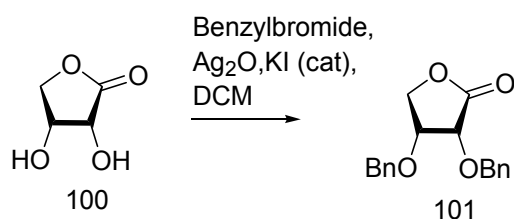
To a solution of methyl 3,4:5,6-di-*O*-isopropylidene-2-deoxy-D-*gluco*-enolate **66** (0.11 g, 0.41 mmol) in dry tetrahydrofuran (10 mL) under argon at -78 °C, was added NaHMDS (0.01 g, 0.54 mmol) dropwise. After stirring for 3.5 hours, TMSCl (0.06 g, 0.51 mmol) was added at -78 °C and the reaction allowed to warm up to room temperature over a span of 1 hour. The mixture was quenched with NH<sub>4</sub>Cl and diluted with diethyl ether. The mixture was extracted with hexane and washed with cold NaHCO<sub>3</sub>, dried over MgSO<sub>4</sub>, and concentrated under vacuum to give alkene **92** (crude) as a clear oil (0.03 g, 23%).



R<sub>f</sub> (25% ethyl acetate/hexane): 0.8; <sup>1</sup>H NMR (400 MHz, CDCl<sub>3</sub>): δ 0.13 (9H, s); 1.33 (3H, s); 1.42 (3H, s); 3.74 (3H, s); 3.83-3.90 (1H, m); 3.94-4.01 (2H, m); 4.25-4.30 (1H, m); 6.04 (1H, dd, *J*: 15.7, 1.8 Hz); 7.01 (1H, dd, *J*: 15.7, 4.3 Hz).

<sup>13</sup>C NMR (400 MHz, CDCl<sub>3</sub>): δ 0.1, 0.1, 0.1, 25.3, 26.7, 51.6, 66.1, 72.2, 78.3, 109.8, 121.2, 147.7, 166.7.

**(3*R*)-(cis)-Dihydro-3,4-bis(phenylmethoxy)-2(3H)-furanone 101**<sup>63</sup>

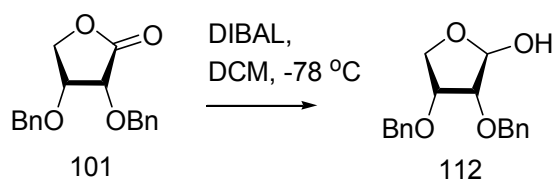


To a stirred solution of (3*R*)-(cis)-dihydro-3,4-dihydroxy-2(3H)-furanone **100** (0.5 g, 4.24 mmol) dissolved in dichloromethane at 0 °C under N<sub>2</sub> was first added potassium iodide (0.2 g, 1.08 mmol), followed by benzyl bromide (2.2 g, 12.7 mmol) and finally silver (I) oxide (2.9 g, 12.7 mmol). The mixture was allowed to stir for 5 minutes at 0 °C then at room temperature until finished (based on TLC). The mixture was filtered through Celite, dissolved in dichloromethane, washed with NaHCO<sub>3</sub>(sat) and brine, dried over MgSO<sub>4</sub>, and concentrated under vacuum. The residue was subjected to column chromatography (25% ethyl acetate/hexane) to give furanone **101** as a white solid (0.7 g, 56%). R<sub>f</sub> (33% ethyl acetate/hexane): 0.38; <sup>1</sup>H NMR (400 MHz, CDCl<sub>3</sub>): δ 4.17 (1H, d, *J*: 4.8 Hz); 4.23-4.24 (2H, m); 4.35-4.40 (1H, m); 4.67 (1H, d, *J*: 12 Hz); 4.76 (1H, d, *J*: 12 Hz); 4.86 (1H, d, *J*: 12 Hz); 4.98 (1H, d, *J*: 12 Hz); 7.31-7.45 (10H, m).

<sup>13</sup>C NMR (400 MHz, CDCl<sub>3</sub>): δ 69.5, 72.1, 72.4, 73.9, 74.0, 127.9, 127.9, 128.1, 128.2, 128.2, 128.2, 128.3, 128.5, 128.5, 128.6, 128.6, 128.6, 158.3.

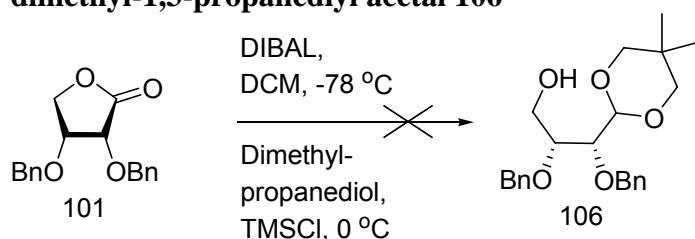
m/z (+ve ESMS) 299.1292 (M+H, 100%, calculated mass: 299.1283).

**(3*R*,4*R*)-Tetrahydro-3,4-bis(phenylmethoxy)-2-furanol **112**<sup>74</sup>**

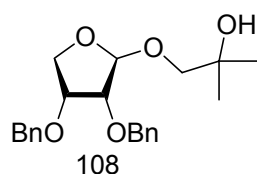


To a stirred solution of (3*R*)-(*cis*)-dihydro-3,4-bis(phenylmethoxy)-2(3*H*)-furanone **101** (0.11 g, 0.36 mmol) dissolved in dichloromethane at -78 °C under N<sub>2</sub> was slowly added 1 M DIBAL (1.07 mL). The mixture was allowed to stir for 4 hours at -78 °C. The reaction was diluted with dichloromethane and quenched at -78 °C with 10% HCl. The mixture was allowed to warm to room temperature and washed with water, Rochelle's salts, and brine. The organic layer was dried with MgSO<sub>4</sub> and concentrated under vacuum to give furanol **112** as a crude clear syrup (0.10 g, 93%). *R<sub>f</sub>* (50% ethyl acetate/hexane): 0.57; <sup>1</sup>H NMR (400 MHz, CDCl<sub>3</sub>): δ 3.83-3.92 (1H, m); 4.06-4.11 (1H, m); 4.12-4.19 (1H, m); 4.23-4.31 (1H, m); 4.53-4.79 (4H, m); 5.28 (1H, dd, *J*: 12.0, 4.2 Hz); 7.28-7.44 (10H, m). <sup>13</sup>C NMR (400 MHz, CDCl<sub>3</sub>): δ 69.9, 72.2, 72.7, 76.4, 78.3, 95.5, 127.8, 127.8, 127.9, 127.9, 128.0, 128.0, 128.1, 128.4, 128.5, 128.5, 128.5, 128.5.

**Attempted synthesis of (2*R*,3*R*)-2,3-Bis-*O*-(phenylmethyl)-*D*-erythrose-cyclic 2,2-dimethyl-1,3-propanediyl acetal **106**<sup>46</sup>**



To a stirred solution of (3*R*)-(cis)-dihydro-3,4-bis(phenylmethoxy)-2(3*H*)-furanone **101** (0.11 g, 0.37 mmol) dissolved in dichloromethane at -78 °C under N<sub>2</sub> was slowly added 1 M DIBAL (1.11 mL). The reaction mixture was allowed to stir for 4 hours at -78 °C to give solution A. To a stirred solution of dimethylpropanediol (0.06 g, 0.56 mmol) and TMSCl (0.12 g, 1.11 mmol) dissolved in dichloromethane at 0 °C under N<sub>2</sub> was added solution A. The reaction mixture was allowed to stir overnight at room temperature. The reaction mixture was diluted with dichloromethane and washed with NaHCO<sub>3</sub> and brine. The aqueous layers were extracted again with dichloromethane. The organic layers were combined, dried over MgSO<sub>4</sub>, and concentrated under vacuum. The residue was subjected to column chromatography (20% ethyl acetate/hexane) to give ether **108** as a clear syrup (0.12 g, 84%).



R<sub>f</sub> (33% ethyl acetate/hexane): 0.48; <sup>1</sup>H NMR (400 MHz, CDCl<sub>3</sub>): δ 0.74 (3H, s); 1.24 (3H, s); 1.26-1.28 (2H, m); 3.35-3.47 (1H, m); 3.69-3.72 (1H, m), 3.73-3.87 (2H, m); 4.74 (1H, d, *J*: 11.5 Hz); 4.91 (1H, d, *J*: 11.5 Hz); 4.65 (1H, d, *J*: 2.2 Hz); 4.55 (1H, d, *J*: 11.5 Hz); 4.59 (1H, d, *J*: 11.5 Hz); 7.26-7.42 (10H, m).

<sup>13</sup>C NMR (400 MHz, CDCl<sub>3</sub>): δ 21.8, 23.1, 30.4, 61.4, 72.0, 74.5, 77.1, 78.4, 78.7, 101.2, 127.7, 127.8, 128.0, 128.0, 128.3, 128.3, 128.3, 128.3, 128.5, 128.5, 138.1, 138.2.

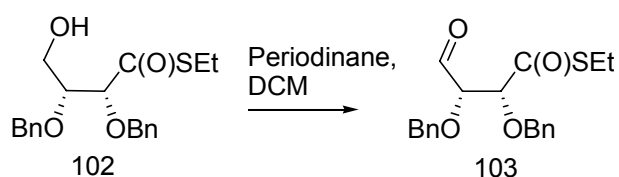
**(2*R*,3*R*)-2,3-Bis-*O*-(phenylmethyl)-*S*-ethylester-*D*-erythrothioic acid **102**<sup>46</sup>**



To a stirred solution of trimethyl aluminium (0.07 g, 1.01 mmol) dissolved in dichloromethane at 0 °C under  $\text{N}_2$  was added ethanethiol (0.06 g, 1.01 mmol). The mixture was stirred and allowed to warm to room temperature. (3*R*)-(*cis*)-dihydro-3,4-bis(phenylmethoxy)-2(3*H*)-furanone **101** (0.15 g, 0.51 mmol) in dichloromethane was then added to the mixture and allowed to stir overnight. The mixture was quenched with ether and 3% HCl. The organic layer was washed with NaOH and brine, dried over  $\text{MgSO}_4$ , and concentrated under vacuum. The residue was subjected to column chromatography (20% ethyl acetate/hexane) to give ethyl thioester **102** as a clear syrup (0.99 g, 54%).  $R_f$  (20% ethyl acetate/hexane): 0.43;  $^1\text{H}$  NMR (400 MHz,  $\text{CDCl}_3$ ):  $\delta$  1.30 (3H, t,  $J$ : 7.3 Hz); 2.94 (2H, q,  $J$ : 7.3 Hz); 3.72-3.85 (1H, m); 3.88 (1H, dd,  $J$ : 9.7, 4.6 Hz); 4.22-4.25 (1H, m); 4.56-4.60 (2H, m); 4.63-4.67 (1H, m); 4.71-4.75 (1H, m); 4.80-4.84 (1H, m); 7.30-7.44 (10H, m).

$m/z$  (+ve ESMS) 375.2080 ( $\text{M}+\text{O}-\text{H}$ , 100%, calculated mass: 375.1283).

**(2*R*,3*R*)-2,3-bis-*O*-(phenylmethyl)-4-formyl-D-erythrothioic acid **103**<sup>64</sup>**



To a solution of Dess-Martin periodinane (0.25 g, 0.58 mmol) in dry dichloromethane under argon was added a solution of (2*R*,3*R*)-2,3-bis-*O*-(phenylmethyl)-D-erythrothioic acid **102** (0.14 g, 0.39 mmol) in dichloromethane. After stirring at room temperature for 4 hours in darkness, the reaction was diluted with dichloromethane and washed with saturated NaHCO<sub>3</sub>, saturated Na<sub>2</sub>S<sub>2</sub>O<sub>3</sub>, water, and brine. The organic layer was dried over MgSO<sub>4</sub> and concentrated under vacuum. The residue was subjected to column chromatography (13% ethyl acetate/hexane) to give **103** as a clear syrup (0.58 g, 42%). *R<sub>f</sub>* (25% ethyl acetate/hexane): 0.63; <sup>1</sup>H NMR (400 MHz, CDCl<sub>3</sub>): δ 1.30 (3H, t, *J*: 7.5 Hz); 2.94 (2H, q, *J*: 7.5 Hz); 4.16 (1H, dd, *J*: 2.9, 0.6, Hz); 4.42 (1H, d, *J*: 2.9 Hz); 4.66 (1H, d, *J*: 11.5 Hz); 4.73 (1H, d, *J*: 12.1 Hz); 4.77 (1H, d, *J*: 12.1 Hz); 4.81 (1H, d, *J*: 11.5 Hz); 7.30-7.44 (10H, m); 9.67 (1H, d, *J*: 0.6 Hz).

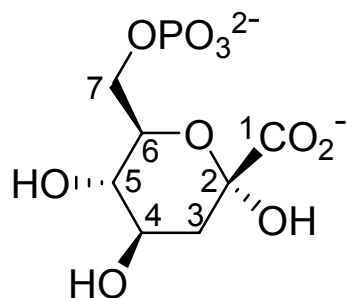
<sup>13</sup>C NMR (400 MHz, CDCl<sub>3</sub>): δ 14.3, 22.9, 73.3, 74.1, 83.3, 85.7, 128.1, 128.1, 128.1, 128.1, 128.2, 128.3, 128.5, 128.5, 128.6, 128.6, 136.5, 136.9, 200.1, 200.3.

## **Appendices**

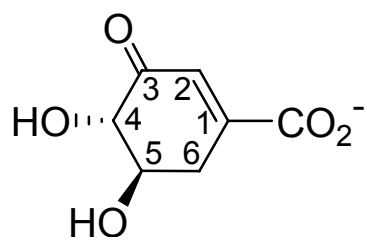
*Appendix one*

**Nomenclature**

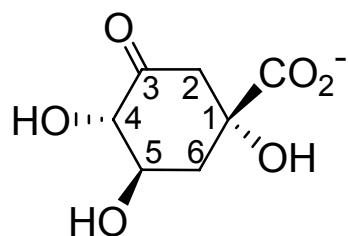
The numbering for DAH7P begins at the carboxylate group:



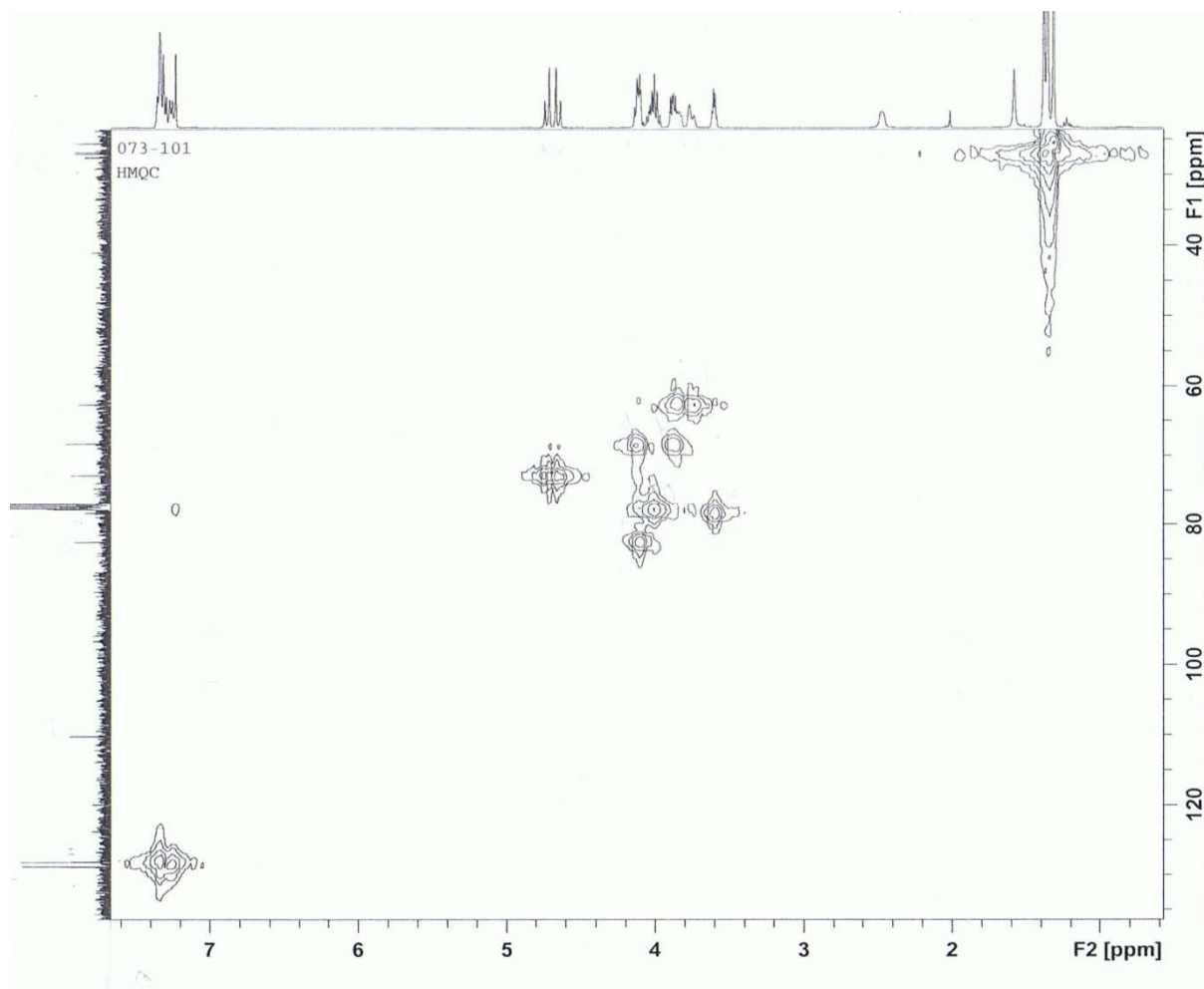
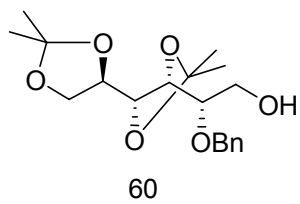
The numbering for shikimate begins at the carbon adjacent to the carboxylate group and continues through the double bond:



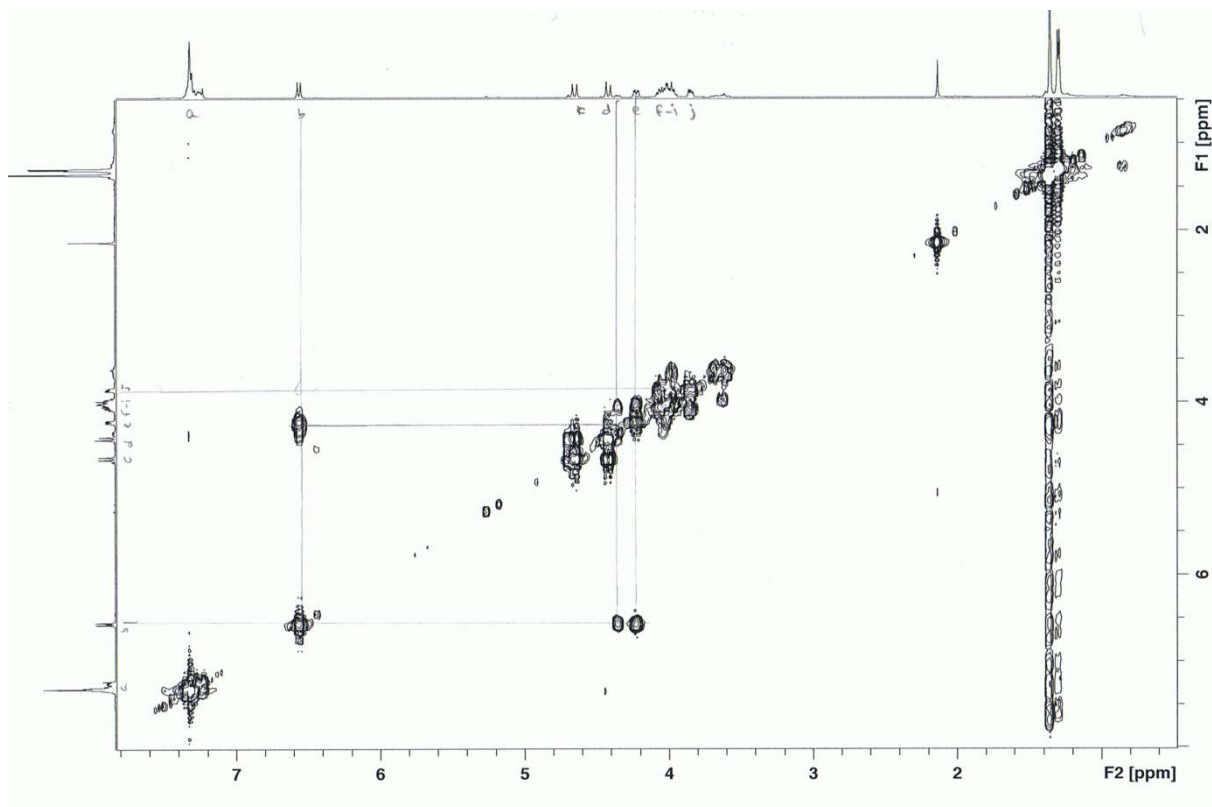
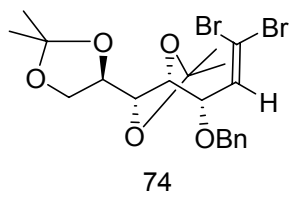
The numbering used for dehydroquinic acid is in the same sense:



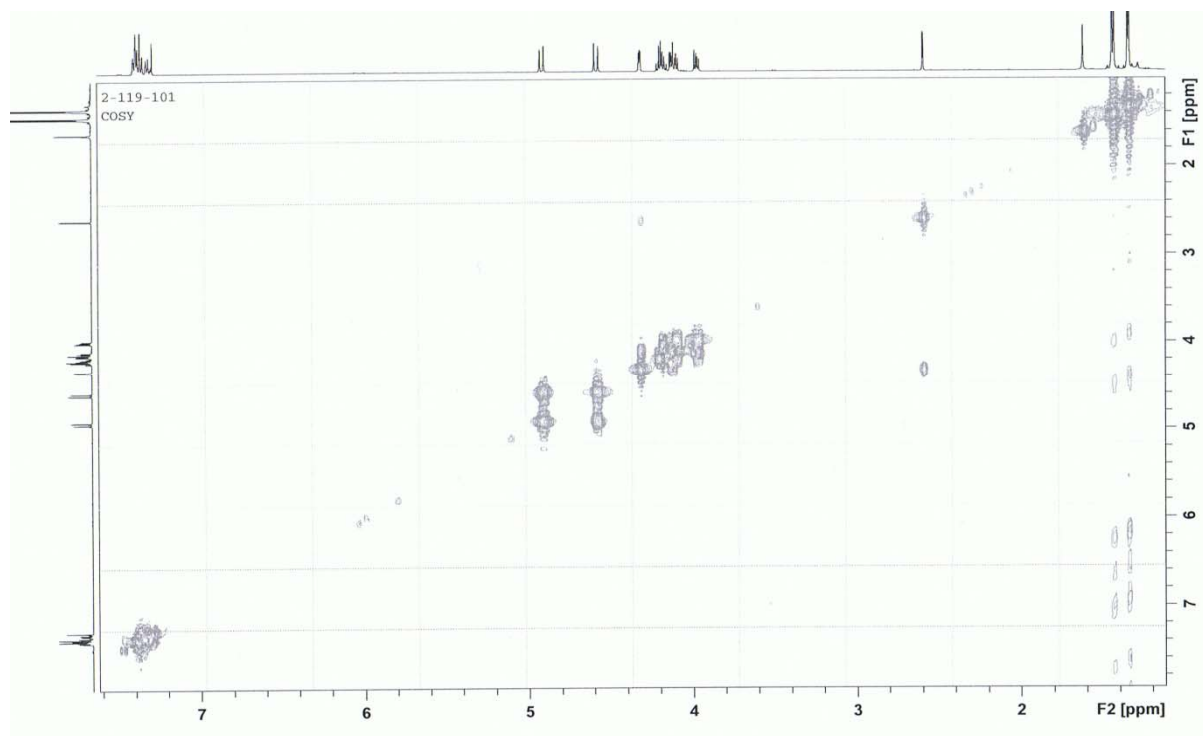
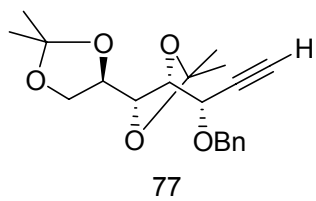
Appendix two



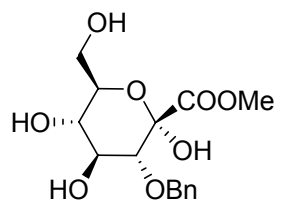
Appendix three



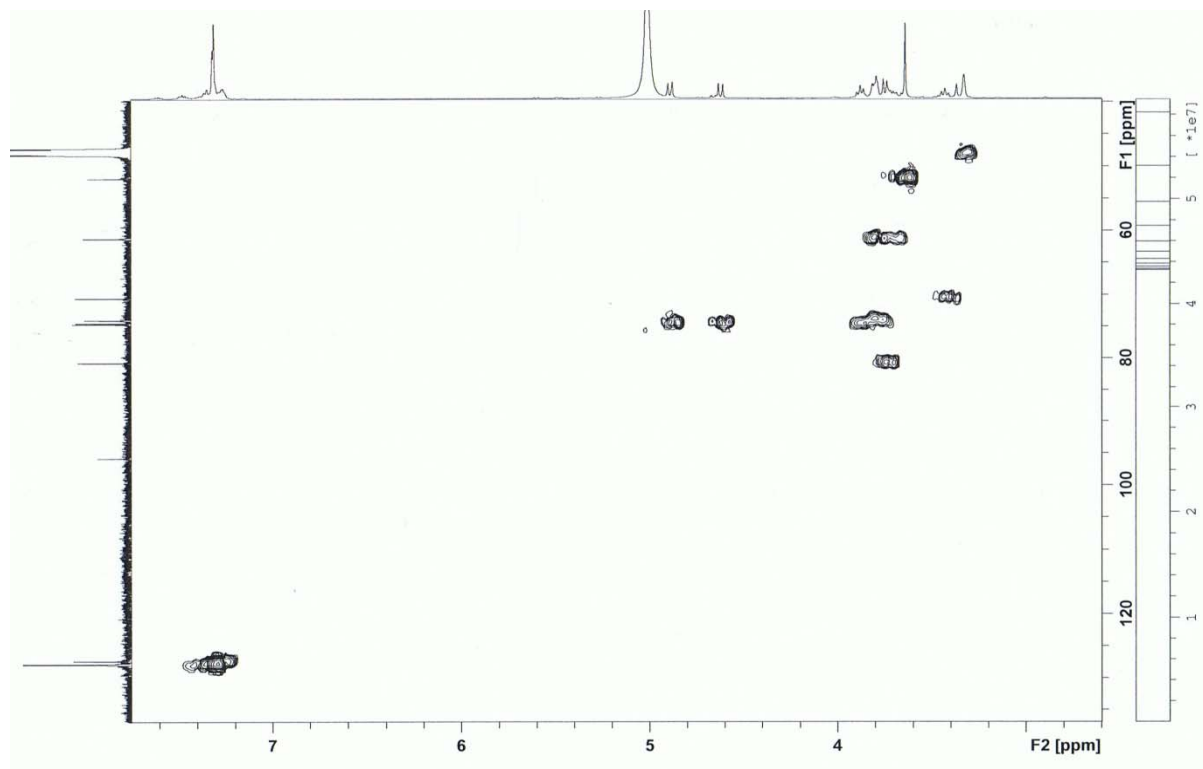
Appendix four



Appendix five



83



## References

- (1) Lancini, G.; Parenti, F.; Gallo, G. G. *Antibiotics: A Multidisciplinary Approach*; Plenum Press: New York, 1995; 278.
- (2) Ganem, B. Shikimate derived metabolites .4. From glucose to aromatics - recent developments in natural products of shikimic acid pathway. *Tetrahedron* **1978**, *34*, 3353-3383.
- (3) Knowles, J. R. Mechanistic ingenuity in enzyme catalysis: dehydroquinase synthase. *Aldrichimica Acta* **1989**, *22*, 59-66.
- (4) Gibson, F.; Pittard, J. Pathways of biosynthesis of aromatic amino acids and vitamins and their control in microorganisms. *Bacteriol. Rev.* **1968**, *32*, 465-492.
- (5) Franz, J.; Mao, M.; Sikorski, J. Glyphosate: A unique global herbicide. In *ACS Monograph, 189*: Washington DC, US, 1997.
- (6) Bentley, R. The shikimate pathway—A metabolic tree with many branches. *Crit. Rev. Biochem. Mol. Biol.* **1990**, *25*, 307–384.
- (7) Hawkins, A. R.; Moore, J. D.; Adeokun, A. M. Characterization of the 3-dehydroquinase domain of the pentafunctional AROM protein, and the quinase dehydrogenase from *Aspergillus nidulans*, and the overproduction of the type-II 3-dehydroquinase from *Neurospora crassa*. *Biochem. J.* **1993**, *296*, 451-457.
- (8) Carpenter, E. P.; Hawkins, A. R.; Frost, J. W.; Brown, K. A. Structure of dehydroquinase synthase reveals an active site capable of multistep catalysis. *Nature* **1998**, *394*, 299-302.
- (9) Nichols, C. E.; Ren, J.; Leslie, K.; Dhaliwal, B.; Lockyer, M. et al. Comparison of Ligand-induced Conformational Changes and Domain Closure Mechanisms, Between Prokaryotic and Eukaryotic Dehydroquinase Synthases. *J. Mol. Biol.* **2004**, *343*, 533-546.
- (10) Sugahara, M.; Nodake, Y.; Sugahara, M.; Kunishima, N. Crystal structure of dehydroquinase synthase from *Thermus thermophilus* HB8 showing functional importance of the dimeric state. *Proteins* **2005**, *58*, 249-252.
- (11) Liu, J. S.; Cheng, W. C.; Wang, H. J.; Chen, Y. C.; Wang, W. C. Structure-based inhibitor discovery of *Helicobacter pylori* dehydroquinase synthase. *Biochem. Biophys. Res. Commun.* **2008**, *373*, 1-7.
- (12) Ngo, P.-T. H.; Natarajan, S.; Kim, H.; Hung, H. K.; Kim, J.-G. et al. Cloning, expression, crystallization and preliminary X-ray crystallographic analysis of 3-dehydroquinase synthase, Xoo1243, from *Xanthomonas oryzae* pv. *oryzae*. *Acta Crystallogr., Sect. F: Struct. Biol. Cryst. Commun.* **2008**, *64*, 1128-1131.
- (13) Bender, S. L.; Mehdi, S.; Knowles, J. R. Dehydroquinase synthase: the role of divalent metal cations and of nicotinamide adenine dinucleotide in catalysis. *Biochemistry* **1989**, *28*, 7555-7560.
- (14) Rotenberg, S. L.; Sprinson, D. B. Mechanism and Stereochemistry of 5-Dehydroquinase Synthetase. *Proc. Natl. Acad. Sci. U. S. A.* **1970**, *67*, 1669-1672.
- (15) Rotenberg, S. L.; Sprinson, D. B. Isotope effects in 3-dehydroquinase synthase and dehydratase. *J. Biol. Chem.* **1978**, *253*, 2210-2215.
- (16) Turner, M. J.; Smith, B. W.; Haslam, E. Shikimate Pathway .4. Stereochemistry of 3-dehydroquinase dehydratase reaction and observations on 3-dehydroquinase synthetase. *J. Chem. Soc., Perkin Trans. 1* **1975**, 52-55.

- (17) Widlanski, T. S.; Bender, S. L.; Knowles, J. R. Stereochemical course of the cryptic elimination and cyclization steps in the reaction catalyzed by dehydroquinase synthase. *J. Am. Chem. Soc.* **1987**, *109*, 1873-1875.
- (18) Lambert, J. M.; Boocock, M. R.; Coggins, J. R. The 3-dehydroquinase synthase activity of the pentafunctional *arom* enzyme complex of *Neurospora crassa* is Zn<sup>2+</sup>-dependent. *Biochem. J.* **1985**, *226*, 817-829.
- (19) Hasan, N.; Nester, E. W. Dehydroquinase Synthase in *Bacillus subtilis*. *J. Biol. Chem.* **1978**, *253*, 4999-5004.
- (20) Yamamoto, E. Purification and Metal Requirements of 3-Dehydroquinase Synthase from *Phaseolus mungo* Seedlings. *Phytochemistry* **1980**, *19*, 779-781.
- (21) Saijo, R.; Kosuge, T. The Conversion of 3-Deoxy-D-arabino-heptulosonate 7-Phosphate to 3-Dehydroquinase by *Sorghum* Seedling Preparations. *Phytochemistry* **1978**, *17*, 223-225.
- (22) Widlanski, T.; Bender, S. L.; Knowles, J. R. Dehydroquinase synthase: the use of substrate analogs to probe the late steps of the catalyzed reaction. *Biochemistry* **1989**, *28*, 7572-7582.
- (23) Widlanski, T.; Bender, S. L.; Knowles, J. R. Dehydroquinase synthase: a sheep in wolf's clothing? *J. Am. Chem. Soc.* **1989**, *111*, 2299-2300.
- (24) Montchamp, J.-L.; Peng, J.; Frost, J. W. Inversion of an asymmetric center in carbocyclic inhibitors of 3-dehydroquinase synthase: examining and exploiting the mechanism for *syn*-elimination during substrate turnover. *J. Org. Chem.* **1994**, *59*, 6999-7007.
- (25) Bartlett, P. A.; Satake, K. Does dehydroquinase synthase synthesize dehydroquinase. *J. Am. Chem. Soc.* **1988**, *110*, 1628-1630.
- (26) Bartlett, P. A.; McLaren, K. L.; Marx, M. A. Divergence between the enzyme-catalyzed and noncatalyzed synthesis of 3-dehydroquinase. *J. Org. Chem.* **1994**, *59*, 2082-2085.
- (27) Parker, E. J.; Coggins, J. R.; Abell, C. Derailing dehydroquinase synthase by introducing a stabilizing stereoelectronic effect in a reaction intermediate. *J. Org. Chem.* **1997**, *62*, 8582-8585.
- (28) Street, I. P.; Rupitz, K.; Withers, S. G. Fluorinated and deoxygenated substrates as probes of transition state structure in glycogen phosphorylase. *Biochemistry* **1989**, *28*, 1581-1587.
- (29) Anh, N. T.; Eisenstein, O. *New J. Chem.* **1977**, *1*, 61-70.
- (30) Frost, J. W.; Bender, J. L.; Kadonaga, J. T.; Knowles, J. R. Dehydroquinase synthetase from *Escherichia coli*: purification, cloning, and construction of overproducers of the enzyme. *Biochemistry* **1984**, *23*, 4470-4475.
- (31) Schofield, L. R.; Anderson, B. F.; Patchett, M. L.; Norris, G. E.; Jameson, G. B. et al. Substrate Ambiguity and Crystal Structure of *Pyrococcus furiosus* 3-Deoxy-D-arabino-heptulosonate-7-phosphate Synthase: An Ancestral 3-Deoxyald-2-ulosonate-phosphate Synthase. *Biochemistry* **2005**, *44*, 11950-11962.
- (32) Robb, F. T.; Maeder, D. L.; Brown, J. R.; DiRuggiero, J.; Stump, M. D. et al. Genomic sequence of hyperthermophile, *Pyrococcus furiosus*: implications for physiology and enzymology. *Methods Enzymol.* **2001**, *330*, 134-157.
- (33) Novy, R.; Drott, D.; Yaeger, K.; Mierendorf, R. Overcoming the codon bias of *E. coli* for enhanced protein expression. *InNovations* **2001**, *12*, 1-3.

- (34) Neisen, F. H.; Berglund, H.; Vedadi, M. The use of differential scanning fluorimetry to detect ligand interactions that promote protein stability. *Nat. Protoc.* **2007**, *2*, 2212-2221.
- (35) Moore, J. D.; Coggins, J. R.; Virden, R.; Hawkins, A. R. Efficient independent activity of a monomeric, monofunctional dehydroquinase synthase derived from the N-terminus of the pentafunctional AROM protein of *Aspergillus nidulans*. *Biochem. J.* **1994**, *301*, 297-304.
- (36) Lumsden, J.; Coggins, J. R. The Subunit Structure of the *arom* Multienzyme Complex of *Neurospora crassa*. *Biochem. J.* **1977**, *161*, 599-607.
- (37) Baxter, J. N.; Perlin, A. S.; Simpson, F. J. Preparation and assay of D-erythrose 4-phosphate. *Can. J. Biochem. Physiol.* **1959**, *37*, 199-209.
- (38) Bergmann, E. D.; Shahak, I. Organic Fluorine Compounds .13. An Ester of Phospho-Enol-Fluoropyruvic Acid 1-Alkoxy-carbonyl-2-Fluorovinyl Dialkyl Phosphate and Related Compounds. *J. Chem. Soc.* **1960**, 462-463.
- (39) Stubbe, J. A.; Kenyon, G. L. Analogs of Phosphoenolpyruvate. Substrate Specificities of Enolase and Pyruvate Kinase from Rabbit Muscle. *Biochemistry* **1972**, *11*, 338-345.
- (40) Lanzetta, P. A.; Alvarez, L. J.; Reinach, P. S.; Candia, O. A. An Improved Assay for Nanomole Amounts of Inorganic Phosphate. *Anal. Biochem.* **1979**, *100*, 95-97.
- (41) Anderson, B. M.; Anderson, C. D. The Effect of Buffers on Nicotinamide Adenine Dinucleotide Hydrolysis. *J. Biol. Chem.* **1963**, *238*, 1475-1478.
- (42) Hilvers, A. G.; van Dam, K. The decomposition of nicotinamide adenine dinucleotide (NAD) under alkaline conditions. *Biochim. Biophys. Acta* **1964**, *81*, 391-394.
- (43) Card, P. J. Fluorinated Carbohydrates. Use of (Diethylamino)sulfur Trifluoride in the Synthesis of Fluorinated Sugars. *J. Org. Chem.* **1983**, *48*, 393-395.
- (44) Tewson, T. J.; Welch, M. J. New Approaches to the Synthesis of 3-Deoxy-3-fluoro-D-glucose. *J. Org. Chem.* **1978**, *43*, 1090-1092.
- (45) Frost, J. W.; Knowles, J. R. 3-Deoxy-D-arabino-heptulosonic acid 7-phosphate - chemical synthesis and isolation from *Escherichia-coli* auxotrophs. *Biochemistry* **1984**, *23*, 4465-4469.
- (46) Kocienski, P. L. *Protecting Groups*; 3rd ed.; Stuttgart ; Georg Thieme: New York, 2004; 679.
- (47) Liu, K. G.; Hu, S. G.; Wu, Y. K.; Yao, Z. J.; Wu, Y. L. A straight forward synthesis of DAH (3-deoxy-D-arabino-hept-2-ulosonic acid) and DRH (3-deoxy-D-ribo-hept-2-ulosonic acid). *J. Chem. Soc., Perkin Trans. 1* **2002**, 1890-1895.
- (48) Gonzalez, I. C.; Forsyth, C. J. Total synthesis of thyriferyl 23-acetate, a specific inhibitor of protein phosphatase 2A and an anti-leukemic inducer of apoptosis. *J. Am. Chem. Soc.* **2000**, *122*, 9099-9108.
- (49) Durand-Reville, T.; Gobbi, L. B.; Gray, B. L.; Ley, S. V.; Scott, J. S. Highly selective entry to the azadirachtin skeleton via a Claisen rearrangement/radical cyclization sequence. *Org. Lett.* **2002**, *4*, 3847-3850.
- (50) Dalarcao, M.; Leonard, N. J. Synthesis and transilience of a 1,3-diazabiphenylene. *J. Am. Chem. Soc.* **1983**, *105*, 5958-5960.
- (51) Michel, P.; Gennet, D.; Rassat, A. A one-pot procedure for the synthesis of alkynes and bromoalkynes from aldehydes. *Tetrahedron Lett.* **1999**, *40*, 8575-8578.

- (52) Le Marechal, P.; Froussios, C.; Level, M.; Azerad, R. The Interaction of Phosphonate and Homophosphonate analogues of 3-deoxy-D-arabino heptulosonate 7-phosphate with 3-Dehydroquinase Synthetase from *Escherichia Coli*. *Biochem. Biophys. Res. Commun.* **1980**, *92*, 1104-1109.
- (53) Middleton, W. J. New Fluorinating Reagents. Dialkylaminosulfur Fluorides. *J. Org. Chem.* **1975**, *40*, 574-578.
- (54) Lal, G. S.; Pez, G. P.; Syvret, R. G. Electrophilic NF Fluorinating Agents. *Chem. Rev.* **1996**, *96*, 1737-1756.
- (55) Nyffeler, P. T.; Gonzalez Duron, S.; Burkart, M. D.; Vincent, S. P.; Wong, C. Selectfluor: Mechanistic Insight and Applications. *Angew. Chem., Int. Ed. Engl.* **2005**, *44*, 192-212.
- (56) Banks, R. E. Selectfluor<sup>TM</sup> reagent F-TEDA-BF<sub>4</sub> in action: tamed fluorine at your service. *J. Fluorine Chem.* **1998**, *87*, 1-17.
- (57) Hess, H. H.; Der, J. E. Assay of Inorganic and Organic Phosphorus in the 0.1-5 Nanomole Range. *Anal. Biochem.* **1975**, *63*, 607-613.
- (58) Bradford, M. M. A rapid and sensitive method for the quantitation of microgram quantities of protein utilizing the principle of protein-dye binding. *Anal. Biochem.* **1976**, *72*, 248-254.
- (59) Englard, S.; Seifter, S. Precipitation techniques. *Methods Enzymol.* **1990**, *182*, 285-300.
- (60) *Prime, version 1.5*; Schrödinger, LLC: New York, NY.
- (61) *MacroModel, version 9.1*; Schrödinger, LLC: New York, NY.
- (62) Regeling, H.; de Rouville, E.; Chittenden, G. J. F. The chemistry of D-gluconic acid derivatives. Part 1. Synthesis of 3,4;5,6-di-O-isopropylidene-D-gluconol and 2,3;4,5-di-O-isopropylidene-aldehydo-D-arabinose from D-glucono-1,5-lactone. *Recl. Trav. Chim. Pays-Bas* **1987**, *106*, 461-464.
- (63) Bouzide, A.; S., G. Highly Selective Silver(I) Oxide Mediated Monoprotection of Symmetrical Diols. *Tetrahedron Lett.* **1997**, *38*, 5945-5948.
- (64) Dess, D. B.; Martin, J. C. Readily accessible 12-I-5 oxidant for the conversion of primary and secondary alcohols to aldehydes and ketones. *J. Org. Chem.* **1983**, *48*, 4155-4156.
- (65) Corey, E. J.; Fuchs, P. L. A synthetic method for formyl → ethynyl conversion (RCHO → RC triple bond CH or RC triple bond CR'). *Tetrahedron Lett.* **1972**, *13*, 3769-3772.
- (66) Hofmeister, H.; Annen, K.; Laurent, H.; Wiechert, R. Ein neuer Zugang zu 17alpha-Brom- und 17alpha-Iodethinyl-Steroiden. *Angew. Chem.* **1984**, *96*, 720-721.
- (67) Lee, D. G.; Chang, V. S. Oxidation of Hydrocarbons. 9. The Oxidation of Alkynes by Potassium Permanganate. *J. Org. Chem.* **1979**, *44*, 2726-2730.
- (68) Dickson, H. D.; Smith, B. W.; Hinkle, K. W. A convenient scalable one-pot conversion of esters and Weinreb amides to terminal alkynes. *Tetrahedron Lett.* **2004**, *45*, 5597-5599.
- (69) Ermolenko, L.; Sasaki, N. A. Diastereoselective Synthesis of All Eight L-Hexoses from L-Ascorbic Acid. *J. Org. Chem.* **2006**, *71*, 693-703.
- (70) Brown, D. G.; Velthuisen, E. J.; Commerford, J. R.; Brisbois, R. G.; Hoye, T. R. A Convenient Synthesis of Dimethyl (Diazomethyl)phosphonate (Seyferth/Gilbert Reagent). *J. Org. Chem.* **1996**, *61*, 2540-2541.
- (71) Barton, D. H. R.; Liu, W. A New and Concise Synthesis of 3-Deoxy-D-arabino-2-heptulopyranosonic Acid (DAH) and Derivatives through the Radical Chemistry of Barton Esters. *Tetrahedron Lett.* **1997**, *38*, 367-370.

- (72) Hoffman, R. V.; Tao, J. A Stereocontrolled Synthesis of Monofluoro Ketomethylene Dipeptide Isosteres. *J. Org. Chem.* **1999**, *64*, 126-132.
- (73) McAtee, J. J.; Schinazi, R. F.; Liotta, D. C. A Completely Diastereoselective Electrophilic Fluorination of a Chiral, Noncarbohydrate Sugar Ring Precursor: Application to the Synthesis of Several Novel 2'-Fluoronucleosides. *J. Org. Chem.* **1998**, *63*, 2161-2167.
- (74) Takano, S.; Tanaka, M.; Seo, K.; Hirama, M.; Ogasawara, K. General chiral route to irregular monoterpenes via a common intermediate: syntheses of (*S*)-lavandulol, *cis*(1*S*,3*R*)-chrysanthemol, (1*R*,2*S*)-rothrockene, and (*R*)-santolinatriene. *J. Org. Chem.* **1985**, *50*, 931-936.